Comparing properties of CA3 engram neurons over initial periods of encoding and early phase of consolidation

Dario Cupolillo

université de BORDEAUX

THÈSE PRÉSENTÉE
POUR OBTENIR LE GRADE DE

DOCTEUR DE
L'UNIVERSITÉ DE BORDEAUX

École doctorale
Science de la Vie et de la Santé

Spécialité: Neurosciences

Par Dario Cupolillo

Early properties of CA3 engram neurons involved in information encoding

Sous la direction de: Christophe Mulle

Soutenue publiquement le 25 Mars 2021

Membres du jury:

Dr. Andreas Frick	Directeur de recherche, INSERM	*Président*
Dr. Christine Gee	Directeur de recherche, Univ. Hamburg	*Rapporteur*
Dr. Valérie Crépel	Directeur de recherche, INSERM	*Rapporteur*
Dr. Magdalena Sauvage	Professeur, Leibniz Inst. Magdeburg	Examinateur
Dr. Christophe Mulle	Directeur de Recherche, CNRS	*Directeur de thése*

Unité de recherche

Interdisciplinary Institute for Neuroscience

CNRS UMR 5297

Centre Broca Nouvelle-Aquitaine

Université Bordeaux

38 Rue Albert Marquet

33000 Bordeaux cédex

Acknowledgements

First of all, I thank all the jury members for accepting the invitation to participate in the evaluation of my doctoral project: Valérie Crépel, Christine Gee, Magdalena Sauvage and Andreas Frick.
I would like thank Christophe Mulle for welcoming me into his team and giving me the opportunity to work in a stimulating scientific environment. His support, encouragement and supervision have been fundamental not only to the development of my work, but also for creating solid bases for my career progress.
I would like to thank Mario Carta not only for his help in making an electrophysiologist out of me, but also for his constant support, encouragement, fruitful discussion, and for setting an example that kept my motivation strong.
This work could not have been carried out without the help of Noelle Grosjean, who I thank for the massive amounts of work she helped me with, between behavior tests and viral injections.
I would like to thank Ashley Kees for her help, all the useful discussions and her inspiring work that motivated me to learn computer programming from which I will benefit in my career.
I also thank Julio Viotti for his support, for being a fellow patcher, and for all his valuable insights.
Thanks to Ania Gonçalves for all her help, support, for always giving me confidence and for teaching me to accept our limitations.
I also thank Catherine Marneffe and Célia Reynauld for their valuable help with my experiments and for all the useful discussions. I would like to thank Sandrine Pouvreau, Gael Barthet and Thierry Amedee for all their help with electrophysiology and for useful exchanges. I also want to acknowledge Severine Deforges work, that created the bases for the realization of this work. Finally, I wish to thank all the present and past team members that created a friendly working environment during the years: Meryl, Mariela, Eva, Ruth, Pei, Tomas, Nan, Anael, Justine, Mathilde, Cindie, Ana, Ana Sofia, Mariana, Jorge, Julie, Marine, Christophe

I would also like to thank the IINS staff: Remi Sterling for his precious work keeping the institute up and running, the IINS administration and IT team for their help.

Last but not least, I thank the animal facility Pole in Vivo (PIV) staff for all the help and for the working environment they created from which my work benefited, the Bordeaux Imaging Center (BIC) for their help with microscopy and in particular to Sebastian Marais for his help with the 2p microscope and for introducing me to image analysis programming.

Abstract

Forming new memories after a one-time experience requires initial encoding then consolidation over time. During learning, multimodal information converges onto the hippocampus, activating sparse neuronal assemblies. Activated neurons are believed to form a memory representation through concerted activity and synaptic interconnectivity. Computational and behavioral studies point at the hippocampal CA3 region as a key structure involved in multimodal information integration and initial memory storage. In this work, we describe the development and validation of a novel tool for fast labeling of engram neurons (FLEN). FLEN is based on c-Fos activity-dependent transient expression of a destabilized fluorescent marker ZsGreen1 rapidly after one-trial learning (few hours). With FLEN, we explore the electrophysiological properties of c-Fos activated CA3 neurons following one-trial learning of an episodic-like memory. In parallel, we employ the Robust Activity Marker (RAM) system, which provides activity-dependent labelling 24 hours following a novel experience. Comparing FLEN+ and RAM+ neurons allows to characterize how the properties of neuronal assemblies evolve after an initial phase of consolidation. We found that CA3 cellular recruitment in an engram is not predetermined by their excitability state, but rather they progressively acquire increased excitability as compared to neurons which were not activated by the one-trial contextual memory task. Early CA3 neuronal engram showed an increased number of excitatory inputs which overall did not appear to be more efficient, suggesting that LTP-like synaptic plasticity does not occurs early during the process of memory formation. Control of local inhibition of spiking influence CA3 PNs capacity to be engaged in an active ensemble of neurons. A comparison of FLEN+ and FLEN– CA3 neurons finally suggests less Mf-driven feedforward inhibition in the putative engram neurons which may facilitate spike transfer from the DG hence increased excitation. Overall, the FLEN strategy appears as an excellent complement to the previously used labeling strategies which have assessed changes in engram neuron properties in the time range of days. With this approach, we can show that both the intrinsic excitability and the synaptic properties of CA3 pyramidal neurons undergo progressive plastic changes over the first day following a one-trial memory task.

Keywords: episodic memory, engram, electrophysiology, neural circuits, behavior

Résumé

La formation de nouveaux mémoires après une expérience unique nécessite un encodage initial puis une consolidation dans le temps. Pendant l'apprentissage, les informations multimodales convergent vers l'hippocampe, activant des assemblées neuronales épars. Les neurons activée sont considérés forments une représentation de la mémoire par une activité concertée et une interconnectivité synaptique. Des études computationnelles et comportementales montrent que la région CA3 de l'hippocampe est une structure clé impliquée dans l'intégration d'informations multimodales et le stockage initial de la mémoire. Dans ce travail, nous décrivons le développement et la validation d'un nouvel outil pour le marquage rapide des neurones d'engramme (FLEN). FLEN est basé sur l'expression transitoire dépendant de l'activité de c-Fos d'un marqueur fluorescent déstabilisé ZsGreen1 rapidement après un apprentissage en procès unique (quelques heures). Avec FLEN, nous explorons les propriétés électrophysiologiques des neurones CA3 activés par c-Fos après l'apprentissage d'une mémoire de type épisodique en procès unique. En parallèle, nous utilisons le système Robust activity marking (RAM), qui fournit un marquage dépendant de l'activité 24 heures après une nouvelle expérience. La comparaison des neurones FLEN+ et RAM+ permet de caractériser l'évolution des propriétés des assemblages neuronaux après une phase initiale de consolidation. Nous avons constaté que le recrutement cellulaire des CA3 dans un engramme n'est pas prédéterminé par leur état d'excitabilité, mais qu'ils acquièrent plutôt progressivement une excitabilité accrue par rapport aux neurones qui n'ont pas été activés par la tâche de mémoire contextuelle en procès unique. Les premiers engrammes neuronaux CA3 ont montré un nombre accru d'entrées excitatrices qui, dans l'ensemble, ne semblaient pas plus efficaces, ce qui suggère que la plasticité synaptique de type LTP ne se produit pas à un stade précoce du processus de formation de la mémoire. Le contrôle de l'inhibition locale de l'effet de pointe influence la capacité des PN CA3 à s'engager dans un ensemble actif de neurones. Une comparaison des neurones FLEN+ et FLEN- CA3 suggère finalement une inhibition moins importante de la feedforward induite par la Mf dans les neurones d'engramme putatifs, ce qui pourrait faciliter le transfert de pic à partir de la DG, d'où une excitation accrue. Globalement, la stratégie FLEN apparaît comme un excellent complément aux stratégies de marquage utilisées précédemment, qui ont permis d'évaluer les changements des propriétés des neurones d'engramme dans l0intervalle de temps des jours. Avec cette approche, nous pouvons montrer que l'excitabilité intrinsèque et les propriétés synaptiques des neurones pyramidales CA3 subissent des changements plastiques progressifs au cours du premier jour suivant une tâche de mémoire en procès unique.

Mots clés: memoire episodique, engramme, electrophysiologie, circuit neuronal, comportement

Preface

This work has been carried out at the Interdisciplinary Institute of Neuroscience (IINS) in Bordeaux, in the 'Synaptic circuits of memory' team, under the supervision of Christophe Mulle. The project was initially part of a Horizon 2020 initiative supported by Marie Skłodowska-Curie program, called 'synaptic dysfunction in Alzheimer's disease' (SyDAD) with a transversal focus on synaptic dysfunction, the main connection point between pathology and cognitive decline in Alzheimer's disease. The project has then gained a focus on a more basic aspects of the cellular and circuit mechanisms of memory encoding.

The 'synaptic circuits of memory' team is interested in episodic memory, a form of declarative autobiographical memory of specific episodes, bearing information about the context (where), elements (what), and when they happened relative to one's sense of time. The hippocampal CA3 region performs the neural computation necessary for rapid encoding and retrieval of episodic memory. CA3 circuits allow the formation of associations of multimodal sensory and spatial information. During novel experiences, this multimodal information converges and activates a subset of pyramidal neurons, called engram neurons. These specific neurons are co-active during encoding of a new memory, and their orchestrated pattern of activity is thought to form the initial trace of a memory. Specific plasticity events at the level of engram neurons and their interconnections allow to store these specific memories.

During my PhD studies I mainly employed a combination of behavioral tests, viral injections and *ex vivo* electrophysiology recordings to study the properties of CA3 neurons specifically involved in episodic memory encoding and storing. I used and tested different one-trial behavioral assays as a task for encoding of episodic-like memories in mice. These were combined with viral tools for activity-dependent expression of a fluorescent reporter to observe the emergence of an engram associated with the novel experience. Different viral constructs were tested under different conditions. Our team developed a novel activity-dependent labeling tool that allow rapid identification of engram cells within few hours following an encoding event. This approach differs from conventional engram labeling strategies, that instead enable engram identification several hours after the novel experience when consolidation processes have already been engaged. This represents an opportunity to investigate properties of neurons involved in memory formation within few hours from the encoded experience, this way providing a bridge between *in vivo* real-time assessment of neuronal ensembles dynamics during a task and *ex vivo* investigation of neuronal properties far in time from the encoded experience.

To describe this work, I introduce the general anatomy of the hippocampus, focusing then on the connectivity and the physiological activity of CA3 pyramidal neurons. Then, I illustrate the involvement of the hippocampus and in particular CA3 in episodic memory function, as well as the main plasticity mechanisms at the base of memory encoding. Then, I introduce Immediate Early Genes, and how they have been used as a readout of recent neuronal activity to identify engram cells involved in a specific computation. I describe some of the strategies reported in the literature to identify engram cells, but also used to manipulate them. Functional manipulation of engram is in fact important to establish a causal role for these IEG-labeled cells in memory function.

In a second part, I illustrate the main methodological approaches used in my work. I introduce some example behavioral tasks used to assess episodic-like memory that are currently adopted in the lab, with a focus on contextual fear conditioning, the principal behavioral task used in this work. Then I describe some of the implications of using viral vectors to specifically label engram cells. I will illustrate the principles and practical indications of electrophysiological recordings in acute slices.

The results of this work are reported in the article '*A novel viral tool for exploring the early properties of CA3 engram cells*', which is currently in preparation. The presented work is not a finished version, as additional experiments are planned, and some others are ongoing. Specific experiments ongoing are specified along the article. The most important work has to be done regarding electrophysiological recordings of FLEN and RAM neurons. Part of this work is being carried out, to complete the groups, and different recordings are planned. In addition, we are optimizing morphological analysis of FLEN cells. Morphological features could be interesting to sustain the corresponding functional changes occurring in CA3 engram cells.

Table of Contents

List of figures and tables

Abbreviations

A/C: associational/commissural

AD: Alzheimer's disease

ACSF: artificial cerebrospinal fluid

AMPA: α-amino-3-hydroxy-5-méthylisoazol-4-propionate

AMPAR: AMPA receptor

CA1/2/3: *cornu ammonis* 1/2 /3

CC: current clamp

CFC: contextual fear conditioning

DIV: days *in vitro*

DG: dentate gyrus

EC: entorhinal cortex

GC: granule cell

GCL: granule cell layer

IEG: immediate-early gene

IML: inner molecular layer

LEC: lateral entorhinal cortex

LFP: local field potential

LTD: long-term depontentiation

LTP: long-term potentiation

MC: mossy cell

MEC: medial entorhinal cortex

MF: mossy fiber

MFB: mossy fiber bouton

MFT: mossy fiber terminal

MML: medial molecular layer

NMDA: N-methyl-D-aspartate

NMDAR: NMDA receptor

OML: outer molecular layer

PN: pyramidal neuron

PP: perforant path

PV: parvalbumin

SP: synaptic plasticity

TE: thorny excrescence

VC: voltage clamp

Introduction

1.1- Hippocampal CA3: anatomy and connectivity

1.1.1 – Hippocampal formation

The hippocampal formation is a brain system that is found bilaterally in the medial temporal lobe (Fig. 1.1A). It is a compound structure that includes:

- *Hippocampus proper*
- Dentate Gyrus
- Subiculum
- Parasubiculum
- Presubiculum
- Entorihnal cortex

The *hippocampus proper* (or hippocampus) is named after the greek word for 'seahorse', given its curved shape. It spans along a dorsal (septal) to ventral (temporal) axis in rodents, corresponding to a anterior-to-posterior axis in humans (**Fig. 1.1C**). Given its fundamental role in memory formation and spatial navigation, hippocampus architecture and basic intrinsic circuitry is evolutionarily preserved across different mammalian species (**Fig. 1.1A**) (Strange et al., 2014). The hippocampus is composed by different *cornu Ammonis* subfields CA1, CA2, and CA3 (and CA4 in humans, also known as *hilus* if considered as a part of the dentate gyrus) (**Fig. 1.1B**).

All the hippocampal formation structures are functionally interconnected by strong forward connections, forming the canonical 'trisynaptic loop' (**Fig. 1.2A**). The entorhinal cortex (EC) constitutes the major excitatory input, projecting axons to the dentate gyrus (DG), CA3, CA1 and the subiculum. Information flows following the trisynaptic loop, with DG sending projections to CA3 through the mossy fibers (MFs), which in turns projects to CA1 through the Schaffer collateral. CA3 also consists of an extensive self-connected network ipsi- and contralaterally, forming the CA3-CA3 associative/commissural (A/C) network. CA1 projects the main output of the hippocampus to the subiculum and back to the EC. Subiculum is in turn connected to pre- and parasubiculum and the EC.

For sake of convenience, the term "hippocampus" will refer to the hippocampus and dentate gyrus collectively, although it is acknowledged that the term is sometimes used to include the subicular complex and the entorhinal cortex (Amaral and Witter, 1989).

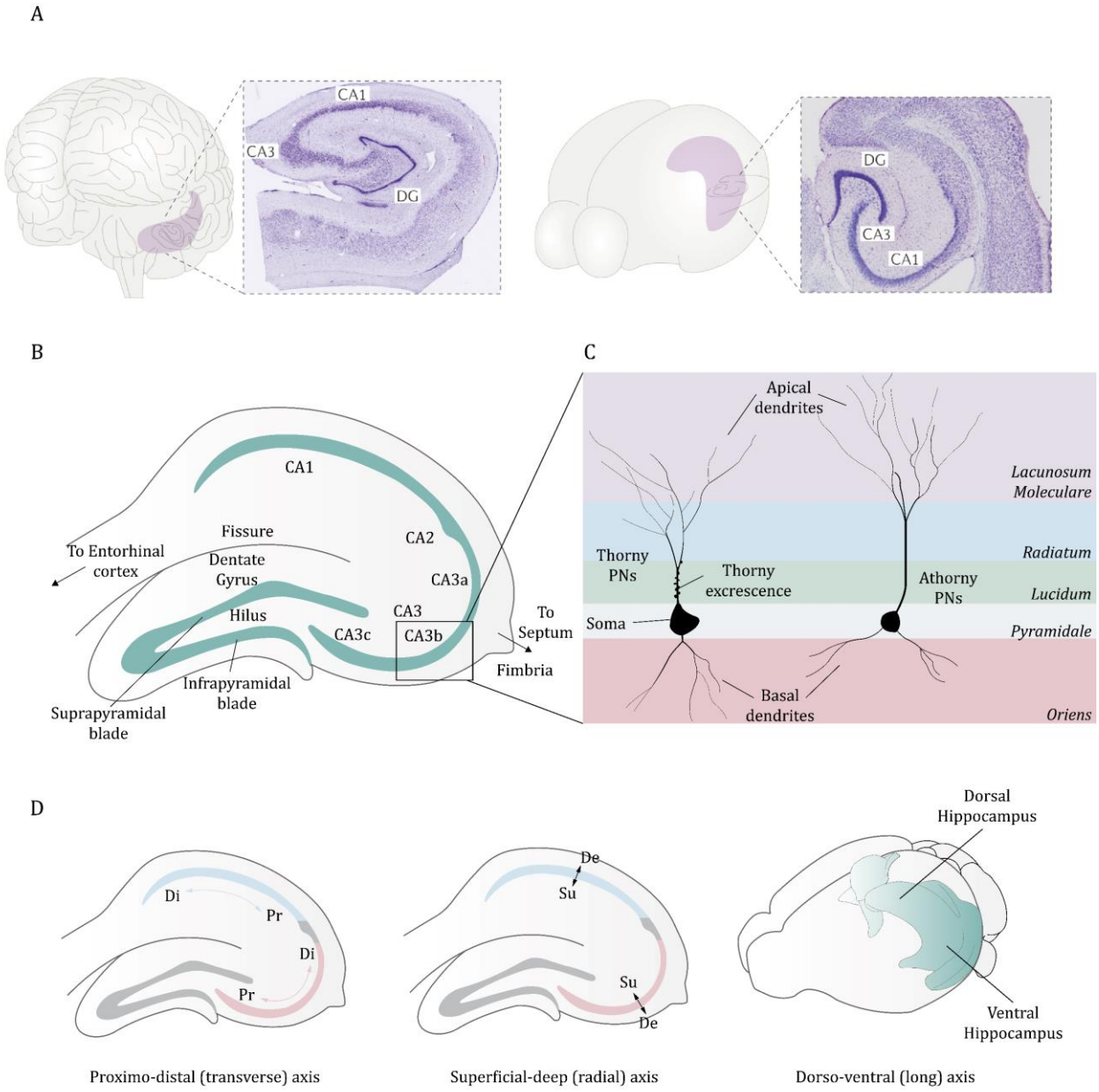

Figure 1.1 | Hippocampal anatomy and CA3. A. *Representation of the hippocampus position in the human (left) and mouse brain (right). The hippocampus and the entorhinal cortex are found bilaterally in the medial temporal lobe. Cross sections of the human and mouse hippocampus are reported on the side. Adapted from (Hainmueller and Bartos, 2018a).* **B.** *Representation of a sagittal section of the mouse hippocampus to show the anatomical organization of the main hippocampal subregions. The hippocampus is composed by the Dentate Gyrus (DG), CA3, CA2 and CA1.* **C.** *Schematic of Pyramidal neurons (PNs) in CA3. An example thorny neuron as it could be found closer to the DG is represented on the left and an example athorny neuron as it could be found closer to CA2 is represented on the right. PNs cell bodies (soma) are located within the stratum pyramidale. Apical dendrites extend through the stratum lucidum, radiatum and lacunosum moleculare, whereas basal dendrites extend in the stratum oriens.* **D.** *Schematic illustration of the spatial axis of a sagittal section of the hippocampus (Pr: proximal, Di; distal, Su: superficial, De: deep).*

1.1.2 - CA3

1.1.2.a – CA3 pyramidal neurons

The early historical descriptions of hippocampal neurons date back to the reports of Golgi (1886) and Ramon y Cajal (1901). These descriptions provided a first portrayal of size and shape of neurons in the region CA1, CA2 and CA3, populated by pyramidal neurons (PNs). In rodents, CA3 PNs are estimated to number approximately 3 x 10^5, with a somatic cross surface of 400-500 μm^2 (2-4 times larger than those of CA1 PNs). CA3 PNs are arranged in a cellular layer, the *stratum pyramidale,* spanning medio-laterally and antero-posteriorly from the DG curving to CA2 (**Fig. 1.1D**). CA3 PNs have 1-3 primary apical dendrites originating from the soma, and 2-7 primary basal dendrites, both further branching into secondary and then into side branches (Ishizuka et al., 1995a). Apical dendrites extend towards the hippocampal fissure through *stratum lucidum*, *stratum radiatum*, and *stratum lacunosum moleculare*, whereas basal dendrites expand within the *stratum oriens in* the opposite direction (**Fig. 1.1C**). In his pioneering work, Lorente del No (1934) further divided CA3 into three equal-size subfields along the proximodistal axis (CA3a, CA3b, CA3c), even in the absence of precise anatomical boundaries. CA3a field distally intermingles with CA2, CA3b region lies in the middle and CA3c is proximal to DG (**Fig. 1.1B**). Despite the discrete naming of these subregions, the differences between them appear graded rather than exhibiting sharp borders. Most experimental studies describe and consider CA3 as populated by homogeneous pyramidal cells. However, many reports describe instead a striking heterogeneity within it. In fact, a gradual marked proximodistal heterogeneity in CA3 PN dendritic morphology, electrophysiological properties, axonal projections, synaptic inputs, engagement in behavior, and gene expression patterns exists (Balind et al., 2019a; Ishizuka et al., 1995a; Sun et al., 2017a). A morphological signature of CA3 PNs is the presence of iconic structures found on the proximal part of apical and basal dendrites, the thorny excrescences (TEs), or spiny excrescences. TEs are specialized dendritic spines with a complex morphology, contacted exclusively by single large MF boutons (MFBs) originating from the DG. Recent findings of the presence of athorny PNs neighboring classical thorny neurons further enhance the degree of complexity of CA3 (Hunt et al., 2018a). Athorny PNs are preferentially located at distal regions (CA3a and CA3b) and deeper in the pyramidal-cell layer (closer to stratum oriens). The two types of CA3 PNs have distinct morphological and physiological phenotypes, as well as different roles during hippocampal-dependent memory function (**Fig. 1.1C**, **Fig, 1.2B**).

1.1.2.b – CA3 interneurons

INs in CA3, unlike PNs, are not found in a specific layer, but rather they are distributed in all the layers. Even if they represent only 10% of all neurons, there is a rich diversity of inhibitory interneurons (INs) in the hippocampus, playing a major role in CA3 activity. Distinct types of inhibitory neurons can be classified based on their molecular, morphological and connectivity features. INs can be classified according to their connectivity relative to CA3 PNs. There can be distinguished perisomatic INs, that target the soma or the initial segment of the axon and a large population of incompletely characterized interneurons that innervate the distal dendrites exist

(Hájos et al., 2004). A detailed description of interneurons type and their connections is provided in 1.1.4b.

1.1.3 – Other hippocampal neuronal types

1.1.3a –Granule cells

Dentate gyrus principal cells are the granule neurons, which number almost 1 million in the rat and 5 million in the monkey (Claiborne et al., 1986, 1990; Seress, 1988). Granule cells (GCs) have a relatively small soma (8-12 μm in diameter) and are organized in a densely packed layer called *stratum granulosum* (or granule cell layer, GCL), but there are misplaced GCs known as semilunar granule cells and ectopic granule cells. The GCL possesses a 'V' shape, whose upper and lower blades (suprapyramidal and infrapyramidal respectively) border the hilar region (or *hilus*) (**Fig. 1.1B**). GCs characteristically have two main radially oriented apical dendrites emitting several fine densely spiny branches, which extend into the DG *stratum moleculare*, reaching the hippocampal fissure. GC basal dendrites are extremely rare in rodents.

Functionally, the DG is the first stage of the hippocampal trisynaptic loop. It is targeted by many entorhinal afferents. The molecular layer is divided into the outer molecular layer (OML), the middle molecular layer (MML) and the inner molecular layer (IML). Afferents from the lateral EC (LEC) terminate in the OML and those from the medial EC (MEC) terminate in the MML, where dendrites of dentate principal cells arborize. Major afferents to the IML comes from hilar mossy cells. Axons of GCs, called mossy fibers (MFs), originate at the opposite pole of the soma and enter the hilus, where they give rise to several local collaterals that largely remain in the hilar region.

The DG also is one of the few regions in the brain where adult neurongenesis is observed. The subgranular zone at the interface between GCL and the hilus is occupied by stem cells, progenitors divide throughout adult life and migrate primarily to the GCL where they become granule cells and integrate into the dentate gyrus circuitry.

1.1.3b – Mossy cells

The hilus, the region bordered by CA3c and the upper and lower blades of the DG, is mainly populated by mossy cells (MCs). MCs are named for their characteristic 'mossy' appearance, with clusters of complex spines (TEs) on their proximal dendrites and on the cell body that are contacted by massive MFBs (Amaral, 1978). Athorny spiny hilar cells also exist. MCs dendrites usually span the hilar region (Amaral, 1978), but some of them have been found to have a single dendritic branch penetrating the DG ML (Buckmaster et al., 1996; Laurberg and Sørensen, 1981; Ribak et al., 1985; Scharfman, 1995; Soltesz and Mody, 1994). Large MC axon projections (known as a 'distant' or 'intralamellar' projection) terminates away from the cell body in both the ipsilateral and contralateral dentate gyrus.

The effect of MCs input on GCs is complex. MCs are glutamatergic (Soriano and Frotscher, 1994) and can excite granule cells through direct inputs (Scharfman, 1995). But mossy cells also activate DG INs that inhibit granule cells. MCs provide a weak monosynaptic input to GCs that generate an excitatory postsynaptic potential (EPSP) only during blocking of GABAergic inhibition. In addition, MCs can have a robust excitatory effect on depolarized GCs (Scharfman, 1995). Optogenetic selective stimulation of MCs evoke both excitatory and inhibitory responses in GCs. However, light stimulus preceding PP stimulation give rise to reduced GCs response to PP input. This suggested that the dominant effect of MCs on PP evoked responses of granule cells is inhibitory. Repetitive light pulses that were more similar to patterns of activity observed *in vivo* were also tested and revealed that the excitation of GABAergic INs was more persistent than the excitation of granule cells. Thus, the inhibitory effects of mossy cells might be stronger than their excitatory effects *in vivo* (Hsu et al., 2016).

1.1.3c – CA2

CA2 is a relatively small region interpolated between CA3a and CA1. CA2 has been little studied because of its small size and difficulty encountered in precisely defining its borders, nevertheless it has a distinctive pattern of expression of specific cellular markers (Williams et al, 1996; Ochiishi et al, 1999; Tucker et al, 1993, Zhao et al., 2001; Lein et al., 2005). It is populated by PNs that share most of their morphological feature with CA3. Although CA2 is a distinct region, the anatomical boundary is not abrupt. Indeed, CA3a and CA2 neurons are highly intermingled at their interface area (Sun et al., 2017b). The major distinguishing characteristic is the lack of thorny excrescences on the proximal apical dendrites as a consequence of lack of mossy fiber connections. CA2 PNs basal dendrites length is slightly less than the very distal CA3 cells, while in *stratum radiatum* the dendritic pattern closely matched that of the CA3 cells, although the dendritic length was slightly higher than in the distal CA3 PNs. The amount of dendritic tree in *stratum lacunosum-moleculare* of CA2 PNs was slightly higher than in distal CA3 cells. The axons of CA2 PNs emerge from the soma and arborized either in SO of CA2 with some branches reaching CA1 or CA3.

CA2 neurons receive uniquely strong, convergent excitatory input from layer 2 and 3 of the EC, the only site of such convergence in the hippocampus. In addition, CA2 is the only CA region receiving inputs from the hypothalamic supramammillary nucleus (Vertes and McKenna, 2000). Synaptic inputs from CA3 largely inhibit CA2 pyramidal neurons by recruiting strong feedforward inhibition (Chevaleyre and Siegelbaum, 2010). CA2 neurons strongly excite CA1 pyramidal neurons through potent excitatory synaptic connections. With this organization, CA2 forms the nexus of a powerful disynaptic circuit linking EC input with CA1 output (Bartesaghi and Gessi, 2004; Bartesaghi et al., 2006).

Selective inactivation of CA2 synaptic output does not alter contextual-dependent memories, but it affects social recognition as determined by three-chamber social novelty testbetween a subject mouse and a novel mouse, demonstrating an important role for CA2 in social memory(Hitti and Siegelbaum, 2014; Leroy et al., 2017).

1.1.3d – CA1

CA1 pyramidal cells are among the most studied neurons in the mammalian brain. The CA1 region possess a layer organization in continuity with CA3 and CA2, with cell bodies located in the *stratum pyramidale*. The transition from CA2 to CA1 is more marked because of the organization of pyramidal cell structure, starting from the smaller dimension of CA1 cell bodies compared to CA3 and CA2. Interestingly, unlike CA3 and CA2, distal apical dendrites of CA1 cells do not extend into the *stratum lacunosum-moleculare*. The dendritic organization of CA1 cells is far more homogeneous than CA3 and CA2 cells, with the general form of the dendritic tree remarkably more similar from neuron to neuron. Apical dendrites of CA1 PNs typically have a more distinctive main apical dendrite and tuft. The basal and proximal apical dendrites of CA1 pyramidal cells receive input primarily from CA3 cells, whereas the apical tuft receives input from the entorhinal cortex (Ishizuka et al., 1995b).

CA1 receives inputs primarily from the EC, with cells in the LEC and MEC preferentially targeting the distal and proximal regions of CA1, respectively (Tamamaki and Nojyo, 1995). The proximal portion of CA1 (adjacent to CA2) is preferentially connected with circuits that determine the animal's position in space like the medial entorhinal cortex and the retrosplenial cortex ((Deshmukh and Knierim, 2013; Naber et al., 2001; Witter et al., 2000). Distal CA1, in contrast, connects with brain areas important for processing items and objects in the environment like the lateral entorhinal cortex and perirhinal cortex(Deshmukh and Knierim, 2013; Naber et al., 2001; Witter et al., 2000). Therefore, the MEC predominantly represented spatial information, encoding the animal's position in space, whereas the LEC represented non-spatial information, contributing to the encoding of object and item location (Deshmukh and Knierim, 2013; Hargreaves et al., 2005), suggesting different roles of CA1 in spatial and non-spatial tasks (Igarashi et al., 2014; Ito and Schuman, 2012). To support the emergence of non-uniform parallel circuits modules, CA1 PNs also exhibit a significant degree of heterogeneity (Soltesz and Losonczy, 2018). In particular, a clear morphological subdivision, transcriptional gradient, and interneuron inputs (Lee et al., 2014) between deep and superficial CA1PCs exists along the radial axis, which could manifest in cell-intrinsic differences in protein expression and functional properties (Bannister and Larkman, 1995; Jarsky et al., 2008). This has been shown with lesion studies, that determined that proximal CA1 is involved in the expression of associative memories (Nakazawa et al., 2016).

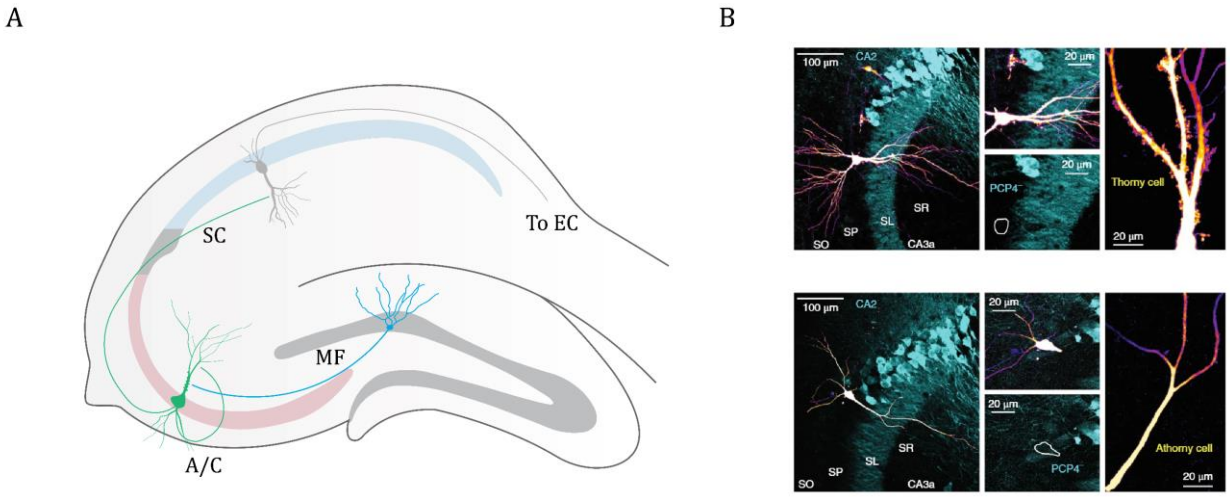

Figure 1.2 | Main hippocampal circuitry and CA3 features. A. *Schematic of the organization of the classical trisynaptic loop. The main excitatory input to the hippocampus is provided by perforant path projection from the EC, contacting granule cells in the DG and CA3 pyramidal neurons. Granule neurons send forward mossy fibers (MFs) excitatory inputs to CA3, who in turn sends projection to CA1 through the Schaffer collateral (SC). The main output of the hippocampus is generated from CA1, projecting back to the EC.* **B.** *Images of thorny and athorny CA3 pyramidal cells, negative for CA2 marker PCP4. SO: stratum oriens, SP: stratum pyramidale, SL: satrutm lucidum, SR: stratum radiatum. Adapted from (Hunt et al., 2018b).*

1.1.4 - CA3 local circuitry

The neural computation required for memory function depends on the specific organization and information flow across the different hippocampal regions (**Fig. 1.2A**). The characteristic architecture and wiring of CA3 seems to be well adapted for rapid storage and retrieval of associative memories.

1.1.4a – DG inputs to CA3

DG granule cells project unmyelinated axons along the septo-temporal axis of the hippocampus, travelling below, within or just above the pyramidal cell layer. Three main functionally specialized type of terminals characterize these axons: large 'giant' MF boutons (MFBs), small *en passant* boutons and filopodial extensions emerging from the MFBs. Giant MFBs contact TEs on the proximal dendrites of CA3 PNs and hilar mossy cells (**Fig. 1.3A**). Mossy fibers also target interneurons through the *en passant* boutons in the dentate hilus and stratum lucidum, as well as through the small terminals and MFTs-emerging filopodial extensions. In rodents, the estimated number of granule cells in the DG is 10^6, each giving rise to around 15 large MFBs. An individual CA3 PN receives inputs from up to 50 DG cells (Gonzales et al., 2001), meaning that 0.005% of the total granule neurons influence a single CA3 PNs. GC activity is exceptionally sparse (Diamantaki et al., 2016) and fewer than 5% of a rodent's GCs are active when the animal explores a given environment (Hainmueller and Bartos, 2020).

The synapse between MFBs and CA3 PNs is distinctive on different levels. MFBs are complex and large pre-synaptic structures enveloping the intricate TEs. They contain intracellular organelles such as clustered mithocondria, endoplasmic reticulum and several vescicular structures. Large boutons contacting TEs also contain an average of 20 release sites. These synapses exhibit several different types of synaptic plasticity (Henze et al., 2000; Nicoll and Schmitz, 2005; Rebola et al., 2017). The amplitude of MF-CA3excitatory post-synaptic currents (EPSCs) depends on the pattern of presynaptic activity. When presynaptic activity frequency is low (<0.1 Hz), MF-driven excitatory post-synaptic potentials (EPSPs) have small amplitudes, insufficient to trigger action potential discharge in CA3 PNs because of the low (<0.01) release probability at individual release sites (Lanore et al., 2012). However, single MF–CA3 synapses triggers post-synaptic action potentials in response to a short burst of presynaptic activity (**Fig. 1.3B, C**), as demonstrated in slices (Sachidhanandam et al., 2009)and in anaesthetized animals *in vivo* (Henze et al., 2002; Zucca et al., 2017). MF-CA3 synapses are therefore known as 'conditional detonator' synapse and this property could be explained by a large presynaptic short-term facilitation upon repeated stimulation (frequency facilitation or bursting mode), by the large number of release sites and the large vesicle pool size and the occurrence of multivesicular release (Hallermann et al., 2003). *In vivo* patch clamp recordings of identified cells in awake mice have shown that GCs fire action potentials sparsely, and preferentially in bursts (Pernía-Andrade and Jonas, 2014), at frequencies that are compatible with such short-term plasticity of MF–CA3 synapses.

By contrast, markedly smaller MF synapses targeting GABAergic interneurons show high initial release probability (Zucca et al., 2017) with little or no frequency-dependent facilitation. Therefore, presynaptic burst discharges >10 Hz (Henze et al., 2002; Vyleta et al., 2016) reliably recruit CA3 pyramidal cells, whereas low-frequency presynaptic firing at <1Hz mostly recruits interneurons, which in turn inhibit the CA3 network (**Fig. 1.3C**). Thus, particularly low-frequency GC activity may exert a net inhibitory effect on the CA3 by recruiting feedforward interneurons.

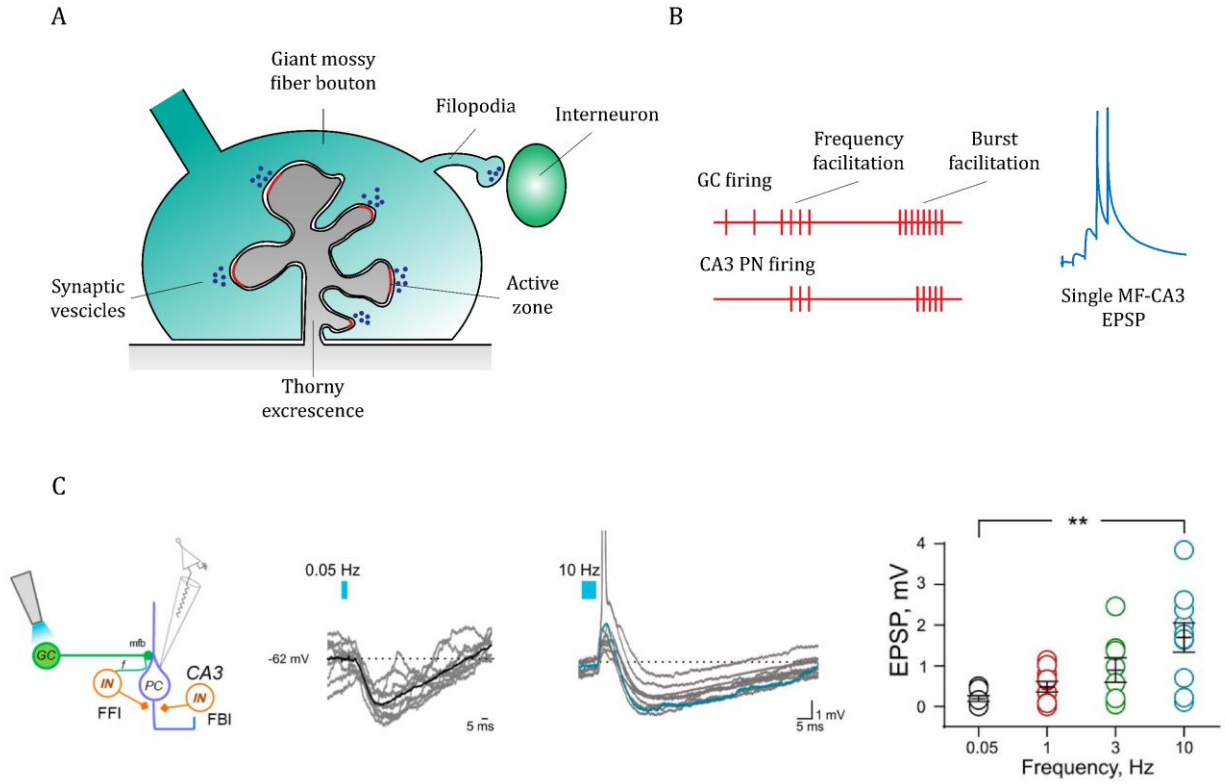

Figure 1.3 | Mossy fiber input to CA3. A. *Representation of the different types of GCs terminals. The main excitatory inputs are giant MFBs contacting TEs on CA3 PNs. Filopodia emerge from MFBs to contact CA3 interneurons.* **B.** *The conditional detonator property of MF-CA3 synapses makes them able to drive post-synaptic action potential firing in a CA3 PN in response to a short burst of pre-synaptic activity. Adapted from (Rebola et al., 2017).* **C.** *Frequency facilitation recorded in vivo in anesthetized mice. Left panel, illustration of optogenetic stimulation of GCs while recording in CA3 PNs. Center panel, synaptic potentials evoked by GCs stimulation at 0.05 Hz and 10 Hz. Low frequency stimulation leads mainly to inhibitory potentials because of feed-forward inhibition by filopodia-contacted interneurons. Increasing the stimulation frequency leads to effective post-synaptic firing in CA3. Right panel, quantification of frequency facilitation. Adapted from (Zucca et al., 2017).*

1.1.4b – Inputs from entorhinal cortex

The entorhinal cortex (EC) provides the major cortical input to the hippocampal formation through the performant path (PP). PNs in CA3 receive direct synaptic contacts from both the lateral EC (LEC) and the medial EC (MEC) layer 2 neurons, within the more superficial and deeper layers of the stratum *lacunosum moleculare* respectively. These connections transfer the spatial information essential for the development of place fields. EC also sends indirect projection to CA3 through granule cells in the DG, which then project mossy fibers.

Despite the distal location of these synapses, PP stimulation results in a strong and rapid activation of CA3 PNs, able to drive them to fire. PP–CA3 PC synapses also display NMDAR-dependent plasticity (Do et al., 2002; McMahon and Barrionuevo, 2002; Tsukamoto et al., 2003). During initial exploration of a novel environments, inputs from the entorhinal cortex have been proposed to be differentially regulated in relation to activity in the CA3-CA3 synapses (according to theta phase). According to this model, PP axons dominate CA3 inputs regulating its activity, without interacting with recurrent

collaterals. Conversely, when CA3-CA3 inputs are favored, extrinsic PP input are attenuated. This modulation of CA3 inputs attenuates with familiarity with the context (Villarreal et al., 2007).

1.1.4c – CA3 recurrent connection

Recurrent collaterals of CA3 are ramified axons that contacts neighbor CA3 PNs as well as interneurons. Recurrent axons expand within the *stratum oriens* and *stratum radiatum* contacting basal and apical dendrites of other CA3 PNs, rarely contacting back to themselves. Recurrent collaterals can extend over 70% of the dorsal-ventral axis of the hippocampus in rodents (Sik et al., 1993). Axons from CA3 PNs make between 30000 and 60000 contacts on both pyramidal cells and interneurons. The highly interconnected network of CA3 PNs is a strikingly extensive synaptic matrix, with a reported sparse connection probability of 0.92% (Guzman et al., 2016). These connections are largely non-aleatory, but rather they are enriched in motifs of multiple connections, such as convergent and divergent triple connections. Localized at both apical and basal dendrites, these synaptic contacts are characterized by a single post-synaptic active zone and a large number of postsynaptic receptor and efficient spatiotemporal summation. Together with a high probability of release, this makes CA3-CA3 connections efficient, so that inputs from relatively few neurons is sufficient to trigger action potential in a post-synaptic CA3 PN. It has been proposed that ensembles of interconnected CA3 are contacted by the same MF axon, to achieve synaptic plasticity within specific CA3 ensembles (Henze et al., 2002; Vyleta and Jonas, 2014). CA3-CA3 synapses show robust NMDAR-dependent associative long-term plasticity. A recent study shows a peculiar symmetric and broad form of spike-timing dependent plasticity, regardless of the order in which the presynaptic and postsynaptic stimulation occurs (Mishra et al., 2016). CA3 recurrent collaterals role in memory is explained in detail in 1.2.4.

1.1.4d – Inhibitory inputs to CA3

GABAergic inputs to CA3 regulate neuronal excitability, firing and synaptic integration. In addition to fine control of PNs activity, INs also have the ability to synchronize populations of neurons and therefore play an important role in the generation or maintenance of certain oscillations present in the hippocampus such as theta, gamma and sharp-waves oscillations (Klausberger et al., 2003).

Functionally, the main GABAergic cell types are perisomatic inhibitory neurons limiting the generation and propagation of the firing of principal cells, dendritic inhibitory interneurons regulating synaptic input (and Ca^{+2} signaling), and GABAergic cells specifically innervating other inhibitory interneurons, providing disinhibition (Gulyás et al., 1996).

Perisomatic inhibition is provided by fast-spiking PV-positive basket cells, CCK-positive basket cells and PV-positive AACs. Basket cell axons arborize in the *stratum pyramidale*, whereas axon branches of axo-axonic cells are restricted to the bottom part of the *stratum pyramidale* and the top part of the *stratum oriens*. These INs are contacted by dentate GCs via MFT-originated filopodia or *en passant* MFTs, constituting feed-forward inhibition (FFI) limiting PNs depolarization and burst firing (Torborg et al., 2010), or alternatively from CA3 PNs constituting feedback inhibition (FBI)

controlling the precise timing of PNs firing and synchronization of neuronal networks during gamma oscillations (Hájos et al., 2004).

CA3 PNs also receive distal dendrites inhibitory inputs, but their precise function is unclear. Distal inhibition may serve as a filter to favor a selective excitatory input arising either from the EC or from recurrent collaterals. Among them, there can be found INs with dendritic tree in *stratum oriens* and axonal projection into SLM (OLM). INs in the *stratum radiatum* with both the dendritic and axonal arborization localized in the *stratum radiatum* (RC) also provide distal dendritic inhibition. Also, INs with dendritic tree found primarily in stratum radiatum with axon restricted to stratum lacunosum-moleculare (RLM) can provide dendritic inhibition (Hájos et al., 2004).

Inhibition in CA3 is also provided by from long-projection GABAergic projection neurons (GPNs) in the medial septum, that suppress the firing of AACs during SPWs *in vivo*, suggesting a major role for these projections in coordinating CA3 PC firing.

1.1.4e – CA3 output – Schaffer Collateral

The main projection of CA3 to CA1 are called Schaffer collaterals. CA3 is the predominant driver of CA1 cells activity. The *stratum radiatum* of CA3 can be divided into a projection zone (superficial) and associational zone (deeper, where recurrent axons extend). Fibers from CA3 run along the projection zone to contact CA1, travelling within the *stratum oriens* directed towards the fimbria. Axons in this region are quite thick and bear few varicosities. The principal axon of the CA3 pyramidal cell generally arose from the basal surface of the cell soma, but in some cases originated from the proximal portion of a basal dendrite. Cells located proximally in CA3 projected preferentially to the superficial portion of *stratum radiatum* in CA1, whereas cells in the midportion of CA3 projected preferentially to the deep part of *stratum radiatum* and CA3 cells located close to the CA2 border projected mainly to *stratum oriens* of CA1 (Ishizuka et al., 1990). The exact number of synapses that a single CA3 PNs makes onto a CA1 PNs is unknown, but it is experimentally estimated to be around two to four synapses, up to 10 (Andersen et al., 1996; Sorra and Harris, 1993). In addition, Schaffer collaterals contact interneurons in CA1, which in turn contact and inhibit CA1 PNs (McBain and Fisahn, 2001).

Understanding the information content conveyed by CA3 to CA1 through Schaffer collateral has been studied by acute silencing of CA3 activity. This approach, however, does not allow to differentiate between the output to CA1 and that to A/C synapses in the recurrent network. Optogenetic silencing of CA3 cells that were active during encoding of a contextual fear memory prevented the expression of the corresponding memory, suggesting that they are necessary for reactivation of that memory (Denny et al., 2014).

CA3 output contains information critical for rapid formation of a high-quality spatial representation of a novel context in the hippocampus by means of CA1 neurons spatial tuning. In fact, if CA3-CA1 information transfer is inhibited, animals present deficit in place cells function. Information conveyed to CA1 that bypasses CA3 instead (from the EC) can improve CA1 spatial tuning by experience, supporting incremental learning in familiar environments (Nakashiba et al., 2008).

Another acute silencing of CA3 study in awake rats showed that CA3 is crucial for the generation of sharp-wave ripples (oscillations associated with memory replay) and that spatial content of CA1 place

fields depends heavily on CA3 input. In addition, a study using CA3 PNs lacking synaptic transmission in mice show that CA3 input is required for precise temporal coordination of CA1 spiking, important for phase precession (Middleton and McHugh, 2016).

The dense and homogeneous projections that form Schaffer's collaterals facilitated the study of synaptic transmission and plasticity, because they are easily activatable and the CA1 PNs are easily recordable. When two pre-synaptic action potentials arrive at an interval of time short (typically a few tens of ms), we observe a facilitation of synaptic transmission (Andersen et al., 1996). The presence of LTP at these synapses has been established by pioneering *in vitro* evidence in 1975 (Schwartzkroin and Wester, 1975). This form of LTP is the most classic plasticity studied: the tetanic stimulation of Schaffer's collaterals induces a rapid and persistent NMDAR-dependent increase in synaptic responses, whether recorded extra or intracellularly, that lasts several hours, days, weeks.

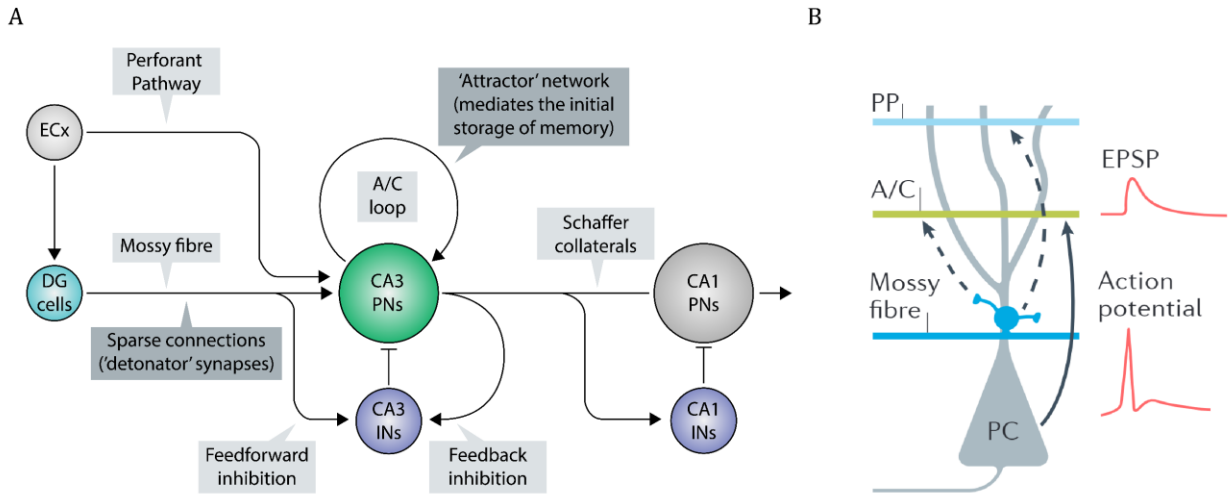

Figure 1.4 | Schematic of the main synaptic inputs to CA3. A. *The main basic circuitry of the hippocampus in relation to CA3. The traditional hippocampal tri-synaptic loop receives information from the EC and it is formed by the DG sending axons to CA3 (through the MFs), which in turns sends connections to CA1 (Schaffer collaterals), that sends the sole output of the hippocampus back to the EC. Perforant path projections from the EC contact dendrites of GCs, dendrites of CA3 PNs as well as dendrites in CA1 (not shown). CA3 PNs also sends extensive recurrent axons to themselves, contacting other CA3 PNs. CA3 interneurons provide strong feed-forward or feed-back inhibition.* **B.** *Organization of the main excitatory inputs along the apical dendrite of CA3 PNs. MFs contact proximally pyramidal cells in CA3, through giant MFTs. Perforant path inputs from the EC are found distally on the apical dendrites, whereas inputs from CA3 recurrent associational/commissural are found in the middle dendritic portion. Adapted from (Rebola et al., 2017).*

Synapse	Role	Experimental evidence
CA3-CA3	• Associative network for initial memory storage • Hebbian-like plasticity • Attractor network • Pattern completion	• Pharmacological inactivation of CA3, GRIN1 deletion in CA3 PNs or NMDAR inhibition perturb one-trial memories (Kesner, 2007; McHugh and Tonegawa, 2009). • One-trial learning deficits when synaptic plasticity is altered (Silva et al., 2016) • Computational models theorize a role in pattern completion (Guzman et al., 2016)
EC-CA3	• Memory recall	• Initial exploration modulates PP inputs and CA3-CA3, minimizing previous association interference (Villarreal et al., 2007)
DG-CA3	• Support memory encoding in CA3-CA3 • Pattern completion	• DG inactivation alters patter separation and completion (Nakashiba et al., 2012) • Pharmacological perturbation of DG-CA3 affects novel context representations (Daumas et al., 2009; Lassalle et al., 2000) • DG-CA3 impairments in LTP result in incremental learning deficits(Otto et al., 2001) • Novel context exposure regulates induced plasticity (Hagena and Manahan-Vaughan, 2011) • Structural rearrangements of MF boutons (Routtenberg, 2010; Ruediger et al., 2011)
GABAergic connections	• Not considered	• Structural rearrangements of MF boutons (Routtenberg, 2010; Ruediger et al., 2011) • PV change in interneurons after one-trial learning (Donato et al., 2013)

Table 1.1 | CA3 local inputs. *Summary of CA3 local circuit inputs and their role in episodic memory. Adapted from (Rebola et al., 2017).*

1.2 – Episodic memory.

1.2.1 - Definition

Over the centuries, the concept of memory has been fragmented into several categories, to account for the different types of memory we empirically recognize. One of such partitions is the dichotomy of implicit (or procedural) and explicit (or declarative) memory. Implicit memory, or skill memory, makes us able to learn to ride a bike or drive a car, whereas declarative memory is the collection of factual information. Declarative memory is in turn divided into semantic memory and episodic memory. Semantic memory is the organized knowledge of an individual, explicitly defining objects, concepts, places or facts independently of temporal context (historical facts).

Episodic memory, on the other hand, is the ability to learn and recall autobiographical discrete experiences in the context of both space and subjective time. The ability to re-experience past occurrences relies on the sense of mental time travel, defined as autonoetic consciousness (Tulving, 1972, 2002). Past events are retained over time with the purpose of influencing or planning future actions. So, episodic memory provides information about the 'when' of events as well as 'what' and 'where' they happened.

Episodic memory has long been debated to be unique to human, arguing that animals, although able to learn stimuli-event relationships and in some instances measure time, lack the sense of subjective time they live within, making them unable to re-experience specific past events (Roberts, 2002; Tulving and Markowitsch, 1998). However, food-storing birds can remember the spatial location and content of their caches, but also the perishability of food stores, suggesting successful recall of 'what-where-when' type of information (Clayton and Dickinson, 1998, 1999). In animals therefore, although not addressing the consciousness aspect of past events recall, memories that integrate 'what-where-when' representation can be defined episodic-like memories (Clayton et al., 2003).

From a mechanistic perspective, encoding, storing (and forgetting), consolidation and retrieval of past events are the different phases characterizing the formation of episodic memories. During every day experiences, information is constantly encoded in the brain in specific patterns of neural activity that can be viewed as an internal representation. This information is initially labile and susceptible to forgetting, but it can be potentially stored over time. In this case, the specific pattern of neural activity results in some circuit physiological changes that constitute a memory trace. Additional processes of consolidation occur during sleep states with the purpose of stabilizing and reinforcing the experience representation in the brain potentially.

1.2.2 – Hippocampal formation and episodic memory

In 1957, Scoville and Milner reported on the severe consequences of the bilateral removal of the hippocampus (and para-hippocampal structures) from the famous patient H.M. (Henry Molaison) in an attempt to treat his severe epileptic seizure (Scoville and Milner, 1957). This pointed for the first time to the fundamental role of the hippocampal complex in memory function. In the following years, similar cases of bilateral or selective medial temporal lobe damage highlighted devastating

effects on memory, with patients strikingly unable to acquire new explicit memories (a deficit known as anterograde anmesia), but with intact short-term, remote (acquired before the lesion), semantic and procedural memories. This extensive body of evidence suggests that the hippocampus is essential for fast encoding and storage of new episodic memories but has a more limited role in remote memory, which is thought to be mainly dependent on the neocortex (McClelland et al., 1995; Nadel and Land, 2000). Memory consolidation in the neocortex appears to be a slow and gradual process based on repeated interactions with the hippocampus.

Hippocampal memories of episodes are expressed as representations with evident correlates to the spatial and nonspatial structure of the external environment. With the discovery of 'place cells' in rats, (O'Keefe and Dostrovsky, 1971) a growing interest in the spatial processing function of the hippocampus arose. Place cells are spatially tuned cells, whose spiking activity is linked to an animal spatial position (the place field). Cells with this property can be found in all hippocampal subregions. As an animal explores an environment, the ensemble of cells provides a stable representation of the animal location in function of environmental boundaries (rather than local environmental feature). Their collective firing pattern is thought to provide animals with an internal map of the local environment (O'Keefe and Dostrovsky, 1971). Another kind of spatially tuned neurons was found in the MEC, named grid cells. Although other kinds of spatial processing cells are found in the MEC (head-direction cells, border cells and speed cells), grid cells are the most abundant. Fyhn et al. (Fyhn et al., 2004) targeted the superficial layers of the dorsal MEC to record neuronal activity as rats explored a large enclosure. They found that the firing fields created a striking hexagonal pattern that tiled the surface of the environment. Populations of grid cells are thought to provide position information in an environment and distance to or from a reference point, such as a start or goal location.

All the different kinds of spatially selective cells in the hippocampal formation contribute to the computation of allocentric location within an environment. Context spatial geometry and the locations of objects within it are an important part of a mental image of the remembered reconstructed event.

1.2.3 - The engram

For long time, the physical nature of memory has been elusive. In 1904, in an attempt to provide a description of the physical and biological identity of internal representations of experiences, Richard Semon introduced the term "engram", defined as "the enduring though primarily latent modifications in the irritable substance produced by a stimulus". In other words, the term engram corresponds roughly to memory trace and refers to the lasting physical changes in brain state and structure that occur in response of an event. Although a precise biological store model was not suggested, Semon believed that engrams are stored via physiochemical processes in the brain. Once formed, an engram becomes dormant but may be recapitulated by presentation of parts of the original (or a similar) event, a process defined ecphory (corresponding to memory retrieval). This means that an engram exists beyond the operation and processes required to form and recover it.

Another important contribution to the engram hypothesis came from Donald Hebb (1949), who developed a cell assembly theory. This theory proposes that reciprocally interconnected neurons are simultaneously active during an experience, and that sufficient activity within the cell assembly induces growth or metabolic changes that strengthen the connections between these cells. According

to Hebb, neurons encoding memory stimuli undergo enduring strengthening of some of their synapses through co-activation, or as he famously stated, 'neurons that fire together wire together'. This increase in synaptic strength between neurons increases the likelihood that the same spatiotemporal pattern of neural activity that occurred during encoding will be recreated at a later time.

Semon's and Hebb's theories are corroborated by contemporary advancement in engram investigation. Assemblies of sparse neurons (neuronal assemblies) are co-active during a specific behavioral condition, carrying out a specific neural computation (Josselyn and Tonegawa, 2020; Josselyn et al., 2015; Tonegawa et al., 2015). Learning is the result of persistent physical/chemical changes in these neurons and their synaptic connections, contributing to the storage of memory and mediating the expression of the encoded memory. The specific synaptic and cellular changes in these populations of selected neurons reflect an engram. With time, the term engram has been more and more used to indicate generally neuronal assemblies active during learning that undergo synaptic/cellular modifications to support learning (engram cells, engram neurons). Neurons belonging to one assembly are not confined to a single brain region, but rather are distributed across several interconnected areas, depending on the specific brain computation required during an event. Nonetheless, the building blocks of the engram can be studied at the level of single brain regions.

Engrams are dynamic structures: they are rapidly formed, undergo modifications and dissolve. Following encoding, consolidation processes alter the physical and chemical organization of engrams, altering its strength and quality (Dudai and Eisenberg, 2004). Memory retrieval may transiently destabilize a previously consolidated engram and initiate a new consolidation cycle that can lead to further changes in the engram. Although the engram is a moving target over time, this characteristic does not preclude tractability and success in capturing the engram at any given moment in time.

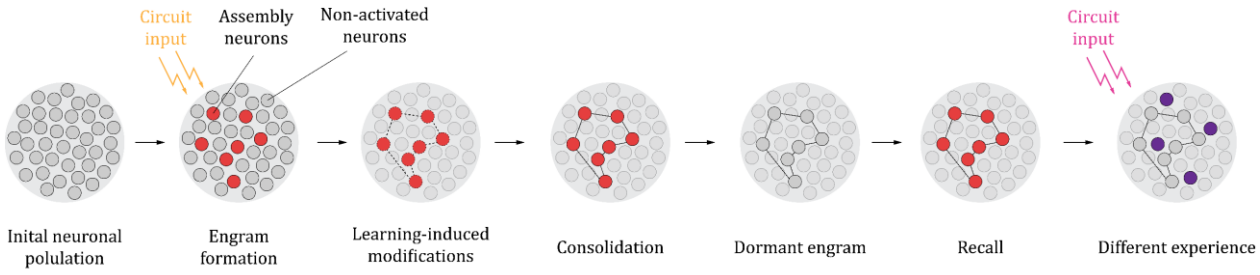

Figure 1. 5. | Schematic representation of the engram formation process. *When information reaches a local neuronal circuit, a selected group of neurons is activated. These neurons undergo neuronal and synaptic strengthening that reflects memory storage. Consolidation of these changes further strengthen the memory. In absence original experience cues, the engram remains silent, whereas when the experience recapitulates the initial cellular orchestrated activity pattern that was present at the time of learning, the memory is retrieved more efficiently. Subsequent different experiences converging in the local circuit activate a different assembly.*

1.2.4 – CA3 and episodic memory

David Marr (Marr, 1971) proposed that the hippocampus should be able to quickly form simple associations of different inputs thanks to modifiable recurrent synaptic connections. Since then, CA3 collateral system has been proposed to operate as such (McNaughton and Morris, 1987). Computational models have suggested that the recurrent network of CA3 function as an attractor network, allowing arbitrary associations to be formed and stored in CA3. This kind of network 'attracts' incoming activity to a stored firing pattern (**Fig. 1.6A**) and activation of some of the neurons in the network by elements of the memory can reactivate the whole pattern of activity through a process called pattern completion (McNaughton and Morris, 1987; Rolls, 2007, 2016). Here, arbitrary associations refer to associations between items regardless of their type, or of their class (such as the association between space and an object). For example, an information from the parietal cortex concerning the localization of an object can be associated with an information coming from the temporal cortex concerning the identity of the object (Rolls 1996).

Data supporting this view comes from studies using genetically modified adult mice lacking NMDAR subunit 1 gene specifically in CA3 PNs (CA3-NR1 KO). Although showing unaltered basal synaptic transmission, mice lacking this gene show impaired synaptic plasticity at the level of CA3. At the behavioral level, these mice are impaired when recalling a memory from degraded spatial information. NMDAR in CA3 is thus involved in the recall of associative memories and in particular in pattern completion (Nakazawa et al., 2002). By extension, NMDAR is necessary for the induction of LTP. These same mice show a deficit when it comes to encoding a new memory quickly in a new experience (**Fig. 1.6B**) (Nakazawa et al., 2003). All these results suggest that rapid changes in the pattern completion and in CA3 are essential in encoding new information, associations between objects and places, odours and places, or visual clues and that NMDAR and the associated synaptic plasticity seem to play an important role in this process (Nakazawa et al., 2004).

1.2.5 – Autoassociative network

Episodic memories are associative memories as relationships between multiple and different elements and places that are not linked are remembered. This is reflected at the neuronal level in coupling of elements of the neuronal population that have been active together. Computationally, an associative network is a matrix consisting in a set of powerful inputs reaching the principal neurons, with the ability to drive intense depolarization and firing. These inputs to the principal cells are associated with their own output, through recurrent connections feeding back into the dendrites of the principal neurons themselves via Hebbian-like modifiable synapse. Temporal coincidence between the input and the recurrent feedback output must occur to reinforce the connection, and activity from the preceding cycle must be terminated before the arrival of new information (McNaughton and Morris, 1987). The main role of such an architecture is to recall a complete representation of a learned input from any partial subset of the original set of inputs (pattern completion). The intrahippocampal cellular organization and synaptic connectivity remind that of the autoassociative network theorized by Marr (Marr, 1971). Granule cells in the DG project specifically to CA3 PNs, making few but powerful detonator-like synapses. CA3 PNs project back into their own dendrites through A/C collaterals. In addition, PP axons from EC that project to DG also terminate

distally on CA3 PNs. In this sense, GCs output to CA3 represents a transform of the PP input to CA3 (indirect connections from EC to CA3). Inhibitory neurons in CA3 also receive excitatory inputs from afferents and provide feedforward and feedback inhibition to CA3 PNs a main current shunt.

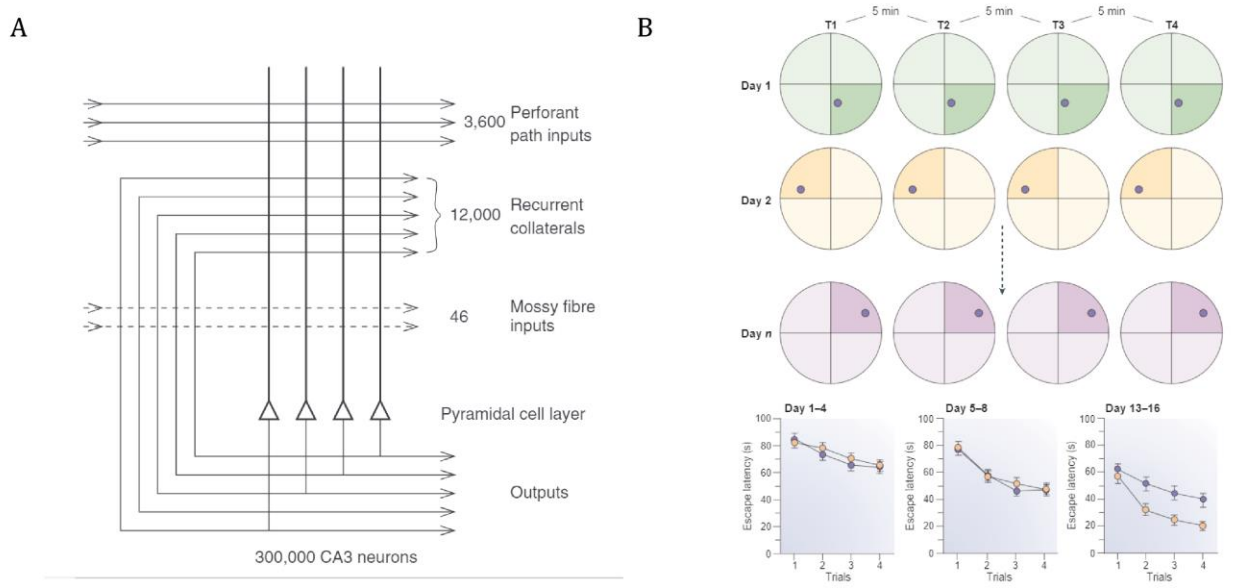

Figure 1.6 | Autoassociative network and its role in memory encoding. A. *A recurrent autoassociative network which associates the input to the principal cells with their own output. The architecture of autoassociative networks allows it to operate as an attractor neural network (Rolls, 2016).* **B.** *CA3-NR1 KO mice are impaired in delayed matching-to-place task in water maze. Mice are given 4 trials every day to learn the position of a hidden platform, which is changed every day. Performance of control mice is gradually improving over the 26 trials, whereas the mutants are impaired and show latency deficits in the last trials. These data indicate that NR1 KO are impaired in the rapid encoding of novel spatial information. Adapted from (Nakazawa et al., 2003).*

1.2.6 – Pattern completion and pattern separation

Computational theories suggest that in order to maximize the storage of information with minimal interference, networks associations such as those present in the hippocampus have to carry out two competitive and complementary processes, called pattern separation and pattern completion (Guzowski et al., 2004; Hainmueller and Bartos, 2020; Hasselmo and Wyble, 1997; McClelland and Goddard, 1996; McNaughton and Morris, 1987; O'Reilly and McClelland, 1994; Rolls et al., 1998). Pattern separation describes a network's response to similar input activity patterns with more distinct output patterns. This results in the ability of the network to reduce overlap of similar information before they are stored, to decrease the probability of interference when the memory is recalled. On the other hand, pattern completion is the ability of the network to retrieve stored patterns when partial or degraded information is presented during memory retrieval. In many models, the DG is indicated to be important to pre-process the information and allow pattern separation of the information from the EC (McNaughton and Morris, 1987; Rolls, 2007; Rolls et al., 1998). GCs outnumber entorhinal neurons by a factor of five and do not communicate directly with each other (Amaral, 1978), so entorhinal-granule cell connections can segregate or ''orthogonalize''

even minuscule, but relevant, differences present in the input patterns (McNaughton and Morris, 1987). This enables each granule cell to carry only a small and distinct fraction of the total input, expanding the relatively few entorhinal cortex neurons inputs onto many more GCs. Therefore, two memories acquired in an environment could be encoded by statistically independent populations of neurons, with independent firing locations in each of the memorized experiences. In addition, active GC ensembles may suppress the activation of competing ensembles by recruiting lateral disynaptic inhibition (Stefanelli et al., 2016). It is assumed that these factors help to separate overlapping PP input patterns and promote representations of similar memories by distinct GC assemblies to provide unique input patterns to the CA3 during memory encoding, determining collective firing of cell assemblies in CA3. Comparison of entorhinal input with DG output activity is used to probe DG pattern separation ability. Functional MRI in humans discriminating similar pictures from memory shows more similar activation patterns in the entorhinal cortex than in the DG and CA3, indicating that the DG–CA3 network may perform pattern separation in this task (Bakker et al., 2008). Rats with selective DG lesions were impaired in tasks thought to rely on spatial pattern separation (Gilbert et al., 2001); genetic knockout of the NR1 subunit of the NMDA receptor in DG impaired the ability of mice to discriminate similar environments in a fear conditioning experiment (McHugh et al., 2007). Proximal CA3c neurons displayed signs of pattern separation, with reported related behaviors for DG and CA3c principal cells in a set of spatial enclosures with gradually dissimilar geometrical shapes (Leutgeb et al., 2007).

Conversely, CA3 is assumed to retrieve previously stored activation patterns from inputs representing parts (cues) of the initially stored experience via its numerous internal recurrent connections and their associated attractor dynamics (Knierim and Neunuebel, 2016). The crucial synaptic modification for this is in the recurrent collateral synapses. CA3 allows arbitrary associations between inputs originating from very different parts of the cerebral cortex to be formed (for instance object information originating in the temporal visual cortex and location information originating in the parietal cortex). Once synaptic plasticity has permanently strengthened the connections of these assemblies, even partial PP inputs may fully reactivate an assembly to promote the recall of the associated memory. A distinctive role of CA3 in pattern completion was indicated through recordings of CA3 cells in behaving rats placed into an environment that was distorted to various degrees across the course of the experiment (Neunuebel and Knierim, 2014). In these experiments, CA3 representations of the standard and degraded environments were well correlated with each other, fulfilling the criteria for pattern completion.

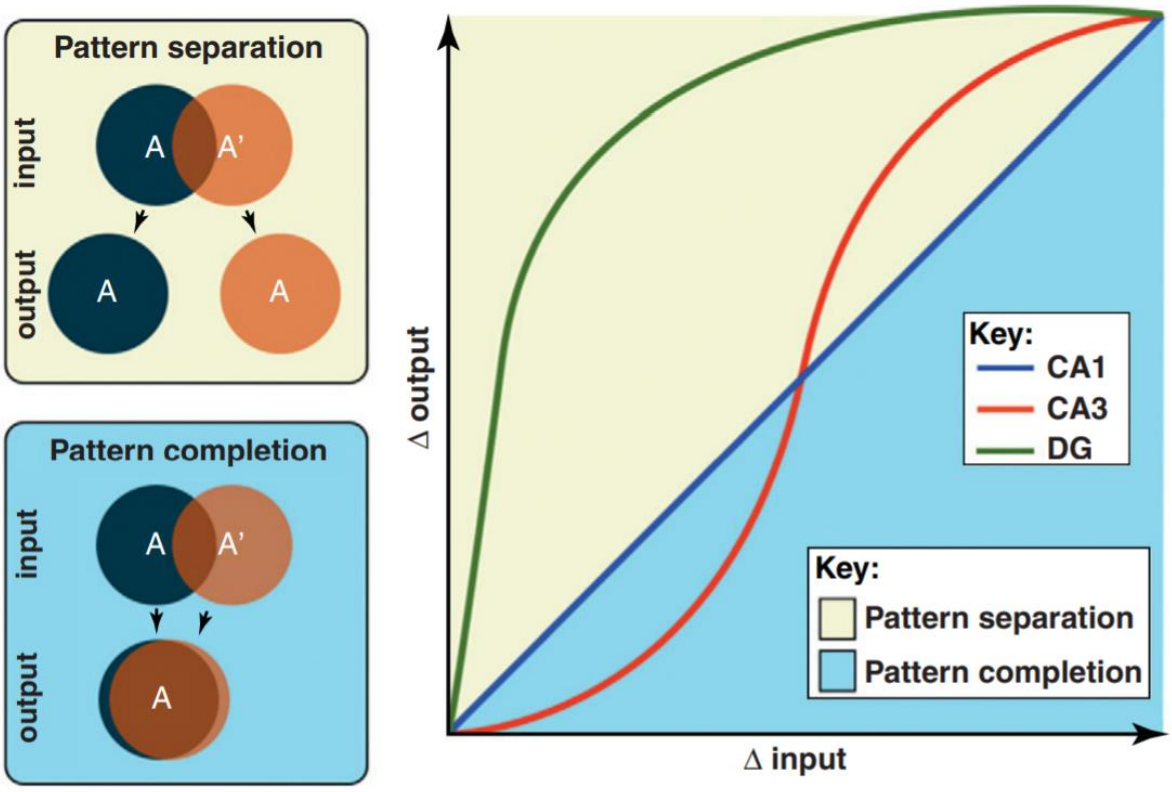

Figure 1.7 | Schematic representation of information transfer within the hippocampus. *Left panel represents the difference between pattern separation and pattern completion. Pattern separation differentiates two similar information (A and A'), while pattern completion recollects an entire representation from degraded cues, and it can be seen as making overlapping representations even more overlapping. The sigmoidal input-output function shows a non-linear transformation of information between the main cellular population of the hippocampus. The diagonal line represents a condition where the input is equal to the output. This line divides the plot into a yellow portion, where the output difference is larger than the input difference, therefore representing orthogonalizing information (pattern separation), and into a blue portion, where differences in the input are larger than differences in the input, representing information convergence (patter completion) (Yassa and Stark, 2011).*

1.3 – CA3 physiology and functions

1.3.1 – Dendritic integration

Single neurons integrate the synaptic inputs received along their dendrite. Several active dendritic mechanisms exist to enhance the integration of inputs above the simple summation of them (supralinear integration). Imaging of synaptic activity in dendritic segments of CA3 PNs showed that synapses that are located close to each other are functionally co-active (Kleindienst and Lohmann, 2014; Takahashi et al., 2016), possibly boosting the local EPSPs generated by spatially and temporally constrained synaptic inputs. This facilitate CA3 PNs firing in response to particular synaptic input patterns. The supralinearity nature of dendritic integration in CA3 PNs is mostly due to activation of NMDARs that modulate local dendritic Ca2+ dynamics (Makara and Magee, 2013). CA3 PNs dendrites also have a relatively high density of voltage gated Na^+ channels, which support the generation of local

dendritic Na^+ spikes and display a marked afterdepolarization (Brown and Randall, 2009) that efficiently propagates into the dendrites and summates with local EPSPs (Mishra et al., 2016). To summarize, active dendritic mechanisms facilitate the interaction of spatially segregated inputs (Hainmueller and Bartos, 2020). The activation of proximal mossy fiber input facilitates the generation of dendritic NMDAR-driven spikes. Thus, active dendritic mechanisms can provide a particularly efficient amplification of coherent synaptic inputs in CA3 PCs.

1.3.2 – CA3 complex spike bursts

Complex spike bursts (CSBs) are the hallmark firing behavior of hippocampal CA3 PNs, as it has been shown *ex vivo* (Balind et al., 2019b) and *in vivo* in anesthetized mice and during navigation and sharp-wave ripples (Ding et al., 2020; Malezieux et al., 2020; Mizuseki et al., 2012; Zucca et al., 2017). CSBs consist of a series of two to six spikes at short interval (<6 ms) with a progressive attenuation of the amplitude of the spikes within the burst. Following an action potential, they generate a slow depolarization on top of which further action potentials are generated. Neurons can generate bursts as a result of intrinsic properties or as a network mechanism (Zeldenrust et al., 2018). Several intrinsic mechanisms to trigger bursts exist, and neurons that generate bursts in isolation are called intrinsic bursters. CA3 PNs are intrinsic bursters, as blocking AMPAR, NMDAR, GABA receptors or adding TTX still allows CA3 PNs to produce regenerative depolarizations (Balind et al., 2019b). CSBs in CA3 PNs are accompanied by large time-locked dendritic Ca^{+2} responses even in distal apical dendrites mediated by voltage-gated calcium channels (VGCCs).

A correlation between topographical distribution of PNs along the proximodistal axis and burst propensity exists in CA3, with PNs close to CA2 having the highest burst propensity, as well as a radial position correlation, with cells in deep layers of distal CA3 having the highest propensity to burst. (Balind et al., 2019b; Ding et al., 2020). Burst firing propensity also correlates with dendritic length in the SLM, possibly due to the strong contribution of perforant path inputs to the generation of spike-bursts in CA2 and CA3 PNs (Helton et al., 2019; Sun et al., 2014). It has also been proposed that bursting propensity belongs to athorny CA3 PNs (Hunt et al., 2018b).

Spike-bursts have been described to have an important role in increasing the efficiency and reliability of information transmission. Thus, they could increase the signal-to-noise ratio of the network information transmission, and therefore appear as a privileged signal for inducing long-term changes during fast learning (Krahe and Gabbiani, 2004). A single burst of activity in Schaffer collaterals induces LTP, when triggering a postsynaptic dendritic spike and activating NMDAR and L-type voltage-gated calcium channels in CA1 pyramidal cells (Pike et al., 1999; Remy and Spruston, 2007; Wittenberg and Wang, 2006). Similarly, a single passage in a maze, inducing few bursting events (Epsztein et al., 2011; O'Keefe and Recce, 1993), leads to new stable place fields (Bittner et al., 2017; Mehta et al., 2000). Altogether, despite the low number of spikes or bursting events, the induction of persistent selective responses can be initiated after a single or few stimulus presentations across the brain and thus serve as neural indicators of acquired memory traces.

1.3.3 – Neuronal excitability

Transient learning-induced increase in neuronal excitability has been reported in the hippocampus (McKay et al., 2009; Moyer et al., 1996; Thompson et al., 1996; Weiss et al., 2006). Intrinsic modulation of neuronal excitability could contribute to induce early changes in neuronal activity (Titley et al., 2017) by alter the responsiveness of neurons to synaptic activation. In this sense, changes in neuronal excitability act as a priming mechanism that will later favor the establishment of synaptic plasticity, even under sparse activity (Faber et al., 2005; Sah and Bekkers, 1996).

Conversely, artificially inducing an increase in excitability may bias the selection of neurons that are involved in a specific memory. This hypothesis of memory allocation was addressed in a series of studies in the hippocampal CA1 and other brain regions. A role for cAMP response element binding protein (CREB) in determining which neurons are recruited in a memory trace has been suggested (Han et al., 2007; Sano et al., 2014; Zhou et al., 2009). CREB is associated with increased excitability, possibly by regulating expression of voltage-dependent ion channels and second messenger systems that modulate those channels. Artificially elevating neuron excitability by CREB upregulation modulate the allocation of memories to specific neurons in the amygdala (Zhou et al., 2009) or in the insular cortex (Sano et al., 2014). Increasing CREB levels in the dorsal hippocampus has been shown to be sufficient to induce robust spatial memory in conditions that do not normally support spatial memory (Sekeres et al., 2010). CREB enhancement selectively in vivo reveals place-cell activity in previously silent neurons (Lee et al., 2012). Alternatively, neuronal excitability can be enhanced by manipulating voltage-dependent potassium channels: neurons with higher excitability are preferentially recruited into the tone conditioning memory trace (Yiu et al, 2014). Furthermore, increasing neuronal excitability with a light-activated opsin, also determines which amygdala neurons are preferentially recruited into encoding a tone fear memory (Rogerson et al, 2016).

In summary, learning naturally induces a temporary increase in excitability. An increase in excitability can equally be triggered artificially, biasing memory allocation to the specific subset of manipulated neurons. Alternatively, two distinct memories could be linked across time because the natural temporary increase in excitability during the first experience would bias the storage of a subsequent memory to many of the same neurons that encoded the first memory. The fundamental idea underlying memory linking is that temporal or content related memories are stored in overlapping populations of neurons, such that the retrieval of one of the memories can activate the recall of the other (Bray, 2016; Cai et al., 2016). In fact, *in vivo* calcium imaging and activity-dependent marker analysis showed a high overlap in ensemble activity in CA1 between two contextual-dependent events spaced by 5 hours but not 7 days. In addition, subsequent pairing of one of the two contexts (encoded shortly after the other context) with a foot-shock enables to transfer the association to the second context, where the foot-shock was never delivered (Cai et al., 2016).

1.3.4 – Spike timing dependent plasticity

Long-term forms of synaptic plasticity (LTP and LTD) were discovered in the 1970s (Bliss and Lømo, 1973) and provided for the first time the experimental analogue of learning-induced changes postulated by Hebb (neurons that fire together wire together).

This pioneer study showed that presynaptic stimulation drives LTP or LTD in a postsynaptic neuron when stimulation is high-frequency or low frequency, respectively (Bliss and Lømo, 1973). Inspired by this work, repeated trains of high-frequency stimulations (generally at 100 Hz) became the standard protocol to induce LTP in dissociated cultures or *ex vivo* to address synaptic plasticity. However, these high firing frequencies are hardly observed in vivo.

The fundamental rule behind high-frequency or low-frequency induced plasticity is the temporal correlation between pre-synaptic spiking and post-synaptic depolarization. This form of synaptic plasticity is named *spike-timing-dependent plasticity* (STDP). In canonical STDP (or Hebbian STDP), temporal distance between presynaptic spiking and postsynaptic depolarization determines the polarity of the potentiation. LTP occurs when presynaptic inputs lead postsynaptic spikes (pre-post pairing), and LTD occurs when presynaptic input followed postsynaptic spikes (post-pre pairing) (Debanne et al., 1994, 1997; Levy and Steward, 1983), within a precise temporal window (10 to 100 ms time scale) (Bi and Poo, 1998; Markram et al., 1997). Canonical STDP is prevalent in excitatory neurons in the cortex and in the hippocampus (Markram et al., 1997; Feldman, 2000; Sjostrom et al., 2001; Nevian and Sakmann, 2006; Bi and Poo, 1998; Nishiyama et al., 2000; Wittenberg and Wang, 2006), but several basic forms of STDP exist at different synapses.

From a mechanistic perspective, temporal proximity of presynaptic release and postsynaptic depolarization triggers calcium influx through postsynaptic NMDARs and voltage-sensitive calcium channels (VSCCs). The magnitude and time course of calcium flux determines LTP versus LTD induction, with brief high calcium generating LTP and sustained moderate calcium-generating LTD. In the case of LTP, AMPAR-mediated EPSPs provide the main local depolarization in the post-synaptic compartment. A generated post-synaptic EPSP also activates voltage gated sodium channels and/or inactivate A-type K^+ channels at the levels of main proximal dendrites, generating a backpropagating action potential (AP) that can activate calcium influx through NMDAR, releasing voltage-dependent Mg2+ block of NMDARs. The more distal dendrites can take advantage of dendritic sodium channels that boosts bAP (Feldman, 2000; Markram et al., 1997; Sjöström et al., 2001).

The primary expression mechanisms are postsynaptic, via addition or removal of postsynaptic AMPA receptors (AMPARs) (Penn et al., 2017) and changes in single-channel conductance (Malinow and Malenka, 2002). Together, these mechanisms result in a reinforced synapse that is more sensitive to glutamate release.

Spike timing-dependent plasticity (STDP) is the primary candidate mechanism for the storage of information in autoassociative networks, such as CA3 A/C. A recent study showed that dendritic backpropagation of AP (bAP) over a short distance is faster than axonal forward propagation over a longer distance (Kim et al., 2012). Thus, excitatory activity on CA3 PNs (for example, during network oscillations or mossy fibre activation) is expected to generate a post–pre sequence, which would favor LTD instead of LTP. CA3 A/C synapses have been demonstrated to result in LTP regardless of the temporal order of the pre-post pairing (Mishra et al., 2016). Given the symmetry and broadness (half width: 150 ms) of synapse potentiation in pre-post and post-pre temporal sequence, STDP at CA3-CA3 synapses has been named symmetric STDP. During a pre–post sequence, bAPs are thought to relieve the Mg^{+2} block of the NMDA receptor. This mechanism may be particularly effective in CA3-CA3 synapses, because of active AP backpropagation caused by the high dendritic Na^+ channel density in these cells (Kim et al., 2012). On the other hand, in a post-pre sequence the marked afterdepolarization (ADP) characteristic of CA3 PNs propagates into dendrites without attenuation, and summates with subsequent EPSPs, producing large dendritic depolarizations that release the

Mg^{+2} block of NMDA receptors and activates voltage-gated Ca^{+2} channels. This mechanism may represent the associative signal for LTP during a post-pre pairing.

1.3.5 – Structural plasticity in CA3

In addition to modifications pre-existing synapses strength, formation of new synapses is an important mechanism of memory formation. In CA3, as a consequence of learning, a large number of filopodia are generated from a substantial fraction of large MF terminals (Ruediger et al., 2011). These filopodia contacts dendrites of fast-spiking PV+ interneurons, which provide feed-forward inhibition (FFI) to CA3 PNs, regulating their depolarization (Zucca et al., 2017). FFI has been described in CA1 and in the neocortex (Pouille et al., 2009) as a mechanism to increase the range of inputs that PNs can respond to. A homogeneous FFI across the post-synaptic population of pyramidal cells ensures that threshold excitatory currents increased with stimulus strength. In contrast, heterogeneities in the distribution of excitatory currents in the post-synaptic population determined the specific set of PNs recruited. This mechanism is probably important for generating a sparse activation of PNs (resembling of sparse neuronal assemblies) upon stimulation to allow sparse storage of information. DG transfer experience information to CA3 through MFs. FFI learning-associated structural rearrangement might be involved in restriction of information transferred to CA3, resulting on the other hand in an increased signal-to-noise ratio in a subset of CA3 whose inputs are unbalanced towards excitation.

1.3.6 – Functional correlates of CA3 activity during memory encoding

Rolls and colleagues suggest that during an encoding phase of memory, the DG-originated MF inputs into CA3 are critical, whereas during a retrieval phase, the direct PP inputs from the entorhinal cortex into CA3 becomes more important than the MF inputs (Rolls et al., 1996; Treves and Rolls, 1992, 1994). A study with selective disruption of MF-CA3 or PP-CA3 revealed that the MF-CA3 network functions mainly during new learning, to create new patterns of ensemble cellular activities in CA3, whereas the PP-CA3 system carries sensory information that serves primarily as a retrieval mechanism for hippocampal memory by partial cues. MF afferents appear to be required for memory acquisition but not for retrieval, whereas PP afferents appear to ini-tiate memory retrieval from the CA3 without the necessity of MF input (Lee and Kesner, 2004).

Many GCs are silent during exploratory behavior (Hainmueller and Bartos, 2018b), but a single GC burst efficiently recruits CA3 PNs, thanks to GCs detonator properties, whilst low-frequency GC firing activates mainly feedforward inhibition. MF activation can induce heterosynaptic plasticity at PP and recurrent inputs onto CA3 pyramidal cells (Kobayashi and Poo, 2004; McMahon and Barrionuevo, 2002; Tsukamoto et al., 2003). Strong MF synapses at proximal pyramidal cell dendrites can elicit large dendritic depolarizations and active dendritic spikes to enable associative encoding of information between the CA3 and its more distal PP and recurrent inputs. In fact, plasticity of recurrent CA3 and PP synapses but not MF synapses requires NMDAR. PP–GC and MF–CA3 synapses are rapidly strengthened, supporting the reactivation of CA3 pyramidal cells during memory recall minutes to hours after the original experience (Kitamura et al., 2017; Ryan et al., 2015), whereas

recurrent synapses between CA3 cells are still weak. Once CA3 ensembles have been permanently established by durable plasticity of PP–CA3 and recurrent synapses, the memory can be reliably recalled without MF input, which is reduced at this stage owing to depotentiation of PP–GC synapses (Kitamura et al., 2017).

1.4 - The engram

1.4.1 – Immediate early genes.

To form memories, the brain stores inputs from the outside world in the form of permanent changes of neurons and connections between them. Therefore, establishment of long-term memory depends on structural and functional modification of synapses. To support these modifications, neurons rapidly respond to synaptic transmission by providing mRNA and protein substrates. In this view, extracellular stimuli can communicate with the nucleus, driving rapid activation of specific genetic transcription events. This communication happens on a timescale of few minutes.

Neurotransmission and neuronal firing results in calcium influx from the extracellular space into the neuron. Calcium can flow through ligand-dependent channels such as N-methyl-D-aspartate (NMDA) and α-amino-3-hydroxy-5-methyl-4-isoxazolepropionic acid (AMPA) glutamate receptor channels as well as through voltage-gated calcium channels, such as the L-type voltage-gated calcium channels (L-VSCCs). Release from intracellular stores can also contribute to calcium concentration increase. Accumulating cytoplasmic calcium activates different signaling cascades, including calcium/calmodulin-dependent kinases (CaMKs), Ras-mitogen-associated protein kinase (MAPK) and the calcineurin-mediated pathways. These signaling cascades finally target constitutively expressed sequence-specific DNA-binding transcription factors (TFs) within the nucleus, such as cyclic adenosine monophosphate (cAMP)-responsive element binding protein (CREB), serum response factor (SRF) and myocyte enhancer factor 2 (MEF2). These TFs rapidly integrate different calcium signals and control the expression of a series of Immediate Early Genes (IEGs) (Bito et al., 1997).

Since these calcium-responding TFs are pre-existing and always available within the cells, IEGs transcription is fast because it does not rely on *de novo* protein synthesis. Once translated, IEGs themselves function as TFs and regulate the transcription of a following wave of late-responding genes (LRGs), who also encodes TFs. Although IEGs are common to several neuronal types, both excitatory and inhibitory, they are differentially regulated in different cell types. LRGs are cell type-specific and tailored to the specific function of the cell within the neural circuits. In this sense, different population (neuronal and not) promptly and more homogenously respond to neural activity and then the following slower response is instead distinct, increasing the variety of neural activity-induced gene regulations. LRGs typically encode effector proteins that coordinate dendritic growth, spine maturation, synapse elimination and development of proper excitation/inhibition balance (Yap and Greenberg, 2018).

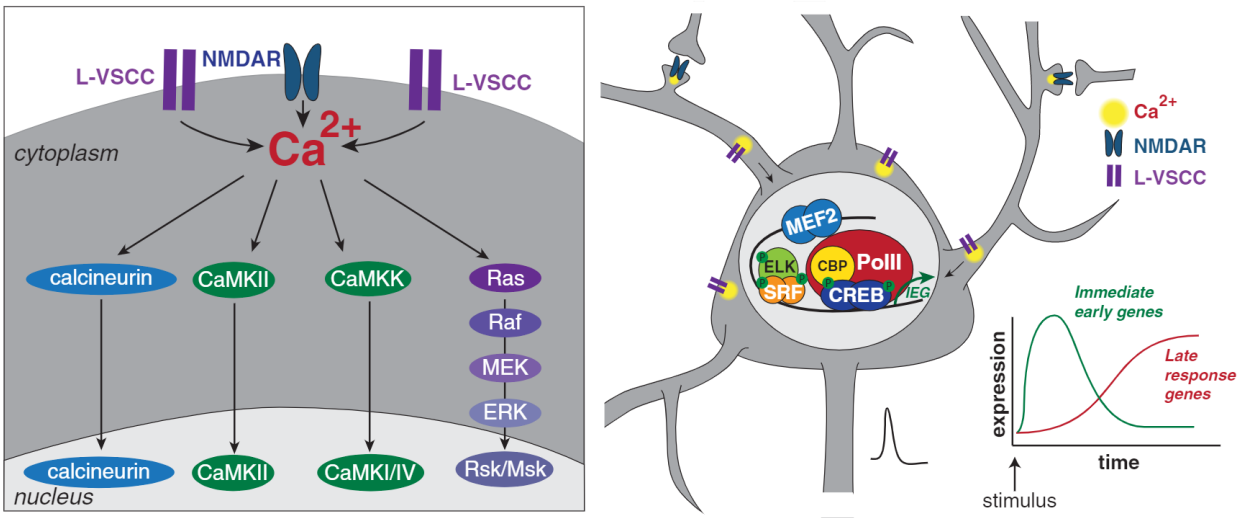

Figure 1.8 | Schematic of Signaling Mechanisms Driving Activity-Dependent Transcription of Immediate Early Genes. *Left. An increase in intracellular Ca^{+2} through NMDAR and L-type voltage-gated calcium channels activate a series of molecules. These molecules belong to cascade pathways that activates pre-existing transcription factors, such as CREB (right) that binds to DNA and regulate the expression of immediate early genes. IEGs are characterized by a rapidly induced and decaying kinetic of activation. IEGs such as c-Fos, Arc regulate other late response genes that will regulate a more neuronal-specific transcription program. Adapted from (Yap and Greenberg, 2018).*

1.4.1a - c-Fos

c-Fos is the most common IEG. Part of the Fos family of proteins (c-Fos, FosB, FosB2 and Fos related antigens Fra-1 and Fra-2). c-Fos transcription depends on calcium influx, but also on various extracellular stimuli. Levels of c-Fos mRNA is detectable in few minutes and peaks 0.5 hours following membrane depolarization (Ramamoorthi et al., 2011). Once in the nucleus, Fos together with its partner Jun for the major heterodimer of the activating protein complex 1 (AP-1).

1.4.1b – Arc

Arc/Arg3.1 (activity-regulated gene, or simply Arc) is a common IEG activated by synaptic activity and growth factors (Link et al., 1992). Arc is a cytoskeleton-associated protein with a high homology with α-spectrin. For this reason, contrarily to the majority of IEG, Arc protein and mRNA can be found also in dendritic processes. Therefore, Arc mRNA can be targeted to specific stimulated synaptic areas, suggesting that it may be translated on site.

Arc transcription is induced extremely rapidly following induced seizures and high-frequency axonal stimulation (that triggers LTP). While Arc mRNA is detectable in around 30 minutes, Arc protein is expressed in 1 hour, reaching maximal induction after 3-4 hours, returning to basal levels by 24 hours after stimulation (Lyford et al., 1995).

Mice lacking Arc gene show loss of long-term memory during a Morris water maze, object recognition and taste aversion test, indicating that Arc is required for the formation of explicit hippocampus-

dependent as well as implicit hippocampus-independent forms of long-term memory (Plath et al., 2006).

1.4.1c – Npas4

Npas4 (Neuronal PAS domain 4) is a TF crucial for activity-dependent regulation of GABAergic synapse development mainly in excitatory neurons. It is rapidly induced by excitatory synaptic activity and turns on a genetic program for inhibitory synapses formation and maintenance, on both perisomatic and dendritic region (different classes of interneurons). Npas4 mRNA is detectable in neurons 5 minutes after training in an episodic-like memory test and return to basal levels in 4.5 hours. Protein levels peaks between 0.5 and 1 hour following training, much earlier than several other IEGs (Ramamoorthi et al., 2011). Npas4 is in fact a key regulator of the activity-dependent expression of c-Fos, Arc and Zif268. Contrarily to c-Fos and Arc, Npas4 expression seems to be unsensitive from several neurotrophic factors, but rather selective for calcium influx (Lin et al., 2008).

In addition, expression of Npas4 in dorsal hippocampus is restricted to CA3 subregion. In fact, selective deletion of Npas4 in CA3 impacts memory formation and retrieval ability, whereas its rescue restores the ability to form long-term contextual memories influx (Lin et al., 2008).

1.4.2 – Relationship between engrams and IEGs

Specific cognitive computations in the brain rely upon orchestrated neuronal activity of a selected population of engram neurons. Activated neurons respond by expressing IEGs to activate a transcription program to sustain neuronal and synaptic modifications. Therefore, IEGs provides a readout of recent activity in single neurons. Many studies exploit learning- and recall-induced expression of IEGs to gain experimental access specifically to neuronal engram for functional investigation.

The view of IEGs as a proxy for recent neural activity is nonetheless simplistic. Although IEGs expression could be triggered by processes different than neuronal activity (growth factors), they in fact reflect a functional transcriptome conversion with the purpose of the establishment of activity-related plasticity. In this sense, IEGs are molecular indicators of those physical/chemical changes that constitute the memory trace (Holtmaat and Caroni, 2016).

IEGs transcription and translation are characterized by specific kinetic of expression. Synaptic inputs and neural activity induce rapid expression of IEGs and, depending on the specific IEG, reach a peak of expression in around 60-90 minutes. This delay likely reflects the time required by the molecular machinery of genetic transcription and translation processes. Elevated levels of IEGs TFs can still be detected several hours after learning.

1.4.3 – IEG-based tool for experimental access to engrams

IEGs are at the base of multiple experimental approaches trying to access specific neuronal engrams. In fact, experience-dependent transcription events represent a promising way to genetically identify neurons responsible for encoding learned experiences *in vivo*. Monitoring of up-regulated expression of IEGs either using immunostaining or in situ hybridization is a standard widely accepted method to map activated circuits at cellular scale.

Pioneering approaches used IEGs combination with a variety of reporter proteins to track activate assembly neurons. Several transgenic mouse lines exist. At first, the promoter of c-Fos was isolated and fused with beta-galactosidase, generating Fos-lacZ transgenic mouse line (Schilling et al., 1991), enabling β-gal staining of activated cells. Subsequently other IEG were coupled to lacZ expression to generate transgenic mouse line. With the improvement of fluorescent reporter protein, additional transgenic mouse lines are introduced. Fos-GFP (Barth et al., 2004).

However, precise identification of active assemblies using fluorescent reporters suffers from 'contamination' from labeling of neurons unrelated to the experience of interest (either activated beforehand or activated by different stimuli). Temporal control of IEG-based reporter expression to the time of the behavior under investigation is therefore crucial. To circumvent this issue, different solutions have been put into action (some are summarized in Table 1).

For instance, using destabilized IEG-controlled fluorescent reporters helps limiting engram labeling in time, preventing unspecific labeling to experiences (or different stimuli) preceding the event of interest. Examples of this approach are Arc-dVenus (Gouty-Colomer et al., 2016) or the artificial E-SARE system (Kawashima et al., 2013).

Different systems rely on inducible control of IEG-based transcription of fluorescent reporters to link in time a specific experience to the engram labeling. An approach used in several studies (Kitamura et al., 2017; Liu et al., 2012; Pignatelli et al., 2019; Roy et al., 2016; Ryan et al., 2015) uses a combination of transgenic mice and viral vectors to achieve a doxycycline (Dox)-dependent control of genetic expression, based on the classical Tet-Off strategy (Gossen et al., 1995). In these studies, c-Fos-based transcription is kept off by Dox administered through the diet but Dox deprivation before a behavioral test is sufficient to disinhibit this genetic control, allowing c-Fos to be activated by the novel experience under study. Another inducible approach, TRAP (targeted recombination in active populations), uses two genetic components. A knock-in mouse line expressing IEG-regulated element (Fos or Arc) that expresses a tamoxifen (TM)-dependent Cre recombinase (CreERT2) is combined with a transgene or virus that expresses an effector protein in a recombination-dependent manner (Guenthner et al., 2013). Using the derivative 4-hydroxytamoxifen (4-OHT) instead of TAM shorten the time needed to achieve effector gene expression. This second element is a R26R-STOP-floxed sequence upstream of a gene of interest. This strategy has been used to label engram cells in a multitude of brain regions following different stimulations, including novel context exploration (Denny et al., 2014; Guenthner et al., 2013). In another knock-in mouse line, c-Fos expression triggers expression of a destabilized exogenous TVA receptor that can later be recognized by EnvA (avian sarcoma and leukosis virus)-coated lentiviruses (LVs) (Sakurai et al., 2016).

IEGs expression can be detected *in vivo* following either acquisition or recall of a memory test. According to the engram theory, the subgroup of neurons activated when an animal is learning is specifically re-engaged when the memory is retrieved, or the task is re-experienced. This is reflected

in the expression of IEGs in the same subset of memory-related neurons during learning and recall. The concept of selective reactivation is at the base of the *overlapping index*, a parameter to investigate to address IEG-based labeling reliability. To calculate it, a memory test consisting of acquisition and retrieval is performed and engrams are labeled with different methods for each phase (Reijmers et al., 2007; Tayler et al., 2013). Artificial transgenic or viral approaches are usually adopted to durably label newly formed engrams in specific brain structures during learning. After a delay, when the animal is re-experiencing the same (or similar) event, neurons can this time be labeled taking advantage of the physiological expression of IEGs, usually through an immunofluorescence method. The selective reactivation is reflected in a high overlap between the durable labeling obtained as a consequence of learning and the label obtained as a consequence of recall.

1.4.3a – TetTag transgenic mouse line

A double transgenic mouse line, called TetTag mouse, was initially developed (Reijmers et al., 2007). This strategy takes advantage of the classical Tet-Off system for inducible activation of genetic expression. These mice express a tetracycline-trans-activator (tTA) under the control of c-Fos promoter. When c-Fos is activated by neuronal activity, tTA is expressed and binds to a tetracycline-responsive elements (TRE) sequence to regulate the expression of tauLacZ (LAC). TetTag mice are raised on food containing Dox, that blocks the activity-dependent expression of tTA through c-Fos promoter. The time window for tagging is opened by switching mice to food without Dox. Neuronal activation will now activate the transcriptional feedback loop and start expression of LAC. The time window can be closed by putting mice back on Dox food. However, neurons activated during the "Dox OFF" time window will continue to express LAC because the feedback loop can maintain its own activation.

A modification to TetTag mice was used in a series of studies, using c-Fos-tTA transgenic mice in combination with a viral vector (generally a AAV (adeno-associated virus) vector) containing TRE-channelrhodopsin 2 (ChR2) -EYFP injected in the brain of region of interest(Kitamura et al., 2017; Liu et al., 2012, 2014a; Pignatelli et al., 2019; Roy et al., 2016; Ryan et al., 2015). In the absence of Dox, training-induced neuronal activity selectively labels active c-Fos-expressing neurons with ChR2–EYFP, which allow not only tagging of neuronal engrams, but also their selective manipulation by light stimulation.

However, the c-Fos-tTA method has high background expressions (Glazewski et al., 2001) and depends on 1–2 days of doxycycline withdrawal, followed by tagging neurons and then reapplication of doxycycline, and thus has a long-time window for labeling c-Fos positive neurons, which include neurons non-specifically activated during the period. Furthermore, several hours (at least 24 hours) are needed to reach reliable expression of the reporter in engram cells.

1.4.3b – ESARE

More recently, a large amount of effort was made to improve endogenous IEG promoters, to create experimentally optimized synthetic activity-dependent promoters. Recently, a novel

engineered synthetic promoter, E-SARE was successfully constructed (Kawashima et al., 2013) based on the SARE enhancer element of the Arc promoter (Kawashima et al., 2009). SARE (Synaptic Activity-Responsive Element) is minimal potent enhancer sequence in the distal promoter of the IEG Arc, which is critical for replicating the amplitude of activity-induced transcriptional response of the full promoter, when placed immediately upstream of the minimal Arc promoter. The SARE element is a short (~100 base pairs) that has cooperative binding sites for three activity-dependent transcription factors, CREB, MEF2, and SRF. To generate an enhanced promoter, a 5-tandem SARE elements repetition was connected to the minimal Arc promoter to yield a much higher downstream reporter expression compared to other IEG promoters (Kawashima et al., 2013).

Contrarily to other activity-dependent labeling systems, E-SARE represent a strategy that allow engram labelling in a rapid manner following an encoding experience, probably because of the lack of a process of inducible regulation of transcription (such as the Tet-OFF system). In this case, the temporal control of gene expression is achieved by fusing the sequence of the fluorescence reporter with a destabilizing domain, as a destabilized GFP (dGFP) protein. This ensures that unspecific neuronal activation occurring before the experience of interest is rapidly degraded. However, the artificial E-SARE construct suffers from high background, possibly due to its greatly enhanced potency of expression, making refined expression of a reporter gene in specific activated neurons difficult.

1.4.3c – RAM system

The Robust Activity Marking (RAM) system is a more recent artificially designed activity-dependent system (Sørensen et al., 2016). This genetic construct is delivered into the brain region of interest through a viral vector. The system is based on a modified version of c-Fos promoter in conjunction with a Tet-OFF control of genetic transcription. This combination brings together the advantages of an artificially induced potency of expression with a time-controlled downstream expression of a gene of interest. A combination of the AP-1 binding site (a consensus sequence for the FOS/JUN family transcription factors) with the binding motif of Npas4 (Ramamoorthi et al., 2011) is inserted into the central midline element (CME), a characterized transcriptional regulatory sequence whose secondary structure is favorable for transcription activation (Wharton et al., 1994) resulting in 'enhancer module'. The RAM promoter (PRAM) is ultimately composed by 4-tandem repeats of this enhancer module inserted upstream of the human Fos minimal promoter. Similarly to the TetTag mouse strategy, the temporal control of gene expression is allowed by a Tet-Off system. PRAM drives the expression of tTA, which activates the TRE promoter in a Dox-dependent manner, driving the effector gene cassette. A destabilized version of tTA, d2tTA, was created, because accumulating tTA outside of the designated experimental window may contributed to the undesirable background expression of effector genes. This system has been efficiently used to identify neuronal engrams in several brain regions (Sørensen et al., 2016), including CA3 (Weng et al., 2018).

The RAM system has a significant higher fold induction compared to E-SARE, mainly because of its lower basal activity in absence of stimulation. However, as the TetTag mouse line, it provides efficient engram labeling only several hours following an activating stimulus. In addition, the artificial PRAM is composed by elements of both c-Fos and Npas4 enhancer sequences. This, although enhancing the

activity-dependent potency of expression, may recapitulate two different patterns of activation (c-Fos-based and Npas4-based).

This has been overcome in another study, where a c-Fos-dependent RAM (FRAM) and Npas4-dependent RAM (N-RAM) reporters were created (Sun et al., 2020). Unlike most activity reporters (and RAM itself), F-RAM and N-RAM are IEG-dependent downstream transcriptional elements rather than IEGs themselves, therefore it is conceivable that the F-RAM and N-RAM ensembles are not identical to those defined by native c-Fos and native Npas4 promoters. Engrams identified by different IEGs represent distinct subpopulations within memory engrams that result from different neuronal activity triggered during learning, that induce a differentiated genetic program in subpopulations of engram cells. Engram neurons identified by F-RAM show an increase in excitatory synaptic inputs as displayed by increased mEPSC frequency, whereas engram neurons identified by N-RAM show increased inhibitory synaptic inputs as displayed by increased mIPSC frequency (Sun et al., 2020). This pointed to the importance of both potentiation of excitatory and inhibitory inputs in mechanisms of memory encoding.

1.4.3d – Cal-Light

Further increasing the spatiotemporal resolution of activity-dependent labeling allows for more precise time control of genetic expression during a behavioral condition under investigation. A quite recent approach, named Cal-Light (Lee et al., 2017a), translates neuronal activity into gene expression in a light-dependent manner. This innovative strategy is actually not IEG-dependent, but rather calcium event-dependent. Therefore, for its activation it does not require the initial events that lead to IEG transcription. The system efficiently translates cytosolic Ca2+ events into gene expression in the nucleus.

Cal-Light consists of two complex synthetic proteins. The first protein a tTA element fused with a transmembrane domain, calmodulin (CaM), the N-terminal of a TEV protease and its corresponding cleavable domain, the tobacco etch virus protease cleavage sequence (TEVseq). This cleavable sequence is hidden by the C terminus of an engineered Jα-helix of Avena sativa phototropin 1 light-oxygen-voltage 2 domains (AsLOV2), making it accessible in a light-dependent manner. The TEV protease was engineered to have calcium-dependent activity. As mentioned, the N-terminal fragment is inserted in the first protein, whereas the C-terminal fragments was fused with M13 calcium sensor, in the second synthetic protein of the system. In this configuration, neuronal activity increases cytosolic Ca2+ levels causing M13 to bind to CaM. The M13–CaM interaction brings TEV-C closer to TEV-N, making them regaining protease activity against the TEVseq, ultimately liberating tTA for nuclear transcription. This chain of molecular interaction events is prevented by the fact that the TEVseq is hidden in a light-dependent manner and therefore not accessible to TEV protease. Light delivery is therefore the limiting event to liberate tTA during intracellular calcium events.

The two protein components of the Cal-Light system can be injected *in vitro* and *in vivo* using two independent viral vectors. A third virus carrying a tetracycline-responding sequence (similar to TRE) controlling the expression of the gene of interest is also necessary. A drawback of this technique is that it requires not only triple virus injection but light canula implantation as well.

Cal-Light-mediated labeling is more affected by the number of light-ON/OFF repetitions and light intensity than by the duration of each light pulse.

A modified version of the Cal-Light system, called DRD2-iTango2 (Lee et al., 2017b), allows for light-dependent neuronal labeling in neurons that are exposed to a specific ligand (such as dopamine).

1.4.3e – CaMPARI

The calcium-modulated photoactivable ratiometric integrator (CaMPARI) is another system to label activated cells independently from IEGs, but rather depending on Ca^{+2} signal and light delivery. CaMPARI is a new type of fluorescent calcium indicator that efficiently undergoes an irreversible green-to-red conversion upon violet light (~400 nm) illumination and binding of calcium (Fosque et al., 2015). At the molecular level, the main component of CaMPARI is a photoconvertible fluorescent protein EosFP. EosFP is a bright fluorescent green protein that irreversibly converts to a red fluorescent protein upon illumination with violet light. EosFP is fused at its end with a Ca^{+2} binding calmodulin (CaM) and its associated M13 peptide. Similarly to conventional calcium indicators (such as GCaMP), presence of calcium ions enables CaM-M13 interaction, inducing EosFP to adopt optimal conformational changes for increasing its fluorescence. This gives rise to a photoconvertible calcium indicator that produces GCaMP-like rises in fluorescent intensity both in the unconverted, green state and in the converted, red state. In other words, this construct allows continuous calcium activity recording, while gradually shifting from green fluorescence to red fluorescence in presence of violet light. The red/green ratio provide information of the degree of calcium activity of a neuron (provided constant violet light illumination). Each fluorescent channel can also, in principle, provide the same information independently. Photoconversion speed is dependent on light intensity. At ideal light intensity range, the intensity of red fluorescence scales with the sum of the calcium levels present at the time of all photoconversion epochs. The resulting covalent fluorophore modification is permanent; thus, the red signal remains for hours to weeks (governed by cellular protein turnover kinetics), providing a post hoc readout of active neurons. Light alone induce negligible photoconversion. This system has been used *ex vivo* in slice preparation (Trojanowski et al., 2020; Zolnik et al., 2017) as well as *in vivo* in larval zebrafish, *Drosophila melanogaster*, and mouse primary cortex (Fosque et al., 2015; Trojanowski et al., 2020).

Because of the large Ca^{+2} influx during action potential, CaMPARI photoconversion is highly sensitive to cell firing, even at low light intensity, markedly increasing the red/green ratio (Zolnik et al., 2017). Post-synaptic potentials induce CaMPARI photoconversion as well, linearly with the number of events, offering a method for functional synaptic connectivity mapping. Subthreshold synaptic potentials typically generate localized dendritic calcium events, which are insufficient to be detected at the soma using transient calcium indicators. Nonetheless, repeatedly combining the violet light illumination with subthreshold stimulation causes a persistent accumulation of photoconverted CaMPARI at the soma (Zolnik et al., 2017). Thus, post hoc measurements based on CaMPARI can reveal a complete functional map of postsynaptic neurons that receive supra- as well as subthreshold inputs. Interestingly CaMPARI can be used for functional mapping synaptic connections, when coupled with optogenetically driven defined inputs. For this experiment, the light-gated channelrhodopsin (ChR2) was expressed in a higher-order cortically projecting thalamic nucleus (POm), and CaMPARI in POm's presumptive recipient layers in somatosensory cortex. Coincident

stimulation of the ChR2-expressing thalamic inputs with CaMPARI photoconversion in the cortical neurons (which could be achieved with the same light) resulted in a 'patchy' labelling in L2/3 with an increased red/green ratio, and a homogeneous labelling of L5, consistent with the anatomical layout of POm-derived synaptic connections (Zolnik et al., 2017).

Background photoconversion in low calcium, slow kinetics and reduced fluorescence after chemical fixation prompted the development of CaMPARI2 (Moeyaert et al., 2018). Using site-directed amino acid mutagenesis was used to increase both green and red calcium-dependent fluorescence as well as improving the photoconversion rate and calcium unbinding kinetic. Reduced background photoconversion is useful for integrating sparse neuronal activity, which requires long illumination periods, whereas faster calcium unbinding kinetics increases the temporal resolution of calcium activity integration, allowing for more precise PC of neurons active during a short epoch of animal behavior. CaMPARI2 has also been used to label neurons based on their *in vivo* activity to then address electrophysiological differences between high- and low-activity neurons, to determine whether neurons with different firing rates *in vivo* retained these properties in acute slices to measure spontaneous firing rates (Trojanowski et al., 2020).

Table 1.2 | Summary of the reported IEG-based engram labeling techniques

Engram labeling strategy	Based on (IEG)	Components	Inducibility	Time to labeling	Labeling time window	Reporter/ effector	Reference
TetTag	• c-Fos	• Transgenic mouse line	• Dox deprivation	>24h	48h	LacZ	(Reijmers et al., 2007)
c-Fos-tTA x TRE-ChR2-EGFP	• c-Fos	• Transgenic mouse line + viral vector	• Dox deprivation	>24h	48h	ChR2-EYFP	(Kitamura et al., 2017; Liu et al., 2012, 2014b; Pignatelli et al., 2019; Ramirez et al., 2013; Redondo et al., 2014; Roy et al., 2017; Ryan et al., 2015)
TRAP	• c-Fos • Arc	• Double transgenic mouse line • Transgenic mouse line + viral vector	• TAM • 4-OHT	>72h	• 24h (with TAM) • <12h (with 4-OHT)	tdTomato	(Guenthner et al., 2013)
E-SARE	• Engineered Arc	• Viral vector	• Destabilized reporter • TAM • 4-OHT	Few hours	• N/A • TAM	• dVenus • RFP	(Kawashima et al., 2013)
RAM system	• Engineered c-Fos	• Viral vector	• Dox deprivation	>24h	48h	EGFP	(Sørensen et al., 2016; Sun et al., 2020; Weng et al., 2018)
CAMPARI2	• IEG-indipendent	• Transgenic animals • viral vector	• Violet light • Ca^{+2} event	24h-72h	During light epochs	Red/green ratio	(Fosque et al., 2015; Moeyaert et al., 2018; Trojanowski et al., 2020)
CalLight	• IEG-indipendent	• Transgenic animals • viral vector	• Blue ight • Ca^{+2} event		During light epochs	EGFP	(Lee et al., 2017a)

1.4.4 – Engram manipulation

Improvements in engram tagging techniques allowed not only for simple engram cells identification, but also for their functional selective manipulations for investigating the specific role of engram cells in memory functions. Modulating memories reveal both how memory naturally works and, when artificially controlled, how memory can work. This has been done by expressing molecular 'switches' (mainly opsins) selectively in engram cells in an IEG-dependent manner, allowing for their specific activation, inhibition or destruction. Engrams formed during a training phase can be perturbed before or during recall to probe the specific role of engrams in memory reactivation.

To study whether neuronal engrams are indispensable for memory function, specific disruption of only those cells activated during encoding is required. This loss-of-function studies show that perturbing engram cell function after an experience impairs subsequent memory retrieval. Josselyin S. and colleagues (Han et al., 2009) performed the first loss-of-function study to probe engram necessity for expression of a memory. At first, an auditory memory was allocated onto a selected population of amygdala neurons during auditory fear conditioning, taking advantage of CREB-based biasing of recruitment in an engram. Injecting HSV viral vector carrying a CREB-Cre construct into transgenic mice that express conditional Cre-dependent diphteria toxin receptor (DTR) allowed for selective tagging of engram cells (through biased allocation) and insertion of a 'switch' to trigger restricted cellular death (through diphteria toxin). A weak auditory conditioning was performed, and recall was assessed after cell death induction by systemic injection of DT. According to the specific re-engagement hypothesis of memory engrams during recall, ablating CREB overexpressing neurons (bearing the memory trace) disrupted freezing to subsequent tone presentation, as if the memory was erased, highlighting the necessity of engram cells to successfully express a memory (Han et al., 2009). Subsequent studies using diverse methods to permanently or reversibly inactivate allocated or tagged engram neurons across several brain areas, in many memory tasks, produced comparable results (Denny et al., 2014; Hsiang et al., 2014; Koya et al., 2009; Lacagnina et al., 2019; Tanaka et al., 2014).

After proving necessity, engrams have been tested for their sufficiency to trigger the expression of a memory. Several works by Tonegawa S. and colleagues probed sufficiency of artificial reactivation of engram cells in absence of natural cues that normally would trigger memory recall. DG c-Fos+ engram cells were functionally labeled with ChR2, using c-Fos-tTA transgenic mice. In few words, GCs involved in a contextual fear conditioning memory trace were tagged to express a switch that allow for specific blue light-mediated reactivation. When tested in a non-training context, mice did not freeze. However, epochs of photostimulation of tagged engram cells in non-training context was sufficient to induce corresponding epochs of freezing, the learning-specific conditioned response, even though mice had never been shocked in this non-training context (Liu et al., 2012). This was the first demonstration that directly activating a subset of cells involved in the formation of a memory is sufficient to mimic patterns of neuronal activation in a dormant engram that recapitulate that memory, inducing the corresponding behavioral expression.

The artificial memory reactivation experiment is based on natural formation of associations between a specific context and an aversive stimulus. A following experiment tested whether it was possible to artificially create this association (Ramirez et al., 2013). Using again c-Fos-tTA transgenic mice, DG engram cells were functionally labeled after mice explored a novel environment. After closing the time window useful for assembly tagging, mice were then placed in a second context, where they were

shocked while optically activating engram cells bearing information about the first context. During this phase, an artificial association between a recalled memory and a novel conditioning stimulus was created. During a memory test, mice replaced in first context froze, even though they had never been shocked in this context. That is, mice retrieved an artificial memory. Mice also froze in the second context (showing natural memory retrieval), but not in a third distinct context. Importantly, memory expression was produced by both "natural" and "artificial" reactivation, meaning the cellular engram retained its identities, but a novel association was added on top of it to form a new but false episodic memory. Similar results were obtained in other studies (Ohkawa et al., 2015) where the conditioning and the unconditioning stimulus were tagged separately and artificially associated, resulting in freezing behavior during optical stimulation in home cage.

The artificial association between a specific context and an aversive or appetitive stimulus can also be bidirectionally reversed to express the opposite valence (Redondo et al., 2014). In this work, c-Fos-tTA mice were injected with a TRE-ChR2-mCherry in the DG as well as in the basolateral amygdala. Mice were initially trained in a context (conditioning stimulus) outside of the time window useful for engram tagging. Then, during the opened window, mice were trained in either an aversive (CFC) or appetitive (female mouse interaction) to tag cells bearing the valence of the memory (unconditioning stimulus). In a third phase, with the time window closed again, mice were placed in the initial context while blue light was delivered to the DG and amygdala and showed either avoidance or appetitive behavior. At this step, the association between the context and the artificially recalled valence of the memory are associated. Then, a during a reversing phase, mice were trained with the unconditioned stimulus of opposite value while blue light was delivered. On the last test day, blue light activation of DG engram cells, but not amygdala, was able to induce the expression of the opposite valence. Depending on the training, DG and amygdala reactivation can drive aversive or appetitive memory expression. However, artificially reactivating labelled neurons in the DG, but not in the BLA, during a subsequent opposite conditioning is sufficient to reverse the dominant valence associated with the memory (Redondo et al., 2014).

Further advancements in the field of engram manipulation allowed to implant an entirely artificial memory. Studies described above achieve artificial memories through the association of a 'learning event' that take place intracranially (optogenetic stimulation) and the presentation of a 'real' external sensory retrieval cue (tone, lights, context). That is, they are composed of an artificial part coupled with a natural part to create a whole new false memory. The behavioral expression of these memories is achieved upon presentation and is restricted to the 'trained' cue. Frankland and colleagues created an artificial association of an odor and an aversive stimulus without the need to expose mice to either natural stimuli (Vetere et al., 2019). This was possible thanks to the selective activation of M72-expressing glomerular olfactory sensory neurons by acetophetone (for the odor part of the memory), and thanks to projections from the lateral habenula (LHb) to the medial ventral tegmental nucleus (VTA) that mediates aversion or alternatively laterodorsal tegmental nucleus (LTD) inputs to the lateral VTA that mediates rewarding signals (Lammel et al., 2012). M72-ChR2 transgenic mice where injected with AAV-ChR2 into the LHb. Paired light stimulation of olfactory bulbs and LHb terminals in the VTA during training leads to selective acetophetone odor avoidance during an odor preference test. In contrast, to mimic opposite valence odor preference, paired light stimulation of olfactory bulbs and LTD terminals in the VTA during training leads to selective odor preference for acetophetone during an odor preference test. That is, the mice either approached or avoided this odor depending on the valence (positive or negative, respectively) of the associated US pathway. This study indicates

that it is possible to entirely bypass experience and, via direct stimulation of the brain, implant a specific memory in mice.

Methodological approaches

Principal techniques used to collect data consist in a combination of viral injection, single-trial behavior and *ex vivo* electrophysiology. Different activity-dependent labeling systems were delivered to CA3 using viral vectors. Injected mice were then subjected to behavioral tasks, mainly contextual fear conditioning (CFC) for acquisition of episodic-like memories that lead to the formation of a neuronal engram in CA3. Brains were then sliced and identified neurons were then targeted for patch-clamp whole cell recordings.

Here principles of the main methodological approaches are reported. For more detailed methods, see the result section 4.3.

2.1 – Single-trial behavior for episodic-like memory

The most striking characteristic of episodic memory is that unique and brief events can be remembered for the whole life of an organism. This type of fast learning is defined by the brevity and rarity of the learning experience, where memory traces are rapidly formed without requiring repetitions of the learning experience (Piette et al., 2020). Fast learning is a crucial component in daily life memory acquisition. Episodic memory are associative memories of context and other elements, and it can be tested in animal models.

In this framework, memory tests can be divided in one-trial learning (for example fear conditioning) and incremental learning tasks (for instance Morris water maze). Both types consist in a learning phase, during which a specific association is learned, and a test phase, during which the learned association is measured. In the case of one-trial tests, associations are learned in a single shot, whereas incremental learning consists of repetitive exposure to the association to reinforce the memory. Single-shot behavioral tests best parallel every-day episodes that can give rise in humans to the formation of an episodic memory.

Before a one-trial behavioral task, mice are isolated from littermates in single cages and are handled by the experimenter for 3 consecutive days. This is an attempt to try to reduce the possibility that uncontrolled episodic-like memories generate memory engrams unrelated to the behavior under investigation. In addition, handling progressively make the animal more comfortable and reduce stressful responses (that are also induced by isolation). Stress may considerably interfere with the animal's natural exploratory behavior, a fundamental component of the formation of a contextual representation (McHugh et al., 2007).

2.1.1 – Contextual fear conditioning

Contextual fear conditioning (CFC) is an aversive hippocampal-dependent memory test, during which an association between a specific context and a foot-shock is learned. It is a widely used

task for testing spatial memories. CFC differs from cued fear conditioning (tone fear conditioning), because the latter is less dependent on the hippocampus since the sound rather than the context predicts the aversive stimulus.

During a learning phase, mice are placed in a conditioning chamber (the conditioning stimulus, CS), where they are allowed to explore the context for a certain period of time. During exploration, the mouse samples the surrounding environment (proximal and distal cues), and all the features (visual, tactile, smells) of the context are encoded and associated in the hippocampus. Then, a series of mild foot-shock (or a single foot-shock) is delivered (the unconditioning stimulus, US), so that the association between the spatial features and the aversive stimulus is created. Memory strength can be tested by placing the mouse in the same chamber in a subsequent retrieval phase. The retrieval phase can take place at different intervals, depending on the need to test short-term memory or long-term memory. If the aversive memory was formed and retained, the mouse displays a stereotypical behavior called freezing, which reflects fear and it is characterized by immobility, muscles rigidity, increased heart rate and breathing frequency. During freezing the mouse usually stays close to walls or corners. The specificity of a CFC memory can also be tested. After being conditioned, mice can be placed in a completely different context, where freezing should not be observed, because no association between the novel environment and the foot-shocks was created. This approach could also be used to investigate generalization, namely the ability of a mouse to discriminate between similar contexts.

2.1.2 – Other single-trial behavioral tasks

2.1.2a – Social transmission of food preference

Rodents have the ability to learn and remember information about potential food sources that are edible by sampling those sources on the breath of conspecifics. This socially transmitted food preference is critical to their survival, as it minimizes the risk of ingesting toxic nutriments. This behavior is at the base of the social transmission of food preference (STFP) test. This test has successfully been used in rats, but it is also has been assessed in mice (Bessières et al., 2017).

Although STFP is more complex than CFC in terms of preparation, as other one-trial learning tests it consists of a single acquisition of an association and a retrieval test phase. At first, a pair of unfamiliar equally preferred scented foods must be identified to avoid biased natural preference of one flavor over the other. During preparation, a 'demonstrator' mouse is first fed one of the two flavored food. The demonstrator mouse is then placed with a naive 'observer' mouse (the test mouse) for few minutes. The two mice can socially interact with each other and collect odor information from their respective breaths. During this interaction, the observer mouse associates the odor present in the demonstrator's breath with the fact that it is harmless, and therefore safe to eat. This stage constitutes the encoding of this novel information.

When presented with a choice between the food consumed by the demonstrator and the other flavored food (that is equally preferred in untrained mice), the observer mouse exhibits enhanced preference for whichever food the demonstrator has eaten, highlighting that it remembers the

association made during social interaction. The memory of this association can be tested at short or long delays, and it was reported to be stable and long-lasting.

STFP is a non-aversive test and underlies a highly ethological innate rodent behavior. It involves creations of associations that do not necessarily have a spatial component. However, as an appetitive task, it requires a diet restriction to elicit adequate motivation for food seeking, that might result in anxiety states.

2.1.2b – Object place recognition

Object place recognition (OPR) is a non-aversive spatial dependent task for assessing episodic-like memories. In this test, the spatial position between objects in relation to cues in a specific context is learned, and therefore this test is strongly dependent on the hippocampus. Mice are placed in a spatial cue-enriched arena, where 2 novel identical objects are placed in specific positions. During the encoding phase, mice sample and explore the two object and learn their specific position within the environment. During the test phase, mice are placed again in the same arena, but this time one novel object is displaced. The learned association is measured by the amount of time mice spend exploring the displaced object over the total amount of time spent exploring both object (ratio). Since the objects are identical between them and between encoding and retrieval, there is no novelty component that could bias sampling and exploration.

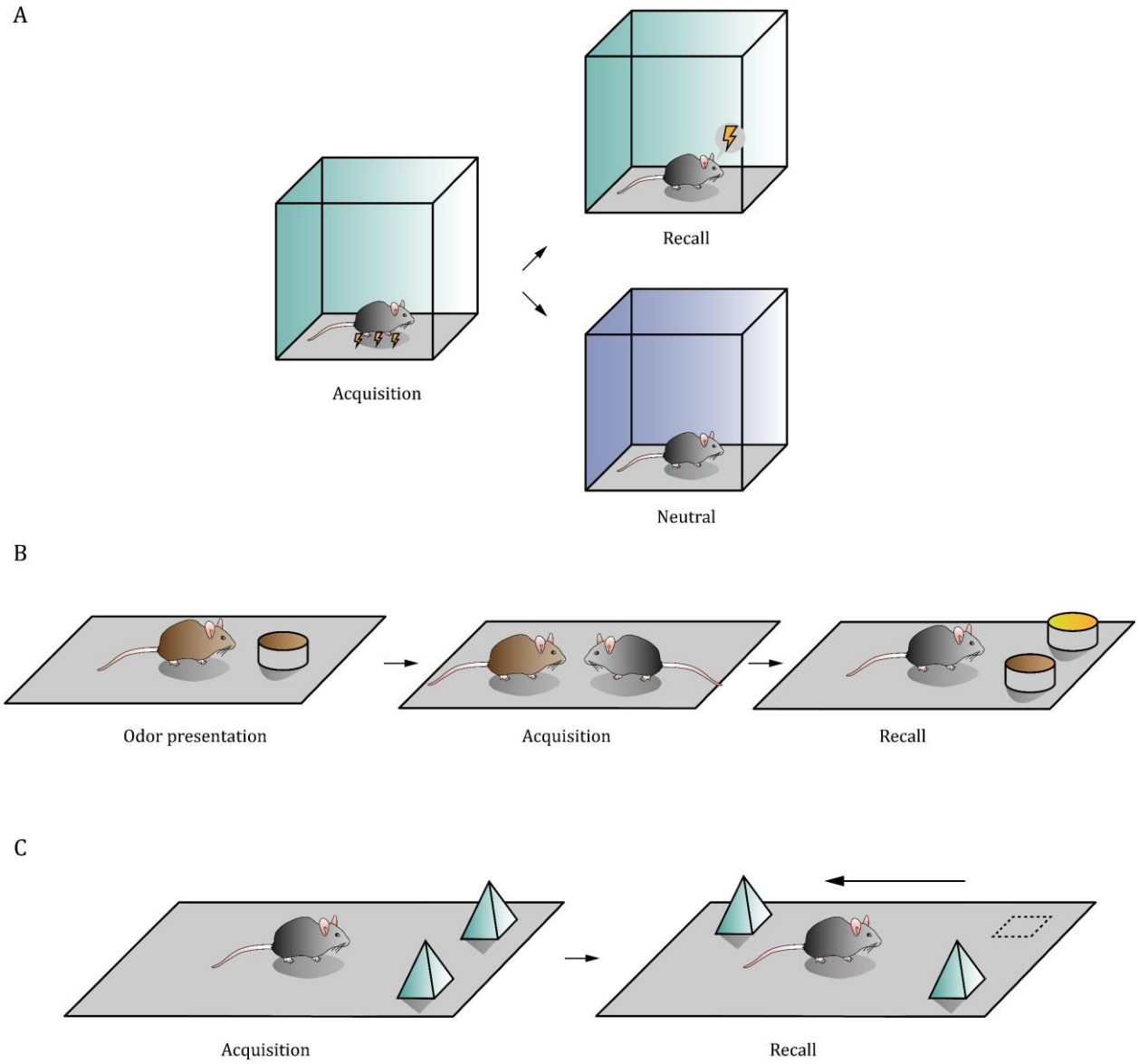

Figure 2.1 | Illustration of one-trial memory tests. *They consist of a training phase, during which an association is acquired and a recall phase to test the generated memory.* **A.** *Contextual fear conditioning (CFC) consists of training in a novel context paired with the delivery of a series of foot-shocks. When the animal is placed in the same conditioning context, freezing behavior is observed, while no freezing is detected in a non-related unfamiliar context.* **B.** *In social transmission of food preference, a food-restricted demonstrator animal eat flavored powder chow. During the subsequent training phase, the demonstrator animal interacts with the test animal, who sample the odor from the breath of the conspecific. Memory is tested when the test mouse is provided a choice between two equally appetible flavored food. If memory is recalled, the demonstrated flavor will be preferred because considered safe to eat.* **C.** *In object place recognition, the spatial organization of two identical objects in a novel arena relative to surrounding cues is acquired. One of the objects is then displaced, and the time the test mouse spends interacting with the displaced object over the familiarly placed object is a measure of memory recall.*

2.2 – Viral vectors

IEGs genetic constructs are delivered using an adeno-associated virus (AAV) vector. AAVs are the most frequently used vectors, since they are safe for use in all tested species, including humans and non-human primates. AAV vectors have three important components: the capsid for cell entry, the promoter that drives transgene expression, and the gene of interest to be expressed in the transduced cells. The size of the capsid limits the dimension (expressed in base pairs, bp) of genetic tools that can be fit into AAVs. The concentration of viral particles in a given volume is defined titer.

Normally, cell-type targeting by AAVs could be achieved using specific promoters. In this case, even though AAVs infect multiple cell populations, the promoter of interest is active only in the desired cell population. Nevertheless, in this study, the use of IEG promoters does not allow for specific cell population discrimination, as IEGs are active in different cell types (mainly excitatory neurons). The infected cell population is rather determined by the targeted brain area and by the viral particles diffusion to adjacent regions. In this study, a diffused neuronal infection to different brain structures does not cause an issue, as long as the neuronal type is visually identified and confirmed during successive investigations.

Neurons infected with an IEG-reporter construct are not identifiable as long as the infected neurons is not involved in any neural computation that trigger IEG activation. As a consequence, single neurons not expressing IEG-reporter could be mistaken for not infected neurons. For this reason, in this study, IEG-based constructs were always co-injected with an infection marker, a second virus (of the same type of the first one) containing a constitutive promoter-driven reporter. Being the same virus type, the two vectors infect in large part the same populations of cells in the brain structure they were targeted to.

AAV injections is performed using a stereotaxic frame to hold the position of the mouse head, mounted with a 3-axis manipulator to guide the virus-containing syringe. In order to precisely orient the injection site to dorsal CA3, a set of coordinates has been created in reference to the bregma, the skull suture between the parietal bones and frontal bone. The head of the mouse is secured between two ear bars and positioned orthogonally to the 3-axis manipulator, to avoid imprecise injection targeting due to head tilt. Head tilt in the 3 different rotation axis: pitch (transverse axis), roll (longitudinal axis) and yaw (vertical axis). Each of these rotations was carefully monitored and head repositioned if excessive.

2.2.1 – Stereotaxic injection

The titer of the viruses was adjusted so that almost all CA3 neurons at the injection site were infected. The injection volume and flow rate (300 nl at 60 nl/min) were controlled with an injection micro-pump (World Precision Instruments). Injection coordinates, using bregma as a reference point, were as follows: AP -1.78, ML ± 2.40, DV -2.35. This site targets dorsal CA3b, but virus infection spread to CA3a, CA3b, CA3c, CA2 and in some cases few granule neurons and hilar cells of the DG.

2.3 – Patch-clamp electrophysiology

Electrophysiological recordings can be performed in different ways. The most direct way to measure the activity generated by several neurons are extracellular field recordings. The extracellular signals are very small, arising from the flow of ionic current through extracellular fluid. It can be performed *in vivo* (tetrodes, silicon probes) or *ex vivo*, using fine electrodes that records the activity of the surrounding neurons. Extracellular recordings can also be performed in very close proximity to single neurons, thus measuring the activity of such neurons rather than field potential. This kind of recordings are called juxtacellular recordings. On the other hand, intracellular recordings are the only way to study intracellular activity (sub- or suprathreshold activity), allowing to measure voltage or currents across the cell membrane. These kinds of recordings are made possible thanks to the development of very fine glass micro-electrodes with a very fine tip, called sharp electrodes, able to penetrates the cell membrane without damaging the neuron. Perforated patch clamp prevents irreversible 'washout' of diffusible intracellular constituents into the relatively larger volume of the pipette through dialysis, preserving the physiological properties and functions of ion channels. However, a small tip introduces a remarkable resistance in the recordings. To overcome this issue, the evolution of glass electrodes made a different type of contact between the electrode and the cell membrane possible, to make patch clamp recordings (**Fig. 2.2**).

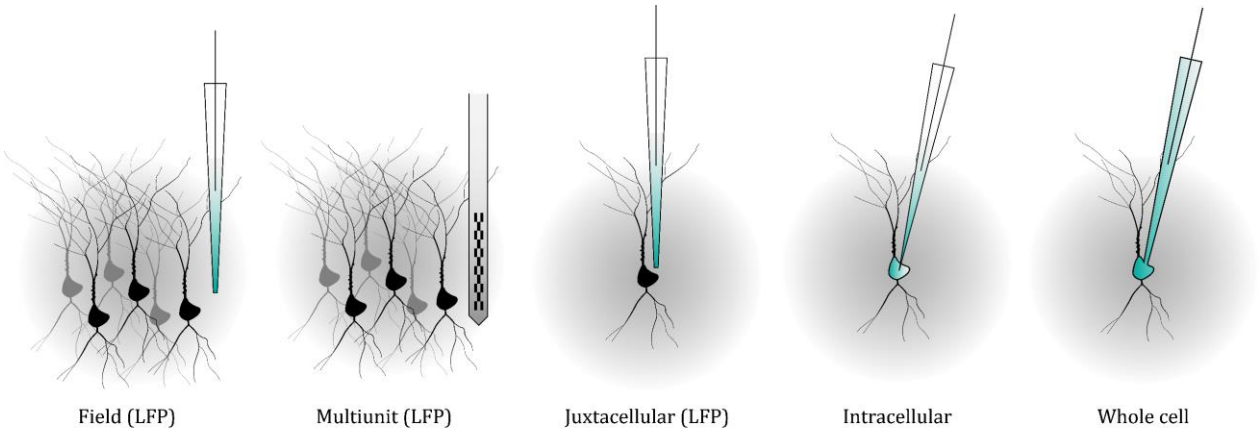

Figure 2.2 | Different types of electrophysiological recordings. *Local field potential (LFP) can be measured using a glass pipette or a multiunit probe (in the example a silicone probe with several recording electrodes). Extracellular recordings of single neurons can be performed when a pipette is in close proximity with a neuron. Intracellular recordings give information about intracellular activity and can be performed using sharp electrodes for perforating the cell membrane or patch clamp whole cell configuration.*

2.3.1 – Principles of electrophysiology

Excitable cells, including neurons, act electrically. A cell delimited by a double lipid membrane separates different electrically conductive ionic solution on the inside and outside. For this configuration, a cell can be seen as an insulator. An electrical potential difference exists between the

interior and exterior of cells, and the ions gains or loses energy as they move between places of different electrical potential. Electrical potential differences are usually denoted as V or ΔV and measured in volts. The typical potential difference ("transmembrane potential") amounts to 30 to 90 mV in most animal cells. The charges stored by the membrane (Q, measured in Coulombs) are proportional to the potential or voltage, giving the equation Q = CV, where the constant of proportionality is the capacitance C measured in Faraday (F).

However, the membrane of neurons cannot be considered as pure capacitors, because they contain numerous proteins and transmembrane ion conducting channels, introducing a conductance in parallel with the capacitance of the cell. The movement of ions through channels according to the potential difference across the membrane generates currents (I, measured in Ampere), varying the membrane potential. Usually, currents measured by electrophysiological equipment range from picoamperes to microamperes. Parallel conductances (as the ones through several ion channels along the plasma membrane) simply sum up. Conductance is always reciprocated with resistances (R, measured in Ω), that defines opposition to the flow of electrical charges. The relationship between potential, conductance and resistance is defined by Ohm's law: V = R(Ω)x I(A).

2.3.2 – Principles of patch clamp

Patch clamp is an electrophysiological technique to measure intracellular activity that can be performed *in vitro* (in cultured neurons), *ex vivo* (in acute slices or organotypic slices) or *in vivo* (in awake or anesthetized animals). Many variations to the patch clamp technique exist, but the most common one is the whole-cell configuration (**Fig. 2.3**).

Electrophysiological equipment enables researchers to measure potential (voltage, V) differences or alternatively current (I) across the membrane. When measuring potential, the patch clamp recording is in the current-clamp (CC) mode. In a current-clamp experiment, a known constant or time-varying current is applied and the corresponding change in membrane potential caused by the applied current is measured. Alternatively, currents can be measured during a patch clamp recording in the voltage clamp (VC) configuration. In a voltage clamp experiment, the membrane voltage is controlled, and transmembrane current required to maintain that voltage are measured. Usually, the investigator has no interest in the membrane current, but is interested in the membrane conductance, since conductance is directly proportional to the ion-channel activity, generated for instance by a synaptic input.

Patch clamp is made possible thanks to small glass capillaries with a fine tip opening. Glass pipettes are filled with an intracellular-like medium in which a recording electrode is submerged. A corresponding ground electrode (usually Ag/AgCl that mediates a redox reaction) is submerged in an extracellular medium (**Fig. 2.4**). While the patch pipette acts simply as a fluid bridge between a cell and the corresponding Ag/AgCl electrode, its properties and forming materials determine the outcome of the recordings. The correct pipette profile and tip opening is determined during pulling and fire polishing.

The potential difference (in CC) or the current flowing (in VC) from one electrode to the other is measured. In the baths, potential differences are negligible or, in VC, current freely flows between the electrodes. However, during a patch clamp experiment, the recording electrode is positioned inside a

cell, thus the recorded potential across the membrane is measured and it represents the potential difference between the inside and the outside of the cell. In VC instead, all currents flow through the pipette into the cell, then out through the cell membrane into the bath grounding electrode. These currents therefore represent conductances across the cell membrane.

Series resistance, equal to the sum of pipette resistance and cell access resistance (**Fig. 2.4**), prevent the pipette from maintaining and precisely control of the cell voltage. These resistances limit the amount of current that can be used to charge the membrane, which means that the actual voltage inside the membrane is different and higher than the theoretically imposed voltage. Access resistance generally is up to 100 MΩ *in vivo* or less than 20 MΩ *in vitro*.

Another limitation of *in vitro* and *in vivo* voltage-imposed recordings is the difficulty of holding an imposed voltage across the whole neurons, due to the complex geometry of neurons (distant dendritic portions). The injected holding current used to maintain potential spreads radially from the patch but decays across distance, therefore not being uniform. Therefore, inhibitory and excitatory synaptic inputs are distorted in relation to their distance on the dendritic tree from the soma (Armstrong and Gilly, 1992; Spruston et al., 1993; Williams and Mitchell, 2008). The ability to control imposed voltage, named space clamp, can be partially improved by increasing the cell impedance, by blocking K^+ conductance or using Cs-based intracellular solution (that reduces potassium currents).

2.3.2a – Practical underpinnings of patch clamp

When the recording pipette is inserted into the bath, a short pulse of voltage potential (test pulse) generates a corresponding square response (**Fig. 2.4**). The amplitude of this square current is inversely proportional to the dimension of the pipette opening. This value usually represents the pipette resistance calculated through Ohm's law, and it is useful to determine whether the tip opening is appropriate to the cell of interest (smaller cells require smaller tips). An initial positive pressure is applied to the pipette to prevent the pipette tip from clogging up. The pipette is then brought in contact with a cell, until the membrane is delicately deformed. Contact with the membrane partially occludes the pipette tip, with a resultant small decrease in square current amplitude. At this point the positive pressure is released, negative pressure is applied so that the membrane attaches to the opening of the pipette. This initial non-invasive configuration is called cell-attached (**Fig. 2.3-2.4**). In cell attached, the tight seal between the pipette and the membrane creates a great resistance, called a giga-seal, because current can't flow between electrodes. In cell attached, the square test current decreases, while leaving transients due to pipette capacitance (Cp), that could cause voltage response slower. Cp is electronically eliminated or corrected. In cell-attached, the intracellular environment of the cell is not controlled, and the membrane potential can't be determined. Nonetheless, cell-attached configuration allows to isolate currents from a single ion channel without perturbing cytoplasm composition and membrane structure.

Cell-excised configurations of membrane can be achieved by withdrawing the pipette from the rest of the cell. After a gigaseal is formed, quick micropipette withdrawing pulls off a patch of membrane from the cell, leaving the membrane patch attached to the micropipette. This configuration, inside-out mode (**Fig. 2.3**), leaves the intracellular surface of the membrane exposed to the external media. This is useful when pharmacological manipulation of the intracellular side of the ion channels is desired. On the other hand, withdrawing the pipette from whole-cell configuration establishes the

'outside-out' configuration (**Fig. 2.3**) which generally results in a resealing of the cell membrane in a convex bulb so that the outside of the membrane faces the bath solution. Outside-out patching gives the opportunity to examine the properties of an ion channel when it is isolated from the cell and exposed to different solutions on the extracellular membrane surface.

The most used technique is the whole-cell configuration. Whole-cell is obtained by rupturing the patch of membrane created during cell-attached with a pulse of suction or voltage, thus establishing low-resistance electrical and physical continuity between the cell and the pipette lumen. In VC, access to the cell interior enable the control the voltage of the whole cell, allowing to measure the ensemble currents from all the ion channels in the cell membrane to be observed. The amount of current required to simply maintain the desired voltage is the holding current. If the contact between the membrane and the pipette is tight, ideally the holding current approaches 0. A great holding current is due to a leak from the cell and may indicate a loose membrane-pipette contact or a damaged cell. In CC, the whole-cell configuration permits to constantly measure the membrane potential, allowing to study potential variation or APs discharge.

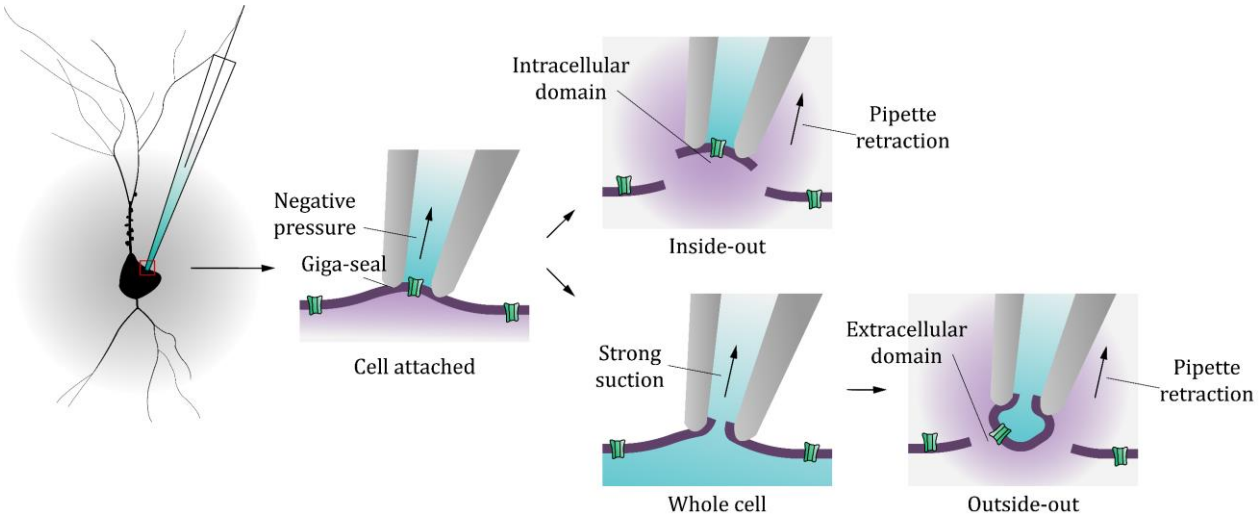

Figure 2.3 | Illustration of the different variations to patch clamp. *When the pipette tip is in contact with the membrane and negative pressure is applied, a giga-seal is obtained, and the cell-attached configuration is achieved. From this configuration, pipette withdrawn detaches a small patch of the membrane from the cell, exposing the intracellular side of the membrane receptors. Alternatively, form cell attached, a strong suction breaks the plasma membrane that remains attached to the pipette tip, bringing the cytosol in continuity with the pipette-filling intracellular solution. Pipette withdrawn from this configuration ruptures a portion of the membrane around the pipette opening, that will tend to close back forming a little bulb that exposes the extracellular side of the membrane receptors to the extracellular environment.*

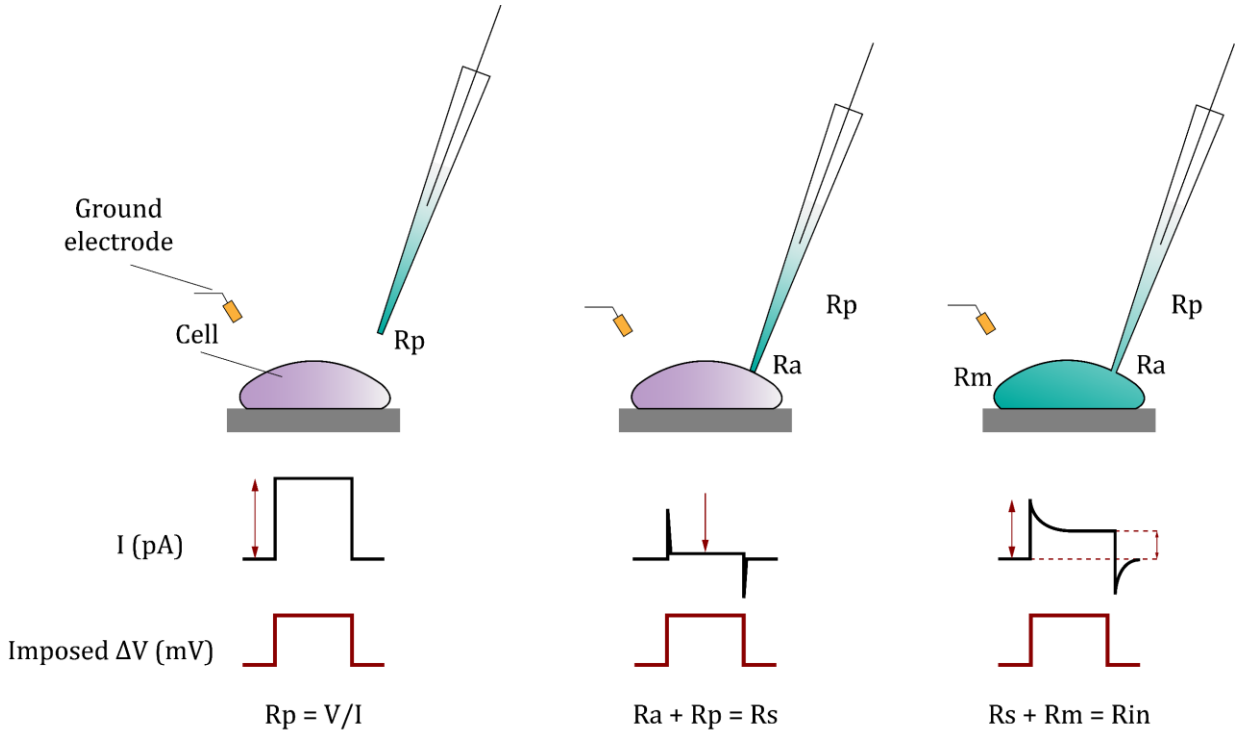

Figure 2.1 | Illustration of the steps that lead to whole cell configuration. *A step of voltage applied in the bath give rise to a square current response. The amplitude of this response is indicative of the pipette resistance that reflects its tip shape and opening. When a giga-seal is created, the tight contact between the pipette and the cell membrane does not allow passage of current, leaving however pipette capacitance transients that needs to be artificially corrected. Whole-cell is obtained by rupturing the patch of membrane through a strong suction. This establishes a low-resistance electrical and physical continuity between the cell and the pipette lumen.*

2.4 – Data analysis and statistics

All the analysis has been performed with custom-written Python scripts and ImageJ scripts (for image analysis) available upon request.

2.4.1 – Image analysis

To determine the activation dynamic of c-Fos-ZsGreen1-DR *in vitro*, the fraction of ZsGreen+ cells among the total number of mCherry+ was calculated. Neurons were fixed using paraformaldehyde (PFA) at different intervals after pharmacological activation. Coverslips were washed in phosphate buffer solution (PBS) and directly mounted on slides and coverslip applied using a DAPI mounting medium and acquired using a confocal microscope. Analysis was carried out through a custom-written ImageJ. Activated neurons were counted based on an intensity threshold detection. The percentage of activated cells is also calculated in histological section to determine the relationship between acquisition of new memories and the development of an engram. Mice injected

with an activity dependent construct were subjected to a specific behavioral test, and then sacrificed at different time points. Mice were perfused with 4% PFA. Brains were post-fixed in PFA over-night at 4°C and conserved in a sucrose 30% solution until they sank. Then, brains were sliced in 25 µm-thick coronal sections using a cryostat. Slices were washed in phosphate buffer solution (PBS) and directly mounted on slides and coverslip applied using a DAPI mounting medium and acquired using a confocal microscope.

Image analysis was performed using self-written ImageJ scripts. At first, total number of DAPI+ cells in CA3 was quantified. A mask of DAPI+ cells was created using a pixel intensity-based threshold, and the detected elements were counted based on their size and circularity (empirically determined). The final DAPI mask was then used to score the constitutively expressed infection marker (mCherry) expression in DAPI+ neurons using a threshold. The fraction of DAPI+ cells that were also mCherry+ gives a measure of how many CA3 PNs were infected. Mice showing less than 60% of infected pyramidal cells in CA3 were discarded from the analysis. Subsequently, activated neurons were counted again using a pixel-intensity threshold, and the percentage of activated cells over the total amount of mCherry+ cells was calculated.

The position of activated cells in CA3 along the proximo-distal axis and the superficial-deep axis was also addressed. To do so, CA3 area was isolated and straighten in a rectangle while maintaining the cellular relative position. The two-dimensional centroid position of each activated cell was calculated in a relative scale from 0 to 1 on both axes.

2.4.2 – Electrophysiology analysis

2.4.2a - Analysis of membrane potential

In the current clamp configuration, membrane potential (Vm) variations in function of injection of current steps was calculated. Series of hyper- and depolarizing current steps were applied and the relative change in Vm (ΔV) was measured at the steady state. The slope of the resulting I-V curve correspond to the input resistance of the cell (Rin). Action potentials were detected when the trace derivative (dV/dt) was greater than 5 mV/ms.

2.4.2b – Analysis of synaptic activity

Access resistance is derived from Ohm's law based on the amplitude of the test pulse in response to a step of imposed voltage. Ra is carefully monitored over every single experiment, and cells whose Ra changes more than 20% (or bigger than 25 ΩM) were discarded. Holding current was carefully monitored to determine the stability of the patch, and cells were discarded if it changes more than 20% or lower than -200 pA. Spontaneous synaptic events were detected using a deconvolution-based approach (Pernía-Andrade et al., 2012). At first, events are detected with any method. Then, a template of a synaptic event was determined for each cell, by randomly averaging 20% of the total number of events. The template is deconvoluted from the trace, and peaks in the resulting trace were

considered if surpassing 4 times the standard deviation of the deconvoluted trace. The time points of peaks correspond to the time of synaptic inputs events.

2.4.3 – Statistical analysis

First, the normality of data set was tested using the D'Agostino-Pearson omnibus normality test. If data was normally distributed, a Student's t-test or two-way ANOVA (Analysis of Variance) was performed; otherwise, nonparametric tests such as Mann–Whitney test (for unpaired data) and Wilcoxon test (for paired data) was used. Results are presented as mean, first and third quartile by boxplots. Statistical differences were considered significant at $P<0.05$ (*: $p \leq 0.05$, **: $p \leq 0.01$; ***: $p \leq 0.001$).

Objectives

3.1 – Background

Episodic memories are distinctive from other forms of declarative memories as they can be remembered over a lifetime of an organism despite happening only once. Indeed, what distinguishes this kind of fast learning are the features of the encoding stage (or learning experience). Fast learning refers to situations where memory traces are rapidly formed without requiring repetitions of the learning experience. In the hippocampus, pattern of activity of selected neuronal engrams are present during a novel experience. These cells are simultaneously active during learning, and subsequently preferentially strengthened their structural and functional connectivity relative to quiescent cells. Durable changes of engram neurons and their circuits allow these activity pattern to be recollected in future circumstances. Computational models propose that fast encoding of episodic memory take place in CA3 circuits, because its unique architecture and organization allow storing of associative remembrances. The recurrent connection network between CA3 principal neurons form an attractor network that favor this process.

Neuronal activation can be inferred from the histological visualization of IEG expression, such as that of c-Fos or Arc, in the brains of animals after they have performed a behavioral task. Several methods based on IEGs allow to isolate cells active during defined periods of learning and recollection to observe their behavior. Many advances in modulating memories in mice have been made to test engrams necessity and sufficiency to provide behavioral expressions of memories. Studies of engram manipulation permit not only to visualize memories at the cellular level, but a specific memory can be allocated, erased or reactivated, artificially created.

3.2 – Objectives

Recent data and technical development suggest that the functional consequences of spatial and non-spatial (multimodal) information processing and fast encoding in CA3 should be observable at the single cell and local circuit level. In this framework, our goal is to understand the cellular and circuit changes necessary for fast information encoding, that are crucial to lay the groundwork for subsequent memory recall.

Cells participating in CA3 engrams of one-trial episodic-like memories can be tracked for further analysis of underlying morpho-functional changes. However, to our knowledge, limited work has been done to investigate the specific changes that neuronal engrams undergo in a very short timescale following learning. The main obstacle in investigating neuronal engrams shortly after learning is the limitation of existing activity dependent markers in providing fast, reliable and specific activity-dependent labelling. Our lab developed an AAV vector carrying a c-Fos-based activity dependent construct to rapidly label recently activated neurons.

Using this construct, we can investigate how exploration of a novel environment generates an early engram. In addition to our developed construct, a second activity-dependent system is used, that differs in terms of labeling timescale. These two constructs provide respectively a few hours and 24 hours delayed tagging of neurons involved in a specific memory. Depending on the system used, brain slices are prepared for histochemistry and cell counting, as well as for electrophysiological experiments.

Whole cell patch clamp in acute slices allow to study neuron intrinsic properties as well as specific synaptic properties. This work attempts to provide a functional characterization of how engram cells behave following a learning experiences occur and how the passage of time influences the physical properties of engram cells. In this work we address these issues by evaluating changes in excitability and synaptic integration following multimodal information encoding, by comparing the labelled engram CA3 PNs and non-labelled CA3 PNs.

Results

4.1 – Preface to the results

In this work, we investigated the properties of early engram cells in CA3, involved in rapid memory encoding, and how these properties evolve within a time scale up to 24 hours. To do this, we introduce a novel viral construct driven by c-Fos to achieve fast labeling of engram neurons (FLEN) based on a destabilized version of the green fluorescent reporter ZsGreen1. Given the novelty of this approach, a large effort has been spent on studying activation dynamics following a stimulation *in vitro* and *in vivo* to validate the FLEN properties of the construct. To our knowledge, the only other activity-dependent construct reported to allow rapid labeling of engram cells is E-SARE (Kawashima et al., 2013). Conceptually, our activity-dependent construct resembles E-SARE design, as it is characterized by a destabilized fluorescent reporter under the control of an IEG. However, E-SARE is an engineered artificial promoter (based on Arc) that provide enhanced gene expression and thus bright labeling in response to neuronal activation. In our hands, this characteristic gives rise to a high background expression in CA3 compared to our c-Fos-ZsGreen1-DR construct, making specific targeting of engram cells difficult. Furthermore, and probably because of this limitation, E-SARE has not been extensively used to investigate early changes in brain regions involved in a specific computation in selected neuronal population.

We sought to probe neuronal properties of early engram cells by mean of patch clamp recordings. Using this strategy in acute slices proved to be challenging. Slice quality is crucial for *ex vivo* electrophysiology, to favor neuronal survival and preserve cell membrane integrity. Neuronal engrams are sparse by nature (>6% of CA3 neurons in our hands), and by consequence, the number of identified engram cells in 300 μm -thick sections is limited. The process of slice cutting and recovery is therefore fundamental in targeting the few available cells. Although many properties have been addressed, more work on this is currently in progress.

To address whether neuronal engram undergo protracted changes to sustain memory encoding after 24 hours, we used a second activity-dependent system, the robust activity marking (RAM) system (Sørensen et al., 2016) that provides a strong durable engram labeling reported to peak 24 hours following a novel experience. Similarly to FLEN-based strategy, a thorough comparison between early engram cells and cells that undergo initial phases of consolidation.

4.2 – Results

To study how a novel episodic-like experience rapidly shapes the formation of a CA3 engram and the corresponding neuronal and circuit changes, we sought to provide an IEG-based activity dependent construct producing a fast labeling of engram neurons (FLEN). c-Fos-ZsGreen1-DR is composed by the full-length c-Fos promoter, which recapitulate the natural activity-dependent

induction and regulation of expression of its downstream genes. c-Fos controls the expression of ZsGreen1, a bright whole cell fluorescent reporter. This green fluorescent protein is fused with a destabilizing domain (DR) that targets it for degradation, causing ZsGreen1 labeling to be unstable and thus transitory. Together, these characteristics enable c-Fos-ZsGreen1-DR to specifically and rapidly label activated cells, with a high signal-to-noise ratio, and a low degree of labeling of cells activated outside the time window of interest.

We then determined the precise expression kinetic of c-Fos-ZsGreen1-DR *in vitro* and *in vivo*. We first injected the viral construct in mouse cortical neurons and calculated the fraction of activated cells over time after a 30-minute step of pharmacologically induced neuronal activation followed by tetrodotoxin-mediated inactivation. This experiment confirmed the rapid and transient nature of c-Fos-ZsGreen1-DR expression. Then, we investigated FLEN *in vivo* in the hippocampus following one-time acquisition of contextual fear conditioning. Mice were foot-shocked during a novel context exploration and then returned to their home cage. Mice were perfused at different time intervals within a 12h period to assess engram labeling development and weakening compared to untrained mice. Untrained mice show a small percentage of basally activated cells, similar to the number of activated cells 1.5 hours post-CFC (the conventional time of c-Fos peak expression). However, the number of activated cells rapidly increases 3 hours post-CFC and rapidly decrease back to basal-like levels within 6 hours. This experiment confirmed that our construct selectively and rapidly labels CA3 engrams, and its expression decays in few hours. We then assessed FLEN labeling under different experimental conditions. We tested mice in a non-aversive novel context exploration (that we called context only CO) and in an immediate shock (IS) version of CFC (were exploration of the novel context is minimal due to early shock delivery). This experiment showed that CO also induce the generation of an engram, although to a smaller extent compared to CFC. On the other hand, the IS group showed very variable results, with mice displaying a large range of FLEN labeled cells.

After establishing FLEN dynamic *in vivo* (time to peak and decay), we tested the viral construct in acute slices for electrophysiological investigation of FLEN+ cells shortly after a learning task. Mice were fear conditioned and then returned to their home cage for 3 hours, to yield FLEN peak expression. Acute slice preparation does not seem to impair the expression of ZsGreen1-DR in CA3 activated cells, that remain detectable for few hours (the duration of an average patch clamp recording session) until slice quality starts to degrade. FLEN+ neurons were identified and targeted for patch clamp recordings and were compared to neighbor non-activated neurons.

First, we investigated the engram cells (E) intrinsic properties. Input resistance, action potential threshold, rheobase and firing pattern were not different between E and non-engram cells (NE). These results show that shortly after encoding, FLEN+ CA3 neurons do not display hyperexcitability or higher firing mode. Then we investigated synaptic properties of FLEN neurons, by measuring spontaneous and miniature excitatory post-synaptic currents (sEPSCs and mEPSCs). Both spontaneous and excitatory events were similar in amplitude between E and NE, but they were slightly more frequent. We also investigated miniature inhibitory post-synaptic currents, and also found them to be slightly increased. MF-CA3 synapse plays a major role in assisting CA3 in the encoding of memory (Kesner and Rolls, 2015), so we investigated also evoked MF synaptic currents. We placed a stimulating electrode in the hilus and measured basal synaptic transmission in CA3. Low frequency stimulation generates small excitatory currents in CA3, with no difference between E and NE. Stimulation to higher frequencies leads to short-term presynaptic frequency facilitation to a similar degree in E and NE cells. These results suggest that shortly after a novel experience, LTP at MF-CA3 synapses does not contribute to early encoding. We also measure MF-mediated di-synaptic

feed-forward inhibition (FFI), which could have a critical role in shaping CA3 firing and thus their involvement in an activated neuronal ensemble.

We then used the c-Fos-based robust activity marking (RAM) system to ask whether engram neurons undergo protracted changes from a few hours (3-6 hours) to >24 hours by comparing the electrophysiological properties of FLEN-label and RAM-labeled CA3 PNs. At first, we validated the robustness of the system in our conditions. Doxycycline-fed mice were injected with the RAM viral vector together with the AAV-CB7-mCherry infection marker. 48 hours after Dox deprivation, mice were fear conditioned and sacrificed 24 hours later. In accordance with previous results (Sørensen et al., 2016), few RAM+ cells were found in absence of an experience, whereas a larger fraction of RAM+ cells was induced following CFC.

We investigated intrinsic property of RAM-engram cells in CA3 and found that in RAM+ neurons showed prolonged spike firing in response to a depolarizing pulse of current, hence decreased accommodation in comparison with NE neurons. Our data strongly suggest that engram neurons in CA3 progressively acquire increased excitability as compared to neurons which were not activated by the one-trial contextual memory task. In addition, we observed a comparable increase in the frequency of sEPSCs in RAM+ CA3 neurons 24 hours after CFC, as previously reported (Weng et al., 2018), without any change in the amplitude.

4.3 – Article

"A novel viral tool for exploring the early properties of CA3 engram cells"

In preparation

Dario Cupollilo[1,2], Noëlle Grosjean[1,2], Catherine Marneffe[1,2], Célia Reynaud[1,2], Séverine Deforges[1,2] and Christophe Mulle[1,2,3]

[1] Interdisciplinary Institute for Neuroscience, CNRS UMR 5297

[2] University of Bordeaux, F-33000 Bordeaux, France

[3] Lead contact; correspondence: christophe.mulle@u-bordeaux.fr

A novel viral tool for exploring the early properties of CA3 engram cells

Dario Cupollilo[1,2], Noëlle Grosjean[1,2], Catherine Marneffe[1,2], Célia Reynaud[1,2], Séverine Deforges[1,2] and Christophe Mulle[1,2,3]

[1]Interdisciplinary Institute for Neuroscience, CNRS UMR 5297

[2]University of Bordeaux, F-33000 Bordeaux, France

[3]Lead contact; correspondence: christophe.mulle@u-bordeaux.fr

ABSTRACT

Forming new memories after a one-time experience requires initial encoding then consolidation over time. During learning, multimodal information converges onto the hippocampus, activating sparse neuronal assemblies. Activated neurons are believed to form a memory representation through concerted activity and synaptic interconnectivity. Computational and behavioral studies point at the hippocampal CA3 region as a key structure involved in multimodal information integration and initial memory storage. In this work, we describe the development and validation of a novel tool for fast-labeling of engram neurons (FLEN). FLEN is based on c-Fos activity-dependent transient expression of a destabilized fluorescent marker ZsGreen1 rapidly after one-trial learning (few hours). With FLEN, we explore the electrophysiological properties of c-Fos activated CA3 neurons following one-trial learning of an episodic-like memory. In parallel, we employ the Robust Activity Marker (RAM) system, which provides activity-dependent labelling 24 hours following a novel experience. Comparing FLEN+ and RAM+ neurons allows to characterize how the properties of neuronal assemblies evolve after an initial phase of consolidation. We found that CA3 cellular recruitment in an engram is not predetermined by their excitability state, but rather they progressively acquire increased excitability as compared to neurons which were not activated by the one-trial contextual memory task. Early CA3 neuronal engram showed an increased number of excitatory inputs which overall did not appear to be more efficient, suggesting that LTP-like synaptic plasticity does not occurs early during the process of memory formation. Control of local inhibition of spiking influence CA3 PNs capacity to be engaged in an active ensemble of neurons. A comparison of FLEN+ and FLEN– CA3 neurons finally suggests less Mf-driven feedforward inhibition in the putative engram neurons which may facilitate spike transfer from the DG hence increased excitation. Overall, the FLEN strategy appears as an

excellent complement to the previously used labeling strategies which have assessed changes in engram neuron properties in the time rage of days. With this approach, we can show that both the intrinsic excitability and the synaptic properties of CA3 pyramidal neurons undergo progressive plastic changes over the first day following a one-trial memory task.

INTRODUCTION

Animals survival depends on the ability to rapidly form new and durable memories after one-time meaningful events. Collections of personal past experiences, called episodic memories, modulate behavior when recalled, adapting it for future relevant circumstances (Tulving, 1972, 2002). The episodic memory process relies on the hippocampus and consists in fast encoding of novel experiences followed by consolidation. During encoding, pattern of activity of selected neuronal groups, called engram neurons, represent the initial memory traces. These neural ensembles are co-active during a behavioral task, undergo long-lasting synaptic modifications during consolidation and are specifically re-engaged when the memory is retrieved. Manipulation of neuronal engrams in the hippocampus allows for selective memory erasure (Han et al., 2009), artificial memory recall (Liu et al., 2012) and creation of a synthetic memory (Vetere et al., 2019), indicating their necessity and sufficiency for memory functions. Computational models of memory highlight a crucial role of hippocampal CA3 region in episodic memory encoding and retrieval (Kesner and Rolls, 2015; Rolls, 2007). The activity of CA3 pyramidal neurons (PNs) is driven by excitatory inputs from the entorhinal cortex (EC) and inputs from the dentate gyrus (DG) through the hippocampal mossy fibers which display detonator-like properties (Henze et al., 2000; Nicoll and Schmitz, 2005). Multimodal information converging on CA3 during memory encoding is allocated on a sparse subset of engram PNs. CA3 distinctive recurrent excitatory collateral network, characterized by NMDAR-dependent modifiable synaptic strength, forms an auto-associative circuit well adapted for the rapid storage and retrieval of associative memories (Guzman et al., 2016; McNaughton and Morris, 1987). Indeed, mice with CA3-specific impairment of synaptic plasticity (CA3 NR1-KO mice) are unable to encode the novel location of a hidden platform in a delayed matching-to-place version of the Morris water maze (Nakazawa et al., 2003) and to retrieve the learned position of a submerged platform when partial cues are presented (Nakazawa et al., 2002).

Experimental access to neuronal engrams commonly relies on genetically encoded activity reporters controlled by immediate-early genes (IEGs), such as *c-Fos*, *Arc* (activity-regulated cytoskeleton-associated protein), *Zif268* (zinc finger protein 225) or *Npas4* (neuronal PAS domain protein 4). These activity-dependent transcription factors regulate plasticity-related transcription programs in engram cells (Yap and Greenberg, 2018). In fact, genetic perturbation of IEGs leads to deficits in neuronal plasticity and memory (Weng et al., 2018). Different IEGs possess specific expression kinetics; transcription is delayed from the learning of the event and remain detectable for several hours before decaying back to basal levels, producing a broad expression time frame. Therefore, IEG-controlled activity reporters suffer from high background due to labeling of neurons unrelated to the experience under investigation. Temporal control

of IEG-based systems is crucial to accurately link engram labeling to specific events during a desired time window. To date, common engram labeling techniques address this issue using inducible transgenic systems. However, induction of genetic expression in conventional systems requires a relatively long time window. For instance, in several studies using transgenic mouse lines, engram labeling depends on deprivation of doxycycline (Dox) from the animal diet approximately 48 hours before the new experience (Kitamura et al., 2017; Liu et al., 2012; Pignatelli et al., 2019; Roy et al., 2017; Ryan et al., 2015). During this period, uncontrolled events happening before the behavior of interest may contaminate the specificity of labeled engram cells. In addition, most of these approaches cause labeling to be relatively late, allowing investigation of learning-induced modifications more than 24 hours after a novel experience (e.g RAM system, (Sørensen et al., 2016)) or shortly after recall for neurons which have been labeled several days before (Pignatelli et al., 2019), when consolidation processes have already been engaged. To our knowledge, only E-SARE, based on a synthetic promoter, appears to provide fast labeling of engram neurons shortly after an experience (Kawashima et al., 2013). These engineered promoters are designed to achieve powerful reporter regulation, but their enhanced cellular labeling capabilities may result in a poor signal-to-noise ratio due to high background fluorescence, that makes identification of engram cells unprecise.

Little has been learned about how neuronal engrams in the hippocampus rapidly adapt their physiological properties to support rapid storage and how they evolve with time. In this sense, it is unknown whether initial memory storage is enabled by engram cell modifications of intrinsic properties, morphological changes, synaptic plasticity or a combination of them. Here, we tackle these questions using a virally delivered c-Fos-based genetic construct that provides physiological-like fast expression and fast-decay of the bright fluorescent marker ZsGreen1. This novel viral strategy allows to identify and target neuronal engram rapidly (up to 3-4 hours) following a novel experience, extending current neuron tagging strategies in the investigation of early processes of memory formation. In addition, in order to understand how initial engram cell properties evolve within a 24-hour time scale, we employ the more durable c-Fos-based artificial RAM system (Sørensen et al., 2016) to label neurons and characterize their properties 24 hours after the exposure to a one-trial memory task.

RESULTS

Creation and validation of c-Fos-ZsGreen1-DR for fast-labeling of engram neurons (FLEN).

We constructed an adeno-associated virus (AAV) vector containing a full-length c-Fos promoter driving the expression of a destabilized version of the green fluorescent protein ZsGreen1 sequence (Fig. 1A). The

complete sequence of the c-Fos promoter ensures a physiological-like kinetic of activity-dependent gene expression, whilst expression of the ZsGreen1 fluorescent protein provides a bright whole-cell labelling of activated neurons. In order to restrict the labelling time window, and so to reduce experience-independent labeling, ZsGreen1 was fused with a destabilizing domain (DR) that targets it for degradation.

To determine the expression kinetics of c-Fos-ZsGreen1-DR in response to stimulation, P0 mouse cortical neurons were cultured (cellular density approximately 300 000 cells/well) and then co-infected at DIV3 with activity-dependent AAV2.9-c-Fos/ZsGreen1-DR and a secondary AAV2.9-CB7/mCherry, which constitutively expresses mCherry in infected neurons. Neurons were cultured until DIV14 in regular neurobasal medium, before switching to a medium containing 4-aminopyridine (4-AP, 100 µM) and bicuculline (Bic, 10 µM) for 30 minutes. The drugs were then washed out, and tetrodotoxin (TTX, 0.5 µM) was added to block further neuronal activity until cells were fixed (Fig. 1B). The percentage of activated neurons (ZsGreen1+/mCherry+) among the total number of infected neurons (mCherry+) was calculated at different time points within a 6-hour period after pharmacological stimulation in order to determine the time course of ZsGreen1DR neuronal expression (Fig. 1C). We observed that only a minimal number of activated neurons could be found in unstimulated conditions. The activating medium triggered ZsGreen1-DR expression in neurons as early as 2 hours, reaching a peak in 3 hours (Fig. 1D).

In vivo FLEN optimization

We next investigated the time course of expression of ZsGreen1-DR *in vivo* in response to exposure of the mice to a salient novel experience. We virally targeted dorsal CA3 in young adult mice (2-3 months of age), bilaterally co-injecting AAV2.9-c-Fos-ZsGreen1-DR and the infection control AAV2.9-CB7/mCherry (Fig. 2A, 2B). Mice then were subjected to contextual fear conditioning (CFC) as a hippocampal-dependent one-trial behavioral paradigm (Fig. 2A, 2B). We found that one-time CFC training generates a strong context-dependent fear memory, as mice responded by freezing when re-exposed to the conditioning environment 1 hour (untrained: 14.68% ± 2.28%, 1h post-CFC: 47.38% ± 7.86%, unpaired t-test, p=0. 0018) and 24 hours after training, but not in an unfamiliar novel environment (untrained: 18.66% ± 3.48%, 24h post-CFC: 61.54% ± 7.52%, neutral: 14.34% ± 4.47%, one-way ANOVA, Tukey's post-hoc test, T1:T2 p =0 .00004, T1:T3 p=0 .84116, T2:T3 p=0 .00001) (Fig. S1).

The percentage of mCherry+ PNs that were ZsGreen1-DR+ was quantified 1.5, 3, 4.5, 6 and 12 hours following CFC training and compared to that of untrained mice that never left their home cage (HC) (Fig. 2D). As previously reported (Sørensen et al., 2016; Weng et al., 2018) in the absence of any exposure to a

novel experience, less than 1% of infected CA3 neurons are activated using a c-Fos-based labeling strategy (Fig. 2C). Here we find that in the HC condition, the percentage of FLEN+ neurons was very variable.

One-trial CFC conditioning generated an engram, as indicated by an increase in FLEN+ neurons in all hippocampal subregions, including CA3 (data for other regions not shown). The CA3 region displayed less than 1.6% of FLEN+ neurons shortly (1.5 hours) after CFC. This number sharply increased 3 hours post-CFC (3.7%), remained high over 4.5- and 6-hours post-CFC, and decayed back to basal-like levels 12 hours post-CFC. This time course faithfully mimics the expression of native c-Fos (Holtmaat and Caroni, 2016). Because of the reported functional heterogeneity of CA3 PNs in relation to memory encoding and recall (Nakamura et al., 2013; Nakazawa et al., 2016; Sun et al., 2017b), we went further in analyzing the distribution of the FLEN+ CA3 PNs following one-trial CFC along the proximo-distal gradient of CA3. We found a clear asymmetry in the localization of FLEN+ neurons 3 hours following CFC along the proximo-distal axis. FLEN+ neurons appear to be preferentially located in CA3a and CA3b along the proximo-distal axis, whilst they are evenly distributed along the superficial-deep axis (Fig. 2S). We thus established that c-Fos-ZsGreen1DR peaks at 3 hours following an experience and remains detectable for a few hours. The decay in ZsGreen1DR levels observed 12 hours after CFC likely reflects the combined result of reduced c-Fos promoter activity and ZsGreen1-DR clearance.

We then sought to probe CA3 engram formation under different behavioral situations by quantifying FLEN+ CA3 PNs 3 hours later. We tested mice in context-only (CO) conditions, allowing them to explore a novel cue-enriched arena without a shock at the end of exploration. In line with published studies showing that the hippocampus forms contextual representations independent of shock delivery (Fanselow, 2000; Rudy and O'Reilly, 1999), we found a significant increase in the number of FLEN+ CA3 PNs 3h following CO mice, which was only slightly smaller than the number of FLEN+ neurons 3 hours following CFC. We then tested mice in an immediate-shock (IS) version of CFC, where a 6-second foot-shock was delivered only after 2-second exploration of a novel context. Contrarily to previous reports in other hippocampal sub-region (like DG) (Sørensen et al., 2016) and in CA3 (looking at IEG mRNA levels (Ramamoorthi et al., 2011)), IS also seems to induce ZsGreen1-DR expression in CA3 PNs, even though spatial exploration was minimal. We thus tested whether a foot-shock-free version of IS (that we called short exploration SE) also drives ZsGreen1-DR expression in CA3 PNs (experiment ongoing). Interestingly, the proximo-distal distribution of FLEN+ CA3 neurons in CO conditions mirrored the CFC conditions, whilst this distribution appears to be more homogenous in the HC conditions.

Overall, these data indicate that the FLEN labeling strategy faithfully labels neurons activated during the one-trial exposure to a novel context and allows to characterize the morphofunctional properties of CA3 engram neurons shortly (<6 hours) following the experience.

Intrinsic properties of FLEN+ neurons

To study the functional properties of engram cell rapidly after encoding of a novel memory, we performed whole cell patch clamp recordings in CA3 PNs in acute hippocampal slices of young adult mice subjected to CFC, comparing engram neurons (E) (FLEN+ neurons) and neighboring non-engram neurons (NE) (FLEN- neurons). AAV2.9-c-Fos/ZsGreen1-DR and AAV2.9-CB7/mCherry were co-injected bilaterally in dorsal CA3. After CFC, mice were returned to their home cage for 3 hours, to yield peak expression of ZsGreen1-DR and then sacrificed to collect sagittal slices (Fig. 3A). Activity-dependent FLEN+ neurons remained detectable in slices, allowing specific targeting of engram PNs neurons for approximately 4 to 5 hours after slicing (Fig. 3B).

We first investigated the intrinsic physiological properties of FLEN+/mCherry+ and FLEN-/mCherry+ PNs. Indeed, the probability for a neuron to be recruited in a memory engram is thought to depend on its excitability level at the moment of information acquisition during learning (Cai et al., 2016; Sano et al., 2014; Zhou et al., 2009). We assessed input resistance (Ri) by injecting a series of hyper- and depolarizing current pulses with the membrane potential held at -70 mV (Fig. 3C). Although slightly higher in E neurons, Ri did not change significantly between E and NE neurons. Further depolarizing steps of current were injected until an action potential was fired. Action potential threshold and the amount of current required to trigger it (rheobase) were not statistically different (Fig. 3D). Computational and experimental evidence reports that spike-bursts are important for the rapid formation of memory engrams (Kaifosh and Losonczy, 2016; Treves and Rolls, 1992). CA3 PNs have been reported to have a burst-like firing pattern thanks to the generation of dendritic Ca^{2+} spikes (Balind et al., 2019b; Ding et al., 2020). To study the action potential firing pattern, we injected 1 s-long pulses of current just above rheobase. As expected, more than half of the total number of action potentials occurred within the first 100 ms for all CA3 PNs, with no differences observed between E and NE cells (Fig. 3E).

Altogether, these results show that early after encoding, FLEN+ CA3 neurons do not show differences in excitability or patterns of bursting activity, as compared to control neurons, suggesting that intrinsic hyperexcitability or higher firing mode is not a prerequisite for CA3 PN neuron to be part of an engram following exposure to a novel context.

Synaptic properties of FLEN+ neurons

Neurons recruited in an engram express c-Fos in response to strong neuronal activation induced by behavior-guided excitatory inputs. We investigated the specific degree of excitatory drive in FLEN+ CA3 PNs by recording spontaneous Excitatory Post-Synaptic Currents (sEPSCs), while blocking GABAA-dependent inhibitory currents (Bicuculline, 10 µM). The amplitude of sEPSCs was on average similar between E and NE neurons, whereas their frequency appeared to be slightly increased (Fig. 4A). Then, we measured the miniature EPSC (mEPSCs) in presence of TTX (0.5 µM) to prevent action potential generation. Although not statistically significant, we observed a tendency of higher frequency of mEPSCs in FLEN+ neurons as compared to control neurons (NE: 0.698 ± 0.074 Hz; E: 0.983 ± 0.197 Hz), whereas the amplitude was similar between E (23.226 ± 5.10 pA) and NE neurons (18.189 ± 1.668 pA) (Fig. 4B). Thus, neurons recruited in an engram appear to retain in slices an increased excitatory drive onto them for a few hours, which may be linked to a higher number of synaptic contacts. The existence of mEPSCs with larger amplitudes may be related to synaptic plasticity in a subset of synapses, or theoretically to an increased participation of Mf-driven mEPSCs.

Inhibitory neurons are important in controlling spike generation of principal CA3 neurons, shaping network activity and participation in neuronal assembly formation (Pouille et al., 2009). We therefore probed spontaneous inhibitory post-synaptic currents (mIPSCs), comparing E vs. NE neurons, in the presence of NBQX (20 µM), D-AP5 (50 µM) and TTX (0.5 µM) (Fig 4). We found that mIPSCs were statistically more frequent (NE: 1.952 ± 0.140 Hz; E: 3.047 ± 0.348 Hz), but their amplitude was on average comparable in E vs NE neurons (NE: 30.936 ± 2.174 pA; E: 35.148 ± 2.275 pA) (Fig 4C).

Mf-CA3 synapses and feedforward inhibition

Mf-CA3 connections between the DG and CA3 pyramidal cells provide powerful inputs via ‘giant’ Mf boutons to CA3 PCs, which are thought to assist CA3 in the encoding of memory. Mf–CA3 PC synapses display a high dynamic range of presynaptic plasticity which causes Mf-CA3 synapses to act as "conditional detonators", discharging their postsynaptic CA3 PC targets with bursts of presynaptic activity from single Mf or with patterns of spiking readily observed in DG cells of awake mice (Henze et al., 2002; Sachidhanandam et al., 2009). One-trial memory tasks have been shown to alter the morphological feature of Mf synaptic complexes, in a rapid (within hours) and reversible manner (Ruediger et al., 2011). In particular, one-trial memory tasks induce a robust increase in the number of filopodia emanating from Mf synaptic terminals which contact GABAergic interneurons (Ruediger et al., 2011), lending support to the hypothesis of an increase in feedforward inhibition in most CA3 PNs. We set out to explore a functional

counterpart to the structural plasticity of Mf-CA3 synapses, and to address whether the change in feedforward inhibition was differentially affected in E vs. NE CA3 PNs. We first recorded EPSCs evoked by minimal stimulation of Mfs (Marchal and Mulle, 2004) (Fig 5 A). We observed no difference in the initial amplitude of Mf-CA3 EPSCs between E and NE neurons (Fig. 5B, NE: 80.748 pA ± 13.487, n=8; E: 85.083 pA ± 22.167, n = 4). Similarly, short-term presynaptic plasticity assessed using frequency facilitation was not different between E vs. NE CA3 PNs (Fig. 5C). We then stimulated Mfs and recorded excitatory and inhibitory synaptic currents in CA3 PCs to explore if and how CFC affected feedforward inhibition. To quantify feedforward inhibition, we first recorded EPSCs at the experimentally determined GABAA reversal potential (ECl^-=-70 mV), and then at reversal potential for cations (ENa^+ = +5 mV) (Fig. 5D) (Torborg et al., 2010). We measured the ratio of the peak amplitude of evoked EPSCs vs IPSCs at a stimulation rate of 0.1 Hz (Fig. 5E). We found that the EPSC/IPSC ratio was lower when recorded in FLEN+ vs FLEN- cells (NE: 3.277 ± 0.565, n=8; E: 3.167 ± 0.500, n=4, *to be increased*). This result indicates an imbalance towards excitation at Mf-CA3 connections, suggesting facilitation of information transfer between DG and CA3 in engram CA3 PNs through decreased feedforward inhibition but not through increased excitatory transmission.

Electrophysiological properties of RAM+ neurons

The robust activity marking (RAM) system (Sørensen et al., 2016) is a powerful tool based on an engineered c-Fos promoter allowing to tag neurons selectively activated by CFC. The RAM system has been used to assess the structural and electrophysiological properties of CA3 engram neurons (Sørensen et al., 2016; Weng et al., 2018). However, at variance with FLEN, these properties are only assessed 24 hours after the contextual fear conditioning experience. We then went on to use the RAM system to ask whether engram neurons undergo protracted plastic changes from a few hours (3-6 hours) to >24 hours by comparing the electrophysiological properties of FLEN+ and RAM+ CA3 PNs.

To identify RAM+ neurons 24 hours following CFC, we stereotaxically injected AAV2.9-RAM/tTA::TRE/EGFP which expresses the reporter gene EGFP in activated neurons and AAV2.9-CB7/mCherry to label all infected neurons into the CA3 region of wild-type mice. The mice were Dox fed starting one day before injection and then their diet was switched to regular food for 48 hours before being subjected to CFC (Fig. 6A). Adapting the RAM system approach, we found that the number of RAM+ neurons as compared mCherry neurons (all infected neurons) was notably higher 24 hours after CFC than in the HC conditions (Fig. 6B, 6C), although not to the same extend as previous reports (Sørensen et al., 2016). Provided that RAM is an artificial promoter engineered to enable strong labeling induction upon neuronal activation, the

ratio of RAM+ neurons 24 hours after CFC over untrained conditions (approximately 5:1) was found to be in slightly higher than the ratio of FLEN+ neurons 3 hours after CFC (approximately 4:1).

We performed *ex vivo* patch-clamp recordings 24 hours after CFC on RAM+ neurons and compared their properties to those of RAM- neurons which were positive for mCherry. We assessed input resistance (Ri), and found that it was not statistically different between the two populations (Fig. 6D). We then studied the action potential firing pattern and bursting activity, by injecting 1 s-long pulses of current just above rheobase. In contrast to FLEN+ neurons, RAM+ neurons showed a prolonged spiking activity which outlasted the first burst occurring at the start of the depolarizing pulse (Fig. 6E). This result strongly suggests that c-Fos expressing neurons progressively acquire increased excitability, but increased excitability and propensity to bursts is not an initial property of engram neurons. Finally, we then recorded sEPSCs in RAM-positive and RAM-negative neurons (Figure 8A, B), and we found no difference in the amplitude *(additional experiments are in progress)*.

DISCUSSION

In the past decade, the search for engrams and the characterization of engram cells has immensely benefited from new gene targeting approaches to label the cells and to control their reactivation (Josselyn and Tonegawa, 2020; Tonegawa et al., 2015). Here we have developed a viral tool allowing to functionally characterize the properties of hippocampal cells activated as shortly as possible after the encoding of a contextual memory. The primary goal of our work was to test two parallel hypotheses; first that the subpopulation of hippocampal cells activated during a one-trial contextual memory task possessed different functional properties as compared to the surrounding neurons quickly after encoding, and second, that these properties were subject to progressive plastic changes which could be linked to a first phase of memory consolidation.

The expression of immediate early genes (IEGs) such as Arc, c-Fos and Zif268 has been invaluable in localizing and quantifying cells activated by the encoding of different types of memories (Beer et al., 2014; Guzowski et al., 1999; Kubik et al., 2007).The time course of expression of these rapidly activated genes is in the order of a few hours. In order to characterize the functional properties and/or to manipulate engram neurons, these neurons are tagged with a viable fluorescent marker and /or express an actuator for opto- or chemogenetics. Most techniques currently employed to study the properties of engram cells in mice combine promoter expression based on IEGs, intersectional transgenic strategies, optogenetics and pharmacogenetics with behavioral paradigms (Guenthner et al., 2013; Tonegawa et al., 2015). Using these techniques, the expression of the fluorescent tag and/or the actuator is not immediate, precluding the

functional characterization of engram neurons immediately after the execution of the memory task by the animal. In addition, the main caveat for using activity-dependent promoter/enhancers in either transgenic mice or using viral vectors is the background basal expression which could result in random labeling of non-functionally relevant neurons. The timing of expression of the fluorescent marker and/or actuator can be controlled by directly coupling the promoter of c-Fos, or a synthetic promoter (in the RAM system) to the tetracycline transactivator (tTA), a key component of the doxycycline (Dox) system (Gossen et al., 1995) for inducible expression of a gene of interest (Liu et al., 2012; Sørensen et al., 2016). With these approaches, the physiological properties of reporter-positive engram and reporter-negative non-engram cells could be examined by *ex vivo* patch-clamp recordings 24 hours to several days after the initial contextual memory task (Pignatelli et al., 2019; Sørensen et al., 2016; Weng et al., 2018; Yap et al., 2020). Other transgenic strategies have favored a long-lasting tagging of c-Fos active neurons (Reijmers et al., 2007). Similarly, mice harboring the Arc-CreERT2 bacterial artificial chromosome (BAC) were used to fluorescently label engram neurons several days after exposure to CFC conditioning (Denny et al., 2014). In search of a method to label neurons with a much shorter delay after the initial memory encoding phase, we functionally labeled activated neurons using the E-SARE (enhanced synaptic activity–responsive element) synthetic promoter, that potentially drives activity–dependent gene expression within a few hours (Kawashima et al., 2013). In our hands, using virally expressed E-SARE-EGFP in the hippocampus, we found that the background labeling of neurons did not allow to clearly discriminate between the HC and the CFC conditions (data not shown).

We thus developed a viral strategy for rapid and transient neuronal expression of a fluorescent protein (FLEN) following the exposure of mice to a novel context making use of the full-length c-Fos promoter and of the brightly fluorescent ZsGreen1 protein engineered to be quickly destabilized. The time course of expression of ZsGreen1 in FLEN labeled neurons peaked at 3 hours both after the pharmacological activation in cultured neurons and *in vivo* after a 5-minutes exposure to a novel context. The native protein c-Fos peaks its expression between 60 and 90 minutes (Holtmaat and Caroni, 2016). The difference in peak expression compared to c-Fos-ZsGreen1-DR can be accounted on the fact that AAV vector genomes usually persist in cells as circular episomes, which may be not readily accessible to the translational molecular machinery that physiologically regulates c-Fos-mediated expression. The labeling of neurons persisted for a few hours, enabling *ex vivo* electrophysiological characterization of neurons thought to be involved in the initial encoding of contextual memory. As in all techniques based on IEG promoters, a small percentage of AAV-transduced neurons showed ZsGreen1 fluorescence in control conditions (HC or no activation of cultured neurons). However, the number of FLEN labeled neurons increased by at least a factor of 3

following CFC, allowing for the electrophysiological characterization of FLEN+ neurons which are for their great majority (>66%) activated in relation to the CFC memory task. Contrarily to reported engineered IEG promoters that provides a boost of induction of cell labeling in CA3 and in the amygdala (Sørensen et al., 2016) the activation fold increase of FLEN was small but in accordance with native IEG-based strategies, for instance approximately doubling the number of labeled neurons in the DG (Liu et al., 2012).

We have used this tool to label neurons in the CA3 region of the hippocampus, which is involved in the rapid encoding of new spatial and contextual information (Kesner and Rolls, 2015). One of the key features of CA3 is the presence of recurrent excitatory connections which are subject to NMDA-dependent synaptic plasticity (Rebola et al., 2017), and this appears essential for memory of a one-trial experience (Nakazawa et al., 2003). It has been proposed that the excitability state of neurons may contribute to memory formation (Disterhoft and Oh, 2006). We first examined whether FLEN+ neurons showed distinctive intrinsic excitability properties. We observed no difference in the membrane potential, input resistance, rheobase or bursting activity between FLEN-positive and FLEN-negative neurons 3 to 6 hours following CFC. This strongly suggests that the subpopulation of CA3 PCs engaged in a one-trial learning task are not initially more excitable than the general population of neurons, hence are not predetermined by their excitability state. In apparent contrast with our finding that FLEN+ CA3 PNs did not show increased excitability, a simple associative memory task, trace eye-blink conditioning, appears to increase the excitability of a sizeable fraction (more than half) of CA3 neurons starting at 1 hour and decreasing after several days (Thompson et al., 1996). Beyond the difference in the task and in the species, these contrasting results may be explained by an overall increased activity of CA3 neurons related to the learning task (Cai et al., 2016; Moyer et al., 1996), however not specific to engram neurons. This does not preclude however the possibility that relative neuronal excitability immediately before training could contribute to the selection of neurons to an engram as proposed in the amygdala (Yiu et al., 2014). However, the one-trial memory task does not per se trigger a selective increase in the excitability of engram neurons as compared to the general population of CA3 neurons. In the DG, recall of a previously stored contextual memory (48 hours before), hence reactivation of engram neurons, rapidly (within 1 hour) increased the excitability of these engram neurons with respect to engram neurons which were not subject to reactivation in a separate group of mice (Pignatelli et al., 2019). A learning-related task may however induce plasticity of intrinsic excitability of engram neurons on a longer time scale. To test this possibility, we compared the intrinsic excitability of FLEN+ neurons to those labeled more than 24 hours after CFC by using the previously described RAM system (Sørensen et al., 2016). We found that in RAM+ neurons showed prolonged spike firing in response to a depolarizing pulse of current, hence decreased

accommodation in comparison with non-labeled neurons. Considering that the set of neurons labeled by these two strategies are of the same set, based on the expression of a fluorescent marker under the control of the c-Fos promoter, our data strongly suggest that engram neurons in CA3 progressively acquire increased excitability as compared to neurons which were not activated by the one-trial contextual memory task.

Overall, our data do not favor the possibility that engram neurons are selected from a larger pool of neurons on the basis of their intrinsic membrane properties. The excitability of neurons at the time of encoding, as evidenced by c-Fos driven expression of the fluorescent marker may result from more efficient or more synchronous excitatory synaptic inputs to these neurons. In favor of this interpretation, we observed that FLEN+ neurons showed an increased excitatory drive, which may be explained by a higher number of synaptic contacts. A morphological analysis of the density of spines in FLEN+ neurons as compared to the general population would provide a useful counterpart to the electrophysiological analysis *(this experiment is currently under way)*. It is difficult to discriminate whether the increased number of synaptic inputs preexists to the formation of the engram, or whether it is a plastic mechanism taking place shortly following the contextual memory. The time course of appearance of additional synapses, by unmuting of silent synapses following contextual memory acquisition, is compatible with experimentally induced functional and structural synaptic plasticity (Holtmaat and Caroni, 2016). On the other hand, if FLEN+ neurons showed higher synaptic inputs at the time of memory encoding, this would increase the chance that these neurons show increased excitation (c-Fos activation) hence participate in the engram. The amplitude of mEPSCs in FLEN+ neurons does not appear to increase on average in comparison with FLEN- CA3 PNs. This finding may not favor the possibility that LTP-like synaptic plasticity occurs early during the process of memory formation. In this event, NMDA-dependent forms of synaptic plasticity are more likely to occur later on during the early phase of consolidation of the memory trace (Humeau and Choquet, 2019). Interestingly, we observed a comparable increase in the frequency of sEPSCs in RAM+ CA3 neurons 24 hours after CFC, as previously reported (Weng et al., 2018), without any change in the amplitude of sEPSCs. Using a pharmacological agent which selectively inhibits Mf-CA3 transmission, it is hypothesized that the increased mEPSC frequency is mainly due to more active Mf-CA3 synapses (Weng et al., 2018). However, if such was the case, we would also expect an increase in the amplitude of mEPSCs. In addition, we did not find evidence for an increase in Mf-CA3 evoked EPSC (see below). Overall, our data indicate that CA3 engram neurons show a higher level of excitatory synaptic inputs shortly after memory encoding, and this feature seems to extend to 24 hours. This increased synaptic input in CA3 engram neurons may result either from a preexisting property of these neurons,

prior to contextual memory encoding, or to a form of synaptic plasticity which leads to unmuting of silent synapses or the rapid creation of additional synapses. This later aspect needs to be directly evaluated by quantifying the number of spines in labeled vs. unlabeled CA3 neurons following contextual memory encoding (*experiment in progress*). We found no evidence for increased amplitude of EPSCs in FLEN+ CA3 PNs which could have been indicative of postsynaptic plasticity through an increased number of synaptic AMPA receptors (Takeuchi et al., 2014). One reason may be that synaptic plasticity only occurs in a subset of synaptic contacts, and the recording of mEPSCs is not resolutive enough to capture these modifications.

Local inhibition controls the spiking of CA3 pyramidal cells, hence their capacity to be engaged in an active ensemble of neurons at the time of contextual memory encoding. In CA1 there is a fine control of inhibition upon novel environment exploration (Yap et al., 2020), or fear learning (Lovett-Barron et al., 2014). Little is known about the plasticity of GABAergic circuits in the process of memory encoding in CA3. Our experimental findings do not allow, yet, to improve our understanding of this mechanism (experiments in progress). However, we were able to provide some information on the process of Mf-driven feedforward inhibition. Mf-CA3 synapses have been proposed to play a major role in assisting CA3 in the encoding of memory (Kesner and Rolls, 2015). There is abundant evidence that the structural properties of Mf-CA3 synapses are modified by experience, albeit most of these modifications were observed in the context of chronic behavioral conditions (Maruo et al., 2016). For these reasons, it is important to directly characterize the properties of Mf-CA3 synapses impinging on CA3 engram neurons. We observed no difference in the amplitude and short-term plasticity of Mf-CA3 EPSCs evoked in FLEN+ CA3 neurons vs. FLEN- neurons, which would have been expected if presynaptic Mf-CA3 LTP contributed to the encoding of memory in CA3. It has been proposed that 24 hours after CFC, the increased amplitude of mEPSCs in RAM+ neurons can be attributed to modifications of Mf-CA3 synapses (Weng et al., 2018), which may suggest progressive plasticity of these inputs. More work is however needed to characterize these changes possibly occurring 24h after contextual memory encoding, but not present rapidly after. An important parameter in the transmission of information from the DG to CA3 is feedforward inhibition, which, combined with short-term plasticity of Mf-CA3 synapses, defines the physiological conditions for efficient spike transfer (Henze et al., 2002; Torborg et al., 2010; Zucca et al., 2017). It is noteworthy that CFC induces a robust increase in the number of filopodia emanating from the giant Mf terminals, which peaks between 1 and 5 hours after the one-trial memory task and is related to the precision of memory and the size of engrams (Ruediger et al., 2011). Because filopodia contact GABAergic interneurons, this structural plasticity has been proposed to increase feedforward inhibition, albeit this has not yet been demonstrated. Here we compared the excitation/inhibition ratio of Mf-evoked synaptic responses between FLEN+ and

FLEN- neurons. Although this ratio was found to be quite variable (*more recordings are in progress*), there is a tendency towards comparatively less feedforward inhibition in the putative engram neurons. Hence this leads us to hypothesize that shortly following contextual memory formation, Mf-driven feedforward inhibition is increased in the general population of neurons (Ruediger et al., 2011) but not in Mf inputs onto engram neurons, thus allowing for a comparative stronger input from the DG to the engram neurons. It will be interesting to test whether this increased signal to noise ratio is maintained 24 hours after contextual memory encoding, given that the number of filopodia per Mf bouton has returned to basal level (Ruediger et al., 2011).

In conclusion, the development of a viral tool allowing for the identification of neurons involved in a behavioral task within 3-6 hours appears as an excellent complement to the transgenic mouse strategies and viral vectors which have been used to assess changes in engram neuron properties in the time rage of days (Josselyn and Tonegawa, 2020). Although it is not possible to fully assess the functional properties of engram neurons at the time of the encoding, this work shows that the engram neurons are not different in their intrinsic membrane properties shortly after encoding, a set of properties which however may follow delayed (progressive) plastic changes which are evident at 24h, and which have also been shown to change upon recall (Pignatelli et al., 2019). Overall, we propose that engram neurons do not show higher excitability preexisting to the selection of neurons to the engram during the memory encoding task. Hence the increased activation state of the FLEN+ neurons at the time of encoding rather relates to a higher number of active synaptic inputs providing more efficient excitation. Interestingly, although more work is needed to confirm this tendency, increased excitation may also be linked to decreased Mf-driven feedforward inhibition, thus favoring spike transfer from the DG to CA3 at the time or shortly after memory encoding. The FLEN viral tool will be useful to assess how the properties of neurons in brain regions involved in the contextual memory encoding process, including the entorhinal cortex and the DG.

METHODS

Animals. C57Bl6j female mice were obtained from Janvier and cared according to the regulations of the University of Bordeaux/CNRS Animal Care and Use Committee. Animals were housed with their littermates with ad libitum access to food and water. Cages were kept in a temperature-regulated room on a 12 h light/dark cycle. Prior to any behavioral test, all mice were single housed for 4-5 days and then handled for at least 3 consecutive days. Mice injected with the RAM system were kept on a doxycycline diet (4mg/Kg) starting 1 day before the viral injection.

Viral vectors. Adeno-associated virus (AAV) serotype 2/9 vectors containing our custom-made c-Fos-ZsGreen1-DR (titer 4.00E13) were generated in our lab, whereas AAV2/9 vectors containing the RAM system (titer 3.39E13) were purchased from AddGene. Each vector was mixed with an infection marker virus AAV2/9-CB7/mCherry (titer 1.50E13) and diluted 1:10 for co-injection.

Cell Culture. P0 mouse cortical neurons were plated (300000 cells/well) and allowed to grow on glia cells. At DIV3 cells were infected with the viral mix of c-Fos-ZsGreen1-DR and CB7-mCherry. At DIV14, neurons were switched to an activating medium containing 4-AP (100 µM) and Bicuculline (10 µM) for 30 minutes. Then this activating medium was washed and tetrodotoxin was added (0.5 µM) to prevent action potential firing and stop neuronal activation. Neurons were then fixed using 0.4% paraformaldehyde (PFA) in 0.1 mM PBS at the different intervals following pharmacological activation.

Stereotaxic injection. 2-month-old C57Bl6j mice were bilaterally injected with either c-Fos-ZsGreen1-DR or the RAM system virus mixed with the infection control virus into dorsal hippocampus. Mice were gas-anesthetized with 4% isoflurane and placed in a stereotaxic apparatus, where they were kept under 1.5-2% isoflurane anesthesia, and injected with buprenorphine and carprofene to prevent post-surgery pain. The injection volume and flow rate (300 nl at 60 nl/min) were controlled with an injection micro-pump (World Precision Instruments). Injection coordinates, using bregma as a reference point, were as follows: AP -1.78, ML ± 2.40, DV -2.35. This site targets dorsal CA3b, but virus spreading resulted the infection of CA3a, CA3b, CA3c, CA2 and in some cases few granule neurons and hilar cells of the DG. Mice were carefully monitored for 4 days following surgery, and behavioral manipulation started after a recovery period of approximately 2 weeks.

Behavioral tests. Once recovered, mice were single-housed to reduce uncontrolled experiences that could contaminate the ensemble of CFC-related labelled engram cells. Then, mice were handled to habituate to the experimenter for at least 3 consecutive days prior to CFC. Mice injected with the RAM system were deprived of doxycycline, switching to a regular diet, 48h before CFC training. On the one-trial learning day, mice were transported in the experimental room and immediately placed in a novel conditioning chamber, enriched with visual cues, and allowed to explore it for a total duration of 300s. After an initial exploration period, 3 mild foot-shocks (2s, 0.7 mA) were delivered at a 150s, 210s, and 270s, leaving 30s for additional context sampling at the end. Mice were recorded and freezing behavior was scored using AnyMaze 6 software. Freezing was detected as the absence of movement apart from respiration, and freezing events were scored when immobility lasted more than a threshold of 300ms. Mice were then returned to their home cage. For context only (CO) exploration, mice were placed in a 50 cm x 50 cm open field, where some

objects were distributed. Mice were allowed to explore for 5 minutes before returned to their home cage. The immediate shock test was carried out in the fear conditioning system. Mice explored the conditioning chamber for only 2 seconds before receiving a 6-second-long foot-shock and were then returned to their home cage.

Histology. Mice were anesthetized with intraperitoneal administration of a ketamine/xylazine mix (100 mg/kg/10 mg/kg) at different time intervals following CFC (1.5h, 3h, 4.5h, 6h, 12h for c-Fos-ZsGreen1-DR, 24h for RAM). Mice were then intracardially perfused with 0.9% NaCl solution followed by 4% paraformaldehyde (PFA) in 0.1 mM PBS. Brains were removed and postfixed in 4% PFA overnight at 4°C. Brains were transferred in sucrose 30% in 0.1 mM PBS at 4°C until they sank. Brains were cut on a cryostat into 25µm-thick coronal sections and collected in PBS with 0.3% Triton X-100. No further immunostaining was applied. Slices were immediately mounted on glass slides and covered in DAPI-based mounting medium.

Confocal microscope. Confocal acquisitions were performed using a Leica SP8 White Light Laser 2 on an inverted stand (Leica Microsystems, Mannheim, Germany) and with a x20 (NA 0.75) immersion objective. Images were analyzed using ImageJ. At least 5 slices per animal were acquired. Imaging of neuronal cultures was carried out as well using confocal Leica SP8 White Light Laser 2 (Leica Microsystems, Mannheim, Germany) and with a x20 (NA 0.75) immersion objective. In all experiments, the settings (laser power, gain, offset) were fixed between goups as well as the pixel size (120 nm).

Ex-vivo slice preparation. Slices were prepared 3h or 24h following CFC for c-Fos-ZsGreen1-DR-injected mice and RAM-injected mice respectively. To attempt to reduce stress-related unspecific c-Fos activation, mice were anesthetized with a ketamine/xylazine mix (100 mg/kg/10 mg/kg; i.p.) in their holding room, and only once anesthetized transferred to slice preparation room. There, they were intracardially perfused with an ice-cold oxygenated (95% O2 and 5% CO2) cutting solution containing (in mM): 87 NaCl, 2.5 KCl, 1.25 NaH2PO4, 25 NaHCO3, 25 glucose, 75 sucrose, 0.5 CaCl2, 7 MgCl2, pH 7.4, 315 mOsm/kg. Brains were quickly dissected out and parasagittal slices from both hemispheres (300 µm thick) were cut on a vibratome (Leica VT1200S, Germany) in the same oxygenated ice-cold cutting solution. Slices were then incubated at 34°C in a resting chamber containing the same cutting solution for 20-30 minutes for recovery. Slices where then transferred in a resting chamber filled with an oxygenated (95% O2 and 5% CO2) artificial cerebrospinal fluid (aCSF) containing (mM): 125 NaCl, 2.5 KCl, 1.25 NaH2PO4, 26 NaHCO3, 1.3 MgCl2, 2.3 CaCl2, 10 glucose, pH 7.4, 300 mOsm/kg at room temperature for the rest of the day.

Electrophysiology. When transferred to a recording chamber, slices were continuously superfused with aCSF. CA3 pyramidal cells were identified with an infrared differential interference contrast (IR-DIC) microscope with a water immersion 63X objective (N.A. 0.8). Neurons were then classified as engram neurons (simultaneous expression of ZsGreen1-DR/mCherry or EGFP/mCherry when RAM was used) or non-engram neuron (mCherry expression only) with a 2p microscope. Whole-cell recordings were made at room temperature using borosilicate glass capillaries with resistances between 4-6 MΩ. For current clamp recordings, the intracellular solution contained (in mM): 135 K-gluconate, 5 KCl, 2 NaCl, 10 Na2-phosphocreatine, 0.1 EGTA, 10 HEPES, 5 Mg-ATP, 0.4 Na-GTP, pH 7.2 adjusted with KOH, 280 mOsm/Kg. For voltage clamp mode, the patch pipettes were filled with a solution containing (mM): 140 Cs-methanesulfonate, 2 MgCl2, 4 NaCl, 5 Na-phosphocreatine, 0.2 EGTA, 10 HEPES, 3 Na2-ATP, 0.3 GTP, P, pH 7.2 adjusted with CsOH, 280 mOsm/Kg. No liquid-junction correction was used. Neurons were held at –70 mV. Leak current and series resistance were monitored throughout each experiment; neurons with a leak current >200 pA and a series resistance >25MΩ or if these parameters changed more than 20% were excluded from analysis. Series resistance compensation and bridge balance were used for current clamp recordings. Resting membrane potential was measured immediately upon break-in. All other recordings were performed 5-10 min after opening the membrane. Input resistance was quantified by linearly fitting the voltage change against injected current. Steps of hyper- and depolarizing current steps were injected to determine action potential threshold and rheobase. Action potential firing pattern was determined by injecting repeated 200 pA steps of current. sEPSC were isolated by bath application of bicuculline (10 µM), while mEPSC were recorded in presence of bicuculline (10 µM) and tetrodotoxin (0.5 µM). sIPSC were recorded in presence of D-AP5 (50 µM) and NBQX (20 µM), while mIPSC were isolated in presence of D-AP5 (50 µM), NBQX (20 µM) and TTX (0.5 µM). Spontaneous and miniature synaptic events were detected using a deconvolution-based approach (Pernía-Andrade et al., 2012). All recordings were obtained with a HEKA EPC10 amplifier, filtered at 3.3 kHz and digitized at 10 kHz via PatchMaster software (Lambrecht, Germany). Data were analyzed offline using custom-made Python scripts. To record evoked EPSCs (eEPSCs), stimulating glass pipettes (World Precision Instruments) were filled with aCSF and placed in the hilus, close to the granule cell layer to stimulate initial portion of Mf axons. Voltage pulses (200 µs) were delivered through a stimulus isolator. Stimulation intensity was adjusted to obtain minimal Mf stimulation (Marchal and Mulle., 2004). Basal synaptic transmission was recorded while holding CA3 neurons at -70 mV with pulses at a low frequency of 0.1 Hz. Frequency was then increased to 1 Hz to induce frequency facilitation. After 2-3 minutes, when facilitation was extinguished, the voltage was switched to +5 mV (reversal potential for cations) to record di-synaptic eIPSC.

Statistical analysis and graphical representations. Statistical analyses and graphical representation were performed with Python. Values were first tested for normality (D'Agostino and Pearson omnibus test). Data were presented as scatter plots and boxplots indicating mean, first and third quartiles. Normally distributed data were compared using a t-test (two-sided) while Mann–Whitney rank test (two-sided) was used for non-normal data set. Analyses involving two factors were tested using two-way ANOVAs. Cumulative frequency distributions were presented as fractions and tested using a Mann–Whitney rank test. Statistical differences were considered as significant at $p < 0.05$.

REFERENCES

Amaral, D.G. (1978). A golgi study of cell types in the hilar region of the hippocampus in the rat. J Comp Neurol *182*, 851–914.

Amaral, D.G., and Witter, M.P. (1989). The three-dimensional organization of the hippocampal formation: A review of anatomical data. Neuroscience *31*, 571–591.

Andersen, P., Moser, E., Moser, M.B., and Trommald, M. (1996). Cellular correlates to spatial learning in the rat hippocampus. J Physiology-Paris *90*, 349.

Armstrong, C.M., and Gilly, W.F. (1992). [5] Access resistance and space clamp problems associated with whole-cell patch clamping. Methods Enzymol *207*, 100–122.

Bakker, A., Kirwan, C.B., Miller, M., and Stark, C.E.L. (2008). Pattern Separation in the Human Hippocampal CA3 and Dentate Gyrus. Science *319*, 1640–1642.

Balind, S.R., Magó, Á., Ahmadi, M., Kis, N., Varga-Németh, Z., Lőrincz, A., and Makara, J.K. (2019a). Diverse synaptic and dendritic mechanisms of complex spike burst generation in hippocampal CA3 pyramidal cells. Nat Commun *10*, 1859.

Balind, S.R., Magó, Á., Ahmadi, M., Kis, N., Varga-Németh, Z., Lőrincz, A., and Makara, J.K. (2019b). Diverse synaptic and dendritic mechanisms of complex spike burst generation in hippocampal CA3 pyramidal cells. Nat Commun *10*, 1859.

Bannister, N.J., and Larkman, A.U. (1995). Dendritic morphology of CA1 pyramidal neurones from the rat hippocampus: II. Spine distributions. J Comp Neurol *360*, 161–171.

Bartesaghi, R., and Gessi, T. (2004). Parallel activation of field CA2 and dentate gyrus by synaptically elicited perforant path volleys. Hippocampus *14*, 948–963.

Bartesaghi, R., Migliore, M., and Gessi, T. (2006). Input–output relations in the entorhinal cortex–dentate–hippocampal system: Evidence for a non-linear transfer of signals. Neuroscience *142*, 247–265.

Barth, A.L., Gerkin, R.C., and Dean, K.L. (2004). Alteration of Neuronal Firing Properties after In Vivo Experience in a FosGFP Transgenic Mouse. J Neurosci *24*, 6466–6475.

Beer, Z., Chwiesko, C., and Sauvage, M.M. (2014). Processing of spatial and non-spatial information reveals functional homogeneity along the dorso-ventral axis of CA3, but not CA1. Neurobiol Learn Mem *111*, 56–64.

Bessières, B., Nicole, O., and Bontempi, B. (2017). Assessing recent and remote associative olfactory memory in rats using the social transmission of food preference paradigm. Nat Protoc *12*, 1415–1436.

Bi, G., and Poo, M. (1998). Synaptic Modifications in Cultured Hippocampal Neurons: Dependence on Spike Timing, Synaptic Strength, and Postsynaptic Cell Type. J Neurosci *18*, 10464–10472.

Bito, H., Deisseroth, K., and Tsien, R.W. (1997). Ca2+-dependent regulation in neuronal gene expression. Curr Opin Neurobiol *7*, 419–429.

Bittner, K.C., Milstein, A.D., Grienberger, C., Romani, S., and Magee, J.C. (2017). Behavioral time scale synaptic plasticity underlies CA1 place fields. Science *357*, 1033–1036.

Bliss, T.V.P., and Lømo, T. (1973). Long-lasting potentiation of synaptic transmission in the dentate area of the anaesthetized rabbit following stimulation of the perforant path. J Physiology *232*, 331–356.

Bray, N. (2016). Once upon a recent time. Nat Rev Neurosci *17*, 397–397.

Brown, J.T., and Randall, A.D. (2009). Activity-dependent depression of the spike after-depolarization generates long-lasting intrinsic plasticity in hippocampal CA3 pyramidal neurons. J Physiology *587*, 1265–1281.

Buckmaster, P.S., Wenzel, H.J., Kunkel, D.D., and Schwartzkroin, P.A. (1996). Axon arbors and synaptic connections of hippocampal mossy cells in the rat in vivo. J Comp Neurol *366*, 270–292.

Cai, D.J., Aharoni, D., Shuman, T., Shobe, J., Biane, J., Song, W., Wei, B., Veshkini, M., La-Vu, M., Lou, J., et al. (2016). A shared neural ensemble links distinct contextual memories encoded close in time. Nature *534*, 115–118.

Chevaleyre, V., and Siegelbaum, S.A. (2010). Strong CA2 Pyramidal Neuron Synapses Define a Powerful Disynaptic Cortico-Hippocampal Loop. Neuron *66*, 560–572.

Chklovskii, D.B., Mel, B.W., and Svoboda, K. (2004). Cortical rewiring and information storage. Nature *431*, 782–788.

Choi, J.-H., Sim, S.-E., Kim, J., Choi, D.I., Oh, J., Ye, S., Lee, J., Kim, T., Ko, H.-G., Lim, C.-S., et al. (2018). Interregional synaptic maps among engram cells underlie memory formation. Science *360*, 430–435.

Claiborne, B.J., Amaral, D.G., and Cowan, W.M. (1986). A light and electron microscopic analysis of the mossy fibers of the rat dentate gyrus. J Comp Neurol *246*, 435–458.

Claiborne, B.J., Amaral, D.G., and Cowan, W.M. (1990). Quantitative, three-dimensional analysis of granule cell dendrites in the rat dentate gyrus. J Comp Neurol *302*, 206–219.

Clayton, N.S., and Dickinson, A. (1998). Episodic-like memory during cache recovery by scrub jays. Nature *395*, 272–274.

Clayton, N.S., and Dickinson, A. (1999). Motivational control of caching behaviour in the scrub jay,Aphelocoma coerulescens. Anim Behav *57*, 435–444.

Clayton, N.S., Bussey, T.J., and Dickinson, A. (2003). Can animals recall the past and plan for the future? Nat Rev Neurosci *4*, 685–691.

Daumas, S., Ceccom, J., Halley, H., Francés, B., and Lassalle, J.-M. (2009). Activation of metabotropic glutamate receptor type 2/3 supports the involvement of the hippocampal mossy fiber pathway on contextual fear memory consolidation. Learn Memory *16*, 504–507.

Debanne, D., Gähwiler, B.H., and Thompson, S.M. (1994). Asynchronous pre- and postsynaptic activity induces associative long-term depression in area CA1 of the rat hippocampus in vitro. Proc National Acad Sci *91*, 1148–1152.

Debanne, D., Gähwiler, B.H., and Thompson, S.M. (1997). Bidirectional Associative Plasticity of Unitary CA3-CA1 EPSPs in the Rat Hippocampus In Vitro. J Neurophysiol *77*, 2851–2855.

Denny, C.A., Kheirbek, M.A., Alba, E.L., Tanaka, K.F., Brachman, R.A., Laughman, K.B., Tomm, N.K., Turi, G.F., Losonczy, A., and Hen, R. (2014). Hippocampal Memory Traces Are Differentially Modulated by Experience, Time, and Adult Neurogenesis. Neuron *83*, 189–201.

Deshmukh, S.S., and Knierim, J.J. (2013). Influence of local objects on hippocampal representations: Landmark vectors and memory. Hippocampus *23*, 253–267.

Diamantaki, M., Frey, M., Berens, P., Preston-Ferrer, P., and Burgalossi, A. (2016). Sparse activity of identified dentate granule cells during spatial exploration. Elife *5*, e20252.

Ding, L., Chen, H., Diamantaki, M., Coletta, S., Preston-Ferrer, P., and Burgalossi, A. (2020). Structural Correlates of CA2 and CA3 Pyramidal Cell Activity in Freely-Moving Mice. J Neurosci *40*, 5797–5806.

Disterhoft, J.F., and Oh, M.M. (2006). Learning, aging and intrinsic neuronal plasticity. Trends Neurosci *29*, 587–599.

Do, V.H., Martinez, C.O., Martinez, J.L., and Derrick, B.E. (2002). Long-Term Potentiation in Direct Perforant Path Projections to the Hippocampal CA3 Region In Vivo. J Neurophysiol *87*, 669–678.

Donato, F., Rompani, S.B., and Caroni, P. (2013). Parvalbumin-expressing basket-cell network plasticity induced by experience regulates adult learning. Nature *504*, 272–276.

Dudai, Y., and Eisenberg, M. (2004). Rites of Passage of the Engram Reconsolidation and the Lingering Consolidation Hypothesis. Neuron *44*, 93–100.

Epsztein, J., Brecht, M., and Lee, A.K. (2011). Intracellular Determinants of Hippocampal CA1 Place and Silent Cell Activity in a Novel Environment. Neuron *70*, 109–120.

Faber, E.S.L., Delaney, A.J., and Sah, P. (2005). SK channels regulate excitatory synaptic transmission and plasticity in the lateral amygdala. Nat Neurosci *8*, 635–641.

Fanselow, M.S. (2000). Contextual fear, gestalt memories, and the hippocampus. Behav Brain Res *110*, 73–81.

Feldman, D.E. (2000). Inhibition and plasticity. Nat Neurosci *3*, 303–304.

Fosque, B.F., Sun, Y., Dana, H., Yang, C.-T., Ohyama, T., Tadross, M.R., Patel, R., Zlatic, M., Kim, D.S., Ahrens, M.B., et al. (2015). Labeling of active neural circuits in vivo with designed calcium integrators. Science *347*, 755–760.

Fyhn, M., Molden, S., Witter, M.P., Moser, E.I., and Moser, M.-B. (2004). Spatial Representation in the Entorhinal Cortex. Science *305*, 1258–1264.

Gilbert, P.E., Kesner, R.P., and Lee, I. (2001). Dissociating hippocampal subregions: A double dissociation between dentate gyrus and CA1. Hippocampus *11*, 626–636.

Glazewski, S., Bejar, R., Mayford, M., and Fox, K. (2001). The effect of autonomous alpha-CaMKII expression on sensory responses and experience-dependent plasticity in mouse barrel cortex. Neuropharmacology *41*, 771–778.

Gonzales, R.B., Galvan, C.J.D., Rangel, Y.M., and Claiborne, B.J. (2001). Distribution of thorny excrescences on CA3 pyramidal neurons in the rat hippocampus. J Comp Neurol *430*, 357–368.

Gossen, M., Freundlieb, S., Bender, G., Muller, G., Hillen, W., and Bujard, H. (1995). Transcriptional activation by tetracyclines in mammalian cells. Science *268*, 1766–1769.

Gouty-Colomer, L.A., Hosseini, B., Marcelo, I.M., Schreiber, J., Slump, D.E., Yamaguchi, S., Houweling, A.R., Jaarsma, D., Elgersma, Y., and Kushner, S.A. (2016). Arc expression identifies the lateral amygdala fear memory trace. Mol Psychiatr *21*, 364–375.

Guenthner, C.J., Miyamichi, K., Yang, H.H., Heller, H.C., and Luo, L. (2013). Permanent Genetic Access to Transiently Active Neurons via TRAP: Targeted Recombination in Active Populations. Neuron *78*, 773–784.

Gulyás, A.I., Hájos, N., and Freund, T.F. (1996). Interneurons Containing Calretinin Are Specialized to Control Other Interneurons in the Rat Hippocampus. J Neurosci *16*, 3397–3411.

Guzman, S.J., Schlögl, A., Frotscher, M., and Jonas, P. (2016). Synaptic mechanisms of pattern completion in the hippocampal CA3 network. Science.

Guzowski, J.F., McNaughton, B.L., Barnes, C.A., and Worley, P.F. (1999). Environment-specific expression of the immediate-early gene Arc in hippocampal neuronal ensembles. Nat Neurosci *2*, 1120–1124.

Guzowski, J.F., Knierim, J.J., and Moser, E.I. (2004). Ensemble Dynamics of Hippocampal Regions CA3 and CA1. Neuron *44*, 581–584.

Hagena, H., and Manahan-Vaughan, D. (2011). Learning-Facilitated Synaptic Plasticity at CA3 Mossy Fiber and Commissural–Associational Synapses Reveals Different Roles in Information Processing. Cereb Cortex *21*, 2442–2449.

Hainmueller, T., and Bartos, M. (2018a). Parallel emergence of stable and dynamic memory engrams in the hippocampus. Nature *558*, 292–296.

Hainmueller, T., and Bartos, M. (2018b). Parallel emergence of stable and dynamic memory engrams in the hippocampus. Nature *558*, 292–296.

Hainmueller, T., and Bartos, M. (2020). Dentate gyrus circuits for encoding, retrieval and discrimination of episodic memories. Nat Rev Neurosci *21*, 153–168.

Hájos, N., Pálhalmi, J., Mann, E.O., Németh, B., Paulsen, O., and Freund, T.F. (2004). Spike Timing of Distinct Types of GABAergic Interneuron during Hippocampal Gamma Oscillations In Vitro. J Neurosci *24*, 9127–9137.

Hallermann, S., Pawlu, C., Jonas, P., and Heckmann, M. (2003). A large pool of releasable vesicles in a cortical glutamatergic synapse. Proc National Acad Sci *100*, 8975–8980.

Han, J.-H., Kushner, S.A., Yiu, A.P., Cole, C.J., Matynia, A., Brown, R.A., Neve, R.L., Guzowski, J.F., Silva, A.J., and Josselyn, S.A. (2007). Neuronal Competition and Selection During Memory Formation. Science *316*, 457–460.

Han, J.-H., Kushner, S.A., Yiu, A.P., Hsiang, H.-L. (Liz), Buch, T., Waisman, A., Bontempi, B., Neve, R.L., Frankland, P.W., and Josselyn, S.A. (2009). Selective Erasure of a Fear Memory. Science *323*, 1492–1496.

Hargreaves, E.L., Rao, G., Lee, I., and Knierim, J.J. (2005). Major Dissociation Between Medial and Lateral Entorhinal Input to Dorsal Hippocampus. Science *308*, 1792–1794.

Hasselmo, M.E., and Wyble, B.P. (1997). Free recall and recognition in a network model of the hippocampus: simulating effects of scopolamine on human memory function. Behav Brain Res *89*, 1–34.

Helton, T.D., Zhao, M., Farris, S., and Dudek, S.M. (2019). Diversity of dendritic morphology and entorhinal cortex synaptic effectiveness in mouse CA2 pyramidal neurons. Hippocampus *29*, 78–92.

Henze, D.A., Urban, N.N., and Barrionuevo, G. (2000). The multifarious hippocampal mossy fiber pathway: a review. Neuroscience *98*, 407–427.

Henze, D.A., McMahon, D.B.T., Harris, K.M., and Barrionuevo, G. (2002). Giant Miniature EPSCs at the Hippocampal Mossy Fiber to CA3 Pyramidal Cell Synapse Are Monoquantal. J Neurophysiol *87*, 15–29.

Hitti, F.L., and Siegelbaum, S.A. (2014). The hippocampal CA2 region is essential for social memory. Nature *508*, 88–92.

Holtmaat, A., and Caroni, P. (2016). Functional and structural underpinnings of neuronal assembly formation in learning. Nat Neurosci *19*, 1553–1562.

Hsiang, H.-L. (Liz), Epp, J.R., Oever, M.C. van den, Yan, C., Rashid, A.J., Insel, N., Ye, L., Niibori, Y., Deisseroth, K., Frankland, P.W., et al. (2014). Manipulating a “Cocaine Engram” in Mice. J Neurosci *34*, 14115–14127.

Hsu, T.-T., Lee, C.-T., Tai, M.-H., and Lien, C.-C. (2016). Differential Recruitment of Dentate Gyrus Interneuron Types by Commissural Versus Perforant Pathways. Cereb Cortex *26*, 2715–2727.

Humeau, Y., and Choquet, D. (2019). The next generation of approaches to investigate the link between synaptic plasticity and learning. Nat Neurosci *22*, 1536–1543.

Hunt, D.L., Linaro, D., Si, B., Romani, S., and Spruston, N. (2018a). A novel pyramidal cell type promotes sharp-wave synchronization in the hippocampus. Nat Neurosci *21*, 985–995.

Hunt, D.L., Linaro, D., Si, B., Romani, S., and Spruston, N. (2018b). A novel pyramidal cell type promotes sharp-wave synchronization in the hippocampus. Nat Neurosci *21*, 985–995.

Igarashi, K.M., Ito, H.T., Moser, E.I., and Moser, M.-B. (2014). Functional diversity along the transverse axis of hippocampal area CA1. Febs Lett *588*, 2470–2476.

Ishizuka, N., Weber, J., and Amaral, D.G. (1990). Organization of intrahippocampal projections originating from CA3 pyramidal cells in the rat. J Comp Neurol *295*, 580–623.

Ishizuka, N., Cowan, W.M., and Amaral, D.G. (1995a). A quantitative analysis of the dendritic organization of pyramidal cells in the rat hippocampus. J Comp Neurol *362*, 17–45.

Ishizuka, N., Cowan, W.M., and Amaral, D.G. (1995b). A quantitative analysis of the dendritic organization of pyramidal cells in the rat hippocampus. J Comp Neurol *362*, 17–45.

Ito, H.T., and Schuman, E.M. (2012). Functional division of hippocampal area CA1 via modulatory gating of entorhinal cortical inputs. Hippocampus *22*, 372–387.

Jarsky, T., Mady, R., Kennedy, B., and Spruston, N. (2008). Distribution of bursting neurons in the CA1 region and the subiculum of the rat hippocampus. J Comp Neurol *506*, 535–547.

Josselyn, S.A., and Tonegawa, S. (2020). Memory engrams: Recalling the past and imagining the future. Science *367*, eaaw4325.

Josselyn, S.A., Köhler, S., and Frankland, P.W. (2015). Finding the engram. Nat Rev Neurosci *16*, 521–534.

Kaifosh, P., and Losonczy, A. (2016). Mnemonic Functions for Nonlinear Dendritic Integration in Hippocampal Pyramidal Circuits. Neuron *90*, 622–634.

Kawashima, T., Okuno, H., Nonaka, M., Adachi-Morishima, A., Kyo, N., Okamura, M., Takemoto-Kimura, S., Worley, P.F., and Bito, H. (2009). Synaptic activity-responsive element in the Arc/Arg3.1 promoter essential for synapse-to-nucleus signaling in activated neurons. Proc National Acad Sci *106*, 316–321.

Kawashima, T., Kitamura, K., Suzuki, K., Nonaka, M., Kamijo, S., Takemoto-Kimura, S., Kano, M., Okuno, H., Ohki, K., and Bito, H. (2013). Functional labeling of neurons and their projections using the synthetic activity–dependent promoter E-SARE. Nat Methods *10*, 889–895.

Kesner, R.P. (2007). Behavioral functions of the CA3 subregion of the hippocampus. Learn Memory *14*, 771–781.

Kesner, R.P., and Rolls, E.T. (2015). A computational theory of hippocampal function, and tests of the theory: New developments. Neurosci Biobehav Rev *48*, 92–147.

Kim, S., Guzman, S.J., Hu, H., and Jonas, P. (2012). Active dendrites support efficient initiation of dendritic spikes in hippocampal CA3 pyramidal neurons. Nat Neurosci *15*, 600–606.

Kitamura, T., Ogawa, S.K., Roy, D.S., Okuyama, T., Morrissey, M.D., Smith, L.M., Redondo, R.L., and Tonegawa, S. (2017). Engrams and circuits crucial for systems consolidation of a memory. Science *356*, 73–78.

Klausberger, T., Magill, P.J., Márton, L.F., Roberts, J.D.B., Cobden, P.M., Buzsáki, G., and Somogyi, P. (2003). Brain-state- and cell-type-specific firing of hippocampal interneurons in vivo. Nature *421*, 844–848.

Kleindienst, T., and Lohmann, C. (2014). Simultaneous Patch-Clamping and Calcium Imaging in Developing Dendrites. Cold Spring Harb Protoc *2014*, pdb.prot080390-pdb.prot080390.

Knierim, J.J., and Neunuebel, J.P. (2016). Tracking the flow of hippocampal computation: Pattern separation, pattern completion, and attractor dynamics. Neurobiol Learn Mem *129*, 38–49.

Kobayashi, K., and Poo, M. (2004). Spike Train Timing-Dependent Associative Modification of Hippocampal CA3 Recurrent Synapses by Mossy Fibers. Neuron *41*, 445–454.

Koya, E., Golden, S.A., Harvey, B.K., Guez-Barber, D.H., Berkow, A., Simmons, D.E., Bossert, J.M., Nair, S.G., Uejima, J.L., Marin, M.T., et al. (2009). Targeted disruption of cocaine-activated nucleus accumbens neurons prevents context-specific sensitization. Nat Neurosci *12*, 1069–1073.

Krahe, R., and Gabbiani, F. (2004). Burst firing in sensory systems. Nat Rev Neurosci *5*, 13–23.

Kubik, S., Miyashita, T., and Guzowski, J.F. (2007). Using immediate-early genes to map hippocampal subregional functions. Learn Memory *14*, 758–770.

Lacagnina, A.F., Brockway, E.T., Crovetti, C.R., Shue, F., McCarty, M.J., Sattler, K.P., Lim, S.C., Santos, S.L., Denny, C.A., and Drew, M.R. (2019). Distinct hippocampal engrams control extinction and relapse of fear memory. Nat Neurosci *22*, 753–761.

Lammel, S., Lim, B.K., Ran, C., Huang, K.W., Betley, M.J., Tye, K.M., Deisseroth, K., and Malenka, R.C. (2012). Input-specific control of reward and aversion in the ventral tegmental area. Nature *491*, 212–217.

Lanore, F., Labrousse, V.F., Szabo, Z., Normand, E., Blanchet, C., and Mulle, C. (2012). Deficits in Morphofunctional Maturation of Hippocampal Mossy Fiber Synapses in a Mouse Model of Intellectual Disability. J Neurosci *32*, 17882–17893.

Lassalle, J.-M., Bataille, T., and Halley, H. (2000). Reversible Inactivation of the Hippocampal Mossy Fiber Synapses in Mice Impairs Spatial Learning, but neither Consolidation nor Memory Retrieval, in the Morris Navigation Task. Neurobiol Learn Mem *73*, 243–257.

Laurberg, S., and Sørensen, K.E. (1981). Associational and commissural collaterals of neurons in the hippocampal formation (Hilus fasciae dentatae and subfield CA3). Brain Res *212*, 287–300.

Lee, I., and Kesner, R.P. (2004). Differential contributions of dorsal hippocampal subregions to memory acquisition and retrieval in contextual fear-conditioning. Hippocampus *14*, 301–310.

Lee, D., Hyun, J.H., Jung, K., Hannan, P., and Kwon, H.-B. (2017a). A calcium- and light-gated switch to induce gene expression in activated neurons. Nat Biotechnol *35*, 858–863.

Lee, D., Creed, M., Jung, K., Stefanelli, T., Wendler, D.J., Oh, W.C., Mignocchi, N.L., Lüscher, C., and Kwon, H.-B. (2017b). Temporally precise labeling and control of neuromodulatory circuits in the mammalian brain. Nat Methods *14*, 495–503.

Lee, S.-H., Kwan, A.C., and Dan, Y. (2014). Interneuron subtypes and orientation tuning. Nature *508*, E1–E2.

Leroy, F., Brann, D.H., Meira, T., and Siegelbaum, S.A. (2017). Input-Timing-Dependent Plasticity in the Hippocampal CA2 Region and Its Potential Role in Social Memory. Neuron *95*, 1089-1102.e5.

Leutgeb, J.K., Leutgeb, S., Moser, M.-B., and Moser, E.I. (2007). Pattern Separation in the Dentate Gyrus and CA3 of the Hippocampus. Science *315*, 961–966.

Levy, W.B., and Steward, O. (1983). Temporal contiguity requirements for long-term associative potentiation/depression in the hippocampus. Neuroscience *8*, 791–797.

Lin, Y., Bloodgood, B.L., Hauser, J.L., Lapan, A.D., Koon, A.C., Kim, T.-K., Hu, L.S., Malik, A.N., and Greenberg, M.E. (2008). Activity-dependent regulation of inhibitory synapse development by Npas4. Nature *455*, 1198–1204.

Link, W.T., Grant, P., Hidaka, H., and Pant, H.C. (1992). Casein kinases I and II from squid brain exhibit selective neurofilament phosphorylation. Mol Cell Neurosci *3*, 548–558.

Lisman, J., Cooper, K., Sehgal, M., and Silva, A.J. (2018). Memory formation depends on both synapse-specific modifications of synaptic strength and cell-specific increases in excitability. Nat Neurosci *21*, 309–314.

Liu, X., Ramirez, S., Pang, P.T., Puryear, C.B., Govindarajan, A., Deisseroth, K., and Tonegawa, S. (2012). Optogenetic stimulation of a hippocampal engram activates fear memory recall. Nature *484*, 381–385.

Liu, X., Ramirez, S., Redondo, R.L., and Tonegawa, S. (2014a). Identification and Manipulation of Memory Engram Cells. Cold Spring Harb Sym *79*, 59–65.

Liu, X., Ramirez, S., and Tonegawa, S. (2014b). Inception of a false memory by optogenetic manipulation of a hippocampal memory engram. Philosophical Transactions Royal Soc B Biological Sci *369*, 20130142.

Lovett-Barron, M., Kaifosh, P., Kheirbek, M.A., Danielson, N., Zaremba, J.D., Reardon, T.R., Turi, G.F., Hen, R., Zemelman, B.V., and Losonczy, A. (2014). Dendritic Inhibition in the Hippocampus Supports Fear Learning. Science *343*, 857–863.

Lyford, G.L., Yamagata, K., Kaufmann, W.E., Barnes, C.A., Sanders, L.K., Copeland, N.G., Gilbert, D.J., Jenkins, N.A., Lanahan, A.A., and Worley, P.F. (1995). Arc, a growth factor and activity-regulated gene, encodes a novel cytoskeleton-associated protein that is enriched in neuronal dendrites. Neuron *14*, 433–445.

Makara, J.K., and Magee, J.C. (2013). Variable Dendritic Integration in Hippocampal CA3 Pyramidal Neurons. Neuron *80*, 1438–1450.

Malezieux, M., Kees, A.L., and Mulle, C. (2020). Theta Oscillations Coincide with Sustained Hyperpolarization in CA3 Pyramidal Cells, Underlying Decreased Firing. Cell Reports *32*, 107868.

Malinow, R., and Malenka, R.C. (2002). AMPA RECEPTOR TRAFFICKING AND SYNAPTIC PLASTICITY. Neuroscience *25*, 103–126.

Marchal, C., and Mulle, C. (2004). Postnatal maturation of mossy fibre excitatory transmission in mouse CA3 pyramidal cells: a potential role for kainate receptors. J Physiology *561*, 27–37.

Markram, H., Lübke, J., Frotscher, M., and Sakmann, B. (1997). Regulation of Synaptic Efficacy by Coincidence of Postsynaptic APs and EPSPs. Science *275*, 213–215.

Marr, D. (1971). Simple memory: a theory for archicortex. Philosophical Transactions Royal Soc Lond B Biological Sci *262*, 23–81.

Maruo, T., Mandai, K., Takai, Y., and Mori, M. (2016). Activity-dependent alteration of the morphology of a hippocampal giant synapse. Mol Cell Neurosci *71*, 25–33.

McBain, C.J., and Fisahn, A. (2001). Interneurons unbound. Nat Rev Neurosci *2*, 11–23.

McClelland, J.L., and Goddard, N.H. (1996). Considerations arising from a complementary learning systems perspective on hippocampus and neocortex. Hippocampus *6*, 654–665.

McClelland, J.L., McNaughton, B.L., and O'Reilly, R.C. (1995). Why There Are Complementary Learning Systems in the Hippocampus and Neocortex: Insights From the Successes and Failures of Connectionist Models of Learning and Memory. Psychol Rev *102*, 419–457.

McHugh, T.J., and Tonegawa, S. (2009). CA3 NMDA receptors are required for the rapid formation of a salient contextual representation. Hippocampus *19*, 1153–1158.

McHugh, T.J., Jones, M.W., Quinn, J.J., Balthasar, N., Coppari, R., Elmquist, J.K., Lowell, B.B., Fanselow, M.S., Wilson, M.A., and Tonegawa, S. (2007). Dentate Gyrus NMDA Receptors Mediate Rapid Pattern Separation in the Hippocampal Network. Science *317*, 94–99.

McKay, B.M., Matthews, E.A., Oliveira, F.A., and Disterhoft, J.F. (2009). Intrinsic Neuronal Excitability Is Reversibly Altered by a Single Experience in Fear Conditioning. J Neurophysiol *102*, 2763–2770.

McMahon, D.B.T., and Barrionuevo, G. (2002). Short- and Long-Term Plasticity of the Perforant Path Synapse in Hippocampal Area CA3. J Neurophysiol *88*, 528–533.

McNaughton, B.L., and Morris, R.G.M. (1987). Hippocampal synaptic enhancement and information storage within a distributed memory system. Trends Neurosci *10*, 408–415.

Mehta, M.R., Quirk, M.C., and Wilson, M.A. (2000). Experience-Dependent Asymmetric Shape of Hippocampal Receptive Fields. Neuron *25*, 707–715.

Middleton, S.J., and McHugh, T.J. (2016). Silencing CA3 disrupts temporal coding in the CA1 ensemble. Nat Neurosci *19*, 945–951.

Mishra, R.K., Kim, S., Guzman, S.J., and Jonas, P. (2016). Symmetric spike timing-dependent plasticity at CA3–CA3 synapses optimizes storage and recall in autoassociative networks. Nat Commun *7*, 11552.

Mizuseki, K., Royer, S., Diba, K., and Buzsáki, G. (2012). Activity dynamics and behavioral correlates of CA3 and CA1 hippocampal pyramidal neurons. Hippocampus *22*, 1659–1680.

Moeyaert, B., Holt, G., Madangopal, R., Perez-Alvarez, A., Fearey, B.C., Trojanowski, N.F., Ledderose, J., Zolnik, T.A., Das, A., Patel, D., et al. (2018). Improved methods for marking active neuron populations. Nat Commun *9*, 4440.

Moyer, J.R., Thompson, L.T., and Disterhoft, J.F. (1996). Trace Eyeblink Conditioning Increases CA1 Excitability in a Transient and Learning-Specific Manner. J Neurosci *16*, 5536–5546.

Naber, P.A., Silva, F.H.L. da, and Witter, M.P. (2001). Reciprocal connections between the entorhinal cortex and hippocampal fields CA1 and the subiculum are in register with the projections from CA1 to the subiculum. Hippocampus *11*, 99–104.

Nadel, L., and Land, C. (2000). Memory traces revisited. Nat Rev Neurosci *1*, 209–212.

Nakamura, N.H., Flasbeck, V., Maingret, N., Kitsukawa, T., and Sauvage, M.M. (2013). Proximodistal Segregation of Nonspatial Information in CA3: Preferential Recruitment of a Proximal CA3-Distal CA1 Network in Nonspatial Recognition Memory. J Neurosci *33*, 11506–11514.

Nakashiba, T., Young, J.Z., McHugh, T.J., Buhl, D.L., and Tonegawa, S. (2008). Transgenic Inhibition of Synaptic Transmission Reveals Role of CA3 Output in Hippocampal Learning. Science *319*, 1260–1264.

Nakashiba, T., Cushman, J.D., Pelkey, K.A., Renaudineau, S., Buhl, D.L., McHugh, T.J., Barrera, V.R., Chittajallu, R., Iwamoto, K.S., McBain, C.J., et al. (2012). Young Dentate Granule Cells Mediate Pattern Separation, whereas Old Granule Cells Facilitate Pattern Completion. Cell *149*, 188–201.

Nakazawa, K., Quirk, M.C., Chitwood, R.A., Watanabe, M., Yeckel, M.F., Sun, L.D., Kato, A., Carr, C.A., Johnston, D., Wilson, M.A., et al. (2002). Requirement for Hippocampal CA3 NMDA Receptors in Associative Memory Recall. Science *297*, 211–218.

Nakazawa, K., Sun, L.D., Quirk, M.C., Rondi-Reig, L., Wilson, M.A., and Tonegawa, S. (2003). Hippocampal CA3 NMDA Receptors Are Crucial for Memory Acquisition of One-Time Experience. Neuron *38*, 305–315.

Nakazawa, K., McHugh, T.J., Wilson, M.A., and Tonegawa, S. (2004). NMDA receptors, place cells and hippocampal spatial memory. Nat Rev Neurosci *5*, 361–372.

Nakazawa, Y., Pevzner, A., Tanaka, K.Z., and Wiltgen, B.J. (2016). Memory retrieval along the proximodistal axis of CA1. Hippocampus *26*, 1140–1148.

Neunuebel, J.P., and Knierim, J.J. (2014). CA3 Retrieves Coherent Representations from Degraded Input: Direct Evidence for CA3 Pattern Completion and Dentate Gyrus Pattern Separation. Neuron *81*, 416–427.

Nicoll, R.A., and Schmitz, D. (2005). Synaptic plasticity at hippocampal mossy fibre synapses. Nat Rev Neurosci *6*, 863–876.

Ohkawa, N., Saitoh, Y., Suzuki, A., Tsujimura, S., Murayama, E., Kosugi, S., Nishizono, H., Matsuo, M., Takahashi, Y., Nagase, M., et al. (2015). Artificial Association of Pre-stored Information to Generate a Qualitatively New Memory. Cell Reports *11*, 261–269.

O'Keefe, J., and Dostrovsky, J. (1971). The hippocampus as a spatial map. Preliminary evidence from unit activity in the freely-moving rat. Brain Res *34*, 171–175.

O'Keefe, J., and Recce, M.L. (1993). Phase relationship between hippocampal place units and the EEG theta rhythm. Hippocampus *3*, 317–330.

O'Reilly, R.C., and McClelland, J.L. (1994). Hippocampal conjunctive encoding, storage, and recall: Avoiding a trade-off. Hippocampus *4*, 661–682.

Otto, C., Kovalchuk, Y., Wolfer, D.P., Gass, P., Martin, M., Zuschratter, W., Gröne, H.J., Kellendonk, C., Tronche, F., Maldonado, R., et al. (2001). Impairment of Mossy Fiber Long-Term Potentiation and Associative Learning in Pituitary Adenylate Cyclase Activating Polypeptide Type I Receptor-Deficient Mice. J Neurosci *21*, 5520–5527.

Penn, A.C., Zhang, C.L., Georges, F., Royer, L., Breillat, C., Hosy, E., Petersen, J.D., Humeau, Y., and Choquet, D. (2017). Hippocampal LTP and contextual learning require surface diffusion of AMPA receptors. Nature *549*, 384–388.

Pernía-Andrade, A.J., and Jonas, P. (2014). Theta-Gamma-Modulated Synaptic Currents in Hippocampal Granule Cells In Vivo Define a Mechanism for Network Oscillations. Neuron *81*, 140–152.

Pernía-Andrade, A.J., Goswami, S.P., Stickler, Y., Fröbe, U., Schlögl, A., and Jonas, P. (2012). A Deconvolution-Based Method with High Sensitivity and Temporal Resolution for Detection of Spontaneous Synaptic Currents In Vitro and In Vivo. Biophys J *103*, 1429–1439.

Piette, C., Touboul, J., and Venance, L. (2020). Engrams of Fast Learning. Front Cell Neurosci *14*, 575915.

Pignatelli, M., Ryan, T.J., Roy, D.S., Lovett, C., Smith, L.M., Muralidhar, S., and Tonegawa, S. (2019). Engram Cell Excitability State Determines the Efficacy of Memory Retrieval. Neuron *101*, 274-284.e5.

Pike, F.G., Meredith, R.M., Olding, A.W.A., and Paulsen, O. (1999). Postsynaptic bursting is essential for 'Hebbian' induction of associative long-term potentiation at excitatory synapses in rat hippocampus. J Physiology *518*, 571–576.

Plath, N., Ohana, O., Dammermann, B., Errington, M.L., Schmitz, D., Gross, C., Mao, X., Engelsberg, A., Mahlke, C., Welzl, H., et al. (2006). Arc/Arg3.1 Is Essential for the Consolidation of Synaptic Plasticity and Memories. Neuron *52*, 437–444.

Pouille, F., Marin-Burgin, A., Adesnik, H., Atallah, B.V., and Scanziani, M. (2009). Input normalization by global feedforward inhibition expands cortical dynamic range. Nat Neurosci *12*, 1577–1585.

Ramamoorthi, K., Fropf, R., Belfort, G.M., Fitzmaurice, H.L., McKinney, R.M., Neve, R.L., Otto, T., and Lin, Y. (2011). Npas4 Regulates a Transcriptional Program in CA3 Required for Contextual Memory Formation. Science *334*, 1669–1675.

Ramirez, S., Liu, X., Lin, P.-A., Suh, J., Pignatelli, M., Redondo, R.L., Ryan, T.J., and Tonegawa, S. (2013). Creating a False Memory in the Hippocampus. Science *341*, 387–391.

Rebola, N., Carta, M., and Mulle, C. (2017). Operation and plasticity of hippocampal CA3 circuits: implications for memory encoding. Nat Rev Neurosci *18*, 208–220.

Redondo, R.L., Kim, J., Arons, A.L., Ramirez, S., Liu, X., and Tonegawa, S. (2014). Bidirectional switch of the valence associated with a hippocampal contextual memory engram. Nature *513*, 426–430.

Reijmers, L.G., Perkins, B.L., Matsuo, N., and Mayford, M.R. (2007). Localization of a Stable Neural Correlate of Associative Memory. Science *317*, 1230–1233.

Remy, S., and Spruston, N. (2007). Dendritic spikes induce single-burst long-term potentiation. Proc National Acad Sci *104*, 17192–17197.

Ribak, C.E., Seress, L., and Amaral, D.G. (1985). The development, ultrastructure and synaptic connections of the mossy cells of the dentate gyrus. J Neurocytol *14*, 835–857.

Roberts, W.A. (2002). Are Animals Stuck in Time? Psychol Bull *128*, 473–489.

Rolls, E.T. (2007). An attractor network in the hippocampus: Theory and neurophysiology. Learn Memory *14*, 714–731.

Rolls, E.T. (2016). Pattern separation, completion, and categorisation in the hippocampus and neocortex. Neurobiol Learn Mem *129*, 4–28.

Rolls, E.T., Critchley, H.D., and Treves, A. (1996). Representation of olfactory information in the primate orbitofrontal cortex. J Neurophysiol *75*, 1982–1996.

Rolls, E.T., Treves, A., Robertson, R.G., Georges-François, P., and Panzeri, S. (1998). Information About Spatial View in an Ensemble of Primate Hippocampal Cells. J Neurophysiol *79*, 1797–1813.

Routtenberg, A. (2010). Adult learning and remodeling of hippocampal mossy fibers: Unheralded participant in circuitry for long-lasting spatial memory. Hippocampus *20*, 44–45.

Roy, D.S., Arons, A., Mitchell, T.I., Pignatelli, M., Ryan, T.J., and Tonegawa, S. (2016). Memory retrieval by activating engram cells in mouse models of early Alzheimer's disease. Nature *531*, 508–512.

Roy, D.S., Kitamura, T., Okuyama, T., Ogawa, S.K., Sun, C., Obata, Y., Yoshiki, A., and Tonegawa, S. (2017). Distinct Neural Circuits for the Formation and Retrieval of Episodic Memories. Cell *170*, 1000-1012.e19.

Rudy, J.W., and O'Reilly, R.C. (1999). Contextual Fear Conditioning, Conjunctive Representations, Pattern Completion, and the Hippocampus. Behav Neurosci *113*, 867–880.

Ruediger, S., Vittori, C., Bednarek, E., Genoud, C., Strata, P., Sacchetti, B., and Caroni, P. (2011). Learning-related feedforward inhibitory connectivity growth required for memory precision. Nature *473*, 514–518.

Ryan, T.J., Roy, D.S., Pignatelli, M., Arons, A., and Tonegawa, S. (2015). Engram cells retain memory under retrograde amnesia. Science *348*, 1007–1013.

Sachidhanandam, S., Blanchet, C., Jeantet, Y., Cho, Y.H., and Mulle, C. (2009). Kainate Receptors Act as Conditional Amplifiers of Spike Transmission at Hippocampal Mossy Fiber Synapses. J Neurosci *29*, 5000–5008.

Sah, P., and Bekkers, J.M. (1996). Apical Dendritic Location of Slow Afterhyperpolarization Current in Hippocampal Pyramidal Neurons: Implications for the Integration of Long-Term Potentiation. J Neurosci *16*, 4537–4542.

Sakurai, K., Zhao, S., Takatoh, J., Rodriguez, E., Lu, J., Leavitt, A.D., Fu, M., Han, B.-X., and Wang, F. (2016). Capturing and Manipulating Activated Neuronal Ensembles with CANE Delineates a Hypothalamic Social-Fear Circuit. Neuron *92*, 739–753.

Sano, Y., Shobe, J.L., Zhou, M., Huang, S., Shuman, T., Cai, D.J., Golshani, P., Kamata, M., and Silva, A.J. (2014). CREB Regulates Memory Allocation in the Insular Cortex. Curr Biol *24*, 2833–2837.

Scharfman, H.E. (1995). Electrophysiological evidence that dentate hilar mossy cells are excitatory and innervate both granule cells and interneurons. J Neurophysiol *74*, 179–194.

Schilling, K., Luk, D., Morgan, J.I., and Curran, T. (1991). Regulation of a fos-lacZ fusion gene: a paradigm for quantitative analysis of stimulus-transcription coupling. Proc National Acad Sci *88*, 5665–5669.

Schwartzkroin, P.A., and Wester, K. (1975). Long-lasting facilitation of a synaptic potential following tetanization in thein vitro hippocampal slice. Brain Res *89*, 107–119.

Scoville, W.B., and Milner, B. (1957). Loss of recent memory after bilateral hippocampal lesions. J Neurology Neurosurg Psychiatry *20*, 11.

Sekeres, M.J., Neve, R.L., Frankland, P.W., and Josselyn, S.A. (2010). Dorsal hippocampal CREB is both necessary and sufficient for spatial memory. Learn Memory *17*, 280–283.

Seress, L. (1988). Interspecies comparison of the hippocampal formation shows increased emphasis on the regio superior in the Ammon's horn of the human brain. J Für Hirnforschung *29*, 335–340.

Sik, A., Tamamaki, N., and Freund, T.F. (1993). Complete Axon Arborization of a Single CA3 Pyramidal Cell in the Rat Hippocampus, and its Relationship With Postsynaptic Parvalbumin-containing Interneurons. Eur J Neurosci *5*, 1719–1728.

Silva, S.V. da, Haberl, M.G., Zhang, P., Bethge, P., Lemos, C., Gonçalves, N., Gorlewicz, A., Malezieux, M., Gonçalves, F.Q., Grosjean, N., et al. (2016). Early synaptic deficits in the APP/PS1 mouse model of Alzheimer's disease involve neuronal adenosine A2A receptors. Nat Commun *7*, 11915.

Šišková, Z., Justus, D., Kaneko, H., Friedrichs, D., Henneberg, N., Beutel, T., Pitsch, J., Schoch, S., Becker, A., von der Kammer, H., et al. (2014). Dendritic Structural Degeneration Is Functionally Linked to Cellular Hyperexcitability in a Mouse Model of Alzheimer's Disease. Neuron *84*, 1023–1033.

Sjöström, P.J., Turrigiano, G.G., and Nelson, S.B. (2001). Rate, Timing, and Cooperativity Jointly Determine Cortical Synaptic Plasticity. Neuron *32*, 1149–1164.

Soltesz, I., and Losonczy, A. (2018). CA1 pyramidal cell diversity enabling parallel information processing in the hippocampus. Nat Neurosci *21*, 484–493.

Soltesz, I., and Mody, I. (1994). Patch-clamp recordings reveal powerful GABAergic inhibition in dentate hilar neurons. J Neurosci *14*, 2365–2376.

Sørensen, A.T., Cooper, Y.A., Baratta, M.V., Weng, F.-J., Zhang, Y., Ramamoorthi, K., Fropf, R., LaVerriere, E., Xue, J., Young, A., et al. (2016). A robust activity marking system for exploring active neuronal ensembles. Elife *5*, e13918.

Soriano, E., and Frotscher, M. (1994). Mossy cells of the rat fascia dentata are glutamate-immunoreactive. Hippocampus *4*, 65–69.

Sorra, K., and Harris, K. (1993). Occurrence and three-dimensional structure of multiple synapses between individual radiatum axons and their target pyramidal cells in hippocampal area CA1. J Neurosci *13*, 3736–3748.

Spruston, N., Jaffe, D.B., Williams, S.H., and Johnston, D. (1993). Voltage- and space-clamp errors associated with the measurement of electrotonically remote synaptic events. J Neurophysiol *70*, 781–802.

Stefanelli, T., Bertollini, C., Lüscher, C., Muller, D., and Mendez, P. (2016). Hippocampal Somatostatin Interneurons Control the Size of Neuronal Memory Ensembles. Neuron *89*, 1074–1085.

Strange, B.A., Witter, M.P., Lein, E.S., and Moser, E.I. (2014). Functional organization of the hippocampal longitudinal axis. Nat Rev Neurosci *15*, 655–669.

Sun, Q., Srinivas, K.V., Sotayo, A., and Siegelbaum, S.A. (2014). Dendritic Na+ spikes enable cortical input to drive action potential output from hippocampal CA2 pyramidal neurons. Elife *3*, e04551.

Sun, Q., Sotayo, A., Cazzulino, A.S., Snyder, A.M., Denny, C.A., and Siegelbaum, S.A. (2017a). Proximodistal Heterogeneity of Hippocampal CA3 Pyramidal Neuron Intrinsic Properties, Connectivity, and Reactivation during Memory Recall. Neuron *95*, 656-672.e3.

Sun, Q., Sotayo, A., Cazzulino, A.S., Snyder, A.M., Denny, C.A., and Siegelbaum, S.A. (2017b). Proximodistal Heterogeneity of Hippocampal CA3 Pyramidal Neuron Intrinsic Properties, Connectivity, and Reactivation during Memory Recall. Neuron *95*, 656-672.e3.

Sun, X., Bernstein, M.J., Meng, M., Rao, S., Sørensen, A.T., Yao, L., Zhang, X., Anikeeva, P.O., and Lin, Y. (2020). Functionally Distinct Neuronal Ensembles within the Memory Engram. Cell *181*, 410-423.e17.

Takahashi, N., Oertner, T.G., Hegemann, P., and Larkum, M.E. (2016). Active cortical dendrites modulate perception. Science *354*, 1587–1590.

Takeuchi, T., Duszkiewicz, A.J., and Morris, R.G.M. (2014). The synaptic plasticity and memory hypothesis: encoding, storage and persistence. Philosophical Transactions Royal Soc B Biological Sci *369*, 20130288.

Tamamaki, N., and Nojyo, Y. (1995). Preservation of topography in the connections between the subiculum, field CA1, and the entorhinal cortex in rats. J Comp Neurol *353*, 379–390.

Tanaka, K.Z., Pevzner, A., Hamidi, A.B., Nakazawa, Y., Graham, J., and Wiltgen, B.J. (2014). Cortical Representations Are Reinstated by the Hippocampus during Memory Retrieval. Neuron *84*, 347–354.

Tayler, K.K., Tanaka, K.Z., Reijmers, L.G., and Wiltgen, B.J. (2013). Reactivation of Neural Ensembles during the Retrieval of Recent and Remote Memory. Curr Biol *23*, 99–106.

Thompson, L.T., Moyer, J.R., and Disterhoft, J.F. (1996). Transient changes in excitability of rabbit CA3 neurons with a time course appropriate to support memory consolidation. J Neurophysiol *76*, 1836–1849.

Titley, H.K., Brunel, N., and Hansel, C. (2017). Toward a Neurocentric View of Learning. Neuron *95*, 19–32.

Tonegawa, S., Liu, X., Ramirez, S., and Redondo, R. (2015). Memory Engram Cells Have Come of Age. Neuron *87*, 918–931.

Torborg, C.L., Nakashiba, T., Tonegawa, S., and McBain, C.J. (2010). Control of CA3 Output by Feedforward Inhibition Despite Developmental Changes in the Excitation–Inhibition Balance. J Neurosci *30*, 15628–15637.

Treves, A., and Rolls, E.T. (1992). Computational constraints suggest the need for two distinct input systems to the hippocampal CA3 network. Hippocampus *2*, 189–199.

Treves, A., and Rolls, E.T. (1994). Computational analysis of the role of the hippocampus in memory. Hippocampus *4*, 374–391.

Trojanowski, N.F., Bottorff, J., and Turrigiano, G.G. (2020). Activity labeling in vivo using CaMPARI2 reveals intrinsic and synaptic differences between neurons with high and low firing rate set points. Neuron.

Tsukamoto, M., Yasui, T., Yamada, M.K., Nishiyama, N., Matsuki, N., and Ikegaya, Y. (2003). Mossy fibre synaptic NMDA receptors trigger non-hebbian long-term potentiation at entorhino-CA3 synapses in the rat. J Physiology *546*, 665–675.

Tulving, E. (1972). Episodic and Semantic Memory. In Undefined, p.

Tulving, E. (2002). EPISODIC MEMORY: From Mind to Brain. Annu Rev Psychol *53*, 1–25.

Tulving, E., and Markowitsch, H.J. (1998). Episodic and declarative memory: Role of the hippocampus. Hippocampus *8*, 198–204.

Vertes, R.P., and McKenna, J.T. (2000). Collateral projections from the supramammillary nucleus to the medial septum and hippocampus. Synapse *38*, 281–293.

Vetere, G., Tran, L.M., Moberg, S., Steadman, P.E., Restivo, L., Morrison, F.G., Ressler, K.J., Josselyn, S.A., and Frankland, P.W. (2019). Memory formation in the absence of experience. Nat Neurosci *22*, 933–940.

Villarreal, D.M., Gross, A.L., and Derrick, B.E. (2007). Modulation of CA3 Afferent Inputs by Novelty and Theta Rhythm. J Neurosci *27*, 13457–13467.

Vyleta, N.P., and Jonas, P. (2014). Loose Coupling Between Ca^{2+} Channels and Release Sensors at a Plastic Hippocampal Synapse. Science *343*, 665–670.

Vyleta, N.P., Borges-Merjane, C., and Jonas, P. (2016). Plasticity-dependent, full detonation at hippocampal mossy fiber–CA3 pyramidal neuron synapses. Elife *5*, e17977.

Wang, Y., Liu, Y., Wang, L., Tang, W., and Wang, Z. (2018). Silent Synapse Unsilencing in Hippocampal CA1 Neurons for Associative Fear Memory Storage. Cereb Cortex *29*, 4067–4076.

Weiss, C., Weible, A.P., Galvez, R., and Disterhoft, J.F. (2006). Forebrain-Cerebellar Interactions During Learning. Cellscience *3*, 200–230.

Weng, F.-J., Garcia, R.I., Lutzu, S., Alviña, K., Zhang, Y., Dushko, M., Ku, T., Zemoura, K., Rich, D., Garcia-Dominguez, D., et al. (2018). Npas4 Is a Critical Regulator of Learning-Induced Plasticity at Mossy Fiber-CA3 Synapses during Contextual Memory Formation. Neuron *97*, 1137-1152.e5.

Wharton, K.A., Franks, R.G., Kasai, Y., and Crews, S.T. (1994). Control of CNS midline transcription by asymmetric E-box-like elements: similarity to xenobiotic responsive regulation. Dev Camb Engl *120*, 3563–3569.

Williams, S.R., and Mitchell, S.J. (2008). Direct measurement of somatic voltage clamp errors in central neurons. Nat Neurosci *11*, 790–798.

Wittenberg, G.M., and Wang, S.S.-H. (2006). Malleability of Spike-Timing-Dependent Plasticity at the CA3–CA1 Synapse. J Neurosci *26*, 6610–6617.

Witter, M.P., Wouterlood, F.G., Naber, P.A., and Haeften, T.V. (2000). Anatomical Organization of the Parahippocampal-Hippocampal Network. Ann Ny Acad Sci *911*, 1–24.

Yap, E.-L., and Greenberg, M.E. (2018). Activity-Regulated Transcription: Bridging the Gap between Neural Activity and Behavior. Neuron *100*, 330–348.

Yap, E.-L., Pettit, N.L., Davis, C.P., Nagy, M.A., Harmin, D.A., Golden, E., Dagliyan, O., Lin, C., Rudolph, S., Sharma, N., et al. (2020). Bidirectional perisomatic inhibitory plasticity of a Fos neuronal network. Nature 1–7.

Yassa, M.A., and Stark, C.E.L. (2011). Pattern separation in the hippocampus. Trends Neurosci *34*, 515–525.

Yiu, A.P., Mercaldo, V., Yan, C., Richards, B., Rashid, A.J., Hsiang, H.-L.L., Pressey, J., Mahadevan, V., Tran, M.M., Kushner, S.A., et al. (2014). Neurons Are Recruited to a Memory Trace Based on Relative Neuronal Excitability Immediately before Training. Neuron *83*, 722–735.

Zeldenrust, F., Wadman, W.J., and Englitz, B. (2018). Neural Coding With Bursts—Current State and Future Perspectives. Front Comput Neurosc *12*, 48.

Zhou, Y., Won, J., Karlsson, M.G., Zhou, M., Rogerson, T., Balaji, J., Neve, R., Poirazi, P., and Silva, A.J. (2009). CREB regulates excitability and the allocation of memory to subsets of neurons in the amygdala. Nat Neurosci *12*, 1438–1443.

Zolnik, T.A., Sha, F., Johenning, F.W., Schreiter, E.R., Looger, L.L., Larkum, M.E., and Sachdev, R.N.S. (2017). All-optical functional synaptic connectivity mapping in acute brain slices using the calcium integrator CaMPARI. J Physiology *595*, 1465–1477.

Zucca, S., Griguoli, M., Malézieux, M., Grosjean, N., Carta, M., and Mulle, C. (2017). Control of Spike Transfer at Hippocampal Mossy Fiber Synapses In Vivo by GABAA and GABAB Receptor-Mediated Inhibition. J Neurosci *37*, 587–598.

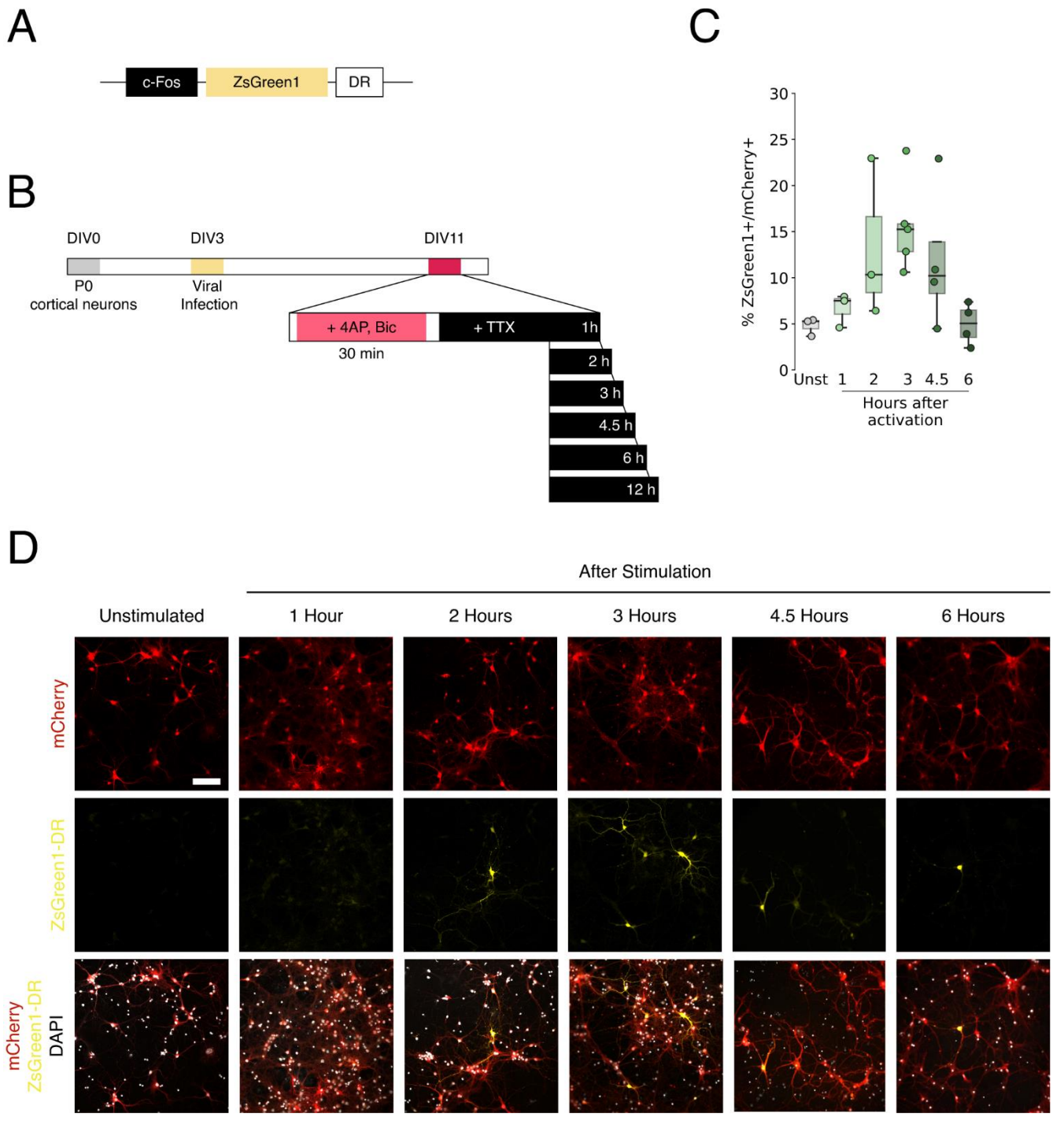
A
c-Fos
ZsGreen1
DR
B
DIV0
DIV3
DIV11
P0
cortical neurons
Viral
Infection
+ 4AP, Bic
30 min
+ TTX
1h
2 h
3 h
4.5 h
6 h
12 h
C
% ZsGreen1+/mCherry+
30
25
20
15
10
5
0
Unst
1
2
3
4.5
6
Hours after
activation
D
After Stimulation
Unstimulated
1 Hour
2 Hours
3 Hours
4.5 Hours
6 Hours
mCherry
ZsGreen1-DR
mCherry
ZsGreen1-DR
DAPI

Figure 1. Construction and validation of c-Fos-ZsGreen1-DR in vitro.

A. FLEN reporter AAV vector.
B. Cultured mouse cortical neurons (~300 000 neurons/well) were infected with the c-Fos-ZsGreen1-DR together with a constitutive mCherry marker on DIV3 and stimulated with an activating medium containing 4-AP and bicuculline (+4AP, Bic) on DIV 11 for 30 minutes. To block further neuronal activity, cells were washed and then incubated in tetrodotoxin-containing medium. Cells were then fixed 1h, 2h, 3h, 4.5h and 6h after activation and compared to unstimulated cells.
C. Quantification of (D). Percentages of mCherry+ neurons that are ZsGreen+ (% ZsGreen1+/mCherry+) are plotted. Unstimulated cells show a low basal activation (4.78% ± 0.56%), and the fraction of labeled cells progressively increases 1 h-post activation (6.68% ± 1.05%), 2 h-post activation (13.26% ± 4.99%) and 3 h-post activation (15.66% ± 2.23%). ZsGreen1-DR labeling then decreases 4.5 h-post activation (11.95% ± 3.90%) and 6 h-post activation (4.97% ± 1.12%). n=3-5 replicates per condition. When comparing basal conditions with 3h post-activation, significance was observed when using t test (p=0.01). With ANOVA, significance was seen (p= 0.044) but post hoc multiple comparison (Dunn's or Tukey's) significance was not observed between pairs.
D. Representative images of cortical neurons in unstimulated and stimulated conditions. DAPI label either neurons or the glial cells on which they were grown on. Neurons are identified by mCherry staining (red), whereas activated neurons are identified by ZsGreen1 expression (yellow). The scale bar is 100 µm and applies to all images.

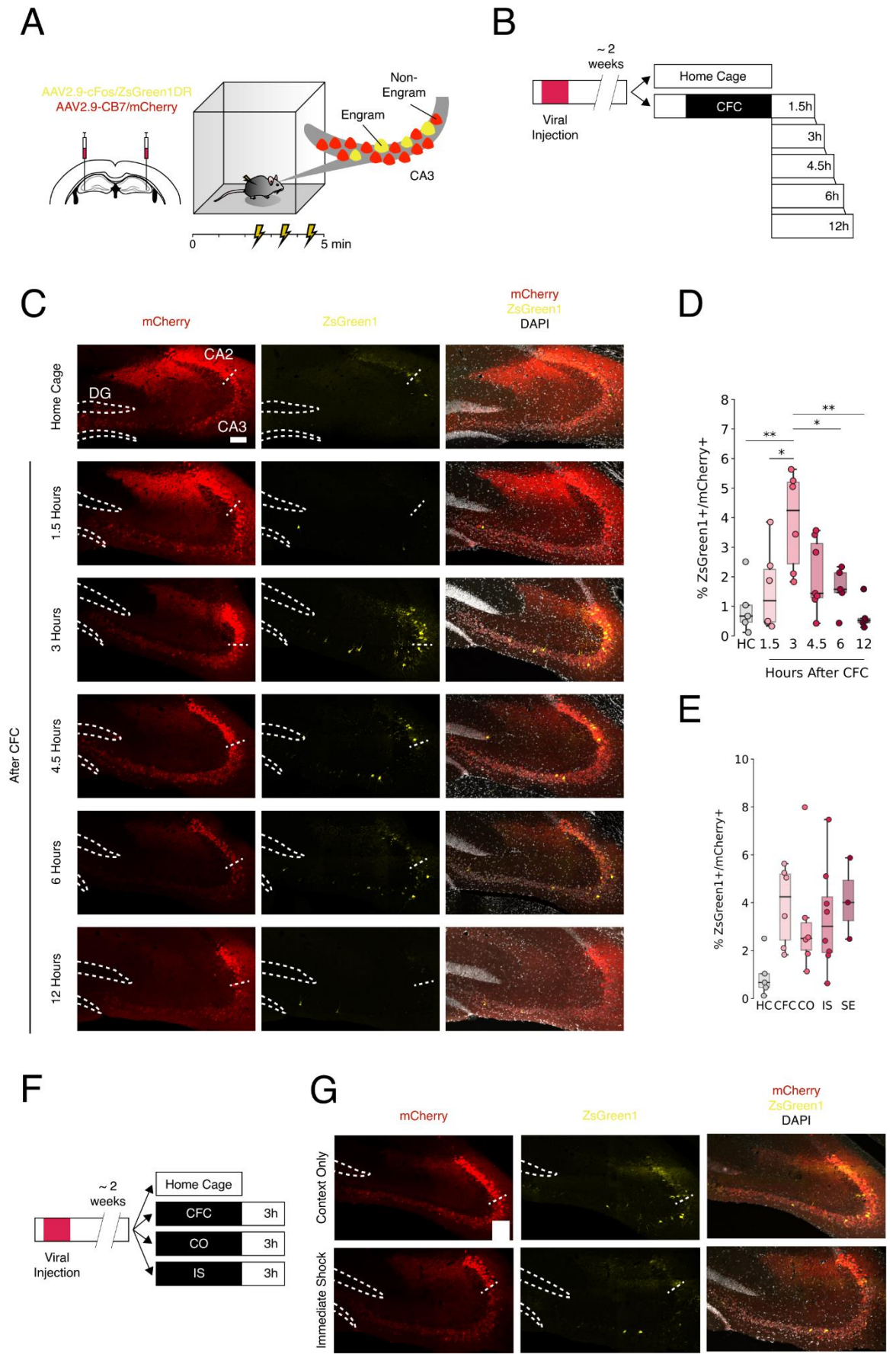
A
AAV2.9-cFos/ZsGreen1DR
AAV2.9-CB7/mCherry
Non-
Engram
Engram
CA3
0
5 min
B
~ 2
weeks
Viral
Injection
Home Cage
CFC
1.5h
3h
4.5h
6h
12h
C
mCherry
ZsGreen1
mCherry
ZsGreen1
DAPI
CA2
DG
CA3
Home Cage
1.5 Hours
3 Hours
4.5 Hours
6 Hours
12 Hours
After CFC
D
% ZsGreen1+/mCherry+
HC 1.5 3 4.5 6 12
Hours After CFC
E
% ZsGreen1+/mCherry+
HC CFC CO IS SE
F
~ 2
weeks
Viral
Injection
Home Cage
CFC 3h
CO 3h
IS 3h
G
mCherry
ZsGreen1
mCherry
ZsGreen1
DAPI
Context Only
Immediate Shock

Figure 2. Characterization of FLEN in vivo.

A. Mice were injected with AAV_9-c-Fos-ZsGreen1-DR and AAV_9-CB7-mCherry targeting CA3b. Then, mice were fear conditioned in a novel context leading to engram formation in CA3 as established by ZsGreen1 expression.
B. Experimental scheme. After injection, mice were allowed to recover for approximately 2 weeks. Mice were then sacrificed either directly from their home cage (unstimulated condition) or at 1.5h, 3h, 4.5h, 6h and 12h intervals after contextual fear conditioning.
C. Representative images of the quantification reported in (D). Total infected neurons are mCherry+, whereas activated cells are ZsGreen1+. DG and the border between CA3 and CA2 are outlined with a dashed white line. The scale bar is 100 μm and applies to all images.
D. Quantification of the percentage of mCherry+ cells that were also ZsGreen1+. HC (home cage) represent the control group of untrained mice (0.96% ± 0.41%). FLEN remain quantitatively low 1.5 hours post-CFC (1.56% ± 0.57%), but it is strikingly increased 3 hours following CFC (3.88% ± 0.68%), 4.5 hours-post CFC (2.04% ± 0.46%) and strat to decay back to basal levels 6 hours-post CFC (1.59% ± 0.33%) and 12 hours-post CFC (0.68% ± 0.23%). n=5-7 mice per condition, p=0.0176 one-way ANOVA, Tukey's post hoc test.
E. Quantification of ZsGreen1+/mCherry+ neurons in mice that undergo context-only (CO) exploration of a novel environment, an immediate-shock (IS) version of CFC and a short-exploration (SE) test compared to HC and 3 hours-post CFC. The fraction of activated cells after CO (3.23% ± 0.99%), IS (3.37% ± 0.77%) and SE (4.12% ± 0.98%) is also similar to that of CFC. n=3-7 per condition.
F. Experimental scheme of different behavioral conditions compared to HC and 3h post-CFC. Mice were sacrifices 3h after the behavior in all conditions.
G. Representative images of (E).

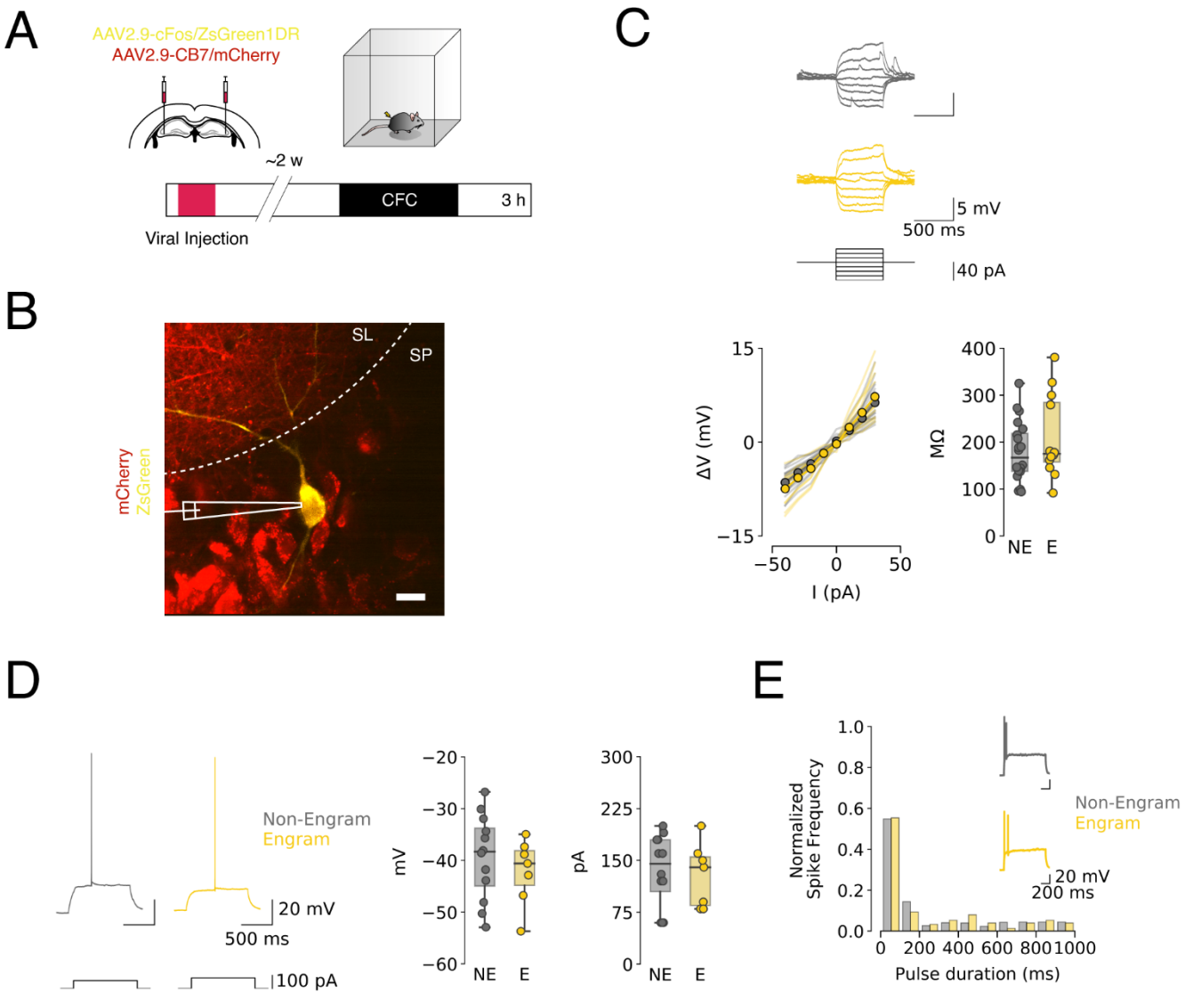
A
AAV2.9-cFos/ZsGreen1DR
AAV2.9-CB7/mCherry
~2 w
CFC
3 h
Viral Injection
B
SL
SP
mCherry
ZsGreen
C
5 mV
500 ms
40 pA
15
0
−15
ΔV (mV)
−50
0
50
I (pA)
400
300
200
100
0
MΩ
NE
E
D
Non-Engram
Engram
20 mV
500 ms
100 pA
−20
−30
−40
−50
−60
mV
NE
E
300
225
150
75
0
pA
NE
E
E
1.0
0.8
0.6
0.4
0.2
0.0
Normalized
Spike Frequency
0
200
400
600
800
1000
Pulse duration (ms)
Non-Engram
Engram
20 mV
200 ms

Figure 3. Intrinsic properties of FLEN neurons.

A. Schematic timeline of the experimental procedure for electrophysiological experiments. After viral infection with AAV-c-Fos-ZsGreen1-DR and AAV-CB7-mCherry in dorsal CA3, mice were subjected to CFC and sacrificed 3h later for acute slice preparation.
B. FLEN+ cells or ZsGreen1-/mCherry+ cells were visually identified and targeted for patch clamp recording. Representative image of FLEN+ patched cell surrounded by not activated control neurons. The border between stratum pyramidale and lucidum is highlighted with the white dashed line. The scale bar is μm.
C. Top: sample traces of subthreshold membrane voltage responses to indicated current injections of engram (yellow) and non-engram (gray) neurons. Bottom: I-V curve. Input resistance was quantified by linearly fitting the voltage change against injected current. NE: 179.596 ± 14.293 MΩ; E: 209.787 ± 25.713 MΩ; t-test p=0.273, n=12-20 neurons per group.
D. Left: sample traces of voltage responses to injected current sufficient to trigger an action potential. Right: quantification of action potential threshold of E (-39.367 ± 2.375 mV) and NE (-42.1473 ±2.405 mV) neurons and rheobase of E (135.0 ± 15.05 pA) and NE (128.571 ± 17.516 pA) neurons. Threshold t-test p= 0.454; Rheobase t-test p=0.791, n=8-12 neurons per group.
E. Action potential firing pattern reveals that both engram (E) and non-engram (NE) CA3 neuron preferentially discharge action potential at the beginning of a current pulse just above the rheobase. Representative traces are shown in the inset. n=12-19 neurons per group.

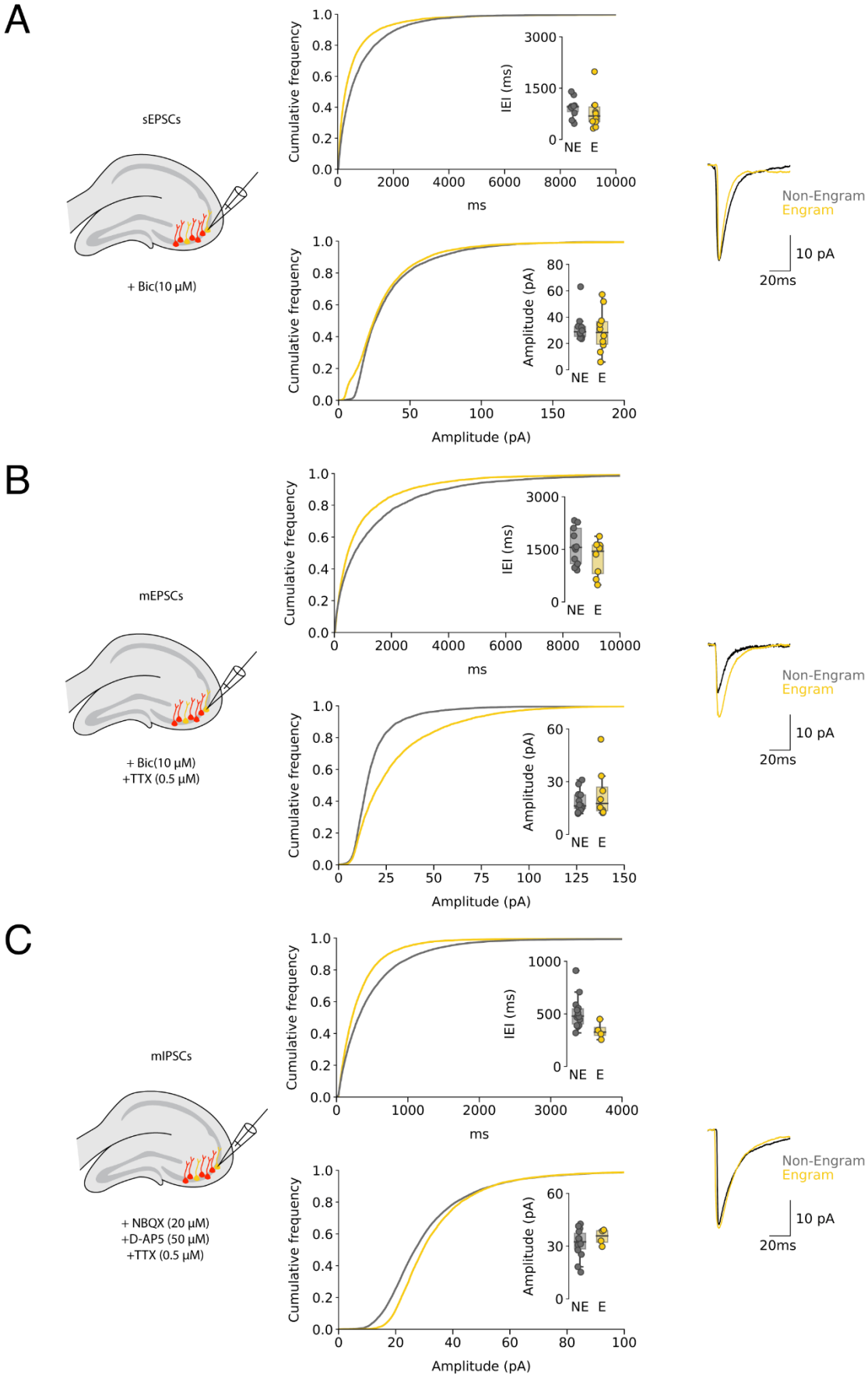
A
sEPSCs
+ Bic(10 μM)
Cumulative frequency
IEI (ms)
NE E
ms
Amplitude (pA)
Non-Engram
Engram
10 pA
20ms
B
mEPSCs
+ Bic(10 μM)
+TTX (0.5 μM)
C
mIPSCs
+ NBQX (20 μM)
+D-AP5 (50 μM)
+TTX (0.5 μM)

Figure 4. Synaptic properties of FLEN neurons.

Excitatory and inhibitory post synaptic currents recordings are represented with cumulative distribution, boxplot and representative cumulative traces recorded from FLEN+ and FLEN- hippocampal CA3 pyramidal neurons.

A. Spontaneous excitatory post-synaptic currents (sEPSCs). Frequency: NE: 1.188 ± 0.142 Hz; E: 1.632 ± 0.25 Hz; t-test p = 0.147. Amplitude: NE, 32.228 ± 3.682 pA; E: 29.667 ± 5.113 pA; n = 10 cells, t-test p = 0.689.
B. Miniature excitatory post-synaptic currents (mEPSCs). Frequency: NE: 0.698 ± 0.073 Hz; E: 0.983 ± 0.197 Hz; t-test p = 0.103. Amplitude: NE, 18.189 ± 1.668 pA; E: 23.226 ± 5.100 pA; n = 8-13 cells, t-test p = 0.308.
C. Miniature inhibitory post-synaptic currents (mEPSCs). Frequency: NE: 1.952 ± 0.140 Hz; E: 3.047 ± 0.348 Hz; t-test p = 0.008. Amplitude: NE, 30.936 ± 2.174 pA; E: 35.148 ± 2.274 pA; n = 4-14 cells, t-test p = 0.435.

A

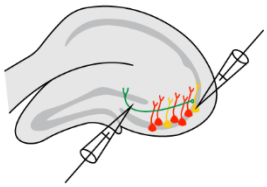

B

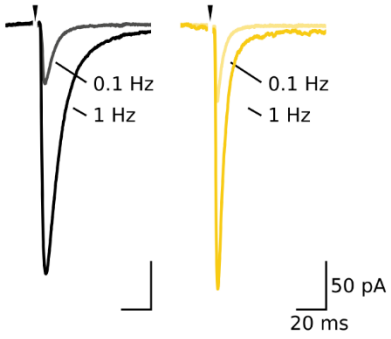
0.1 Hz
1 Hz
0.1 Hz
1 Hz
50 pA
20 ms

C

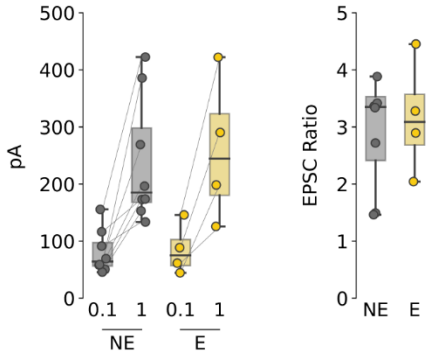
pA
500
400
300
200
100
0
0.1
1
0.1
1
NE
E
EPSC Ratio
5
4
3
2
1
0
NE
E

D

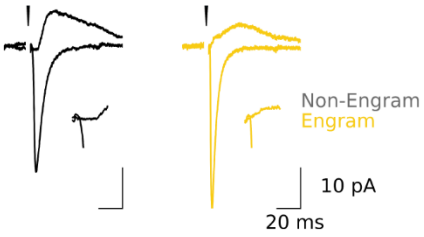
Non-Engram
Engram
10 pA
20 ms

E

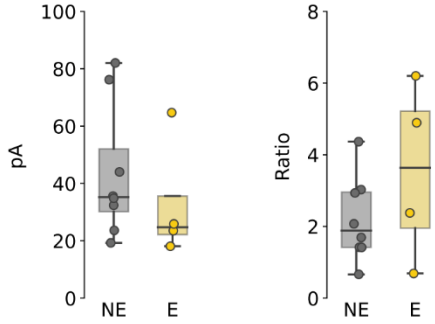
pA
100
80
60
40
20
0
NE
E
Ratio
8
6
4
2
0
NE
E

Figure 5.

A. Schematic representation of Mf stimulation while recording in CA3. The stimulating electrode was placed in the hilus until a response was evoked. Stimulation power was adjusted to achieve Mf minimal stimulation (Marchal and Mulle, 2004).
B. Representative traces of basal and facilitating Mf synaptic inputs onto NE and E CA3 pyramidal cells.
C. Mf-driven excitatory currents were recorded at low frequency for assessing basal transmission in NE (80.748 ± 13.487 pA) and E (85.0836 ± 22.167 pA) CA3 neurons. n=4-8 neurons, t-test p=0.863. All mf-identified currents displayed frequency facilitation when stimulated at 1 Hz in NE (238.230 ± 38.975 pA) and E (259.041 ± 63.900 pA), with a EPSC ratio of NE: 3.277 ± 0.565; E: 3.167 ± 0.500. n=4-8, t-test p=0.904
D. Excitation/inhibition ratio was investigate recording di-synaptic Mf-driven feedforward inhibition, holding the cells at the reversal potential for cations (+5mV). Representative traces of recorded of excitatory and inhibitory currents. The difference in response delay is represented in the inset.
E. Mf-driven inhibitory currents were recorded at +5 mV using a low frequency of stimulation NE (43.487 ± 8.231 pA) and E (33.041 ± 10.674 pA) CA3 neurons. n=4-8 neurons, t-test p=0.470. The excitation/inhibition ratio is NE: 0.648 ±0.046, E: 0.701 ± 0.103. n=4-8, t-test p=0.597.

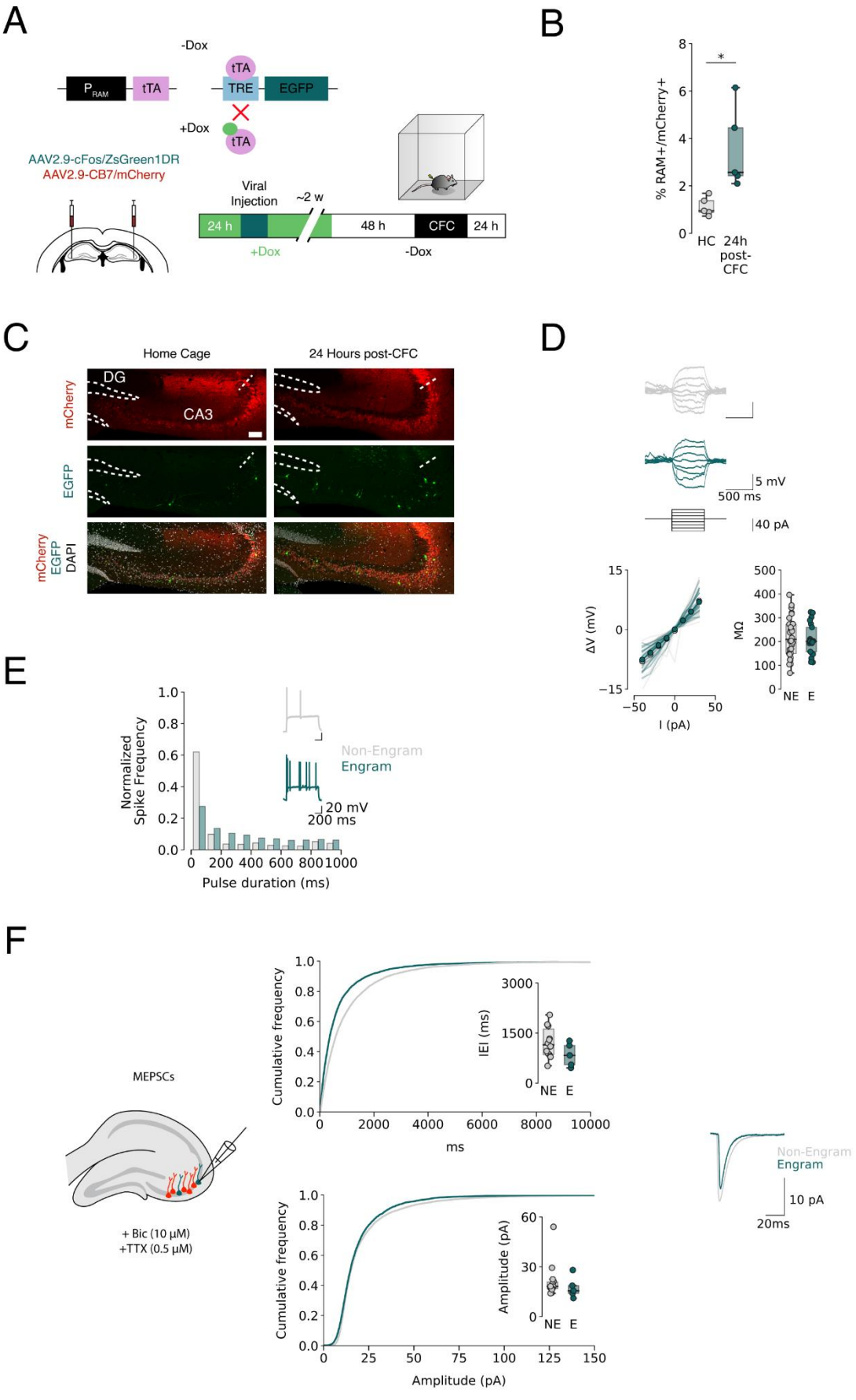
A
-Dox
tTA
P RAM
tTA
TRE
EGFP
+Dox
tTA
AAV2.9-cFos/ZsGreen1DR
AAV2.9-CB7/mCherry
Viral Injection
~2 w
24 h
48 h
CFC
24 h
+Dox
-Dox
B
% RAM+/mCherry+
HC
24h post-CFC
C
Home Cage
24 Hours post-CFC
DG
CA3
mCherry
EGFP
mCherry EGFP DAPI
D
5 mV
500 ms
40 pA
ΔV (mV)
I (pA)
MΩ
NE E
E
Normalized Spike Frequency
Pulse duration (ms)
Non-Engram
Engram
20 mV
200 ms
F
MEPSCs
+ Bic (10 μM)
+TTX (0.5 μM)
Cumulative frequency
ms
IEI (ms)
Amplitude (pA)
Non-Engram
Engram
10 pA
20ms

Figure 6.

A. Schematic representation of the RAM system, with the RAM promoter driving the expression of tTA. tTA in turn bind to the TRE sequence to activate the expression of downstream reporter in absence of doxycycline. Dox-fed mice are injected with AAV_9-RAM-tTA::TRE-EGFP and AAV_9-CB7-mCherry targeting CA3b. Then, mice were Dox deprived and fear conditioned 48 hours later in a novel context (or left in HC conditions) leading to engram formation in CA3. Mice were sacrificed after 24 hours.
B. Quantification of RAM+ cells represented in (C). Control condition leads to labeling of few activated cells, whereas 24h post-CFC RAM-EGFP expression is induced and significantly higher.
C. Representative images of control (HC) and 24 hors post-CFC RAM-based engram labeling. DG and the border between CA3 and CA2 are outlined with a dashed white line. The scale bar is 100 µm and applies to all images.
D. Top: example traces of voltage responses to injected current in RAM labeled cells. Bottom: input resistance calculated for NE (244.189 MΩ ± 15.050) and E 202.493 MΩ ± 14.370) neurons. n=19-30 neurons per group, t-test p=0.702.
E. Distribution of action potential onset within a 1 secon-long pulse of current. Action potential firing pattern reveals that E show prolonged action potential discharge in response to just above rheobase current compared to NE. Representative traces are shown in the inset.
F. Spontaneous excitatory post-synaptic currents (sEPSCs) in RAM+ neurons. Frequency: NE: 0.925867 ± 0.113 Hz; E: 1.263 ± 0.326 Hz; t-test p = 0.089 Amplitude: NE, 21.305 ± 2.721 pA; E: 17.560 ± 2.903 pA; n = 5-14 cells, t-test p = 0.457.

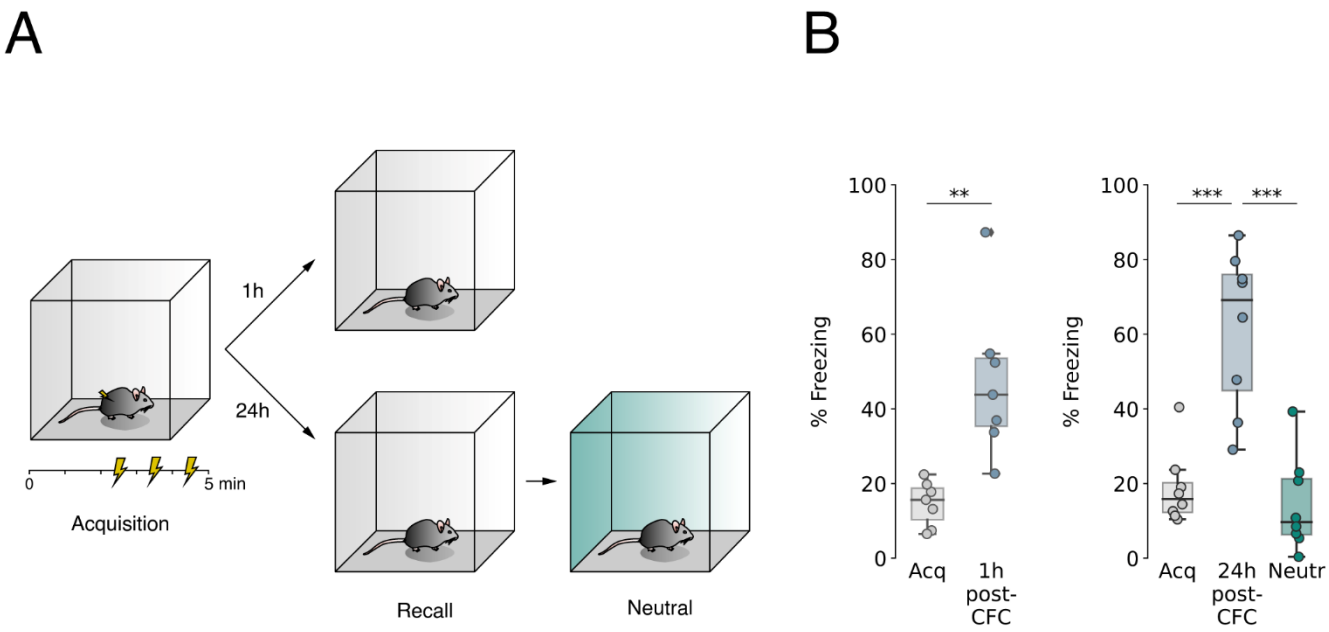
A
1h
24h
0
5 min
Acquisition
Recall
Neutral
B
% Freezing
100
80
60
40
20
0
**
Acq
1h post-CFC
***
***
Acq
24h post-CFC
Neutr

Figure 1S. One-trial contextual fear conditioning rapidly creates a strong memory.

A. Contextual Fear Conditioning (CFC) consist of a one-trial acquisition phase, during which mice explore a novel context. Environmental features (conditioning stimulus) are associated with a series of 3 mild foot-shock (unconditioning stimulus), delivered every 60 seconds after an initial exploration period of 2.5 minutes.
B. This single-time acquisition of episodic-like memories is sufficient to create a strong context specific memory. Mice do not freeze when exposed to a neutral unrelated context, whereas they displayed high levels of freezing when exposed to the conditioning context 1 hour (untrained: 14.68% ± 2.28%, 1h post-CFC: 47.38% ± 7.86%, unpaired t-test, p=0. 0018) or 24 hours post-CFC (untrained: 18.66% ± 3.48%, 24h post-CFC: 61.54% ± 7.52%, neutral: 14.34% ± 4.47%, one-way ANOVA, Tukey's post-hoc test, T1:T2 p =0 .00004, T1:T3 p=0 .84116, T2:T3 p=0 .00001).

A

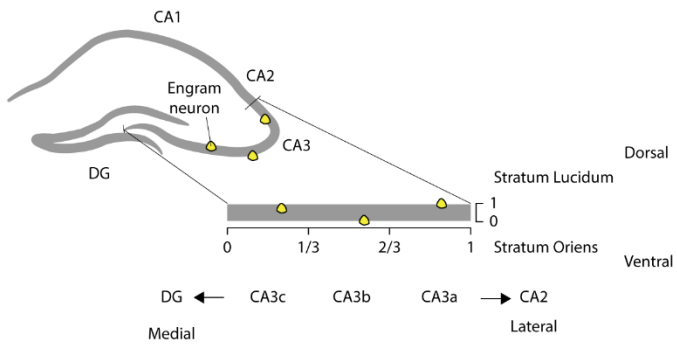
CA1
CA2
Engram neuron
CA3
DG
Dorsal
Stratum Lucidum
1
0
0
1/3
2/3
1
Stratum Oriens
Ventral
DG
CA3c
CA3b
CA3a
CA2
Medial
Lateral

B

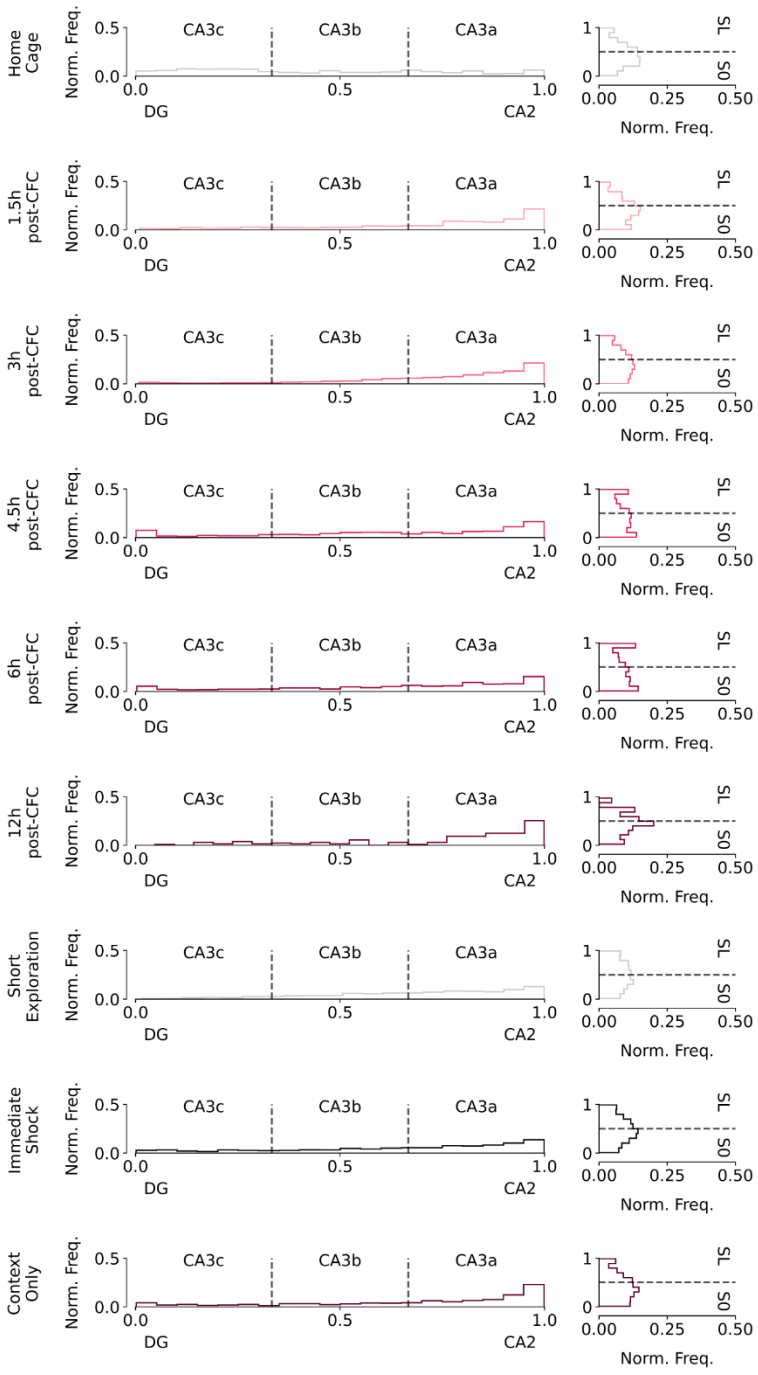
Home Cage
1.5h post-CFC
3h post-CFC
4.5h post-CFC
6h post-CFC
12h post-CFC
Short Exploration
Immediate Shock
Context Only
Norm. Freq.
0.5
0.0
CA3c
CA3b
CA3a
0.0
0.5
1.0
DG
CA2
SL
SO
1
0
0.00
0.25
0.50
Norm. Freq.

Figure 2S. Proximodistal position of FLEN neurons

A. The relative position of FLEN+ neurons from coronal hippocampal sections along the proximodistal axis was scored in a scale from 0 to 1, where 0 lies close to the hippocampus and 1 lies in proximity to CA2. In addition FLEN+ neuron position was scored along the superficial-deep axis, from the *stratum oriens* to the *stratum lucidum*. CA3 was divided in 3 equals third corresponding to CA3a, CA3b and CA3c.
B. Histogram of the normalized frequency of neuronal position according to the proximodistal and the superficial-deep axis of the different groups. Contrarily to the home cage group, where FLEN+ neurons are evenly distributed, all the groups exposed to a contextual exploration showed a marked asymmetry of FLEN+ position. Activated cells appears more abundant in CA3b and CA3a, in proximity to CA2.

Discussion

Investigation of the cellular basis of memory has been strongly reinforced by the availability of strategies to specifically identify and manipulate neuronal engrams in several brain structures. A multitude of IEG-controlled approaches has been developed to label cells, to study their properties and control their reactivation (Josselyn and Tonegawa, 2020; Josselyn et al., 2015), based on the combination of transgenic strategies, optogenetics and pharmacogenetics with behavioral paradigms (Tonegawa et al., 2015). One limitation common to most strategies is that the expression of the fluorescent tag and/or the actuator is not immediate, thus precluding the functional characterization of engram neurons immediately after the execution of a memory task. The period that immediately follows learning is relatively understudied due to these technical limitations and sit in the middle between *in vivo* recordings and current engram labeling strategies. To study recently formed engram cells property, we developed a viral strategy for rapid and transient expression of a fluorescent protein following a one-time short exposure of mice to a novel context. The newly developed c-Fos-ZsGreen1-DR (that we called FLEN) construct is characterized by full-length c-Fos promoter regulation of expression upstream of a bright ZsGreen1 fluorescent protein. To limit neuronal tagging in time and thus avoid out of interest labeling, we fused ZsGreen1 with a domain that targets it for degradation (DR), making it unstable. ZsGreen expression in FLEN labeled neurons peaked at 3 hours both after pharmacological activation in cultured neurons and *in vivo* after a 5-minutes exposure to a novel context. Although FLEN is controlled by full-length c-Fos promoter, it seems that ZsGreen expression does not precisely reflect that of native c-Fos, known to peak between 60- and 90-minutes following activation. This could be due to the fact that AAV vector genomes usually persist in cells as circular episomes, which may be not readily accessible to the translational molecular machinery that physiologically regulates c-Fos-mediated expression.

We have used this tool to label neurons in the CA3 region of the hippocampus, which is involved in the rapid encoding of new spatial and contextual information (Kesner and Rolls, 2015), thanks to the presence of recurrent excitatory connections, which are subject to NMDA-dependent synaptic plasticity (Rebola et al., 2017), essential for memory of a one-trial experience (Nakazawa et al., 2003).

It has been proposed that neurons in the hippocampus and other brain regions are selected to become part of an engram based on their excitability state at the moment of encoding of a novel experience (Disterhoft and Oh, 2006; Sano et al., 2014; Zhou et al., 2009). Therefore, we first examined whether FLEN-labeled neurons showed distinctive intrinsic excitability properties. We observed no difference in the membrane potential, input resistance, rheobase or bursting activity between FLEN-positive and FLEN-negative neurons 3 to 6 hours following CFC. This suggests that the subpopulation of CA3 PNs engaged in one-trial learning task are not initially ore excitable, or alternatively that the enhanced excitability state has passed in the few hours that following the learning task. The first scenario implies that memory allocation in CA3 is not predetermined by PNs excitability state, thus contrasting with previous reports in which memory allocation was biased towards artificially induced more excitable neurons (Lisman et al., 2018; Sano et al., 2014). The second case could support the idea that an engram is formed rapidly and then remain 'silent' in the brain until the memory is replayed (during slow-wave sleep or quiet wakefulness) or recalled for further consolidation. However, the higher excitable state has been reported to persist for long periods after encoding (Cai et al., 2016; Thompson

et al., 1996), and memories of different context can be linked if encoded within a short interval. Beyond the difference in the task and in the species, these contrasting results may be explained by an overall increased activity of CA3 neurons related to the learning task, however not specific to engram neurons. This does not preclude the possibility that relative neuronal excitability immediately before training could contribute to the selection of neurons to an engram as proposed in the amygdala (Yiu et al., 2014), but rather that the memory allocation could be shaped by additional mechanisms such as more efficient and/or synchronous excitatory inputs.

A learning-related task may however induce plasticity of intrinsic excitability of engram neurons on a longer time scale. It has been described that DG neurons show transient higher excitability 24 hours following encoding of CFC, even if only upon memory recall mediated by re-exposure to the conditioning context (Pignatelli et al., 2019). To test the possibility that CA3 engrams build up excitability, we investigated the intrinsic excitability of RAM+ labeled neurons (Sørensen et al., 2016) more than 24 hours after CFC. We observed that RAM+ neurons showed prolonged spike firing in response to a depolarizing pulse of current. This suggests that engram neurons in CA3 progressively acquire increased excitability as compared to neurons which were not activated by the one-trial contextual memory task.

Neurons express c-Fos in response to synaptic activity, it is therefore conceivable that CA3 engram PNs are characterized by increased excitatory inputs. In favor of this interpretation, we observed that FLEN+ neurons showed an increased excitatory drive, a feature that seems to extend to 24 hours post-CFC, which may be explained by a higher number of contacts. However, these contacts do not appear to be more efficient or reinforced, not favoring the hypothesis that LTP -like synaptic plasticity is not a dominant process at this stage of memory encoding. One explanation could be that the higher number of contacts is a pre-existing characteristic of co-active cells that are included in an engram. According to our data, CA3 pyramidal neurons are preferentially activated closer to CA2, where most excitatory inputs are driven mainly by perforant path axons from the entorhinal cortex and recurrent collateral from CA3 rather than MF axons from the DG, and where the dendritic tree is far more extended compared to more proximal CA3 PNs. However, knowing whether CA3 neurons with higher spine density are preselected to become part of an engram is beyond the capabilities defined by the FLEN strategy. Alternatively, increased spine density could depend on learning-induced mechanisms. Formation of new active contacts may be mediated by *de novo* synaptogenesis or unmuting of silent pre-existing synapses (Wang et al., 2018). Formation of synapses at sites where axons and dendrites are close enough to be connected to one another through the outgrowth of a postsynaptic spine or a presynaptic terminal bouton (Chklovskii et al., 2004). Thus, specific neuronal pairs within an assembly may form a higher-than-average number of synapses at shared potential synaptic sites. This does not exclude also the possibility that the two processes may co-exist. In this view, LTP-like processes may appear at later stages to reinforce and stabilized newly formed synapses. Intra-assembly synaptic connectivity between different hippocampal subregion CA3 and CA1) has been reported to be high and enhanced (Choi et al., 2018), although not addressing the hypothesis of pre-existing connectivity.

MF-CA3 synapses have been proposed to be important for memory encoding, by recruiting single CA3 PNs thanks to their conditional 'detonator' behavior, which then become associated with the entorhinal input pattern representing the new information (Treves and Rolls, 1994). However, our data do not suggest increased basal transmission or pre-synaptic plasticity at MF-CA3, suggesting that changes at these synapses might be progressively established.

An important parameter in the transmission of information from the DG to CA3 is feedforward inhibition (FFI), which, combined with short-term plasticity of MF-CA3 synapses, defines the physiological conditions for efficient spike transfer (Henze et al., 2002; Torborg et al., 2010; Zucca et al., 2017). Interestingly, CFC induces a robust increase in the number of interneuron-contacting filopodia emanating from the giant MF terminals, within few hours after the one-trial memory task and is related to the precision of memory and the size of engrams (Ruediger et al., 2011). Although a causal evidence has not been provided, this kind of structural plasticity at has been proposed to increase FFI. In our work, we compared the excitation/inihibition ratio of MF-evoked synaptic responses between FLEN+ and FLEN- neurons. Although this ratio was found to be quite variable (more recordings are in progress), there is a tendency torwards comparatively less FFI in the putative engram neurons. Hence this leads us to hypothetize that shortly following contextual memory formation, MF-driven FFI is increased in the general population of neurons (Ruediger et al., 2011) but not in MF inputs onto engram neurons. A homogeneous FFI across the post-synaptic population of pyramidal cells may be involved in ensuring that threshold excitatory currents increased with stimulus strength, whereas heterogeneities in the distribution of excitatory currents (like a comparative stronger input) in the post-synaptic population can result in selective recruitment of sparse PNs.

Perspectives

The development of a viral tool allowing for the identification of neurons involved in a behavioral task within 3-6 hours appears as an excellent complement to the transgenic mouse strategies and viral vectors which have been used to assess changes in engram neuron properties in the time rage of days (Josselyn and Tonegawa, 2020; Tonegawa et al., 2015).

First of all, the use of a viral approach provides great versatility compared to a transgenic line. This gives the possibility to use this system in combination with transgenic (or with multiple transgene) lines without the need for further crossing, allowing to address functional properties of engram cells in those specific conditions. For instance, multiple transgenic mouse lines can model neurodegenerative diseases, such as APP-PS1 mice are used for Alzheimer's disease (AD) research. AD mice are characterized by memory impairments. A loss of NMDA-dependent LTP at CA3 recurrent collateral, which is crucially involved in the initial encoding of memory, has been observed in early stages of AD in APP-PS1 mice (Silva et al., 2016). In addition, dendritic structural degeneration and hyperexcitability have been observed in CA1 (Šišková et al., 2014). Specific assessment of engram cells properties in AD conditions could provide valuable insights on the deficits that characterized early memory deficits that are not accountable for synaptic degeneration or cellular loss.

Although FLEN do not enable real-time tracking of physiological kinetics of engram cells, it allows identification of neurons involved in a behavioral task within 3-6 hours. This could be useful in situations where *in vivo* recordings are challenging, such as *in vivo* calcium imaging of deep brain regions, or it is important to access intracellular dynamics after an *in vivo* recording.

In addition to complete all the ongoing experiments, further recordings of FLEN+ CA3 PNs are necessary. We believe it would be interesting to interrogate synaptic efficacy at recurrent collaterals of CA3 shortly after CFC and compare E and NE. This specific network is proposed to be crucial in memory encoding (Kesner and Rolls, 2015; Rolls, 2007; Treves and Rolls, 1994), and plasticity at CA3-CA3 synapses allow pattern completion (Nakazawa et al., 2003). Nonetheless, it would be interesting to probe the hypothesis that CA3 cells that are co-active during a behavioral task are also functionally interconnected. It has been suggested that engram cells in CA3 and CA1 are preferentially interconnected following contextual fear conditioning (Choi et al., 2018). Therefore, pairs of activated cells in CA3 could be probed for direct synaptic connections. However, synapses between CA3 cells are extremely sparse, with a proposed probability of connection of 0.92% (Guzman et al., 2016). It cannot be excluded that targeting neurons that show co-activation, for instance using our newly developed FLEN system, may result in an increase in the probability of finding functional pairs. However, a limitation of our approach in this sense is the fact that neurons in acute slices lose part of their dendrites and thus synaptic inputs, so direct connections (especially between neurons farther from each other) may be lost.

As specified before, a morphological analysis would inform us about structural differences between E and NE. In this view, the FLEN system present the limitation that it is not possible to compare single neurons before and after a one-time memory task to directly investigates changes. Any difference observed between E and NE cells following a behavior may be the direct result of learning or a pre-existing condition that biases a certain neuron recruitment in an engram.

References

Amaral, D.G. (1978). A golgi study of cell types in the hilar region of the hippocampus in the rat. J Comp Neurol *182*, 851–914.

Amaral, D.G., and Witter, M.P. (1989). The three-dimensional organization of the hippocampal formation: A review of anatomical data. Neuroscience *31*, 571–591.

Andersen, P., Moser, E., Moser, M.B., and Trommald, M. (1996). Cellular correlates to spatial learning in the rat hippocampus. J Physiology-Paris *90*, 349.

Armstrong, C.M., and Gilly, W.F. (1992). [5] Access resistance and space clamp problems associated with whole-cell patch clamping. Methods Enzymol *207*, 100–122.

Bakker, A., Kirwan, C.B., Miller, M., and Stark, C.E.L. (2008). Pattern Separation in the Human Hippocampal CA3 and Dentate Gyrus. Science *319*, 1640–1642.

Balind, S.R., Magó, Á., Ahmadi, M., Kis, N., Varga-Németh, Z., Lőrincz, A., and Makara, J.K. (2019a). Diverse synaptic and dendritic mechanisms of complex spike burst generation in hippocampal CA3 pyramidal cells. Nat Commun *10*, 1859.

Balind, S.R., Magó, Á., Ahmadi, M., Kis, N., Varga-Németh, Z., Lőrincz, A., and Makara, J.K. (2019b). Diverse synaptic and dendritic mechanisms of complex spike burst generation in hippocampal CA3 pyramidal cells. Nat Commun *10*, 1859.

Bannister, N.J., and Larkman, A.U. (1995). Dendritic morphology of CA1 pyramidal neurones from the rat hippocampus: II. Spine distributions. J Comp Neurol *360*, 161–171.

Bartesaghi, R., and Gessi, T. (2004). Parallel activation of field CA2 and dentate gyrus by synaptically elicited perforant path volleys. Hippocampus *14*, 948–963.

Bartesaghi, R., Migliore, M., and Gessi, T. (2006). Input–output relations in the entorhinal cortex–dentate–hippocampal system: Evidence for a non-linear transfer of signals. Neuroscience *142*, 247–265.

Barth, A.L., Gerkin, R.C., and Dean, K.L. (2004). Alteration of Neuronal Firing Properties after In Vivo Experience in a FosGFP Transgenic Mouse. J Neurosci *24*, 6466–6475.

Bessières, B., Nicole, O., and Bontempi, B. (2017). Assessing recent and remote associative olfactory memory in rats using the social transmission of food preference paradigm. Nat Protoc *12*, 1415–1436.

Bi, G., and Poo, M. (1998). Synaptic Modifications in Cultured Hippocampal Neurons: Dependence on Spike Timing, Synaptic Strength, and Postsynaptic Cell Type. J Neurosci *18*, 10464–10472.

Bito, H., Deisseroth, K., and Tsien, R.W. (1997). Ca2+-dependent regulation in neuronal gene expression. Curr Opin Neurobiol *7*, 419–429.

Bittner, K.C., Milstein, A.D., Grienberger, C., Romani, S., and Magee, J.C. (2017). Behavioral time scale synaptic plasticity underlies CA1 place fields. Science *357*, 1033–1036.

Bliss, T.V.P., and Lømo, T. (1973). Long-lasting potentiation of synaptic transmission in the dentate area of the anaesthetized rabbit following stimulation of the perforant path. J Physiology *232*, 331–356.

Bray, N. (2016). Once upon a recent time. Nat Rev Neurosci *17*, 397–397.

Brown, J.T., and Randall, A.D. (2009). Activity-dependent depression of the spike after-depolarization generates long-lasting intrinsic plasticity in hippocampal CA3 pyramidal neurons. J Physiology *587*, 1265–1281.

Buckmaster, P.S., Wenzel, H.J., Kunkel, D.D., and Schwartzkroin, P.A. (1996). Axon arbors and synaptic connections of hippocampal mossy cells in the rat in vivo. J Comp Neurol *366*, 270–292.

Cai, D.J., Aharoni, D., Shuman, T., Shobe, J., Biane, J., Song, W., Wei, B., Veshkini, M., La-Vu, M., Lou, J., et al. (2016). A shared neural ensemble links distinct contextual memories encoded close in time. Nature *534*, 115–118.

Chevaleyre, V., and Siegelbaum, S.A. (2010). Strong CA2 Pyramidal Neuron Synapses Define a Powerful Disynaptic Cortico-Hippocampal Loop. Neuron *66*, 560–572.

Chklovskii, D.B., Mel, B.W., and Svoboda, K. (2004). Cortical rewiring and information storage. Nature *431*, 782–788.

Choi, J.-H., Sim, S.-E., Kim, J., Choi, D.I., Oh, J., Ye, S., Lee, J., Kim, T., Ko, H.-G., Lim, C.-S., et al. (2018). Interregional synaptic maps among engram cells underlie memory formation. Science *360*, 430–435.

Claiborne, B.J., Amaral, D.G., and Cowan, W.M. (1986). A light and electron microscopic analysis of the mossy fibers of the rat dentate gyrus. J Comp Neurol *246*, 435–458.

Claiborne, B.J., Amaral, D.G., and Cowan, W.M. (1990). Quantitative, three-dimensional analysis of granule cell dendrites in the rat dentate gyrus. J Comp Neurol *302*, 206–219.

Clayton, N.S., and Dickinson, A. (1998). Episodic-like memory during cache recovery by scrub jays. Nature *395*, 272–274.

Clayton, N.S., and Dickinson, A. (1999). Motivational control of caching behaviour in the scrub jay,Aphelocoma coerulescens. Anim Behav *57*, 435–444.

Clayton, N.S., Bussey, T.J., and Dickinson, A. (2003). Can animals recall the past and plan for the future? Nat Rev Neurosci *4*, 685–691.

Daumas, S., Ceccom, J., Halley, H., Francés, B., and Lassalle, J.-M. (2009). Activation of metabotropic glutamate receptor type 2/3 supports the involvement of the hippocampal mossy fiber pathway on contextual fear memory consolidation. Learn Memory *16*, 504–507.

Debanne, D., Gähwiler, B.H., and Thompson, S.M. (1994). Asynchronous pre- and postsynaptic activity induces associative long-term depression in area CA1 of the rat hippocampus in vitro. Proc National Acad Sci *91*, 1148–1152.

Debanne, D., Gähwiler, B.H., and Thompson, S.M. (1997). Bidirectional Associative Plasticity of Unitary CA3-CA1 EPSPs in the Rat Hippocampus In Vitro. J Neurophysiol *77*, 2851–2855.

Denny, C.A., Kheirbek, M.A., Alba, E.L., Tanaka, K.F., Brachman, R.A., Laughman, K.B., Tomm, N.K., Turi, G.F., Losonczy, A., and Hen, R. (2014). Hippocampal Memory Traces Are Differentially Modulated by Experience, Time, and Adult Neurogenesis. Neuron *83*, 189–201.

Deshmukh, S.S., and Knierim, J.J. (2013). Influence of local objects on hippocampal representations: Landmark vectors and memory. Hippocampus *23*, 253–267.

Diamantaki, M., Frey, M., Berens, P., Preston-Ferrer, P., and Burgalossi, A. (2016). Sparse activity of identified dentate granule cells during spatial exploration. Elife *5*, e20252.

Ding, L., Chen, H., Diamantaki, M., Coletta, S., Preston-Ferrer, P., and Burgalossi, A. (2020). Structural Correlates of CA2 and CA3 Pyramidal Cell Activity in Freely-Moving Mice. J Neurosci *40*, 5797–5806.

Disterhoft, J.F., and Oh, M.M. (2006). Learning, aging and intrinsic neuronal plasticity. Trends Neurosci *29*, 587–599.

Do, V.H., Martinez, C.O., Martinez, J.L., and Derrick, B.E. (2002). Long-Term Potentiation in Direct Perforant Path Projections to the Hippocampal CA3 Region In Vivo. J Neurophysiol *87*, 669–678.

Donato, F., Rompani, S.B., and Caroni, P. (2013). Parvalbumin-expressing basket-cell network plasticity induced by experience regulates adult learning. Nature *504*, 272–276.

Dudai, Y., and Eisenberg, M. (2004). Rites of Passage of the Engram Reconsolidation and the Lingering Consolidation Hypothesis. Neuron *44*, 93–100.

Epsztein, J., Brecht, M., and Lee, A.K. (2011). Intracellular Determinants of Hippocampal CA1 Place and Silent Cell Activity in a Novel Environment. Neuron *70*, 109–120.

Faber, E.S.L., Delaney, A.J., and Sah, P. (2005). SK channels regulate excitatory synaptic transmission and plasticity in the lateral amygdala. Nat Neurosci *8*, 635–641.

Feldman, D.E. (2000). Inhibition and plasticity. Nat Neurosci *3*, 303–304.

Fosque, B.F., Sun, Y., Dana, H., Yang, C.-T., Ohyama, T., Tadross, M.R., Patel, R., Zlatic, M., Kim, D.S., Ahrens, M.B., et al. (2015). Labeling of active neural circuits in vivo with designed calcium integrators. Science *347*, 755–760.

Fyhn, M., Molden, S., Witter, M.P., Moser, E.I., and Moser, M.-B. (2004). Spatial Representation in the Entorhinal Cortex. Science *305*, 1258–1264.

Gilbert, P.E., Kesner, R.P., and Lee, I. (2001). Dissociating hippocampal subregions: A double dissociation between dentate gyrus and CA1. Hippocampus *11*, 626–636.

Glazewski, S., Bejar, R., Mayford, M., and Fox, K. (2001). The effect of autonomous alpha-CaMKII expression on sensory responses and experience-dependent plasticity in mouse barrel cortex. Neuropharmacology *41*, 771–778.

Gonzales, R.B., Galvan, C.J.D., Rangel, Y.M., and Claiborne, B.J. (2001). Distribution of thorny excrescences on CA3 pyramidal neurons in the rat hippocampus. J Comp Neurol *430*, 357–368.

Gossen, M., Freundlieb, S., Bender, G., Muller, G., Hillen, W., and Bujard, H. (1995). Transcriptional activation by tetracyclines in mammalian cells. Science *268*, 1766–1769.

Gouty-Colomer, L.A., Hosseini, B., Marcelo, I.M., Schreiber, J., Slump, D.E., Yamaguchi, S., Houweling, A.R., Jaarsma, D., Elgersma, Y., and Kushner, S.A. (2016). Arc expression identifies the lateral amygdala fear memory trace. Mol Psychiatr *21*, 364–375.

Guenthner, C.J., Miyamichi, K., Yang, H.H., Heller, H.C., and Luo, L. (2013). Permanent Genetic Access to Transiently Active Neurons via TRAP: Targeted Recombination in Active Populations. Neuron *78*, 773–784.

Gulyás, A.I., Hájos, N., and Freund, T.F. (1996). Interneurons Containing Calretinin Are Specialized to Control Other Interneurons in the Rat Hippocampus. J Neurosci *16*, 3397–3411.

Guzman, S.J., Schlögl, A., Frotscher, M., and Jonas, P. (2016). Synaptic mechanisms of pattern completion in the hippocampal CA3 network. Science.

Guzowski, J.F., Knierim, J.J., and Moser, E.I. (2004). Ensemble Dynamics of Hippocampal Regions CA3 and CA1. Neuron *44*, 581–584.

Hagena, H., and Manahan-Vaughan, D. (2011). Learning-Facilitated Synaptic Plasticity at CA3 Mossy Fiber and Commissural–Associational Synapses Reveals Different Roles in Information Processing. Cereb Cortex *21*, 2442–2449.

Hainmueller, T., and Bartos, M. (2018a). Parallel emergence of stable and dynamic memory engrams in the hippocampus. Nature *558*, 292–296.

Hainmueller, T., and Bartos, M. (2018b). Parallel emergence of stable and dynamic memory engrams in the hippocampus. Nature *558*, 292–296.

Hainmueller, T., and Bartos, M. (2020). Dentate gyrus circuits for encoding, retrieval and discrimination of episodic memories. Nat Rev Neurosci *21*, 153–168.

Hájos, N., Pálhalmi, J., Mann, E.O., Németh, B., Paulsen, O., and Freund, T.F. (2004). Spike Timing of Distinct Types of GABAergic Interneuron during Hippocampal Gamma Oscillations In Vitro. J Neurosci *24*, 9127–9137.

Hallermann, S., Pawlu, C., Jonas, P., and Heckmann, M. (2003). A large pool of releasable vesicles in a cortical glutamatergic synapse. Proc National Acad Sci *100*, 8975–8980.

Han, J.-H., Kushner, S.A., Yiu, A.P., Cole, C.J., Matynia, A., Brown, R.A., Neve, R.L., Guzowski, J.F., Silva, A.J., and Josselyn, S.A. (2007). Neuronal Competition and Selection During Memory Formation. Science *316*, 457–460.

Han, J.-H., Kushner, S.A., Yiu, A.P., Hsiang, H.-L. (Liz), Buch, T., Waisman, A., Bontempi, B., Neve, R.L., Frankland, P.W., and Josselyn, S.A. (2009). Selective Erasure of a Fear Memory. Science *323*, 1492–1496.

Hargreaves, E.L., Rao, G., Lee, I., and Knierim, J.J. (2005). Major Dissociation Between Medial and Lateral Entorhinal Input to Dorsal Hippocampus. Science *308*, 1792–1794.

Hasselmo, M.E., and Wyble, B.P. (1997). Free recall and recognition in a network model of the hippocampus: simulating effects of scopolamine on human memory function. Behav Brain Res *89*, 1–34.

Helton, T.D., Zhao, M., Farris, S., and Dudek, S.M. (2019). Diversity of dendritic morphology and entorhinal cortex synaptic effectiveness in mouse CA2 pyramidal neurons. Hippocampus *29*, 78–92.

Henze, D.A., Urban, N.N., and Barrionuevo, G. (2000). The multifarious hippocampal mossy fiber pathway: a review. Neuroscience *98*, 407–427.

Henze, D.A., McMahon, D.B.T., Harris, K.M., and Barrionuevo, G. (2002). Giant Miniature EPSCs at the Hippocampal Mossy Fiber to CA3 Pyramidal Cell Synapse Are Monoquantal. J Neurophysiol *87*, 15–29.

Hitti, F.L., and Siegelbaum, S.A. (2014). The hippocampal CA2 region is essential for social memory. Nature *508*, 88–92.

Holtmaat, A., and Caroni, P. (2016). Functional and structural underpinnings of neuronal assembly formation in learning. Nat Neurosci *19*, 1553–1562.

Hsiang, H.-L. (Liz), Epp, J.R., Oever, M.C. van den, Yan, C., Rashid, A.J., Insel, N., Ye, L., Niibori, Y., Deisseroth, K., Frankland, P.W., et al. (2014). Manipulating a "Cocaine Engram" in Mice. J Neurosci *34*, 14115–14127.

Hsu, T.-T., Lee, C.-T., Tai, M.-H., and Lien, C.-C. (2016). Differential Recruitment of Dentate Gyrus Interneuron Types by Commissural Versus Perforant Pathways. Cereb Cortex *26*, 2715–2727.

Hunt, D.L., Linaro, D., Si, B., Romani, S., and Spruston, N. (2018a). A novel pyramidal cell type promotes sharp-wave synchronization in the hippocampus. Nat Neurosci *21*, 985–995.

Hunt, D.L., Linaro, D., Si, B., Romani, S., and Spruston, N. (2018b). A novel pyramidal cell type promotes sharp-wave synchronization in the hippocampus. Nat Neurosci *21*, 985–995.

Igarashi, K.M., Ito, H.T., Moser, E.I., and Moser, M.-B. (2014). Functional diversity along the transverse axis of hippocampal area CA1. Febs Lett *588*, 2470–2476.

Ishizuka, N., Weber, J., and Amaral, D.G. (1990). Organization of intrahippocampal projections originating from CA3 pyramidal cells in the rat. J Comp Neurol *295*, 580–623.

Ishizuka, N., Cowan, W.M., and Amaral, D.G. (1995a). A quantitative analysis of the dendritic organization of pyramidal cells in the rat hippocampus. J Comp Neurol *362*, 17–45.

Ishizuka, N., Cowan, W.M., and Amaral, D.G. (1995b). A quantitative analysis of the dendritic organization of pyramidal cells in the rat hippocampus. J Comp Neurol *362*, 17–45.

Ito, H.T., and Schuman, E.M. (2012). Functional division of hippocampal area CA1 via modulatory gating of entorhinal cortical inputs. Hippocampus *22*, 372–387.

Jarsky, T., Mady, R., Kennedy, B., and Spruston, N. (2008). Distribution of bursting neurons in the CA1 region and the subiculum of the rat hippocampus. J Comp Neurol *506*, 535–547.

Josselyn, S.A., and Tonegawa, S. (2020). Memory engrams: Recalling the past and imagining the future. Science *367*, eaaw4325.

Josselyn, S.A., Köhler, S., and Frankland, P.W. (2015). Finding the engram. Nat Rev Neurosci *16*, 521–534.

Kawashima, T., Okuno, H., Nonaka, M., Adachi-Morishima, A., Kyo, N., Okamura, M., Takemoto-Kimura, S., Worley, P.F., and Bito, H. (2009). Synaptic activity-responsive element

in the Arc/Arg3.1 promoter essential for synapse-to-nucleus signaling in activated neurons. Proc National Acad Sci *106*, 316–321.

Kawashima, T., Kitamura, K., Suzuki, K., Nonaka, M., Kamijo, S., Takemoto-Kimura, S., Kano, M., Okuno, H., Ohki, K., and Bito, H. (2013). Functional labeling of neurons and their projections using the synthetic activity–dependent promoter E-SARE. Nat Methods *10*, 889–895.

Kesner, R.P. (2007). Behavioral functions of the CA3 subregion of the hippocampus. Learn Memory *14*, 771–781.

Kesner, R.P., and Rolls, E.T. (2015). A computational theory of hippocampal function, and tests of the theory: New developments. Neurosci Biobehav Rev *48*, 92–147.

Kim, S., Guzman, S.J., Hu, H., and Jonas, P. (2012). Active dendrites support efficient initiation of dendritic spikes in hippocampal CA3 pyramidal neurons. Nat Neurosci *15*, 600–606.

Kitamura, T., Ogawa, S.K., Roy, D.S., Okuyama, T., Morrissey, M.D., Smith, L.M., Redondo, R.L., and Tonegawa, S. (2017). Engrams and circuits crucial for systems consolidation of a memory. Science *356*, 73–78.

Klausberger, T., Magill, P.J., Márton, L.F., Roberts, J.D.B., Cobden, P.M., Buzsáki, G., and Somogyi, P. (2003). Brain-state- and cell-type-specific firing of hippocampal interneurons in vivo. Nature *421*, 844–848.

Kleindienst, T., and Lohmann, C. (2014). Simultaneous Patch-Clamping and Calcium Imaging in Developing Dendrites. Cold Spring Harb Protoc *2014*, pdb.prot080390-pdb.prot080390.

Knierim, J.J., and Neunuebel, J.P. (2016). Tracking the flow of hippocampal computation: Pattern separation, pattern completion, and attractor dynamics. Neurobiol Learn Mem *129*, 38–49.

Kobayashi, K., and Poo, M. (2004). Spike Train Timing-Dependent Associative Modification of Hippocampal CA3 Recurrent Synapses by Mossy Fibers. Neuron *41*, 445–454.

Koya, E., Golden, S.A., Harvey, B.K., Guez-Barber, D.H., Berkow, A., Simmons, D.E., Bossert, J.M., Nair, S.G., Uejima, J.L., Marin, M.T., et al. (2009). Targeted disruption of cocaine-activated nucleus accumbens neurons prevents context-specific sensitization. Nat Neurosci *12*, 1069–1073.

Krahe, R., and Gabbiani, F. (2004). Burst firing in sensory systems. Nat Rev Neurosci *5*, 13–23.

Lacagnina, A.F., Brockway, E.T., Crovetti, C.R., Shue, F., McCarty, M.J., Sattler, K.P., Lim, S.C., Santos, S.L., Denny, C.A., and Drew, M.R. (2019). Distinct hippocampal engrams control extinction and relapse of fear memory. Nat Neurosci *22*, 753–761.

Lammel, S., Lim, B.K., Ran, C., Huang, K.W., Betley, M.J., Tye, K.M., Deisseroth, K., and Malenka, R.C. (2012). Input-specific control of reward and aversion in the ventral tegmental area. Nature *491*, 212–217.

Lanore, F., Labrousse, V.F., Szabo, Z., Normand, E., Blanchet, C., and Mulle, C. (2012). Deficits in Morphofunctional Maturation of Hippocampal Mossy Fiber Synapses in a Mouse Model of Intellectual Disability. J Neurosci *32*, 17882–17893.

Lassalle, J.-M., Bataille, T., and Halley, H. (2000). Reversible Inactivation of the Hippocampal Mossy Fiber Synapses in Mice Impairs Spatial Learning, but neither Consolidation nor Memory Retrieval, in the Morris Navigation Task. Neurobiol Learn Mem *73*, 243–257.

Laurberg, S., and Sørensen, K.E. (1981). Associational and commissural collaterals of neurons in the hippocampal formation (Hilus fasciae dentatae and subfield CA3). Brain Res *212*, 287–300.

Lee, I., and Kesner, R.P. (2004). Differential contributions of dorsal hippocampal subregions to memory acquisition and retrieval in contextual fear-conditioning. Hippocampus *14*, 301–310.

Lee, D., Hyun, J.H., Jung, K., Hannan, P., and Kwon, H.-B. (2017a). A calcium- and light-gated switch to induce gene expression in activated neurons. Nat Biotechnol *35*, 858–863.

Lee, D., Creed, M., Jung, K., Stefanelli, T., Wendler, D.J., Oh, W.C., Mignocchi, N.L., Lüscher, C., and Kwon, H.-B. (2017b). Temporally precise labeling and control of neuromodulatory circuits in the mammalian brain. Nat Methods *14*, 495–503.

Lee, S.-H., Kwan, A.C., and Dan, Y. (2014). Interneuron subtypes and orientation tuning. Nature *508*, E1–E2.

Leroy, F., Brann, D.H., Meira, T., and Siegelbaum, S.A. (2017). Input-Timing-Dependent Plasticity in the Hippocampal CA2 Region and Its Potential Role in Social Memory. Neuron *95*, 1089-1102.e5.

Leutgeb, J.K., Leutgeb, S., Moser, M.-B., and Moser, E.I. (2007). Pattern Separation in the Dentate Gyrus and CA3 of the Hippocampus. Science *315*, 961–966.

Levy, W.B., and Steward, O. (1983). Temporal contiguity requirements for long-term associative potentiation/depression in the hippocampus. Neuroscience *8*, 791–797.

Lin, Y., Bloodgood, B.L., Hauser, J.L., Lapan, A.D., Koon, A.C., Kim, T.-K., Hu, L.S., Malik, A.N., and Greenberg, M.E. (2008). Activity-dependent regulation of inhibitory synapse development by Npas4. Nature *455*, 1198–1204.

Link, W.T., Grant, P., Hidaka, H., and Pant, H.C. (1992). Casein kinases I and II from squid brain exhibit selective neurofilament phosphorylation. Mol Cell Neurosci *3*, 548–558.

Lisman, J., Cooper, K., Sehgal, M., and Silva, A.J. (2018). Memory formation depends on both synapse-specific modifications of synaptic strength and cell-specific increases in excitability. Nat Neurosci *21*, 309–314.

Liu, X., Ramirez, S., Pang, P.T., Puryear, C.B., Govindarajan, A., Deisseroth, K., and Tonegawa, S. (2012). Optogenetic stimulation of a hippocampal engram activates fear memory recall. Nature *484*, 381–385.

Liu, X., Ramirez, S., Redondo, R.L., and Tonegawa, S. (2014a). Identification and Manipulation of Memory Engram Cells. Cold Spring Harb Sym *79*, 59–65.

Liu, X., Ramirez, S., and Tonegawa, S. (2014b). Inception of a false memory by optogenetic manipulation of a hippocampal memory engram. Philosophical Transactions Royal Soc B Biological Sci *369*, 20130142.

Lyford, G.L., Yamagata, K., Kaufmann, W.E., Barnes, C.A., Sanders, L.K., Copeland, N.G., Gilbert, D.J., Jenkins, N.A., Lanahan, A.A., and Worley, P.F. (1995). Arc, a growth factor and activity-regulated gene, encodes a novel cytoskeleton-associated protein that is enriched in neuronal dendrites. Neuron *14*, 433–445.

Makara, J.K., and Magee, J.C. (2013). Variable Dendritic Integration in Hippocampal CA3 Pyramidal Neurons. Neuron *80*, 1438–1450.

Malezieux, M., Kees, A.L., and Mulle, C. (2020). Theta Oscillations Coincide with Sustained Hyperpolarization in CA3 Pyramidal Cells, Underlying Decreased Firing. Cell Reports *32*, 107868.

Malinow, R., and Malenka, R.C. (2002). AMPA RECEPTOR TRAFFICKING AND SYNAPTIC PLASTICITY. Neuroscience *25*, 103–126.

Markram, H., Lübke, J., Frotscher, M., and Sakmann, B. (1997). Regulation of Synaptic Efficacy by Coincidence of Postsynaptic APs and EPSPs. Science *275*, 213–215.

Marr, D. (1971). Simple memory: a theory for archicortex. Philosophical Transactions Royal Soc Lond B Biological Sci *262*, 23–81.

McBain, C.J., and Fisahn, A. (2001). Interneurons unbound. Nat Rev Neurosci *2*, 11–23.

McClelland, J.L., and Goddard, N.H. (1996). Considerations arising from a complementary learning systems perspective on hippocampus and neocortex. Hippocampus *6*, 654–665.

McClelland, J.L., McNaughton, B.L., and O'Reilly, R.C. (1995). Why There Are Complementary Learning Systems in the Hippocampus and Neocortex: Insights From the Successes and Failures of Connectionist Models of Learning and Memory. Psychol Rev *102*, 419–457.

McHugh, T.J., and Tonegawa, S. (2009). CA3 NMDA receptors are required for the rapid formation of a salient contextual representation. Hippocampus *19*, 1153–1158.

McHugh, T.J., Jones, M.W., Quinn, J.J., Balthasar, N., Coppari, R., Elmquist, J.K., Lowell, B.B., Fanselow, M.S., Wilson, M.A., and Tonegawa, S. (2007). Dentate Gyrus NMDA Receptors Mediate Rapid Pattern Separation in the Hippocampal Network. Science *317*, 94–99.

McKay, B.M., Matthews, E.A., Oliveira, F.A., and Disterhoft, J.F. (2009). Intrinsic Neuronal Excitability Is Reversibly Altered by a Single Experience in Fear Conditioning. J Neurophysiol *102*, 2763–2770.

McMahon, D.B.T., and Barrionuevo, G. (2002). Short- and Long-Term Plasticity of the Perforant Path Synapse in Hippocampal Area CA3. J Neurophysiol *88*, 528–533.

McNaughton, B.L., and Morris, R.G.M. (1987). Hippocampal synaptic enhancement and information storage within a distributed memory system. Trends Neurosci *10*, 408–415.

Mehta, M.R., Quirk, M.C., and Wilson, M.A. (2000). Experience-Dependent Asymmetric Shape of Hippocampal Receptive Fields. Neuron *25*, 707–715.

Middleton, S.J., and McHugh, T.J. (2016). Silencing CA3 disrupts temporal coding in the CA1 ensemble. Nat Neurosci *19*, 945–951.

Mishra, R.K., Kim, S., Guzman, S.J., and Jonas, P. (2016). Symmetric spike timing-dependent plasticity at CA3–CA3 synapses optimizes storage and recall in autoassociative networks. Nat Commun *7*, 11552.

Mizuseki, K., Royer, S., Diba, K., and Buzsáki, G. (2012). Activity dynamics and behavioral correlates of CA3 and CA1 hippocampal pyramidal neurons. Hippocampus *22*, 1659–1680.

Moeyaert, B., Holt, G., Madangopal, R., Perez-Alvarez, A., Fearey, B.C., Trojanowski, N.F., Ledderose, J., Zolnik, T.A., Das, A., Patel, D., et al. (2018). Improved methods for marking active neuron populations. Nat Commun *9*, 4440.

Moyer, J.R., Thompson, L.T., and Disterhoft, J.F. (1996). Trace Eyeblink Conditioning Increases CA1 Excitability in a Transient and Learning-Specific Manner. J Neurosci *16*, 5536–5546.

Naber, P.A., Silva, F.H.L. da, and Witter, M.P. (2001). Reciprocal connections between the entorhinal cortex and hippocampal fields CA1 and the subiculum are in register with the projections from CA1 to the subiculum. Hippocampus *11*, 99–104.

Nadel, L., and Land, C. (2000). Memory traces revisited. Nat Rev Neurosci *1*, 209–212.

Nakashiba, T., Young, J.Z., McHugh, T.J., Buhl, D.L., and Tonegawa, S. (2008). Transgenic Inhibition of Synaptic Transmission Reveals Role of CA3 Output in Hippocampal Learning. Science *319*, 1260–1264.

Nakashiba, T., Cushman, J.D., Pelkey, K.A., Renaudineau, S., Buhl, D.L., McHugh, T.J., Barrera, V.R., Chittajallu, R., Iwamoto, K.S., McBain, C.J., et al. (2012). Young Dentate Granule Cells Mediate Pattern Separation, whereas Old Granule Cells Facilitate Pattern Completion. Cell *149*, 188–201.

Nakazawa, K., Quirk, M.C., Chitwood, R.A., Watanabe, M., Yeckel, M.F., Sun, L.D., Kato, A., Carr, C.A., Johnston, D., Wilson, M.A., et al. (2002). Requirement for Hippocampal CA3 NMDA Receptors in Associative Memory Recall. Science *297*, 211–218.

Nakazawa, K., Sun, L.D., Quirk, M.C., Rondi-Reig, L., Wilson, M.A., and Tonegawa, S. (2003). Hippocampal CA3 NMDA Receptors Are Crucial for Memory Acquisition of One-Time Experience. Neuron *38*, 305–315.

Nakazawa, K., McHugh, T.J., Wilson, M.A., and Tonegawa, S. (2004). NMDA receptors, place cells and hippocampal spatial memory. Nat Rev Neurosci *5*, 361–372.

Nakazawa, Y., Pevzner, A., Tanaka, K.Z., and Wiltgen, B.J. (2016). Memory retrieval along the proximodistal axis of CA1. Hippocampus *26*, 1140–1148.

Neunuebel, J.P., and Knierim, J.J. (2014). CA3 Retrieves Coherent Representations from Degraded Input: Direct Evidence for CA3 Pattern Completion and Dentate Gyrus Pattern Separation. Neuron *81*, 416–427.

Nicoll, R.A., and Schmitz, D. (2005). Synaptic plasticity at hippocampal mossy fibre synapses. Nat Rev Neurosci *6*, 863–876.

Ohkawa, N., Saitoh, Y., Suzuki, A., Tsujimura, S., Murayama, E., Kosugi, S., Nishizono, H., Matsuo, M., Takahashi, Y., Nagase, M., et al. (2015). Artificial Association of Pre-stored Information to Generate a Qualitatively New Memory. Cell Reports *11*, 261–269.

O'Keefe, J., and Dostrovsky, J. (1971). The hippocampus as a spatial map. Preliminary evidence from unit activity in the freely-moving rat. Brain Res *34*, 171–175.

O'Keefe, J., and Recce, M.L. (1993). Phase relationship between hippocampal place units and the EEG theta rhythm. Hippocampus *3*, 317–330.

O'Reilly, R.C., and McClelland, J.L. (1994). Hippocampal conjunctive encoding, storage, and recall: Avoiding a trade-off. Hippocampus *4*, 661–682.

Otto, C., Kovalchuk, Y., Wolfer, D.P., Gass, P., Martin, M., Zuschratter, W., Gröne, H.J., Kellendonk, C., Tronche, F., Maldonado, R., et al. (2001). Impairment of Mossy Fiber Long-Term Potentiation and Associative Learning in Pituitary Adenylate Cyclase Activating Polypeptide Type I Receptor-Deficient Mice. J Neurosci *21*, 5520–5527.

Penn, A.C., Zhang, C.L., Georges, F., Royer, L., Breillat, C., Hosy, E., Petersen, J.D., Humeau, Y., and Choquet, D. (2017). Hippocampal LTP and contextual learning require surface diffusion of AMPA receptors. Nature *549*, 384–388.

Pernía-Andrade, A.J., and Jonas, P. (2014). Theta-Gamma-Modulated Synaptic Currents in Hippocampal Granule Cells In Vivo Define a Mechanism for Network Oscillations. Neuron *81*, 140–152.

Pernía-Andrade, A.J., Goswami, S.P., Stickler, Y., Fröbe, U., Schlögl, A., and Jonas, P. (2012). A Deconvolution-Based Method with High Sensitivity and Temporal Resolution for Detection of Spontaneous Synaptic Currents In Vitro and In Vivo. Biophys J *103*, 1429–1439.

Piette, C., Touboul, J., and Venance, L. (2020). Engrams of Fast Learning. Front Cell Neurosci *14*, 575915.

Pignatelli, M., Ryan, T.J., Roy, D.S., Lovett, C., Smith, L.M., Muralidhar, S., and Tonegawa, S. (2019). Engram Cell Excitability State Determines the Efficacy of Memory Retrieval. Neuron *101*, 274-284.e5.

Pike, F.G., Meredith, R.M., Olding, A.W.A., and Paulsen, O. (1999). Postsynaptic bursting is essential for 'Hebbian' induction of associative long-term potentiation at excitatory synapses in rat hippocampus. J Physiology *518*, 571–576.

Plath, N., Ohana, O., Dammermann, B., Errington, M.L., Schmitz, D., Gross, C., Mao, X., Engelsberg, A., Mahlke, C., Welzl, H., et al. (2006). Arc/Arg3.1 Is Essential for the Consolidation of Synaptic Plasticity and Memories. Neuron *52*, 437–444.

Pouille, F., Marin-Burgin, A., Adesnik, H., Atallah, B.V., and Scanziani, M. (2009). Input normalization by global feedforward inhibition expands cortical dynamic range. Nat Neurosci *12*, 1577–1585.

Ramamoorthi, K., Fropf, R., Belfort, G.M., Fitzmaurice, H.L., McKinney, R.M., Neve, R.L., Otto, T., and Lin, Y. (2011). Npas4 Regulates a Transcriptional Program in CA3 Required for Contextual Memory Formation. Science *334*, 1669–1675.

Ramirez, S., Liu, X., Lin, P.-A., Suh, J., Pignatelli, M., Redondo, R.L., Ryan, T.J., and Tonegawa, S. (2013). Creating a False Memory in the Hippocampus. Science *341*, 387–391.

Rebola, N., Carta, M., and Mulle, C. (2017). Operation and plasticity of hippocampal CA3 circuits: implications for memory encoding. Nat Rev Neurosci *18*, 208–220.

Redondo, R.L., Kim, J., Arons, A.L., Ramirez, S., Liu, X., and Tonegawa, S. (2014). Bidirectional switch of the valence associated with a hippocampal contextual memory engram. Nature *513*, 426–430.

Reijmers, L.G., Perkins, B.L., Matsuo, N., and Mayford, M.R. (2007). Localization of a Stable Neural Correlate of Associative Memory. Science *317*, 1230–1233.

Remy, S., and Spruston, N. (2007). Dendritic spikes induce single-burst long-term potentiation. Proc National Acad Sci *104*, 17192–17197.

Ribak, C.E., Seress, L., and Amaral, D.G. (1985). The development, ultrastructure and synaptic connections of the mossy cells of the dentate gyrus. J Neurocytol *14*, 835–857.

Roberts, W.A. (2002). Are Animals Stuck in Time? Psychol Bull *128*, 473–489.

Rolls, E.T. (2007). An attractor network in the hippocampus: Theory and neurophysiology. Learn Memory *14*, 714–731.

Rolls, E.T. (2016). Pattern separation, completion, and categorisation in the hippocampus and neocortex. Neurobiol Learn Mem *129*, 4–28.

Rolls, E.T., Critchley, H.D., and Treves, A. (1996). Representation of olfactory information in the primate orbitofrontal cortex. J Neurophysiol *75*, 1982–1996.

Rolls, E.T., Treves, A., Robertson, R.G., Georges-François, P., and Panzeri, S. (1998). Information About Spatial View in an Ensemble of Primate Hippocampal Cells. J Neurophysiol *79*, 1797–1813.

Routtenberg, A. (2010). Adult learning and remodeling of hippocampal mossy fibers: Unheralded participant in circuitry for long-lasting spatial memory. Hippocampus *20*, 44–45.

Roy, D.S., Arons, A., Mitchell, T.I., Pignatelli, M., Ryan, T.J., and Tonegawa, S. (2016). Memory retrieval by activating engram cells in mouse models of early Alzheimer's disease. Nature *531*, 508–512.

Roy, D.S., Kitamura, T., Okuyama, T., Ogawa, S.K., Sun, C., Obata, Y., Yoshiki, A., and Tonegawa, S. (2017). Distinct Neural Circuits for the Formation and Retrieval of Episodic Memories. Cell *170*, 1000-1012.e19.

Ruediger, S., Vittori, C., Bednarek, E., Genoud, C., Strata, P., Sacchetti, B., and Caroni, P. (2011). Learning-related feedforward inhibitory connectivity growth required for memory precision. Nature *473*, 514–518.

Ryan, T.J., Roy, D.S., Pignatelli, M., Arons, A., and Tonegawa, S. (2015). Engram cells retain memory under retrograde amnesia. Science *348*, 1007–1013.

Sachidhanandam, S., Blanchet, C., Jeantet, Y., Cho, Y.H., and Mulle, C. (2009). Kainate Receptors Act as Conditional Amplifiers of Spike Transmission at Hippocampal Mossy Fiber Synapses. J Neurosci *29*, 5000–5008.

Sah, P., and Bekkers, J.M. (1996). Apical Dendritic Location of Slow Afterhyperpolarization Current in Hippocampal Pyramidal Neurons: Implications for the Integration of Long-Term Potentiation. J Neurosci *16*, 4537–4542.

Sakurai, K., Zhao, S., Takatoh, J., Rodriguez, E., Lu, J., Leavitt, A.D., Fu, M., Han, B.-X., and Wang, F. (2016). Capturing and Manipulating Activated Neuronal Ensembles with CANE Delineates a Hypothalamic Social-Fear Circuit. Neuron *92*, 739–753.

Sano, Y., Shobe, J.L., Zhou, M., Huang, S., Shuman, T., Cai, D.J., Golshani, P., Kamata, M., and Silva, A.J. (2014). CREB Regulates Memory Allocation in the Insular Cortex. Curr Biol *24*, 2833–2837.

Scharfman, H.E. (1995). Electrophysiological evidence that dentate hilar mossy cells are excitatory and innervate both granule cells and interneurons. J Neurophysiol *74*, 179–194.

Schilling, K., Luk, D., Morgan, J.I., and Curran, T. (1991). Regulation of a fos-lacZ fusion gene: a paradigm for quantitative analysis of stimulus-transcription coupling. Proc National Acad Sci *88*, 5665–5669.

Schwartzkroin, P.A., and Wester, K. (1975). Long-lasting facilitation of a synaptic potential following tetanization in thein vitro hippocampal slice. Brain Res *89*, 107–119.

Scoville, W.B., and Milner, B. (1957). Loss of recent memory after bilateral hippocampal lesions. J Neurology Neurosurg Psychiatry *20*, 11.

Sekeres, M.J., Neve, R.L., Frankland, P.W., and Josselyn, S.A. (2010). Dorsal hippocampal CREB is both necessary and sufficient for spatial memory. Learn Memory *17*, 280–283.

Seress, L. (1988). Interspecies comparison of the hippocampal formation shows increased emphasis on the regio superior in the Ammon's horn of the human brain. J Für Hirnforschung *29*, 335–340.

Sik, A., Tamamaki, N., and Freund, T.F. (1993). Complete Axon Arborization of a Single CA3 Pyramidal Cell in the Rat Hippocampus, and its Relationship With Postsynaptic Parvalbumin-containing Interneurons. Eur J Neurosci *5*, 1719–1728.

Silva, S.V. da, Haberl, M.G., Zhang, P., Bethge, P., Lemos, C., Gonçalves, N., Gorlewicz, A., Malezieux, M., Gonçalves, F.Q., Grosjean, N., et al. (2016). Early synaptic deficits in the

APP/PS1 mouse model of Alzheimer's disease involve neuronal adenosine A2A receptors. Nat Commun *7*, 11915.

Šišková, Z., Justus, D., Kaneko, H., Friedrichs, D., Henneberg, N., Beutel, T., Pitsch, J., Schoch, S., Becker, A., von der Kammer, H., et al. (2014). Dendritic Structural Degeneration Is Functionally Linked to Cellular Hyperexcitability in a Mouse Model of Alzheimer's Disease. Neuron *84*, 1023–1033.

Sjöström, P.J., Turrigiano, G.G., and Nelson, S.B. (2001). Rate, Timing, and Cooperativity Jointly Determine Cortical Synaptic Plasticity. Neuron *32*, 1149–1164.

Soltesz, I., and Losonczy, A. (2018). CA1 pyramidal cell diversity enabling parallel information processing in the hippocampus. Nat Neurosci *21*, 484–493.

Soltesz, I., and Mody, I. (1994). Patch-clamp recordings reveal powerful GABAergic inhibition in dentate hilar neurons. J Neurosci *14*, 2365–2376.

Sørensen, A.T., Cooper, Y.A., Baratta, M.V., Weng, F.-J., Zhang, Y., Ramamoorthi, K., Fropf, R., LaVerriere, E., Xue, J., Young, A., et al. (2016). A robust activity marking system for exploring active neuronal ensembles. Elife *5*, e13918.

Soriano, E., and Frotscher, M. (1994). Mossy cells of the rat fascia dentata are glutamate-immunoreactive. Hippocampus *4*, 65–69.

Sorra, K., and Harris, K. (1993). Occurrence and three-dimensional structure of multiple synapses between individual radiatum axons and their target pyramidal cells in hippocampal area CA1. J Neurosci *13*, 3736–3748.

Spruston, N., Jaffe, D.B., Williams, S.H., and Johnston, D. (1993). Voltage- and space-clamp errors associated with the measurement of electrotonically remote synaptic events. J Neurophysiol *70*, 781–802.

Stefanelli, T., Bertollini, C., Lüscher, C., Muller, D., and Mendez, P. (2016). Hippocampal Somatostatin Interneurons Control the Size of Neuronal Memory Ensembles. Neuron *89*, 1074–1085.

Strange, B.A., Witter, M.P., Lein, E.S., and Moser, E.I. (2014). Functional organization of the hippocampal longitudinal axis. Nat Rev Neurosci *15*, 655–669.

Sun, Q., Srinivas, K.V., Sotayo, A., and Siegelbaum, S.A. (2014). Dendritic Na+ spikes enable cortical input to drive action potential output from hippocampal CA2 pyramidal neurons. Elife *3*, e04551.

Sun, Q., Sotayo, A., Cazzulino, A.S., Snyder, A.M., Denny, C.A., and Siegelbaum, S.A. (2017a). Proximodistal Heterogeneity of Hippocampal CA3 Pyramidal Neuron Intrinsic Properties, Connectivity, and Reactivation during Memory Recall. Neuron *95*, 656-672.e3.

Sun, Q., Sotayo, A., Cazzulino, A.S., Snyder, A.M., Denny, C.A., and Siegelbaum, S.A. (2017b). Proximodistal Heterogeneity of Hippocampal CA3 Pyramidal Neuron Intrinsic Properties, Connectivity, and Reactivation during Memory Recall. Neuron *95*, 656-672.e3.

Sun, X., Bernstein, M.J., Meng, M., Rao, S., Sørensen, A.T., Yao, L., Zhang, X., Anikeeva, P.O., and Lin, Y. (2020). Functionally Distinct Neuronal Ensembles within the Memory Engram. Cell *181*, 410-423.e17.

Takahashi, N., Oertner, T.G., Hegemann, P., and Larkum, M.E. (2016). Active cortical dendrites modulate perception. Science *354*, 1587–1590.

Tamamaki, N., and Nojyo, Y. (1995). Preservation of topography in the connections between the subiculum, field CA1, and the entorhinal cortex in rats. J Comp Neurol *353*, 379–390.

Tanaka, K.Z., Pevzner, A., Hamidi, A.B., Nakazawa, Y., Graham, J., and Wiltgen, B.J. (2014). Cortical Representations Are Reinstated by the Hippocampus during Memory Retrieval. Neuron *84*, 347–354.

Tayler, K.K., Tanaka, K.Z., Reijmers, L.G., and Wiltgen, B.J. (2013). Reactivation of Neural Ensembles during the Retrieval of Recent and Remote Memory. Curr Biol *23*, 99–106.

Thompson, L.T., Moyer, J.R., and Disterhoft, J.F. (1996). Transient changes in excitability of rabbit CA3 neurons with a time course appropriate to support memory consolidation. J Neurophysiol *76*, 1836–1849.

Titley, H.K., Brunel, N., and Hansel, C. (2017). Toward a Neurocentric View of Learning. Neuron *95*, 19–32.

Tonegawa, S., Liu, X., Ramirez, S., and Redondo, R. (2015). Memory Engram Cells Have Come of Age. Neuron *87*, 918–931.

Torborg, C.L., Nakashiba, T., Tonegawa, S., and McBain, C.J. (2010). Control of CA3 Output by Feedforward Inhibition Despite Developmental Changes in the Excitation–Inhibition Balance. J Neurosci *30*, 15628–15637.

Treves, A., and Rolls, E.T. (1992). Computational constraints suggest the need for two distinct input systems to the hippocampal CA3 network. Hippocampus *2*, 189–199.

Treves, A., and Rolls, E.T. (1994). Computational analysis of the role of the hippocampus in memory. Hippocampus *4*, 374–391.

Trojanowski, N.F., Bottorff, J., and Turrigiano, G.G. (2020). Activity labeling in vivo using CaMPARI2 reveals intrinsic and synaptic differences between neurons with high and low firing rate set points. Neuron.

Tsukamoto, M., Yasui, T., Yamada, M.K., Nishiyama, N., Matsuki, N., and Ikegaya, Y. (2003). Mossy fibre synaptic NMDA receptors trigger non-hebbian long-term potentiation at entorhino-CA3 synapses in the rat. J Physiology *546*, 665–675.

Tulving, E. (1972). Episodic and Semantic Memory. In Undefined, p.

Tulving, E. (2002). EPISODIC MEMORY: From Mind to Brain. Annu Rev Psychol *53*, 1–25.

Tulving, E., and Markowitsch, H.J. (1998). Episodic and declarative memory: Role of the hippocampus. Hippocampus *8*, 198–204.

Vertes, R.P., and McKenna, J.T. (2000). Collateral projections from the supramammillary nucleus to the medial septum and hippocampus. Synapse *38*, 281–293.

Vetere, G., Tran, L.M., Moberg, S., Steadman, P.E., Restivo, L., Morrison, F.G., Ressler, K.J., Josselyn, S.A., and Frankland, P.W. (2019). Memory formation in the absence of experience. Nat Neurosci *22*, 933–940.

Villarreal, D.M., Gross, A.L., and Derrick, B.E. (2007). Modulation of CA3 Afferent Inputs by Novelty and Theta Rhythm. J Neurosci *27*, 13457–13467.

Vyleta, N.P., and Jonas, P. (2014). Loose Coupling Between Ca^{2+} Channels and Release Sensors at a Plastic Hippocampal Synapse. Science *343*, 665–670.

Vyleta, N.P., Borges-Merjane, C., and Jonas, P. (2016). Plasticity-dependent, full detonation at hippocampal mossy fiber–CA3 pyramidal neuron synapses. Elife *5*, e17977.

Wang, Y., Liu, Y., Wang, L., Tang, W., and Wang, Z. (2018). Silent Synapse Unsilencing in Hippocampal CA1 Neurons for Associative Fear Memory Storage. Cereb Cortex *29*, 4067–4076.

Weiss, C., Weible, A.P., Galvez, R., and Disterhoft, J.F. (2006). Forebrain-Cerebellar Interactions During Learning. Cellscience *3*, 200–230.

Weng, F.-J., Garcia, R.I., Lutzu, S., Alviña, K., Zhang, Y., Dushko, M., Ku, T., Zemoura, K., Rich, D., Garcia-Dominguez, D., et al. (2018). Npas4 Is a Critical Regulator of Learning-Induced Plasticity at Mossy Fiber-CA3 Synapses during Contextual Memory Formation. Neuron *97*, 1137-1152.e5.

Wharton, K.A., Franks, R.G., Kasai, Y., and Crews, S.T. (1994). Control of CNS midline transcription by asymmetric E-box-like elements: similarity to xenobiotic responsive regulation. Dev Camb Engl *120*, 3563–3569.

Williams, S.R., and Mitchell, S.J. (2008). Direct measurement of somatic voltage clamp errors in central neurons. Nat Neurosci *11*, 790–798.

Wittenberg, G.M., and Wang, S.S.-H. (2006). Malleability of Spike-Timing-Dependent Plasticity at the CA3–CA1 Synapse. J Neurosci *26*, 6610–6617.

Witter, M.P., Wouterlood, F.G., Naber, P.A., and Haeften, T.V. (2000). Anatomical Organization of the Parahippocampal-Hippocampal Network. Ann Ny Acad Sci *911*, 1–24.

Yap, E.-L., and Greenberg, M.E. (2018). Activity-Regulated Transcription: Bridging the Gap between Neural Activity and Behavior. Neuron *100*, 330–348.

Yassa, M.A., and Stark, C.E.L. (2011). Pattern separation in the hippocampus. Trends Neurosci *34*, 515–525.

Yiu, A.P., Mercaldo, V., Yan, C., Richards, B., Rashid, A.J., Hsiang, H.-L.L., Pressey, J., Mahadevan, V., Tran, M.M., Kushner, S.A., et al. (2014). Neurons Are Recruited to a Memory Trace Based on Relative Neuronal Excitability Immediately before Training. Neuron *83*, 722–735.

Zeldenrust, F., Wadman, W.J., and Englitz, B. (2018). Neural Coding With Bursts—Current State and Future Perspectives. Front Comput Neurosc *12*, 48.

Zhou, Y., Won, J., Karlsson, M.G., Zhou, M., Rogerson, T., Balaji, J., Neve, R., Poirazi, P., and Silva, A.J. (2009). CREB regulates excitability and the allocation of memory to subsets of neurons in the amygdala. Nat Neurosci *12*, 1438–1443.

Zolnik, T.A., Sha, F., Johenning, F.W., Schreiter, E.R., Looger, L.L., Larkum, M.E., and Sachdev, R.N.S. (2017). All-optical functional synaptic connectivity mapping in acute brain slices using the calcium integrator CaMPARI. J Physiology *595*, 1465–1477.

Zucca, S., Griguoli, M., Malézieux, M., Grosjean, N., Carta, M., and Mulle, C. (2017). Control of Spike Transfer at Hippocampal Mossy Fiber Synapses In Vivo by GABAA and GABAB Receptor-Mediated Inhibition. J Neurosci *37*, 587–598.

Annex

Impaired plasticity of intrinsic excitability in the dentate gyrus alters spike transfer in a mouse model of Alzheimer's disease

Nan Jiang[1], **Dario Cupolillo**[1], Noelle Grosjean[1], Emeline Muller[1], Séverine Deforges[1], Christophe Mulle[1] and Thierry Amédée[1]

[1]Univ. Bordeaux, CNRS, INSERM, Bordeaux Imaging Center, BIC, UMS 3420, US 4, F-33000 Bordeaux, France

Impaired plasticity of intrinsic excitability in the *dentate gyrus* alters spike transfer in a mouse model of Alzheimer's disease

Nan Jiang [1], Dario Cupolillo [1], Noelle Grosjean [1], Emeline Muller [1], Séverine Deforges [1], Christophe Mulle [1] and Thierry Amédée [1]

[1] Univ. Bordeaux, CNRS, INSERM, Bordeaux Imaging Center, BIC, UMS 3420, US 4, F-33000 Bordeaux, France

Corresponding author: Thierry Amédée, Université de Bordeaux, IINS - UMR 5297 CNRS - Centre Broca Nouvelle Aquitaine, 146 rue Léo Saignat, CS 61292 Case 130, 33076 BORDEAUX Cedex, France. Email: thierry.amedee@u-bordeaux.fr

Abstract: Alzheimer's disease (AD) is a progressive neurodegenerative disease characterized by cognitive decline related to deficits in synaptic transmission and plasticity. We report in APP/PS1 mice, a double transgenic mouse model of AD, that females displayed precocious Aβ plaques load in the *stratum moleculare* of the *dentate gyrus* (DG) together with prominent neuroinflammatory activation of astrocytes and microglia. These cellular alterations were accompanied by robust deficits in spatial memory in APP/PS1 female mice as early as 4 months of age. We then investigated the functional properties of the lateral perforant path (LPP) to DG granule cells. Remarkably DG granule cells displayed higher intrinsic excitability in APP/PS1 female mice. We showed that long term potentiation of population spike amplitude induced by high frequency stimulation (HFS) at LPP-DG granule cells synapse is impaired in APP/PS1 female mice. HFS caused plasticity of intrinsic excitability in DG granule cells without inducing noticeable modification of synaptic strength. Furthermore, the enhanced intrinsic excitability was potentiated to a higher extent in APP/PS1 as compared to control mice following HFS. Our study shows that changes in the intrinsic excitability of DG granule cells in AD contribute to dysfunctional transfer of information from the entorhinal cortex to the hippocampus.

Keywords: Alzheimer's disease, dentate gyrus, intrinsic excitability, perforant pathway, synaptic plasticity, hippocampus, glial cells, neuroinflammation

Introduction: Alzheimer's disease (AD) is a devastating neurodegenerative disease accounting for more than 70 % of dementia in the elderly population worldwide (in "2018 Alzheimer's disease fact and figures", 2018) but despite considerable efforts in research, there is still neither a cure nor even efficient treatments to alleviate the symptoms.

AD is characterized by two major histopathological hallmarks, Aβ plaques mostly in the cortex and the hippocampus and intraneuronal accumulation of fibrillary tangles of hyperphosphorylated Tau (Querfurth and LaFerla, 2010). At late stages, AD's brains display profound structural changes such as shrinkage of the cortex and severe atrophy of the hippocampus. These molecular events are associated with prominent neuroinflammation and a large corpus of data have reported that soluble Aβ and numerous molecules produced by inflamed glial cells contributed to the pathophysiology of AD (Akiyama *et al*., 2000; Heneka and O'Banion, 2007; Heneka *et al*., 2015; Sarlus and Heneka, 2017).

The hippocampus is characterized by an excitatory tri-synaptic pathway formed by the perforant pathway to *dentate gyrus* (DG) granule cells synapse (PP-DG synapse) followed by the projection of DG granule cells axons (mossy fiber, Mf) to CA3 pyramidal neurons (Mf-CA3 synapse) which in turn project to CA1 pyramidal neurons via the Schaffer collateral pathway (SC-CA1 synapse). Entorhinal Cortex - Hippocampus network is among the earliest brain region to be heavily targeted by AD (Stranahan *et al*., 2010; Criscuolo *et al*., 2017) and alterations of hippocampal synaptic/dendritic properties are acknowledged to underlie memory deficits in early AD (Penzes *et al*., 2011). Hence hippocampal synaptic transmission and plasticity have been extensively studied on different transgenic mouse model of the pathology (Marchetti and Marie, 2011) for the past two decades. From this corpus of data has emerged the general picture of an alteration of synaptic circuits at the early stage of the disease (Selkoe, 2002; Spires-Jones and Hyman, 2014; Forner *et al*., 2017). However while the vast majority of the studies have been focused on the alterations of different forms of hippocampal synaptic plasticity, putative alterations in intrinsic neuronal properties, the

other key player of information processing (Daoudal and Debanne, 2003) have been poorly considered so far in the context of the pathology.

The *dentate gyrus* (DG) is the main entry gate for entorhinal cortex inputs to hippocampus. As such, plasticity of synaptic transmission within the DG has long been considered to play a crucial role in the processing of cortical information entering the hippocampus. However, DG granule cells are relatively reluctant to Hebbian-type of synaptic plasticity in response to classical induction protocols (Schmidt-Hieber *et al*., 2004; Lopez-Rojas *et al*., 2016) whereas they display high plasticity of intrinsic excitability (Lopez-Rojas *et al*., 2016). This non-synaptic form of plasticity may be essential to control the transfer of information in the DG since the generation of action potentials, which depends not only on excitatory synaptic drive but also on intrinsic excitability, is the main determinant of neuronal activity.

We therefore decided to investigate the plasticity of intrinsic excitability of DG granule cells in WT female mice and search if and how this plasticity was affected by the pathology in APP/PS1 mice. We took advantage of the recapitulation by amyloidogenic mouse models of AD of the higher prevalence and greater AD neuropathology for women over men (Barnes *et al*., 2005; Sinforiani *et al*., 2010). APP/PS1 females mice display earlier and stronger β amyloid plaque load together with earlier deficits in hippocampal-dependent spatial memory tasks as compared to age-matched males (Gallagher *et al*., 2013; Richetin *et al*., 2017).

We first characterized in APP/PS1 female mice the hippocampal progression of Aβ plaque deposition in relation to the neuroinflammatory status and deficits in hippocampus-

dependent memory task in order to set an early age at which robust histopathological and behavioral alterations were present. We showed that APP/PS1 female mice at 6 months of age displayed a noticeable load of Aβ plaques together with prominent neuroinflammatory activation of astrocytes and microglia in the *stratum moleculare* of the *dentate gyrus*, a region described to be early affected in the spatiotemporal progression of the disease (Hurtado *et al*., 2010). These cellular alterations were accompanied by deficits in contextual fear conditioning, a one-trial hippocampus-dependent task resulting in a robust long lasting memory for a rodent (Phillips and Ledoux, 1992).

Having shown that APP/PS1 female mice at the age of 6 months displayed obvious molecular and behavioral alterations, we focussed our study on the lateral perforant pathway (LPP) which conveys multimodal sensory informations originated in the entorhinal cortex to the DG (Hunsaker *et al*., 2007; Deng *et al.,* 2010). We show that APP/PS1 female mice at 6 months of age display alteration of the plasticity of spike transmission at LPP-synaptic inputs and most remarkably that the plasticity of intrinsic excitability of DG granule cells is prominently impacted by the pathology. Our results reveal new mechanisms potentially leading to dysfunctional transfer of information from the entorhinal cortex to the hippocampus and may delineate new routes for improvement and/or therapeutic intervention.

Materials and Methods

Ethical approval: Animal anesthesia and euthanasia were carried out in accordance with the Animal Protection of ethical standards and the French legislation concerning animal experimentation and were approved by the University of Bordeaux / CNRS Animal care and

Use Committee (authorization #03524). All efforts to improve the animal welfare and to minimize animals suffering were made.

Animals: The animals used in this study were males and females APPswe695/PS1ΔE9 termed APP/PS1 (Stock number: 005864) obtained from Jackson Laboratory (Bar Harbor, ME, USA) and their wild-type (WT) littermates (C57BL6/J). Briefly, the APP/PS1 mice express a chimeric mouse/human amyloid precursor protein APPswe (mouse APP695 harboring a human Aβ domain and mutations K595N and M596L linked to a Swedish familial AD) and a human presenilin 1 mutated in familial AD (PS1ΔE9; deletion of exon 9). These bigenic mice were created by co-injection of both transgenes allowing for a co-segregation of the transgenes as a single locus (Jankowsky *et al*., 2004). Mice were generated in our animal facility from double-transgenic APP/PS1 males mated with C57BL/6J females. Transgenic mice (APP/PS1) and age-matched non-transgenic littermates (WT) were allowed free access to food and water and maintained in a 12 hours dark-light cycle. Mice were genotyped and systematically regenotyped after each experiments (Transcriptomics Platform, Neurocentre Magendie, Bordeaux, France). In all experiments, females have been used without consideration to their estrous cycle.

Acute hippocampal slices: APP/PS1 and WT female mice at 6 months were deeply anaesthetized with a mix of ketamine (80 mg/kg; i.p) and xylazine (16 mg/kg; i.p) and then intracardially perfused for 2-3 minutes with a protective solution at 4°C containing the following (in mM): 2.5 KCl, 1.25 NaH_2PO_4, 0.5 $CaCl_2$, 7 $MgCl_2$, 20 glucose, 26 $NaHCO_3$, 76 sucrose, 3 pyruvic acid, 5 Na ascorbate, equilibrated with 95% 0_2 and 5% CO_2 (300-310 mOsm). When the solution coming out of the heart was free of blood, the mouse was

sacrificed by decapitation and the brain was quickly removed from the skull and stored in the same solution. The isolated brain was glued onto the stage of a vibratome (VT 1200S, Leica Microsystems, Nussloch, Germany) and parasagittal hippocampal slices (320 µm) were cut in the protective solution for which sodium chloride was replaced by sucrose, and then incubated at 33°C for 10-20 min in a resting solution containing the following (in mM): 125 NaCl, 2.5 KCl, 1.25 NaH_2PO_4, 2 $CaCl_2$, 1 $MgCl_2$, 20 glucose, 26 $NaHCO_3$, 5 Na ascorbate equilibrated with 95% 0_2 and 5% CO_2 (300-310 mOsm). Slices were thereafter maintained at room temperature in the same solution until required. Only dorsal slices were retained in this study as the dorsally located hippocampal segment mediate cognitive operations like spatial navigation which is critically impaired in mouse models of AD (Bannerman *et al*., 2014; Strange *et al*., 2014) whereas functions related to emotions are preferentially taken on by the ventral segment of the hippocampus (Kheirbek *et al*., 2013).

Electrophysiological studies on acute hippocampal slices: For recording, slices were transferred into a recording chamber where they were submerged and perfused with an extracellular recording solution containing the following (in mM): 125 NaCl, 2.5 KCl, 1.35 NaH_2PO_4, 2 $CaCl_2$, 1 $MgCl_2$, 16 glucose, 26 $NaHCO_3$ continuously oxygenated (95% 0_2 and 5% CO_2). Recordings were made at room temperature. Whole-cell patch clamp recordings (3-4 MΩ electrodes, -70 mV holding potential) were made from *dentate gyrus* (DG) granule cells visualized by infrared video-microscopy. Patch clamp electrodes were pulled out from borosilicate glass (GF 150 F-10) and filled with an internal solution containing the following (in mM): 140 $CsCH_3SO_3$, 2 $MgCl_2$, 4 NaCl, 5 phospho-creatine, 2 Na_2ATP, 0.2 EGTA, 10 HEPES, and 0.33 GTP adjusted with CsOH (300 mOsm, pH 7.3). For patch-clamp recordings in current-clamp mode, a K^+-based internal solution containing (in mM) was used: 115 K-

gluconate, 10 KCl, 0.2 EGTA, 10 HEPES, 15 phospho-creatine, 4 MgATP and 0.3 NaGTP adjusted with KOH (300-305 mOsm, pH 7.3). Bicuculline (10 µM) was added to the bath to inhibit γ-Aminobutyric acid-A (GABA-A) receptors. Voltage-clamp recordings were performed on DG granule cells identified with a differential interference contrast microscope (Eclipse FN-1, Nikon, Champigny sur Marne, France) equipped with an infrared camera (VX 44, Till Photonics, Gräfelfing, Germany) using an Axopatch-200B amplifier (Axon Instruments, Sunnyvale, CA, USA). Signals were filtered at 2 kHz and digitized at 5 kHz via a DigiData 1322A interface (Axon instruments). In order to ascertain the quality of patch clamp recordings, series resistance (10-20 MΩ) was monitored during the recording using a −10 mV hyperpolarizing voltage step of 50 ms length occurring at the beginning of each recording and DG granule cells were rejected if more than a 20% change occurred during the experiment. Furthermore, DG granule cells with a holding current exceeding 250 pA at a holding potential of -70 mV were also rejected. No liquid-junction potential correction was used. Data were collected and analysed using pClamp software 9.2 (Axon Instruments).

Field recordings were obtained from the granular cell layer using glass electrodes (1- 2 MΩ) filled with extracellular recording solution. Because of the possibility of crosstalk between mossy cell fibers (MCFs) and the more proximal medial perforant path (MPP) we focused our study on lateral perforant path (LPP) transmission. To stimulate selectively the LPP, a stimulating glass electrode (1 - 2 µm tip diameter) filled with extracellular recording solution was placed in the outer molecular layer of the DG (>100 µm away from the granule cell layer) and as close as possible to the hippocampal fissure which is located 180 - 250 µm away from the granule cell layer (Allen Brain Atlas©). In addition to the location of the stimulating electrode, we characterized the LPP by its ability to exhibit paired-pulse

facilitation whereas the MPP does not (Fig. 2B). Signals were recorded using an Axopatch-200B amplifier (Axon Instruments, Sunnyvale, CA, USA), filtered at 20 kHz and digitally sampled at 50 kHz. All experiments were performed in the presence of bicuculline (10 µM) to block GABA-A receptors. GABA-B receptors, which are expressed both by axonal terminal and dendritic compartment of DG granule cells, were not blocked as these receptors primarily exert disinhibition on DG granule cells due to the reduction of GABA release from hilar interneurons (Foster *et al*., 2013). Input-output curves were recorded by varying stimulation strength from 0 to 300 µA in 50 µA intervals. For subsequent experiments on basal transmission and population spike recordings, the stimulus strength was set to a level that produced about 30-35% of the maximal responses. Proper stimulating electrode location was controled by applying a paired-pulse protocol to the recorded population spike. The protocol for population spike potentiation consisted of a high-frequency stimulation (HFS) of 3 bursts of 100 stimuli at 100 Hz with a 10 s interburst interval. In patch clamp experiments, HFS was paired with a postsynaptic depolarization at 0 mV in order to facilitate the removal of the magnesium block of NMDA receptors. E-S curve, which relates EPSP slopes to the associated action potential (AP) firing probability, was generated by measuring slopes during the first 2 ms (reflecting mainly the fast component of AMPA-receptor synaptic transmission) and sorted in 0.5 mV/ms bins to the associated AP firing probability. The AP firing probability was calculated for each bin and the EC_{50} value (the value of the EPSP-slope that elicits an AP with 50 % of probability) was calculated in each cell. EPSP amplitude/slope ratio histograms before and after HFS were generated as follows: at the start of the experiment, for each cell the amplitude of sub-threshold EPSPs (*i.e.* not triggering APs) was measured in current-clamp mode (the membrane potential was set to around -70 mV), and plotted *vs* the EPSP slope. Then a linear regression was fitted yielding a slope value. The cell

was rejected if the goodness of fit, $S_{y.x}$, which quantifies the scatter of the data points around the best fit line was < 1.5. After this, the cell was switched to voltage-clamp mode and held at -70 mV. A baseline was recorded for 5 min and then the HFS protocol was applied followed by a period of 20 min. Then the cell was returned back to current-clamp mode (set around - 70 mV) and a new EPSP amplitude/slope ratio histogram was generated.

Immunohistological staining and analysis: WT and APP/PS1 male and female mice at 3, 6 and 9 months of age were anesthetized with intraperitoneal administration of pentobarbital (50 mg/kg body weight) and were fixed by transcardial perfusion with buffered saline and 50 ml of 4% paraformaldehyde (PFA). Brains were removed, postfixed in 4% PFA overnight and cut into 40 µm-thick frontal sections on a vibratome. Sections were collected into PBS 0.1M and stored at + 4°C until the staining protocol. After a thorough wash in TBST (Tris Buffer Sodium: 0.0384 M Trisma Base -0.1263 M NaCl pH: 7.4 + 0.1 % Tween 20), free-floating sections were incubated with TBST - 10% Normal Goat Serum - 0.3% Triton X-100, for 1 hour at room temperature. Then sections were incubated with primary antibody in TBST - 3.5% Normal Donkey Serum overnight at 4°C (chicken anti - glial fibrillary acidic protein (GFAP): 1/1000 USBiologicals; rabbit anti - ionized calcium-binding adapter molecule Iba-1: 1/5000 Wako. Aβ plaques were stained either using Methoxy-X04 (Congo red derivative, 50 µM, Tocris) or mouse anti-$Aß_{1\text{-}16}$: 1/150 (Millipore). After washes in TBST, sections were incubated with secondary antibodies for 1 hour (Goat anti-chicken Alexa 647, anti-mouse Alexa 555 and anti-rabbit Alexa 488: 1/500, Invitrogen). Slices were finally washed and mounted in mounting medium (Fluoromount + DAPI, SouthernBiotech). Slices were imaged using the up-right widefield microscope Leica DM5000 (Leica Microsystems, Nanterre, France) using objectives HC PL Fluotar 20X NA 0.5. Fluorescence excitation was performed

by a LED SOLA Light (Lumencor, Beaverton, USA). Images were obtained by the resolutive cameras CoolSnap HQ2 (Photometrics, Tucson, USA) and a cooled QICAM (QImaging, Surrey, Canada). A galvanometric stage (Leica Microsystems) allowed the z stack reconstructions. The mosaics were made using a motorized stage Scan (Märzhäuser, Wetzlar, Germany). This system was controlled by MetaMorph software (Molecular Devices, Sunnyvale, USA). Analyses were performed with Image J software (National Institutes of Health, New York, USA) on the maximum intensity fluorescence projections of the 3D mosaics. Images were then calibrated and processed as 8-bits grayscale images (0-255) by Image J software. A high manual threshold was applied to Aβ plaques and to GFAP positive cells and Iba-1 positive cells to remove irrelevant signals. The manual threshold was adjusted to count only dense core Aβ plaques. Between 8 and 10 measurements from 5 mice were acquired per genotype and per stained protein.

Contextual fear conditioning (CFC): Mice were housed individually. Prior to the test, mice were handled 2 minutes per day during 5 days. At day 0, single-trial contextual fear conditioning was performed by placing mice into a conditioning chamber where they were allowed to explore for 150 seconds after which they received a mild electric footshock (2s, 0.7 mA) and were removed 28 seconds after the shock. The conditioning chamber was housed in a sound attenuated box with the four interior walls wearing a checkerboard pattern. The conditioning cage (17 cm wide, 17 cm deep and 25 cm high) was made of clear plexiglas and the floor consisted of a shock grid. Between each animal the cage was cleaned with 70% ethanol solution. At day 1, mice were reexposed to the conditioning chamber during 180 seconds. The cage was cleaned with 1% acetic acid between each mouse. Contextual fear memory retention was studied by measuring the freezing response in the

conditioning chamber. Automatic freezing was detected with the help of a software (Any-Maze, Ugo Basile, Gemonio, Italy). The minimum freeze duration was set at 400 ms with the software distinguishing between freezing detection and immobility detection (Any-Maze, Ugo Basile, Gemonio, Italy).

Experimental design and statistical analysis: In order to minimize biases as much as possible, experimenters were kept blind to the genotype of the mice until analysis was completed. Values are presented as mean ± SEM (standard error of mean) of n experiments. Statistical analyses were performed with Prism 7.0 (GraphPad Software, La Jolla, CA, USA). First the normality of data set was tested using the D'Agostino-Pearson omnibus normality test. If data was normally distributed, a Student's *t* - test for 2 groups and a two way ANOVA with Bonferonni's test for more than two groups were used for statistical comparison. The *P*-values given are two-tailed and were considered significant if $p<0.05$. One-proportion *Z*-test was used for proportion analysis (Fig 3A).

Drugs: Bicuculline, D-2-amino-5-phosphonopentanoate (D-AP5) and Methoxy-X04 were obtained from Tocris, TTX and D-serine from Sigma-Aldrich, NBQX from HelloBio. Stock solutions using appropriate solvent (DMSO for bicuculline, D-AP5 and Methoxy-X04 and acetic acid for TTX) were made and diluted with aCSF just before the application.

Results

Histopathological and behavioral alterations in APP/PS1 female mice

In order to set an age at which a noticeable deposit of hippocampal Aβ plaques occured, we

study the time course of the expression of hippocampal Aβ plaques in APP/PS1 female mice at 3, 6 and 9 months of age (Fig. 1). While there were no detectable plaques at 3 months of age, numerous plaques were noticeable at 6 months of age and there was a heavy load at 9 months of age (Fig. 1A). Remarkably at 6 and 9 months of age, Aβ plaques (red signal) were not uniformely distributed throughout the hippocampus but were clearly concentrated in the *stratum moleculare* (delineated by the white dotted-line) of the DG (Fig. 1A). At a higher magnification (Fig. 1B), Aβ plaques were formed by a dense amyloid core (anti-$A\beta_{1\text{-}16}$, white signal) surrounded by a spider web of microglia (Iba-1, green signal). Activated astrocytes (GFAP, red signal) were located in the vicinity. Aβ plaques were counted in the whole hippocampus and in the *stratum moleculare* (DG area) obtained from 5 mice for both genotype. There was a gradual and clear increase in the number of Aβ plaques over the course of the pathology (Fig. 1C) for both the whole hippocampus (3 months-old: 5.0 ± 1.7, n=20; 6 months-old: 31.1 ± 3.0, n=30; 9 months-old: 59.8 ± 4.2, n=17, *** $p<0.001$) and the DG area (3 months-old: 1.9 ± 0.7, n=29; 6 months-old: 8.5 ± 0.8, n=56; 9 months-old: 21.5 ± 2.9, n=29, *** $p<0.001$).

The neuroinflammatory activation of glial cells is well acknowledged as hallmarks of the course of the disease (for review see Heneka and O'Banion, 2007; Heneka *et al*., 2015; Sarlus and Heneka, 2017). In order to illustrate this in our mouse model, we performed double immunostaining of astrocytes (GFAP, red signal) and microglia (Iba-1, green signal) and compared the pattern of activation between WT and APP/PS1 female mice at 6 months of age (Fig. 1D; Fig. 1E). Whereas, astrocytes displayed elongated bodies with long and thin processes in WT mice, they displayed rounded cell bodies with shortened and enlarged processes, a morphological hallmark of activated astrocytes (Wilhelmsson *et al*., 2006; for

review see Schiweck *et al*., 2018) in APP/PS1 mice (Fig. 1D). Microglia also displayed a typical phenotype of reactive cells (Nimmerjahn *et al*., 2005) shifting from a quiescent morphology with small somas densely arborised with very thin processes in WT mice to an activated status with a prominent enlargement of cell bodies displaying shortened and thickened processes in APP/PS1 mice (Fig. 1E).

Collectively, these data are unambiguous evidence that Aβ plaques deposition accompanied by hypertrophic astrocytes and amoeboid microglia, all of which being acknowledged as neuroinflammatory furnaces, starts after 3 months of age in APP/PS1 female and is robust at 6 months of age. Our findings are consistent with numerous reports describing in the APP/PS1 mouse model the progressive onset of amyloid pathology in the form of Aβ plaques deposits starting around 4-6 months of age (for review see Marchetti and Marie, 2011) and extend those of Richetin et al (2017) reporting the presence of abundant hypertrophic astrocytes in the DG of older APP/PS1 female mice (7-9 months of age).

Hippocampal-dependent memory was tested in APP/PS1 female mice at 3, 4 and 6 months of age and their age-matched WT littermates using a one-trial behavioral paradigm, contextual fear conditioning (CFC). CFC is a hippocampus-dependent task which results in a robust long lasting memory for a rodent (Phillips and Ledoux, 1992). Importantly, both WT and APP/PS1 mice displayed almost no freezing at 3, 4 and 6 months of age (data not shown) during the 150 s period before the footshock at the time of training (3 months-old: WT: 0.75 ± 0.2%, n=11; APP/PS1: 0.71 ± 0.2%, n=11, p=0.911; 4 months-old: WT: 1.0 ± 0.2%, n=14; APP/PS1: 1.0 ± 0.5%, n=9, p=0.997; 6 months-old: WT: 5.6 ± 1.4%, n=15; APP/PS1: 3 ± 0.8%, n=10, p=0.186) evidencing the lack of significant anxiety-related behavior in our

experimental conditions. As early as 3 months of age, APP/PS1 female mice displayed memory deficits with an impaired CFC (3 months-old: WT: 43.7 ± 4.9 %, n=11; APP/PS1: 24.9 ± 5.2%, n=11, *p<0.05, 4 months-old: WT: 37.4 ± 7 %, n=14; APP/PS1: 15.2 ± 4.8%, n=9, *p<0.05; 6 months-old: WT: 50.2 ± 5.1%, n=15; APP/PS1: 30.8 ± 6.8%, n=10, *p<0.05) (Fig. 1F).

Altogether, our results show that memory deficits parallel the prominent increase in Aβ plaques load and in neuroinflammatory astrocytic and microglial activation, preferentially located in the *stratum moleculare* of the DG. Therefore on the basis of robust molecular and behavioral alterations we decided to investigate the functional properties of the lateral perforant pathway to DG granule cells synapse on APP/PS1 female mice at 6 months of age.

Functional properties of LPP-DG synapses

Having shown that Aβ plaques were abundant in the *stratum moleculare* of the DG in female mice, we investigated the functional properties of synaptic circuitry in the close vicinity, that are PP-DG synapses. More specifically, we focused on the lateral perforant path (LPP) - DG synapse which processes multimodal sensory information from the entorhinal cortex (Hunsaker *et al*., 2007; Igarashi *et al*., 2014). We took great care of differentiating between the LPP and the medial perforant path (MPP) by placing the stimulating electrode in the outer one-third molecular layer of the DG suprapyramidal blade and the recording electrode either in the DG granule cell layer for patch-clamp recordings as shown in Fig. 2A, or close to the crest of the suprapyramidal blade for extracellular field recordings. In this way, we achieved reliable and selective activation of LPP projections to the DG. On the other hand, MPP was selectively activated by positioning the electrode in the middle molecular layer, that is at a distance < 100 μm from the DG granule cell layer. We confirmed the anatomical

dissection of the two pathways by using a paired-pulse protocol (McNaughton, 1980; Dahl and Sarvey, 1989; Colino and Malenka, 1993; Petersen *et al.*, 2013) which results in the facilitation of the second pulse when the LPP is stimulated but in either no facilitation or even a depression of the second pulse when the MPP is stimulated (Fig. 2B). Excitatory post synaptic currents (EPSCs) were recorded in DG granule cells in the whole-cell configuration of the patch clamp technique from a holding potential of -70 mV. Stimuli were delivered at a low intensity that produced EPSCs that were approximately 15-20% of maximum possible amplitude in order to minimize as much as possible current spreading to the adjacent pathway (Petersen *et al.*, 2013). The two pulses were separated by 100 ms inter-pulse interval. Both genotypes exhibited a facilitation for the LPP (WT: 1.4 ± 0.1, n=5; APP/PS1: 1.6 ± 0.1, n=8) but not for the MPP (WT: 1.0 ± 0.1, n=6; APP/PS1: 1.0 ± 0.1, n=8) (Fig. 2B).

Then we investigated if the relative amount of AMPA *vs* NMDA mediated synaptic currents at DG granule cells were affected by the genotype in DG granule cells of APP/PS1 and WT mice (Fig. 2C). AMPA currents were recorded at a holding potential of -70 mV, a potential at which NMDA currents are virtually absent due to the Mg^{2+} voltage-dependent block (Nowak *et al.*, 1984; Mayer *et al.*, 1984). NMDA currents were isolated at a holding potential of +40 mV in the presence of 50 μM NBQX to block AMPA and kainate currents. We found no difference in the AMPA/NMDA ratio between WT (2.82 ± 0.45, n=10) and APP/PS1 mice (2.35 ± 0.39, n=9; p=0.452). Furthermore, the AMPA rectification index (AMPA RI), a proxy to investigate for possible changes of AMPA receptor properties did not significantly differ between the genotypes (WT: 0.51 ± 0.06, n=10; APP/PS1: 0.49 ± 0.08, n=9; p=0.794) suggesting no major alteration in AMPA receptor properties in APP/PS1 mice.

DG granule cells display higher excitability in APP/PS1 mice

We next characterized basic intrinsic properties of WT and APP/PS1 DG granule cells, *i.e.* input resistance (R_{in}), total amplitude of AP, amplitude of the overshoot, time to peak of the AP, time to reach the half-maximal amplitude (t_{50}), threshold potential but found no significant differences (Table 1). Only the resting membrane potential was slightly higher for APP/PS1 compared to WT mice (-72.7 ± 0.9 mV, n=23; -75.4 ± 0.7 mV, n=15 respectively, * p<0.05, Table 1). Worthy of note, the minimal current required to trigger APs (I_{thr}) was significantly lower for APP/PS1 compared to WT mice (APP/PS1: 40.3 ± 2 pA, n=31; WT: 56 ± 3.7 pA, n=30, *** p<0.001) (Table 1) indicating a higher intrinsic excitability of APP/PS1 DG granule cells.

DG granule cells in adult mice are constituted of newly born (immature) and mature neurons reflecting their dynamic integration in the DG throughout the entire life of the organism. These two populations of DG granule cells have been previously described in WT rodents (van Praag *et al*., 2002; Schmidt-Hieber *et al*., 2004; Mongiat *et al*., 2009; Spampanato *et al*., 2012) and their relative contribution to memory processing such as pattern separation and pattern completion have been investigated (Aimone *et al*., 2011; Nakashiba *et al*., 2012). Remarkably, these two populations display different intrinsic properties among which the input resistance (R_{in}) and the firing pattern have been used to discriminate them (Nenov *et al*., 2015). This prompted us to ask whether intrinsic properties of DG cells were differentially affected by Aβ pathology in APP/PS1 mice. Whole-cell patch clamp recordings were carried out in DG granule cells from 6 months-old WT and APP/PS1 female mice. Figure 3A shows representative electrotonus and action potentials (APs) in DG granule cells from a WT mouse in response to long (250 ms) depolarizing current step injections of 10 pA

increments from 60 pA up to 200 pA in current-clamp mode at a membrane potential close to -70 mV. On the basis of firing pattern and input resistance, DG granule cells could be divided into two distinct categories, termed type 1 and type 2 according to Nenov et al (2015). When comparing type 1 *vs* type 2 DG granule cells according to the genotype, we found that WT type 1 DG cells had a high R_{in} (368 ± 20 MΩ, n=13) whereas WT type 2 DG cells had a significant lower R_{in} (279 ± 19 MΩ, n=16, ** p<0.01) (Table 2). For APP/PS1 mice, type 1 DG cells had a R_{in} of 368 ± 16 MΩ (n=17) and type 2 DG cells a R_{in} of 294 ± 18 MΩ (n=14, ** p<0.01) (Table 2) but type 1 and type 2 R_{in} were not significantly different with respect to the genotype (p=0.993 and p=0.562 respectively) (Table 2). Type 1 DG granule cells exhibited spikes starting from a moderate intensity (50-60 pA), increasing in frequency following steps increments (Fig. 3A). At current steps of high intensity (>120 pA), type 1 DG granule cells displayed spike frequency adaptation (Benda and Hertz, 2003) as shown by the progressive decrease in the amplitude of APs leading to their complete block before the end of the current step (Fig. 3A). In contrast, type 2 DG granule cells fired throughout all the current step without failure (Fig. 3A) and exhibited firing frequencies linearly proportional to the intensity of the current step, *i.e.* the maximum number of APs was always observed for the highest current intensity (Fig. 3B). The proportion of type 1 *vs* type 2 DG granule cells was similarly distributed (WT: 46.7 % *vs* 53.3 % respectively, n=30; APP/PS1: 54.8 % *vs* 45.2 % respectively, n=31) and did not depend on the genotype (p=0.366, Chi-square = 0.815, Chi-squared test). Whatever the intensity of the current steps, APP/PS1 DG granule cells fired significantly more spikes that WT DG granule cells for both type 1 and type 2 (Fig. 3B; type 1: F=38.44, DF=1, *** p<0.0001; type 2: F=47.25, DF=1, *** p<0.0001, two way ANOVA). Moreover, whatever the type, the interspike interval was shorter for APP/PS1 DG granule cells than WT DG granule cells highlighting the higher excitability of APP/PS1 DG granule

cells (Fig. 3C; type 1: F=25.37, DF=1, *** p<0.0001; type 2: F=15.53, DF=1, *** p<0.0001, two way ANOVA). In order to investigate spike frequency adaptation, *i.e.* the reduction of the firing rate for a stimulus of constant intensity, we examined the last three interspike intervals in type 2 DG granule cells to search for possible differences between WT and APP/PS1 mice. Whatever the interval, *i.e.* the third, the second or the first, they were no differences between genotypes (data not shown). Therefore, APP/PS1 type 1 and type 2 DG granule cells spiked at a higher frequency compared to WT in response to current steps.

The potentiation of population spike amplitude is impaired at the LPP-DG synapse in APP/PS1 mice

It has been recently reported that the excitability of DG granule cells was highly plastic but also remarkably modulated by long-term potentiation of MPP-DG synaptic transmission (Lopez-Rojas *et al*., 2016). We first recorded input-output relationships by stimulating the LPP with increasing intensity (0 - 300 μA; 200 μs at 0.1 Hz). This range of stimuli triggered a population spike reflecting the generation of action potentials in DG granule cells in response to the synaptic stimulation of LPP inputs (Fig. 4A left panel). The population spike amplitude (PSA) plotted against stimulus intensity was best fitted by a non-linear regression which plateaued within 250-300 μA (Fig. 4A right panel). The input-output relationships were significantly different between genotypes (F=26.11, DF=1, *** p<0.0001, two way ANOVA), APP/PS1 mice at 6 months of age always displaying a smaller population spike amplitude (PSA) compared to the aged-matched WT for a given stimulation intensity (Fig. 4A right panel). This indicated an alteration of spike transfer between the entorhinal cortex and DG granule cells in APP/PS1 female mice. Because APP/PS1 DG granule cells displayed higher intrinsic excitability, increased PSA may have been expected in APP/PS1 mice. The decreased

PSA in APP/PS1 mice for a given stimulation intensity may be caused by decreased EPSC amplitude due to less excitable PP fibers through reduced release probability or less PP inputs. However, the mean amplitude of EPSCs (stimulus intensity range: 20-65 µA) was not significantly different between genotypes (WT: 150.8 ± 12.4 pA, n=30; APP/PS1: 150.9 ± 14.3 pA, n=29, *p*=0.997).

We then tested whether spike transfer from the entorhinal cortex to the DG was modulated by a high frequency stimulation (HFS) protocol consisting of 3 bursts of 100 stimuli at 100 Hz with a 10 s interburst interval. HFS triggered a robust and long-lasting potentiation of PSA in WT female mice (187 ± 14%, n=17). The potentiation of PSA was completely blocked by 50 µM AP-V (n=9) (Fig. 4B) evidencing the requirement of NMDA receptors (Errington *et al*., 1987; Jester *et al*., 1995). The potentiation of PSA was significantly reduced by half in APP/PS1 mice (146 ± 8%, n=16, * $p<0.05$) (Fig. 4B). Because the input/output relationships were significant different between genotypes (Fig. 4A), stimulating intensities triggering 30-35% of the maximal amplitude of PSA were not in a same range between WT and APP/PS1 (WT: 60-80 µA; APP/PS1: 70-90 µA). Therefore we checked if the degree of potentiation of PSA induced by the HFS protocol was linked to the baseline amplitude of population spike (0.8 - 1.6 mV) triggered by stimuli intensities within the range 60-100 µA. Whatever the genotype, the degree of potentiation of PSA was not linked to its baseline amplitude (goodness of fit: $R2_{WT} = 0.11$, $Sy.x_{WT} = 57.8$, n=17; $R2_{APP/PS1} = 0.002$, $Sy.x_{APP/PS1} = 35.2$, n=33).

Worthy of note, the robust potentiation of PSA induced by HFS occurred in the absence of noticeable alteration of synaptic strengh as shown by the lack of significant potentiation of EPSCs measured at 50-60 minutes versus the baseline (100%) for both genotype (Fig. 4C)

(WT: 117 ± 12%, n=15, *p*=0.18; APP/PS1: 112 ± 9%, n=16, *p*=0.21). It is very unlikely this lack of potentiation was related to a "wash out" phenomenon that could occur during whole-cell patch clamp recordings as the same HFS protocol induced a significant increase in the EPSP amplitude/slope ratio in the following experiments (see Fig. 5D). An early potentiation of EPSCs following the application of HFS was observed for both genotype although not significantly different (10-20 min, WT: 156 ± 12%, n=16; APP/PS1: 157 ± 10%, n=16, *p*=0.98). Therefore in our experimental conditions, the long term potentiation of PSA does not result from major changes in excitatory synaptic currents.

The excitability of DG granule cells is differently affected by high frequency stimulation in WT *vs* APP/PS1 mice

In order to gain information linking spike transfer at the LPP-DG synapse to DG granule cells excitability, we investigated the coupling between EPSPs and the generation of spikes in whole-cell current clamp recordings. Figure 5A (left panel) shows representative electrotonus and action potentials (APs) in a DG granule cell from a WT mouse in response to the stimulation of LPP by short (200 μs) depolarizing current steps (10 μA increments) in current-clamp mode at a membrane potential close to -70 mV.

The EPSP-to-Spike (E-S) curve, which relates EPSP-slopes to the associated AP firing probability, was generated by applying increasing stimuli to cover from a sub-threshold EPSP evoking no action potential to an EPSP evoking an action potential with 100% probability (Fig. 5B). EPSP slopes were measured during the first two milliseconds (Fig. 5A), a time window which mainly reflects the fast component of AMPA receptor mediated synaptic transmission (Lopez-Rojas *et al.*, 2016). In control conditions, before applying the HFS

protocol, there were no significant differences between genotypes in the E-S curves (p=0.849) (Fig. 5B, solid lines). We searched whether the probability of discharge of the postsynaptic DG granule cells in response to excitatory synaptic stimulation was differently affected in WT *vs* APP/PS1 mice. We compared E-S curves generated in the absence or after applying the HFS protocol triggering PSA potentiation. HFS induced a significant large leftward shift of the E-S curves (Fig. 5B, dotted lines) in both genotypes (EC_{50} WT: 5.96 ± 0.38, n=15, EC_{50} $WT_{after\ HFS}$: 4.51 ± 0.41, n=11, * p<0.05; EC_{50} APP/PS1: 5.85 ± 0.39, n=15, EC_{50} $APP/PS1_{after\ HFS}$: 3.92 ± 0.27, n=10, ** p<0.01) (Fig. 5C). Remarkably this leftward shift was significantly larger for APP/PS1 *vs* WT mice (F=489.9, DF=1, *** p<0.001, 2 way ANOVA), corresponding to a higher increase in E-S coupling following the HFS protocol. E-S potentiation corresponds to the strengthening of the electrical coupling between the dendritic synaptic inputs and the soma which results in greater action potential output for a given synaptic input. It is known to depend on the intrinsic leakiness of dendritic and somatic compartments but also on synaptic inhibition due to GABA-A receptors. As all experiments were performed in the presence of bicuculline, any change in the E-S potentiation would presumably be related to modification in synaptically driven depolarization and propagation to the spike trigger zone within the soma. The leftward shift indicates an increased excitability in DG granule cells induced by HFS, *i.e.* to a given EPSP slope corresponds a higher AP firing probability. These results show that HFS induces long lasting changes in intrinsic properties of DG granule cells, likely related to dendritic properties, with a more pronounced effect for APP/PS1 genotype.

Whereas the coupling EPSP slope - AP firing probability is increased in APP/PS1 mice following HFS, the level of PSA potentiation is lower in APP/PS1 mice than in WT mice. One

possible explanation for these puzzling results may arise from the decreased stimulation - PSA relationship in APP/PS1 mice (Fig. 5A) making the HFS induction protocol less efficient to promote potentiation of PSA in APP/PS1 mice. Because the slope of EPSPs determines to some extent the amplitude of population spike, we considered the values of the slope before and after HFS for both genoype. Within the range of stimulus intensity 20 - 40 µA, EPSPs slope was not significantly different for WT ($WT_{before\ HFS}$: 3.24 ± 0.35 mV/ms, n=10; $WT_{after\ HFS}$: 3.40 ± 0.37 mV/ms, n=17, p=0.772) whether it was significantly decreased in APP/PS1 following HFS ($APP/PS1_{before\ HFS}$: 4.33 ± 0.52 mV/ms, n=12; $APP/PS1_{after\ HFS}$: 2.90 ± 0.42 mV/ms, n=12, * p=0.0458). Therefore, eventhough APP/PS1 DG granule cells are more excitable, *i.e.* able to fire more APs in response to a given synaptic input (EPSPs), the HFS induction protocol was not efficient to potentiate EPSPs slope.

Then we looked at the ratio between the EPSP amplitude and the EPSP slope for subthreshold EPSPs (*i.e.* not triggering APs) before and after HFS. Whereas EPSP slopes relate to synaptic transmission, EPSP amplitudes are strongly determined by dendritic integration due to voltage-dependent ionic channels (Lopez-Rojas *et al*., 2016). We found a significant increase in the EPSP amplitude/slope ratio for APP/PS1 mice ($APP/PS1_{before\ HFS}$: 4.55 ± 0.18, n=15; $APP/PS1_{after\ HFS}$: 6.08 ± 0.31, n=11, *** p<0.001) but not for WT mice ($WT_{before\ HFS}$: 4.9 ± 0.3, n=15; $WT_{after\ HFS}$: 5.7 ± 0.33, n=12, p=0.08) (Fig. 5D).

Discussion

In the present study we investigated the electrophysiological properties of DG granule cells in conditions of a robust Aβ plaque load and unambiguous neuroinflammatory activation of

astrocytes and microglia in APP/PS1 female mice. These molecular and cellular alterations parallel functional deficits in an hippocampus-dependent memory task. We report prominent differences in the intrinsic excitability of DG granule cells and in the plasticity of E-S coupling leading to dysfunctional spike transfer between the entorhinal cortex and the hippocampus.

Histopathological and behavioral alterations in APP/PS1 female mice

We report that APP/PS1 female mice at 6 months of age displayed Aβ plaques and expressed abundant hypertrophic astrocytes and amoeboïd microglia preferentially located in the *stratum moleculare* of the DG, a region early affected in the spatiotemporal progression of the disease (Hurtado *et al*., 2010). Our findings extend those of Richetin et al (2017) reporting in older APP/PS1 female mice (7-9 months) the presence of abundant hypertrophic astrocytes in the DG. Concomitantly, APP/PS1 female mice displayed impaired contextual fear conditioning. These results are in general agreement with other studies reporting impairments of CFC in APP/PS1 mice as early as 4-6 months of age (Kilgore *et al*., 2010; Bonardi *et al*., 2011; Janus *et al*., 2015). However, differences in mice gender and in training protocols such as the foot-shock intensity and/or its duration prevent closer and pertinent comparisons of our results with these previous studies.

Passive and active membrane properties of WT and APP/PS1 DG granule cells

Adult DG granule cells are constituted of newly generated granule cells (immature granule cells) and mature granule cells. These two populations can be divided into type 1 and type 2, on the basis of their input resistance and their firing patterns. Type 1 DG granule cells are considered to be young/immature neurons whereas type 2 DG granule cells would

correspond to more mature neurons (van Praag *et al*., 2002; Mongiat *et al*., 2009; Spampanato *et al*., 2012). We found a ratio of about 50 to 50 percent of type 1 *vs* type 2 DG granule cells in WT DG granule cells. This unexpected result showing a number of type 1 DG granule cells (presumably less mature) almost similar to the number of type 2 DG granule cells (presumably more mature) deserves further investigations given that the majority of granule neurons at 6 months old are presumably mature. Worthy of note, a ratio shifted towards even less type 2 (70 to 30 percent of type 1 *vs* type 2 DG granule cells) has been reported in 9 months old WT mice (Nenov *et al*., 2015).

In contrast to Nenov et al (2015), we report that the ratio between type 1 and type 2 DG granule cells was not significantly affected by the genotype whereas it was unbalanced (60 to 40 percent of type 1 *vs* type 2 DG granule cells) for 9 months old Tg2576 mice (Nenov *et al*., 2015). Furthermore, we did not observe differences in R_{in} due to genotype whereas Nenov et al (2015) reported a significant difference for type 2 DG granule cells between WT and Tg2576 mice. These discrepancies might be related to different experimental conditions. First, the transgenic mouse model was different (Tg2576 *vs* APP/PS1). Second we used only female mice whereas male and female were used indifferently in Nenov's study introducing a gender experimental bias. Last, we studied 6 months old female mice whereas 9 months old male and female mice were used in Nenov's study. Interestingly, Nenov et al (2015) suggested that differences observed in WT *vs* Tg2576 DG granule cells could be due to a decrease in proliferation, survival, maturation or integration of newborn DG neurons within DG. If it holds, the younger age of our mice could blunt differences due to these mechanisms. Worthy of note, the estrous cycle is known to alter hippocampal spinogenesis and spine densities (Gould *et al*., 1990; Hara *et al*., 2015) and adult-born DG cells in APP/PS1

female mice at older age than in our study display impaired dendritic spine density contributing to reduced survival rate (Richetin *et al*., 2017). We clearly show that the population spike amplitude, which is related to the number of DG granule cells discharging, was decreased in APP/PS1 *vs* WT at a given stimulation intensity. In contrast, the intrinsic excitability of DG granule cells was significantly increased in APP/PS1 *vs* WT. In line with these data, the current threshold (I_{thr}) to trigger APs was significantly lower in APP/PS1 *vs* WT for both type 1 and type 2 DG granule cells. Potential mechanisms underlying the increased excitability in APP/PS1 DG granule cells may involve voltage-dependent channels such as A-type K^+ channels (Sun *et al*., 2011) and calcium-activated K^+ channels (Brenner *et al*., 2005; Ye *et al*., 2010).

Plasticity of spike transfer and intrinsic excitability in DG granule cells of WT *vs* APP/PS1

Synaptic and non-synaptic, *i.e.* intrinsic excitability, forms of plasticity likely coexist and interact coherently together to regulate information processing in the brain (Daoudal and Debanne, 2003). As both types of DG granule cells likely participate to the transfert of information at the PP-DG synapse and whereas immature DG granule cells display similar dendritic complexity than mature granule cells (Morgenstern *et al*., 2008), we analysed pathophysiological modulation of the transfert of information at the LPP-DG synapse considering DG granule cells as a whole. We provide strong evidence that plasticity of intrinsic excitability of DG granule cells controls spike transfer at the LPP-DG synapse and is affected in APP/PS1 mice. This plasticity has a lower induction-threshold than the archetypical synaptic plasticity described in DG mature granule cells (Lopez-Rojas *et al*., 2016) and likely accounts for a large part of the partial impairment of the potentiation of PSA following HFS. Indeed, HFS triggered a strong potentiation of PSA in DG granule cells not

related to enhanced synaptic plasticity even though this potentiation requires the activation of NMDA receptors activated by ambiant glutamate (Errington *et al*., 1987; Sah *et al*., 1989) and likely modulating dendritic integration properties (Krueppel *et al*., 2011).

In the present work, we report that the potentiation of PSA following the HFS-induction protocol was impaired in APP/PS1 mice. Interestingly, the exogenous application of soluble Aβ oligomers lead the impairment of the HFS-induced potentiation of PSA in the adjacent *stratum pyramidale* of CA1 neurons in mouse hippocampal slices (Lei *et al*., 2016). The authors attributed this impairment to the reduction of extracellular glutamate uptake leading to an increase in ambiant glutamate and consequently an increase in NMDA receptor-dependent neuronal excitability. However, the exogenous application of soluble Aβ oligomers does not mimic either in time (acute bolus of soluble Aβ oligomers *in vitro* versus progressive increase in soluble Aβ oligomers concentration *in vivo*) or space (homogenous soluble Aβ oligomers concentration within all the slice *in vitro* versus localized soluble Aβ oligomers concentration increase in the vicinity of Aβ plaques *in vivo*) what occurs *in vivo* which renders difficult any relevant comparison. Furthermore the cellular origin of Aβ oligomers (neurons *vs* glia) is not considered in exogenous application.

Although the potentiation of PSA following HFS is decreased in APP/PS1 mice as compared to WT mice, our results reveal that HFS increases the E-S coupling to a larger extent in APP/PS1 mice. Therefore whereas the intrinsic excitability of DG granule cells is enhanced the potentiation of PSA is decreased. This counter intuitive result could be the result of a less efficient HFS protocol in APP/PS1 to induce potentiation of EPSPs. Indeed our results show a significant decrease of EPSP potentiation after HFS in APP/PS1 leading to a decrease of PSA

potentiation. EPSP amplitude is strongly determined by dendritic integration via voltage-dependent ionic channels hence changes in dendritic processing of synaptic input could account for excitability changes. Therefore the increase of EPSP amplitude/slope ratio observed for APP/PS1 mice following HFS, but not for WT mice is likely related to the higher excitability of APP/PS1 DG granule cells but much less to variation in synaptic transmission. In good agreement with a major role of dendritic integration in intrinsic excitability of DG granule cells, the blockade of dendritic A-type potassium channels by 4-aminopyridine significantly increased the EPSP amplitude/slope ratio and decreased EC_{50} value (Lopez-Rojas *et al*., 2016). In line with a significant role of dendritic A-type potassium channels in a mouse model of AD, the observed dendritic depletion of Kv4.2, the potassium channel subunit which mediates the majority of A-type current, induces dendritic hyperexcitability in the CA1 region in hAPP mice (Hall *et al*., 2015).

The E-S coupling following HFS is remarkably different between WT and APP/PS1 mice. Hence not only the increased intrinsic excitability but also a strengthened E-S coupling likely enhance spike transfer between the entorhinal cortex and the DG which may participate in the well known enhanced excitability of hippocampal circuits in the AD pathology. This enhanced spike transfer could act as compensatory mechanisms for the well established early loss of perforant path fibers from the layer II of entorhinal cortex to the hippocampus encountered in the course of the pathology (Llorens-Martin *et al*., 2014).

Worthy of note, the present study focussed on excitatory synaptic drive but one may wants to know how this could relate to the *in vivo* situation with intact inhibitory drive. GABAergic interneurons in the DG are multiple and densely expressed in the hilus (for review, see

Houser, 2007). Hilar interneurons project to perisomatic and proximal dendritic regions of DG granule cells (Amaral *et al*., 2007) exerting synaptic inhibition that shunts AP generation (Ben-Ari *et al.,* 2005). Whereas GABA-A receptors expressed by DG granule cells are responsible for a tonic inhibition (Engin *et al*., 2015) leading to their sparse activation, the activation of GABA-B receptors enhances DG granule cell activity by reducing synaptic inhibition driven by hilar interneurons (Burgard and Sarvey, 1991; Mott and Lewis, 1991; Mott et al., 1993; Foster *et al*., 2013). Therefore blocking GABA-A receptors with bicuculline seems pertinent to suppress the inhibitory drive. However due to the expression of GABA-B receptors, the control of the transfer of information at the perforant path to the hippocampus by GABAergic control of DG granule cells is a complex issue which clearly deserves further investigation.

In conclusion, our study report for the first time that a non-synaptic form of plasticity, *i.e.* the plasticity of intrinsic excitability of DG granule cells, is markedly impacted in a mouse model of AD. This is of paramount importance given the crucial role of the functional integrity of the DG in the formation of new memories which is particularly impacted in AD. Thus in addition to enlarge the fundamental knowledge of AD, our results may open new routes for improvement and/or therapeutic intervention.

Acknowledgments

We deeply thank Jeffrey Lopez-Rojas for his invaluable help with electrophysiological recordings, extremely fruitful discussions and constant availability and kindness. We thank Gaël Barthet for his constant support and very fruitful comments. We thank Benoit Silvestre de Ferron for the cartoon shown in Figure 2. The microscopy was performed in the Bordeaux

Imaging Center (BIC), a service unit of the CNRS-Inserm and Bordeaux University, member of the national infrastructure France BioImaging. We thank Patrice Mascalchi from the BIC for his technical support.

Funding

This work was supported by a joint program between the University of Bordeaux and the China Scholarship Council (CSC) to NJ (Grant: 201506890031)

Conflict of interest

None declared

Author contributions

Nan Jiang: Investigation, Visualization, Formal analysis

Dario Cupollilo: Investigation, Formal analysis

Noelle Grosjean: Investigation, Formal analysis

Emeline Muller: Investigation, Formal analysis

Séverine Deforges: Investigation

Christophe Mulle: Writing - Review & Editing

Thierry Amédée: Conceptualization, Methodology, Validation, Formal analysis, Supervision, Funding acquisition, Writing - Original draft, Writing - Review & Editing

References

Aimone JB, Deng W, Gage FH. 2011. Resolving new memories: a critical look at the dentate gyrus, adult neurogenesis and pattern separation. Neuron 70: 589-596.

Akiyama H, Arai T, Kondo H, Tanno E, Haga C, Ikeda K. 2000. Cell mediators of inflammation in the Alzheimer disease brain. Alzheimer Dis Assoc Disord 14: 47-53.

Alzheimer's Association Report. 2018. Alzheimer's disease fact and figures Alzheimer's & Dementia 14: 367-429.

Barnes LL, Wilson RS, Bienias JL, Schneider JA, Evans DA, Bennett DA. 2005. Sex differences in the clinical manifestations of Alzheimer disease pathology. Arch Gen Psychiatry 62:685–691.

Bonardi C, de Pulford F, Jennings D, Pardon MC. 2011. A detailed analysis of the early context extinction deficits seen in APPswe/PS1dE9 female mice and their relevance to preclinical Alzheimer's disease. Behav Brain Res. 222(1):89-97.

Brenner R, Chen QH, Vilaythong A, Toney GM, Noebels JL, Aldrich RW. 2005. BK channel beta4 subunit reduces dentate gyrus excitability and protects against temporal lobe seizures. Nat Neurosci 8: 1752–1759.

Burgard EC, Sarvey JM. 1991. Long-lasting potentiation and epileptiform activity produced by GABAB receptor activation in the dentate gyrus of rat hippocampal slice. J Neurosci. 11(5):1198-209

Colino A, Malenka RC. 1993. Mechanisms underlying induction of long-term potentiation in rat medial and lateral perforant paths in vitro. J Neurophysiol 69(4):1150-1159.

Criscuolo C, Fontebasso V, Middei S, Stazi M, Ammassari-Teule M, Yan SS, Origlia N. 2017. Entorhinal Cortex dysfunction can be rescued by inhibition of microglial RAGE in an Alzheimer's disease mouse model. Sci Rep. 7:42370.

Dahl D, Sarvey JM. 1989. Norepinephrine induces pathway-specific long-lasting potentiation and depression in the hippocampal dentate gyrus. Proc Natl Acad Sci U S A. 86(12):4776-80

Daoudal G, Debanne D. 2003. Long-term plasticity of intrinsic excitability: learning rules and mechanisms. Learn Mem. 10(6):456-465.

Deng W, Aimone JB, Gage FH. 2010. New neurons and new memories: how does adult hippocampal neurogenesis affect learning and memory? Nat Rev Neurosci 11:339-350.

Errington ML, Lynch MA, Bliss TV. 1987. Long-term potentiation in the dentate gyrus: induction and increased glutamate release are blocked by D(-)aminophosphonovalerate. Neuroscience. 20(1):279-284.

Foster JD, Kitchen I, Bettler B, Chen Y. 2013. GABAB receptor subtypes differentially modulate synaptic inhibition in the dentate gyrus to enhance granule cell output. Br J Pharmacol. 168(8):1808-19

Gallagher JJ, Minogue A, Lynch M. 2013. Impaired performance of female APP/PS1 mice in the Morris water maze is coupled with increased Aβ accumulation and microglial activation. Neurodegener Dis 11:33–41.

Gould E, Woolley C, Frankfurt M, McEwen BS. 1990. Gonadal steroids regulate dendritic spine density in hippocampal pyramidal cells in adulthood. J Neurosci 10: 1286–1291.

Hall AM, Throesch BT, Buckingham SC, Markwardt SJ, Peng Y, Wang Q, Hoffman DA, Roberson ED. 2015. Tau-dependent Kv4.2 depletion and dendritic hyperexcitability in a mouse model of Alzheimer's disease. J Neurosci 35:6221-6230.

Hara Y, Waters E, McEwen B, Morrison J. 2015. Estrogen effects on cognitive and synaptic health over the lifecourse. Physiol Rev. 95:785-807.

Heneka MT, Golenbock DT, Latz E. 2015. Innate immunity in Alzheimer's disease. Nat Immunol 16:229-236.

Heneka MT, Obanion M. 2007. Inflammatory processes in Alzheimer's disease. Journal of Neuroimmunology 184(1-2):69–91.

Hunsaker MR, Mooy GG, Swift JS, Kesner RP. 2007. Dissociations of the medial and lateral perforant path projections into dorsal DG, CA3, and CA1 for spatial and nonspatial (visual object) information processing. Behav Neurosci 121:742-750.

Hurtado DE, Molina-Porcel L, Iba M, Aboagye AK, Paul SM, Trojanowski JQ, Lee VM. 2010. Aβ accelerates the spatiotemporal progression of tau pathology and augments tau amyloidosis in an Alzheimer mouse model. Am J Pathol 177:1977-1988.

Jankowsky JL, Fadale DJ, Anderson J, Xu GM, Gonzales V, Jenkins NA, Copeland NG, Lee MK, Younkin LH, Wagner SL, Younkin SG, Borchelt DR. 2004. Mutant presenilins specifically elevate the levels of the 42 residue β-amyloid peptide in vivo: evidence for augmentation of a 42-specific γ secretase. Human Molecular Genetics 13:159–170

Janus C, Flores AY, Xu G, Borchelt DR. 2015. Behavioral abnormalities in APPSwe/PS1dE9 mouse model of AD-like pathology: comparative analysis across multiple behavioral domains. Neurobiol Aging. 36(9):2519-2532.

Jester JM, Campbell LW, Sejnowski TJ. 1995. Associative EPSP—spike potentiation induced by pairing orthodromic and antidromic stimulation in rat hippocampal slices. J Physiol (Lond) 484: 689–705.

Kilgore M , Miller CA, Fass DM, Hennig KM, Haggarty SJ, Sweatt JD, Rumbaugh G. 2010. Inhibitors of class 1 histone deacetylases reverse contextual memory deficits in a mouse model of Alzheimer's disease. Neuropsychopharmacology. 35(4):870-880.

Krueppel R, Remy S, Beck H. 2011. Dendritic integration in hippocampal dentate granule cells. Neuron 71(3):512-528

Lei M, Xu H, Li Z, Wang Z, O'Malley TT, Zhang D, Walsh DM, Xu P, Selkoe DJ, Li S. 2016. Soluble Aβ oligomers impair hippocampal LTP by disrupting glutamatergic/GABAergic balance. Neurobiology of Disease 85:111–121.

Llorens-Martín M, Blazquez-Llorca L, Benavides-Piccione R, Rabano A, Hernandez F, Avila J, DeFelipe J. 2014. Selective alterations of neurons and circuits related to early memory loss in Alzheimer's disease. Front Neuroanat. 8, 38:1-12.

Lopez-Rojas J, Heine M, Kreutz MR. 2016. Plasticity of intrinsic excitability in mature granule cells of the dentate gyrus. Scientific Reports 6:21615.

Marchetti C, Marie H. 2011. Hippocampal synaptic plasticity in Alzheimer's disease: what have we learned so far from transgenic models? Rev Neurosci 22:373-402.

McNaughton BL. 1980. Evidence for two physiologically distinct perforant pathways to the fascia dentata. Brain Res 199:1-19.

Mayer ML, Westbrook GL, Guthrie PB. 1984. Voltage-dependent block by Mg^{2+} of NMDA responses in spinal cord neurones. Nature 309:261–263

Mott DD, Lewis DV. 1991. Facilitation of the induction of long-term potentiation by GABAB receptors. Science. 252(5013):1718-20

Mott DD, Xie CW, Wilson WA, Swartzwelder HS, Lewis DV. 1993. GABAB autoreceptors mediate activity-dependent disinhibition and enhance signal transmission in the dentate gyrus. J Neurophysiol. 69(3):674-91.

Nakashiba T, Cushman JD, Pelkey KA, Renaudineau S, Buhl DL, McHugh TJ, Rodriguez Barrera V, Chittajallu R, Iwamoto KS, McBain CJ, Fanselow MS, Tonegawa S. 2012. Young dentate granule cells mediate pattern separation, whereas old granule cells facilitate pattern completion. Cell 149:188-201.

Nenov MN, Tempia F, Denner L, Dineley KT, Laezza F. 2015. Impaired firing properties of dentate granule neurons in an Alzheimer's disease animal model are rescued by PPARγ agonism. J Neurophysiol 113:1712-1726.

Nimmerjahn A, Kirchhoff F, Helmchen F. 2005. Resting Microglial Cells Are Highly Dynamic Surveillants of Brain Parenchyma in Vivo. Science. 308: 1314-1318.

Nowak L, Bregestovski P, Ascher P, Herbet A, Prochiantz A. 1984. Magnesium gates glutamate-activated channels in mouse central neurones. Nature. 307:462–465

Petersen RP, Moradpour F, Eadie BD, Shin JD, Kannangara TS, Delaney KR, Christie BR. 2013. Electrophysiological identification of medial and lateral perforant path inputs to the dentate gyrus. Neuroscience 252:154-168.

Penzes P, Cahill ME, Jones KA, VanLeeuwen JE, Woolfrey KM. 2011. Dendritic spine pathology in neuropsychiatric disorders. Nat Neurosci. 14(3):285-293

Phillips RG, LeDoux JE. 1992. Differential contribution of amygdala and hippocampus to cued and contextual fear conditioning. Behav Neurosci 106:274-278.

Querfurth HW, LaFerla FM. 2010. Alzheimer's disease. N Engl J Med 362:329-344.

Richetin K, Petsophonsakul P, Roybon L, Guiard BP, Rampon C. 2017. Differential alteration of hippocampal function and plasticity in females and males of the APPxPS1 mouse model of Alzheimer's disease. Neurobiol Aging 57:220-231.

Sah P, Hestrin S, Nicoll RA. 1989. Tonic activation of NMDA receptors by ambient glutamate enhances excitability of neurons. Science 246:815-818.

Sarlus H, Heneka MT. 2017. Microglia in Alzheimer's disease. J Clin Invest. 127(9):3240-3249

Schmidt-Hieber C, Jonas P, Bischofberger J. 2004. Enhanced synaptic plasticity in newly generated granule cells of the adult hippocampus. Nature 429(6988):184-187.

Schiweck J, Eickholt BJ, Murk K. 2018. Important Shapeshifter: Mechanisms Allowing Astrocytes to Respond to the Changing Nervous System During Development, Injury and Disease. Front Cell Neurosci 12:261.

Selkoe DJ. 2002. Alzheimer's disease is a synaptic failure. Science 298:789-791.

Sinforiani E, Citterio A, Zucchella C, Bono G, Corbetta S, Merlo P, Mauri M. 2010. Impact of gender differences on the outcome of Alzheimer’s disease. Dement Geriatr Cogn Disord 30:147–154.

Spampanato J, Sullivan RK, Turpin FR, Bartlett PF, Sah P. 2012. Properties of doublecortin expressing neurons in the adult mouse dentate gyrus. PLoS One 7:e41029.

Spires-Jones TL, Hyman BT. 2014. The intersection of amyloid beta and tau at synapses in Alzheimer's disease. Neuron 82:756-771.

Stranahan AM, Mattson MP. 2010. Selective vulnerability of neurons in layer II of the entorhinal cortex during aging and Alzheimer's disease. Neural Plast. 2010:108190

Sun W, Maffie JK, Lin L, Petralia RS, Rudy B, Hoffman DA. 2011. DPP6 establishes the A-type K^+ current gradient critical for the regulation of dendritic excitability in CA1 hippocampal neurons. Neuron 71: 1102–1115.

van Praag H, Schinder AF, Christie BR, Toni N, Palmer TD, Gage FH. 2002. Functional neurogenesis in the adult hippocampus. Nature 415:1030-1034.

Wilhelmsson U, Bushong EA, Price DL, Smarr BL, Phung V, Terada M, Ellisman MH, Pekny M. 2006. Redefining the concept of reactive astrocytes as cells that remain within their unique domains upon reaction to injury. PNAS 103:17513–17518.

Figure Legends

Figure 1: APP/PS1 female mice display molecular and behavioral alterations. **A**. Representative micrographs of a hippocampus in APP/PS1 female mice at 3, 6 and 9 months

of age. Slices were double stained for nuclei with 4',6-diamidino-2-phenylindole (DAPI, blue signal) and for Aβ plaques with 2,5-Bis(2-(4-hydroxyphenyl)vinyl) anisole (methoxy-X04, red signal). Note the virtual lack of Aβ plaques at 3 months of age and the progressive expression at 6 and 9 months of age (white arrow heads). At 9 months of age, there is an heavy load of Aβ plaques in the hippocampus but more concentrated in the upper molecular layer (delineated by the white dotted-line), i.e. the *stratum moleculare* of the DG. Bar scale = 250 µm. **B.** Representative micrograph of an Aβ plaque formed of an amyloid core (anti-$A\beta_{1-16}$ antibody, white signal) embedded in a spider web of microglia (Iba-1, green signal) and activated astrocytes (GFAP, red signal) in the vicinity in a 9 months old female mouse. Bar scale = 10 µm. **C**. Bar graphs represent the number of Aβ plaques counted per imaged slice (n) in the whole hippocampus (left panel) and in the DG area as delineated in A (right panel) at 3, 6 and 9 months of age (5 mice). Note the progressive increase of Aβ plaques at each age (female: 3 *vs* 6 months old *** $p<0.001$; 6 *vs* 9 months old *** $p<0.001$; 3 *vs* 9 months old *** $p<0.001$) both in all hippocampus and in the *stratum moleculare* (termed DG area). **D**. Astrocytic status in the DG area for WT and APP/PS1 female mice at 6 months of age. Note the prominent morphological changes in GFAP positive cells (astrocytes) in APP/PS1 *vs* WT female mice (white arrow head), (DAPI, blue signal). Bar scale = 10 µm**. E**. Microglial status in the DG area for WT and APP/PS1 female mice at 6 months of age. Note the morphological changes in Iba-1 positive cells (microglia) in APP/PS *vs* WT female mice (white arrow head). Bar scale = 10 µm**. F.** At day 0, WT and APP/PS1 female mice were placed in a training chamber where they received a mild electric footshock (2s, 0.75 mA). At day 1, mice were reexposed to the same chamber. Contextual fear memory retention was studied by measuring the freezing response in the chamber and freezing percentage was calculated for each animal (left panel). As early as 3 months of age when compared to WT mice, APP/PS1

female mice show impairment of contextual fear conditioning when reexposed to the training chamber. (* p<0.05).

Figure 2: Electrophysiological characterization of the lateral perforant path (LPP) inputs to the hippocampal *dentate gyrus* (DG). **A**. Diagram shows the positions of the stimulating electrode (located in the outer DG molecular layer) and of the recording electrode in patch clamp experiments. Please note that the position of the recording electrode is only for illustrative purpose but does not indicate the exact location of recorded DG granule cells. For field recordings, the electrode is placed near the crest of the suprapyramidal blade. **B**. Electrophysiological dissection of the LPP and medial perforant path (MPP) by paired-pulse experiments in whole-cell patch clamp recordings. DG cells were clamped at - 70 mV and the two pulses were separated by 100 ms. For both genotype the paired-pulse ratio was significantly higher for the LPP *vs* MPP (WT: 1.4±0.07, n=5 *vs* 1.01±0.06, n=6, ** p<0.01; APP/PS1: 1.58±0.07, n=8 *vs* 1.03±0.08, n=8, *** p<0.001). **C**. Representative traces from whole-cell patch clamp experiments showing AMPA-receptor- and NMDA-receptor evoked currents (in the presence of 50 µM NBQX) in DG granule cells. Histograms showing the AMPA to NMDA ratio for WT and APP/PS1 mice (WT:2.82±0.45, n=10; APP/PS1:2.35±0.39, n=9, p=0.452). The AMPA rectification index (AMPA RI) was obtained by dividing the AMPA current amplitude measured at +40 mV by the one measured at -70 mV for WT and APP/PS1 mice (WT:0.51±0.06, n=10; APP/PS1:0.49±0.08, n=9, p=0.794).

Figure 3: APP/PS1 DG granule cells display higher excitability than WT. A. Representative trains of APs elicited by long depolarizing current steps (250 ms) of increasing intensity in WT DG granule cells. Cells were recorded from a membrane potential close to -70 mV in the

whole-cell configuration of the patch clamp technique. DG granule cells were sorted into type 1 and type 2 cells according to their firing patterns. Whatever the genotype, type 1 and type 2 cells were similarly distributed (Type 1: WT = 45.1 %, n=14, APP/PS1 = 54.9 %, n=17; Type 2: WT = 53.3 %, n=16, APP/PS1 = 46.7 %, n=14; *p*=0.366, 1-proportion *Z* test). **B**. Input-output curves for type 1 and type 2 DG granule cells. The number of spikes elicited in response to 250 ms-long depolarizing current steps with 10 pA increments was significantly higher in APP/PS1 *vs* WT DG cells for both type 1 and type 2 (type 1: WT, black circles; APP/PS1, red circles, F=38.44, DF=1, *** *p*<0.0001, 2 way ANOVA; type 2: WT, black squares, APP/PS1, red squares, F=47.25, DF=1, *** *p*<0.0001, 2 way ANOVA). Whatever the genotype the number of spikes elicited in response to 250 ms-long depolarizing current steps with 10 pA increments increased linearly for type 2 but reached a plateau for type 1. **C**. Interspike interval (ISI) plotted as a function of the first three intervals (first spike interval type 1: WT: 15.5±1.6 ms, n=13; APP/PS1: 10.4±0.8, n=17, ** *p*<0.01; first spike interval type 2: WT: 14.6±1.4 ms, n=17; APP/PS1: 9.6±0.7, n=14, ** *p*<0.01) (second spike interval type 1: WT: 20.1±1.9 ms, n=13; APP/PS1: 13.3±1, n=17, ** p<0.01; second spike interval type 2: WT: 19.6±1.9 ms, n=17; APP/PS1: 13.5±1.2 ms, n=14, * *p*=0.05) (third spike interval type 1: WT: 23.2±2.1 ms, n=13; APP/PS1: 17.1±1.5, n=16, * p<0.05; third spike interval type 2: WT: 23.1±1.3 ms, n=17; APP/PS1: 18.2±1.9, n=14, p=0.08). Whatever the type, the first three ISI were significantly higher for WT mice compared to APP/PS1 mice (WT type 1 black circles, APP/PS1 type 1 black squares; F=25.37, DF=1, *** *p*<0.0001; WT type 2 red circles, APP/PS1 type 2 red squares, F=15.53, DF=1, *** *p*=0.0002, 2 way ANOVA).

Figure 4: Transfert of information at the LPP-GE synapse is altered in APP/PS1 female mice. A. Left panel shows representative traces of population spike in DG granule cells from

a WT mouse. The double arrows dotted line represents the amplitude of the population spike. Right panel shows input-output relationship between the population spike amplitude and the stimulus intensity. For each intensity, WT (black circles) and APP/PS1 (red circles) relationships were significantly different (50 µA: WT=0.68±0.12, APP/PS1=0.40±0.07; 100 µA: WT=1.79±0.19, APP/PS1=1.14±0.10; 150 µA: WT=2.54±0.22, APP/PS1=1.71±0.17; 200 µA: WT=2.85±0.26, APP/PS1=2.14±0.16; 250 µA: WT=3.10±0.25, APP/PS1=2.50±0.17; 300 µA: WT=3.20±0.27, APP/PS1=2.62±0.18, F:26.11, DF:1, *** p<0.0001, 2 way ANOVA). Both genotypes were best fitted by a non-linear regression. The goodness-of-fit was assessed by the coefficient of determination R2 ($R2_{WT}$ = 0.998; $R2_{APP/PS1}$ = 0.852). **B.** Left panel shows representative traces of population spike before (white circle) and after HFS (black circle) in DG granule cells. Population spike amplitude were recorded from a membrane potential close to -70 mV in the presence of bicuculline (10 µM). The potentiation of population spike was induced by 3 bursts of 100 stimuli at 100 Hz with a 10-second interburst interval (HFS). Light grey traces are individual traces and black traces are the averaged traces of 60 sweeps before and after HFS. Right panel shows the time course of potentiation of population spike (WT:black circles, APP/PS1:red circles). The average of normalized population spike amplitude (PSA) between 50 and 60 minutes after HFS protocol showed a significant reduction in APP/PS1 female mice (WT: 187±14%, n=17; APP/PS1: 146±8%, n=16; * p<0.05, t test). The potentiation was completely blocked by AP-V (50 µM, light grey circles) (n=9). **C.** Left panel shows representative averaged EPSCs recorded from a holding potential of -70 mV in voltage-clamp during the baseline (0-10 minutes) and after (50-60 minutes) HFS in DG granule cells from WT and APP/PS1 mice. Right panel shows representative time course of EPSCs before and after HFS in WT and APP/PS1. Note the lack of significant long-term potentiation of EPSCs at 50-60 minutes whatever the genotype (WT: 117±12%, n=15,

p=0.18; APP/PS1: 112±9%, n=16, *p*=0.21). All experiments were done in the presence of bicuculline (10 μM).

Figure 5: Plasticity of itrinsic excitability in DG granule cells. A. Representative action potentials (APs) elicited in response to 200 μs depolarizing current steps with 10 μA increments in a DG granule cell from WT mouse. The DG granule cell was recorded from a membrane potential close to -70 mV in the whole cell configuration of the patch clamp technique. **B.** E-S curves before and after high frequency stimulation (HFS). For each genotype (WT, black circles; APP/PS1, red circles) EPSP-slope values were calculated for the first two milliseconds and plotted versus the probability to fire action potentials. EPSP slope value giving a spike probability of 50% were graphically determined from the sigmoidal curves. In the absence of HFS, E-S curves were similar for both genotype (WT: 5.97, Hill slope=0,37, n=15; APP/PS1: 5.98, Hill slope=0.39, n=15). HFS induced prominent shifts of E-S curves to the left (WT:4.98, n=11, F=661.8, DF=1, *** *p*<0.0001, 2 way ANOVA; APP/PS1:3.88, n=10, F=724.9, DF=1, *** *p*<0.0001, 2 way ANOVA) which were significant for both genotype (WT: -1.45±0.57 mV/ms, * *p*=0.018; APP/PS1: -1.93±0.53 mV/ms, ** *p*= 0.0014) but larger for APP/S1 *vs* WT (F=489.9, DF=1, *** *p*<0.0001, 2 way ANOVA). **C.** A significant shift of EC_{50} in the E-S relation was induced by HFS for both WT (WT: 5.96±0.38, n=15, $WT_{after\ HFS}$: 4.51±0.41, n=11, * *p*<0.05) and APP/PS1 (APP/PS1: 5.85±0.39, n=15, $APP/PS1_{after\ HFS}$: 3.92±0.27, n=10, ** *p*<0.01) although with a larger amplitude for the APP/PS1 genotype. **D**. EPSP amplitude/slope ratio before and after synaptic potentiation induced by HFS. The amplitude/slope ratio was not different between WT and APP/PS1 mice before (WT: 4.90±0.30, n=15; APP/PS1: 4.55±0.18, n=15, *p*=0.332) or after synaptic potentiation induced by HFS ($WT_{after\ HFS}$: 5.72±0.33, n=11; $APP/PS1_{after\ HFS}$: 6.08±0.31, n=10,

p=0.406) whereas it was significantly increased by HFS in APP/PS1 mice (APP/PS1: 4.55±0.18, n=15; $APP/PS1_{after\ HFS}$: 6.08±0.31, n=10, *** *p*<0.001) but not for WT (WT: 4.90±0.30, n=15; $WT_{after\ HFS}$: 5.72±0.33, n=11, *p*=0.088).

	Amplitude (mV)	Overshoot (mV)	Peak time (ms)	RMP (mV)	AP threshold (mV)	I_{thr} (pA)	t_{50} (ms)	R_{in} (MΩ)
WT	132.2 ± 2.1 (12)	62.5 ± 2.1 (12)	2.4 ± 0.1 (12)	-72.7 ± 0.9 (23)	-33.2 ± 2.7 (10)	56±3.7 (30)	1.76 ± 0.09 (12)	323 ± 15 (32)
APP/PS1	125.4 ± 2.8 (13)	55.7 ± 2.7 (13)	2.4 ± 0.1 (13)	-75.4 ± 0.7 (15)	-32.1 ± 2.2 (10)	40.3±2 (31)	1.74 ± 0.09 (13)	335 ± 14 (31)

Table 1. Comparison between action potentials properties in DG granule cells from WT and APP/PS1 female mice. Data are mean ± SEM. Values between brackets are n values. *p* values were obtained with Student's *t*-test (amplitude: p=0.070; overshoot: p=0.064; peak time: p=0.885; RMP: * p<0.05; AP threshold: p=0.764; I_{thr}: *** p<0.001; t_{50}: p=0.848; R_{in}: p=0.552). RMP: resting membrane potential. t_{50}: time to get half amplitude of AP. R_{in}: input resistance

	WT				APP/PS1			
	Type 1	*p* (1 *vs* 2)	Type 2	*p* Type 1 (WT *vs* APP/PS1)	Type 1	*p* (1 *vs* 2)	Type 2	*p* Type 2 (WT *vs* APP/PS1)
1^{st} AP latency (ms)	160 ± 9.1 (13)	0.178	177.4 ± 8.5 (17)	0.809	163 ± 8.2 (17)	0.746	158.4 ± 12.1 (14)	0.198
ADP (mV)	8.2 ± 0.7 (13)	0.244	9.5 ± 0.8 (16)	0.217	9.4 ± 0.7 (17)	0.824	9.7 ± 0.8 (14)	0.897
fast AHP (mV)	18 ± 0.9 (13)	0.086	15.3 ± 1.1 (17)	0.525	17.2 ± 0.8 (17)	0.018 *	14.4 ± 0.8 (14)	0.561
slow AHP (mV)	10.3 ± 1 (13)	0.209	8.6 ± 0.9 (16)	0.318	9.2 ± 0.7 (17)	0.343	8.2 ± 0.7 (12)	0.764
I_{thr} (pA)	53.1 ± 3.4 (13)	0.493	58.2 ± 5.9 (17)	0.001 **	37.1 ± 2.9 (17)	0.078	43.6 ± 2.5 (14)	0.042 *
R_{in} (MΩ)	368 ± 20 (13)	0.003 **	279 ± 19 (16)	0.993	368 ± 16 (17)	0.004 **	294 ± 17 (14)	0.562

Table 2. Comparison of action potentials properties of type 1 and type 2 DG granule cells between WT and APP/PS1 female mice. Data are mean ± SEM. For the calculation of the 1^{ST} AP latency, minimal current step intensity was about 54 pA for WT and 40 pA for APP/PS1. Fast and slow AHP were measured in current clamp mode using a 250 ms pulse duration. The fast AHP was measured as the amplitude between the AP threshold and the peak of its fast repolarization. The slow AHP was measured as the amplitude between the AP threshold and the amplitude at the end of the 250 ms pulse. Values between brackets are n values. *p* values were obtained with Student's *t*-test. ADP: after depolarisation. AHP: after hyperpolarisation. I_{thr}: AP current threshold (minimal current intensity inducing an AP).

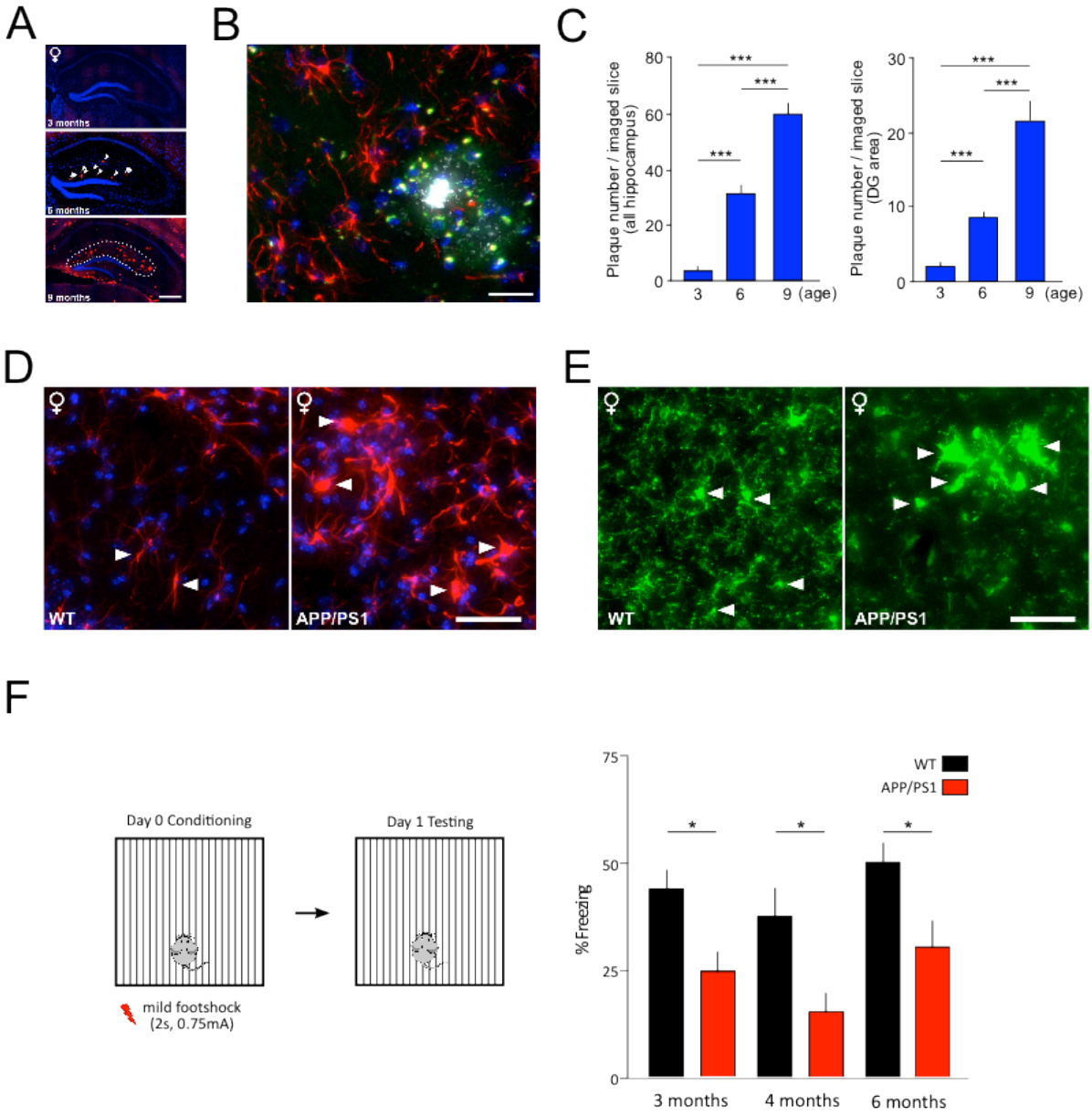
A
3 months
6 months
9 months
B
C
Plaque number / imaged slice (all hippocampus)
80
60
40
20
0
***
***
***
3
6
9 (age)
Plaque number / imaged slice (DG area)
30
20
10
0
***
***
***
3
6
9 (age)
D
WT
APP/PS1
E
WT
APP/PS1
F
Day 0 Conditioning
Day 1 Testing
mild footshock
(2s, 0.75mA)
% Freezing
75
50
25
0
WT
APP/PS1
*
*
*
3 months
4 months
6 months

Figure 1

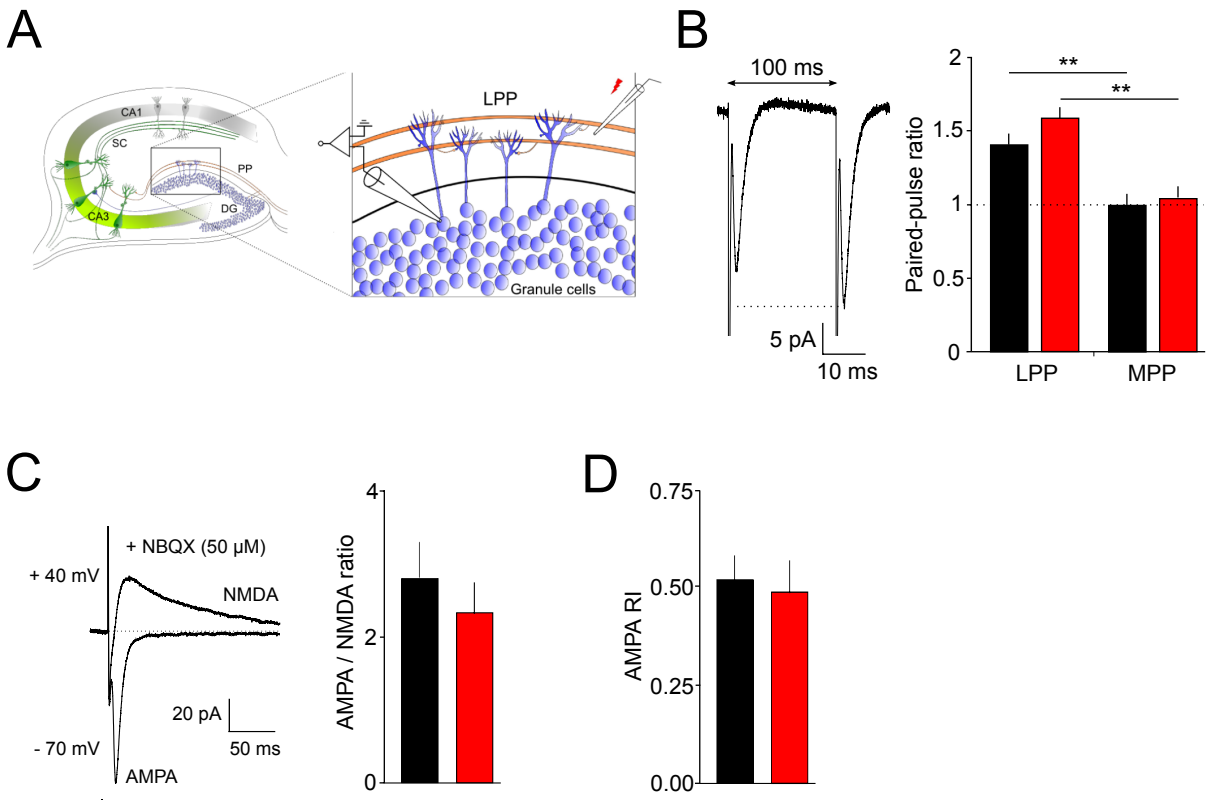
A
CA1
SC
PP
DG
CA3
LPP
Granule cells
B
100 ms
5 pA
10 ms
Paired-pulse ratio
2
1.5
1
0.5
0
**
**
LPP
MPP
C
+ NBQX (50 µM)
+ 40 mV
NMDA
20 pA
50 ms
- 70 mV
AMPA
AMPA / NMDA ratio
4
2
0
D
AMPA RI
0.75
0.50
0.25
0.00

Figure 2

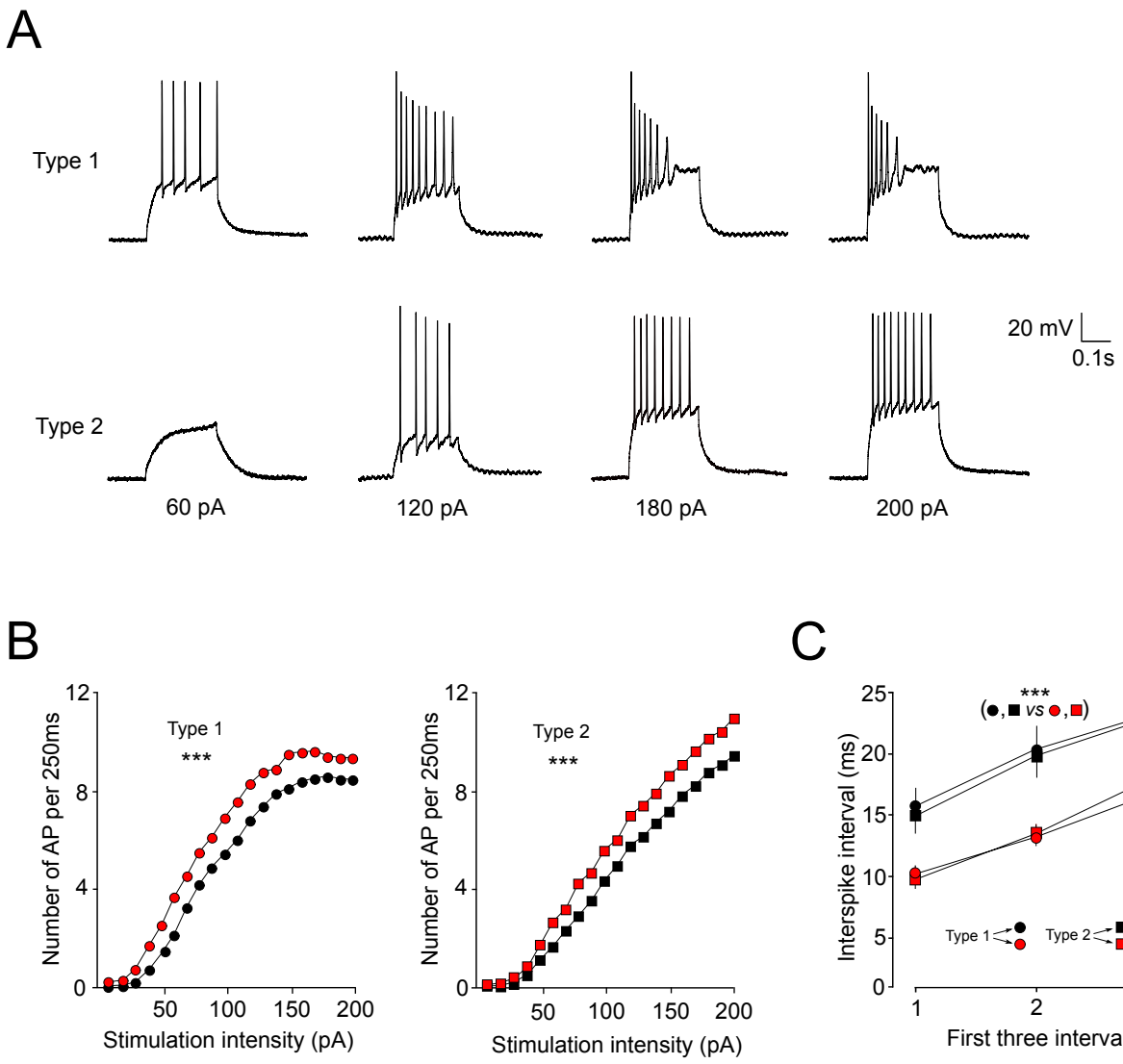
A
Type 1
Type 2
20 mV
0.1s
60 pA
120 pA
180 pA
200 pA
B
Type 1
***
Number of AP per 250ms
Stimulation intensity (pA)
Type 2
***
Number of AP per 250ms
Stimulation intensity (pA)
C
***
(●,■ vs ●,■)
Interspike interval (ms)
Type 1
Type 2
First three intervals

Figure 3

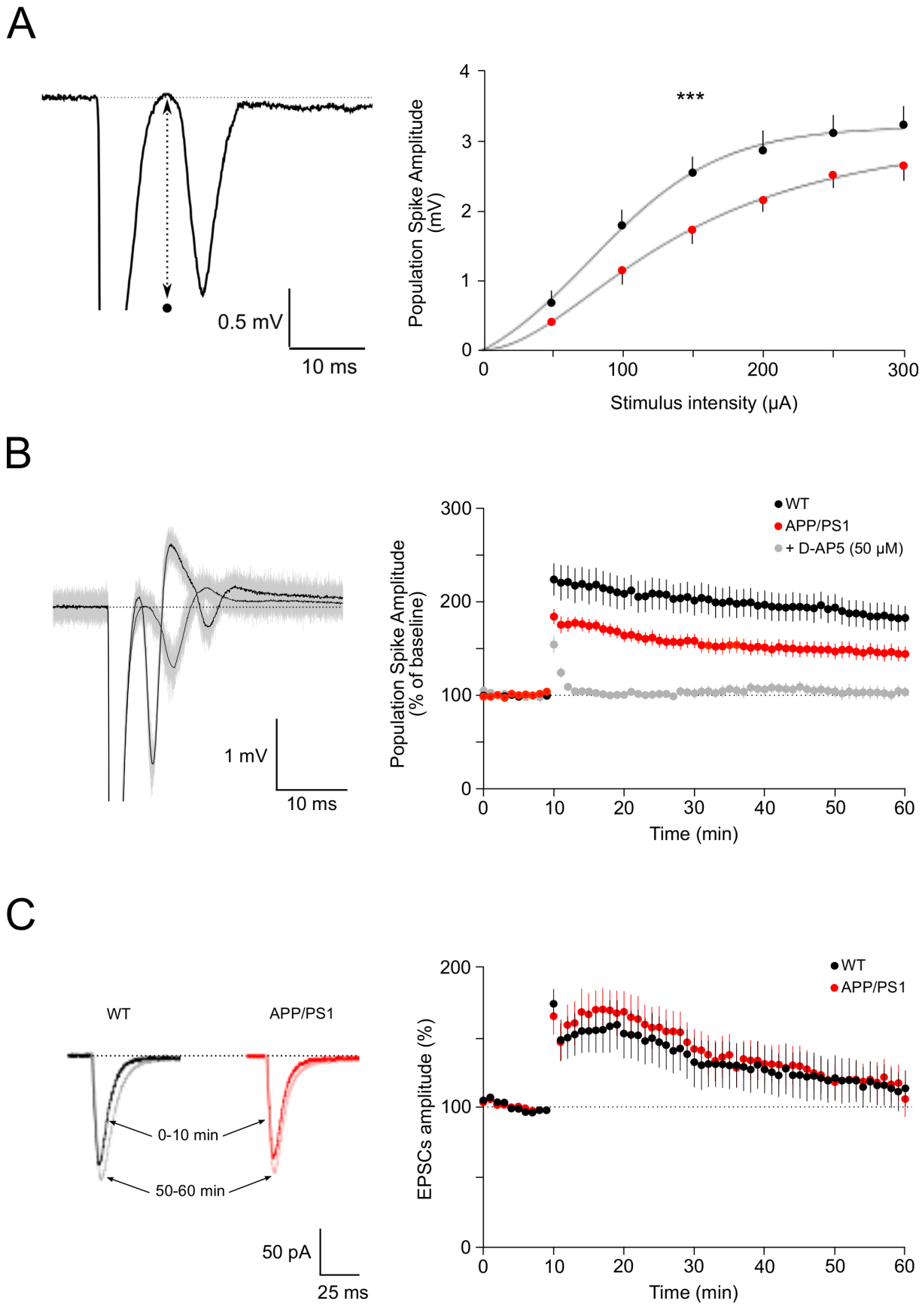
A
0.5 mV
10 ms
***
Population Spike Amplitude (mV)
Stimulus intensity (µA)
B
1 mV
10 ms
WT
APP/PS1
+ D-AP5 (50 µM)
Population Spike Amplitude (% of baseline)
Time (min)
C
WT
APP/PS1
0-10 min
50-60 min
50 pA
25 ms
EPSCs amplitude (%)
Time (min)

Figure 4

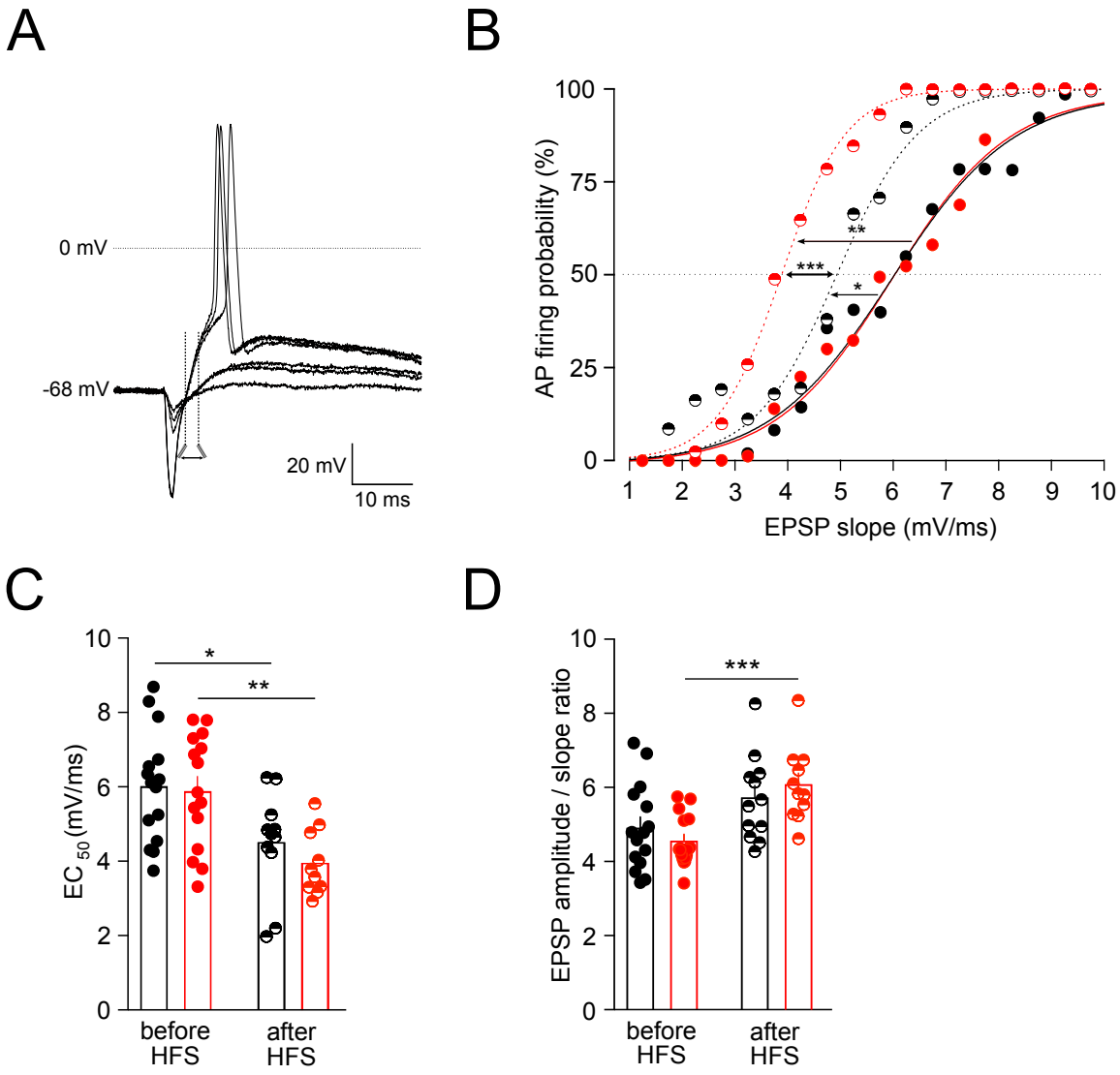
A
0 mV
-68 mV
20 mV
10 ms
B
AP firing probability (%)
EPSP slope (mV/ms)
C
EC50 (mV/ms)
before HFS
after HFS
D
EPSP amplitude / slope ratio
before HFS
after HFS

Figure 5